DOCTORAL THESIS

Trends and Variability of Rainfall, Temperature and Associated Extremes, and Their Future Projections in Rwanda Using Regional Climate Models

VOLUME I

by Ndakize Joseph Sebaziga

2025

Trends and Variability of Rainfall, Temperature and Associated Extremes, and Their Future Projections in Rwanda Using Regional Climate Models

By

Ndakize Joseph Sebaziga

A Thesis submitted in fulfillment of the requirements for the degree of:

Doctor of Philosophy in Physics (Atmospheric and Climate Science)

Department of Physics
School of Science
College of Science and Technology
University of Rwanda

August 2025

Copyright

Declaration

I declare that this dissertation contains my work except where acknowledged, and it has been passed through the antiplagiarism system and found to be compliant and this is the approved version of the PhD Thesis: ***Trends and Variabilities of Rainfall, Temperature and Associated Extremes, and Their Future Projections in Rwanda using Regional Climate Models*.**

Ndakize Joseph Sebaziga, Reg N°: 217290981 Date:10 /10/2025

Name and signature of the PhD candidate

The PhD Thesis Supervisory Team of Mr. Ndakize Joseph Sebaziga

Professor Bonfils Safari Date: 10/10/2025

Name and signature of the Main Supervisor

Dr. Joshua Ndiwa Ngaina Date: 06/10/2025

Name and signature of the Co-supervisor

Dr. Didier Ntwali Date: 08/10/2025

Name and signature of the Co-supervisor

Dedication

To my family, whose unwavering support and encouragement made my academic journey possible, this dissertation is dedicated.

Acknowledgement

I would like to express my deep and sincere gratitude to my supervisor, Professor Bonfils Safari, for his invaluable guidance and encouragement during this PhD journey. I am also deeply thankful to Dr. Joshua Ndiwa Ngaina and Dr. Didier Ntwali who co-supervised this dissertation. Their support has been a source of inspiration and have significantly contributed to the success of my research.

I am grateful to the Rwanda Astrophysics, Space, and Climate Science Research Group (RASCRG) for having fully supported my studies, thanks to its collaboration (Grant No. ISP/RWA: 01) with the International Science Programme (ISP) funded by the Swedish International Development Cooperation Agency (SIDA).

I thank the Rwanda Meteorology Agency (METEO-RWANDA) for providing observed meteorological data used in this study, and to the Rwanda Environment Management Authority (REMA) for facilities made available.

I owe everything to my family, whose encouragement and support have been a constant source of strength throughout my personal and academic journey. I am especially grateful to my parents, my lovely brothers, sisters, and other family members for their unwavering and unconditional support. Very special thanks goes to my wife, Solange Nyirashimwe, for her unwavering support and for taking care of our children throughout my PhD journey. I am especially thankful to my daughters Lucie Ishimwe Sebaziga, Pretty Ineza Sebaziga, Gianna Gasaro Sebaziga and my son Joshua Shema Sebaziga for standing by me throughout this research. Thank you for sharing in both the challenges and triumphs along the way.

My success in this PhD journey has not only depended on scientific focus but also on the positive and supportive people I met along the way. While it would be difficult to mention everyone, a few names truly stand out. Special thanks go to Dr. Antony Twahirwa, Abdou Kagabo Safari, Dr. Vedaste Iyakaremye, Michel Rwema, Dr. Jonah Kazora, Bernard Niyigena, Aminadab Tuyisenge, Eric R. Mudakikwa, David Ukwishaka, Herman Hakuzimana, Bernardin Bavuge and Alex Nizeyimana. Every word of encouragement and every chat during moments of exhaustion made a meaningful contribution to the completion of this research.

Abstract

This study examines observed trends, variability, and future projections of rainfall, temperature, and associated extremes in Rwanda using outputs from the Coordinated Regional Climate Downscaling Experiment-Coordinated Output for Regional Evaluation (CORDEX-CORE) regional climate models (RCMs). Observational trends and variability were analyzed for 1983-2021 using data from the Rwanda Meteorology Agency, while future projections were examined for 2026-2060 and 2066-2100 under two representative concentration pathways (RCP2.6 and RCP8.5). The performance of CORDEX-CORE RCMs in simulating observed rainfall was evaluated for 1983-2005. The study also assesses the influence of large-scale climate drivers, particularly the El Niño-Southern Oscillation (ENSO) and the Indian Ocean Dipole (IOD), on Rwanda's rainfall patterns. For the observational period, trends and magnitudes were assessed using the Modified Mann-Kendall test and Theil-Sen estimator, while temporal variability was analyzed using standard deviation and coefficient of variation. Rainfall characteristics, namely onset day (OD) and cessation day (CD) of the rainy season, were determined using methods based on accumulation thresholds, rainy day counts, dry spell and potential evapotranspiration analysis. Climate extremes were evaluated following the methodology of the Expert Team on Climate Change Detection and Indices (ETCCDI). Results show that the multi-model ensemble (CORDEX-CORE-MME) outperforms individual models in simulating Rwanda's present climate. During the observational period, maximum temperatures exhibited higher variability than minimum temperatures. However, minimum temperatures exhibited greater warming magnitudes than maximum temperatures. Rainfall showed high spatial and temporal variability, with mostly non-significant trends across regions. Rainfall onset and cessation dates revealed west-east and east-west progression patterns, respectively. Seasonal length (SL) and number of rainy days (RD) were generally longer and more frequent in the southern, western, and northern regions, while central and eastern areas had shorter seasons and fewer rainy days. Climate extreme indices for rainfall and temperature displayed spatially and seasonally heterogeneous trends, with significant increases or decreases depending on the index and emission scenario. Future projections suggest shifts in OD and CD, with earlier onsets and longer seasons more common under RCP2.6 than RCP8.5. Rainy days are projected to increase during the long rains, but exhibit more complex patterns in the short rains, including regional decreases under RCP8.5 by century's end. Heavy

(R10mm) and very heavy (R20mm) precipitation days are projected to decline during long rains, while consecutive wet days (CWD) are expected to rise, particularly under RCP2.6 in 2026-2060. For temperature extremes, cold days (Tx10p) are projected to increase during long rains for 2026-2060 but decline in 2066-2100, while warm days (Tx90p) show the opposite pattern. These findings provide crucial insights to inform climate-resilient planning and policy development across key socio-economic sectors, including agriculture, health, water resources, infrastructure, tourism, and disaster risk reduction, and support the formulation of effective adaptation strategies at local and national levels.

Key word: CORDEX-CORE RCMs, Extreme Indices, Projection, Rainfall, Rainfall Characteristics, Rwanda, Temperatures, Trend and Variability.

List of symbols, acronyms and abbreviations

CCl: Commission on Climatology

CD: Cessation Day

CDV: Variation of Cessation Days

CGCMs: Coupled Global Climate Models

CHIRPS: Climate Hazards Group InfraRed Rainfall and Stations

CLIVAR: Climate Variability and Prediction

CMORPH: Climate Prediction Center Morphing Technique

CORDEX: Coordinated Regional Climate Downscaling Experiment

CORDEX-CORE: CORDEX-Coordinated Output for Regional Evaluation

CORDEX-CORE-MME: CORDEX-CORE Multi-Model Ensemble

CPC: Climate Prediction Centre

CRU: Climatic Research Unit

CWD: Consecutive dry days

DTR: Diurnal temperature range

EA: East Africa

ENACTS: Enhancing National Climate Services

ENSO: El Niño-Southern Oscillation

ERA-Interim: European Centre for Medium-Range Weather Forecasts (ECMWF) Interim Re-Analysis

ETCCDI: Expert Team on Climate Change Detection and Indices

GCM: Global Climate Model

GDP: Gross Domestic Product.

GIS: Geographic Information Systems

GPCC: Global Precipitation Climatology Centre

GPCP: Global Precipitation Climatology Project

IDW: Inverse Distance Weighted

IOD: Indian Ocean Dipole

ISP: International Science Programme

ITCZ: Inter-tropical Convergence Zone

ITD: Inter-Tropical Discontinuity

JF: January-February

JJA: June-July-August

JRA55: Japanese 55-year reanalysis project

LR: Long Rain season

MAE: Mean Absolute Error

MAM: March-April-May (MAM)

MBE: Mean Bias Error

METEO-RWANDA: Rwanda Meteorology Agency

MJO: Madden-Julian Oscillation

MK: Modified Mann–Kendall

mm: Milimeter

$mm \cdot day^{-1}$: Milimeter per day

$mm^2 \cdot day^{-1}$: Milimeter square per day

mm/decade: Milimeter per decade

MSR: Mean Seasonal Rainfall

NOAA: National Oceanic and Atmospheric Administration

NRMSE: Normalized Root Mean-Square Error

OD: Onset Day

ODV: Variation of Onset Days

OND: October-November-December

ONI: Oceanic Niño Indices

PET: Potential Evapotranspiration

PhD: Doctor of Philosophy

PRCPTOT: Total wet-day precipitation

r: Pearson correlation coefficient

RCM: Regional Climate Model

RCP: Representative Concentration Pathway

RD: Number of Rainy Day

RDV: Variation of Number of Rainy Days

REMA: Rwanda Environment Management Authority

RI: Rainfall Intensity

RMSE: Root Mean-Square Error

Rx1day: Maximum 1-day precipitation amount

R10 mm: Heavy precipitation days

R20 mm: Very heavy precipitation days

R95pTOT: Precipitation due to very wet days

T: Mean temperature

TAMSAT: Tropical Applications of Meteorology using SATellite

Tn: Minimum temperature

Tn10p: Cold nights

Tn90p: Warm nights

TRMM-3B42: Tropical Rainfall Measuring Mission

TS: Theil–Sen

Tx: Maximum temperature

Tx10p: Cold days

Tx90p: Warm days

SDE: standard error of the mean bias

SDII: Simple Daily Intensity Index

SIDA: Swedish International Development Cooperation Agency

SL: Seasonal Length

SLV: Variation of Seasonal Length

SOND: September-October-November-December

SR: Short Rain season

SSA: Sub-Saharan African

SST: Sea Surface Temperature

UDEL: University of Delaware

WMO: World Meteorological Organization

WRF: Weather Research and Forecasting

X: mean rainfall

˚C: Degree Celsius

˚C/decade: Degree Celsius per decade

σ^2: variance

$\delta_{RD:}$ projected change of mean number of rainy days

$\delta_{OD:}$ projected change of mean Onset Days

$\delta_{CD:}$ projected change of mean Cessation days

$\delta_{SL:}$ projected change of mean Seasonal Length

Table of Content

List of figures

List of tables

List of publications

This dissertation is a monograph based on seven journal articles. Details about these publications and their contributions to the respective chapters of the dissertation are outlined below.

1. Safari, B., Sebaziga, J. N., & Siebert, A. (2022). Evaluation of CORDEX-CORE regional climate models in simulating rainfall variability in Rwanda. International Journal of Climatology, 43(2), 1112–1140. https://doi.org/10.1002/joc.7891 (Chapter 2)
2. Safari, B., & Sebaziga, J. N. (2023). Trends and Variability in Temperature and Related Extreme Indices in Rwanda during the Past Four Decades. Atmosphere, 14(9), 1449. https://doi.org/10.3390/atmos14091449 (Chapter 3)
3. Sebaziga, N. J., Safari, B., Ngaina, N. J., Ntwali, D., Mutai, B. K., Safari, A., & Rwema, M. (2022). Rainfall variability and trends over Rwanda. Journal of Climate Change and Sustainability, 4(1), 26–34. https://doi.org/10.20987/jccs.04.06.2022 (Chapter 4)
4. Sebaziga, N.J., Safari B., Ngaina, N. J., Ntwali, D. (2024). Spatial variability of seasonal rainfall onset, cessation, length and rainy days in Rwanda," Theoretical and Applied Climatology, 2024, https://doi.org/10.1007/s00704-024-05086-3 (Chapter 5)
5. Sebaziga, N.J., Safari B., Ngaina, N. J., Ntwali, D. (2025). Observed trends and variability of seasonal extreme rainfall indices and projected changes in Rwanda., Theoretical and Applied Climatology, 2025, https://doi.org/10.1007/s00704-025-05474-3 (Chapter 6)
6. Trends and Projected Changes in Seasonal Rainfall Onset, Cessation Dates, Seasonal Length, and Rainy Days in Rwanda (Chapter 7)
   Authrors: Ndakize Joseph Sebaziga, Bonfils Safari, Didier Ntwali, Joshua Ndiwa Ngaina
   Submitted in: Advances in Meteorology.
7. Observed and Future Projections of Seasonal Extreme Temperature Indices in Rwanda (Chapter 8)
   Authrors: Ndakize Joseph Sebaziga, Bonfils Safari, Joshua Ndiwa Ngaina, Didier Ntwali
   Submitted in: Theoretical and Applied Climatology.

Chapter 1 General introduction and thesis outline

1.1 Introduction

Climate variability and change are among the most critical challenges today, deeply impacting natural ecosystems and human activities. Key meteorological variables such as rainfall and temperature are central to climate change impact studies as they influence agriculture, water availability, ecosystems, and human livelihoods (Mikova, 2015). Understanding the variability and trends of these variables under a changing climate is essential for forecasting future conditions and developing adaptation strategies. In many African countries, the seasonality of rainfall is especially important because communities depend heavily on seasonal rains for farming and domestic needs (Ramirez-villegas et al., 2017). However, rainfall patterns have become increasingly variable in both frequency and intensity, with Africa experiencing significant shifts over the past century century (Huq et al., 2004). In sub-Saharan Africa (SSA), where rain-fed agriculture is the main source of livelihood, climate change has already caused declines in crop production, severely affecting smallholder farmers (Ayanlade et al., 2022).

In East Africa (EA), rainfall is marked by high spatial and temporal variability, often leading to extreme weather events such as droughts and floods. These events have had devastating effects on economies, infrastructure, and human and animal lives (Nicholson, 2017). Recent decades have shown declining rainfall and longer, more intense droughts, often stretching across rainy seasons in the region (Palmer et al., 2023). At the same time, extremely high rainfall events have caused flooding, destruction, and social and economic disruption (Chang'a et al., 2020). For example, the October-December 2019 floods in EA, which caused landslides and displacement, were linked to unusually high rainfall (Chang'a et al., 2020). Meanwhile, rainy seasns in some areas have shown slight decreases, with no major changes in the annual rainfall average (Ogega et al., 2020). In EA region, significant rise in temperatures was observed across major cities, with warming levels nearly double the global average since pre-industrial times (Engelbrecht et al., 2015). This trend is evident in observed increases in maximum, minimum, and mean temperatures throughout the region (Gebrechorkos et al., 2019). In Rwanda, similar warming patterns have been observed, particularly in urban areas such as Kigali City, where the annual mean temperature has significantly increased (Safari, 2012; Kagabo et al., 2024). Across the country, studies indicate

that minimum temperatures have increased at a faster rate than maximum temperatures, which tend to show higher variability (Ngarukiyimana et al., 2021; Safari and Sebaziga, 2023).

The rainfall in the EA and Rwanda, is primarily controlled by the seasonal north-south migration of the Inter-tropical Convergence Zone (ITCZ) (Nicholson, 2000). The main drivers of the rainfall inter-annual variability are the El Niño-Southern Oscillation (ENSO) and the Indian Ocean Dipole (IOD) climate modes associated with sea surface temperature (SST) anomalies across the tropical Pacific and Indian Oceans, respectively (Mutai and Neil., 2000; Goddard and Mason, 2002; Oettli & Camberlin, 2005; Lyon & Dewitt, 2012; Liebmann et al., 2014; Nicholson, 2017). Sea surface temperatures (SSTs) are commonly used to predict seasonal rainfall, with warmer or cooler waters in the Indian and Atlantic Oceans linked to enhanced or suppressed rainfall over EA (Owiti, 2008). Typically, El Niño and positive IOD events lead to increased rainfall, while La Niña and negative IOD events result in reduced rainfall (Indeje et al., 2000; Nicholson, 2017; Ingeri et al., 2024). Tropical cyclones in the Mozambique Channel also influence rainfall, especially during March to May by altering low-level winds while rainfall tends to increase during December and January, sometimes causing flooding (Nyakwada et al., 2009). In additional, topography also plays a critical role where highland areas generally receive more rainfall and experience cooler temperatures than lowland regions (Ogwang et al., 2014)(Ntwali et al., 2016).

1.2 Climate Modelling and Simulation

Information derived from meteorological variables is important for policy and decision makers, who use it for development of smart decisions for long-term planning and managing risks (Giorgi et al., 2009; Akinsanola et al., 2015). To create this information, scientists mainly use climate models to predict how climate might change in the coming decades (Lee et al., 2014). The development of global climate models (GCMs) has evolved significantly over the past century, emerging as a key scientific tool for understanding and projecting changes in the Earth's climate system. The evaluation of GCMs helped scientists and researchers to recognize the limitations of coarse-resolution in capturing local and regional climate variations. This led to the development of Regional Climate Models (RCMs), which provide higher spatial resolution and are better suited for impact studies at the regional and national levels to provide detailed climate information on local climate change hot spots within regions that forms the basis of a community-led solution

(Lobell et al., 2008).To get more detailed climate information at the local level, scientists use a process called downscaling, which improves the resolution of the model. There are two main types of downscaling namely, dynamical downscaling and statistical downscaling (Trzaska and Schnarr, 2014).

Dynamical downscaling uses an RCM which operates on principles similar to those of GCMs but work at a much finer scale (Giorgi and Gutowski, 2015; Fotso-Nguemo et al., 2017). This approach involves nesting a finer-meshed RCM within the GCM, which provides the boundary and lateral conditions and incorporates more detailed topography, land-sea contrasts, surface heterogeneities, and physical processes, allowing it to produce realistic climate information at a spatial resolution of approximately 50 kilometers (Trzaska and Schnarr, 2014). However, dynamical downscaling is computationally intensive and sensitive to the biases inherited from the driving GCM. On the other hand, statistical downscaling is based on building mathematical relationships between large-scale climate patterns (called predictors) and local weather conditions (called predictands) developed using past climate data (Trzaska and Schnarr, 2014; Worku et al., 2018). A key idea in this method is that the relationship between large and local-scale variables remains valid in the future under different forcing conditions of possible future climates (Trzaska and Schnarr, 2014).This method is less demanding on computers but depends heavily on how well GCMs capture the large-scale patterns and how strong are the statistical links.

To coordinate and advance regional downscaling efforts worldwide, the World Climate Research Programme (WCRP) established the Coordinated Regional Climate Downscaling Experiment (CORDEX). CORDEX provides a global framework for producing and evaluating RCMs to produce regional climate projections based on a consistent set of GCMs and RCMs that are consistent and comparable across different regions and institutions (Giorgi et al., 2009). CORDEX is organized around a set of regional domains, including CORDEX-Africa, and uses standardized protocols for driving data, simulation periods, spatial resolution, and output formats. This enables ensemble modelling, where multiple RCMs driven by multiple GCMs are used to quantify uncertainty and improve confidence in projections. The CORDEX-Africa initiative has been particularly valuable for the African continent, enabling high-resolution projections (0.44°) tailored to African needs, addressing the continent's unique climate dynamics and vulnerabilities and demonstrated the utility of CORDEX RCMs in simulating key climate features, such as the seasonal and diurnal cycles of rainfall and temperature across Africa, while also highlighting

substantial inter-model biases (Nikulin et al., 2012; Endris et al., 2013) (Dosio et al., 2015; Giorgi & Gutowski, 2015).

With the growing demand for high-resolution information about regional climate change and its impact all over the world and to streamline modelling efforts and improve interoperability, the WCRP CORDEX developed the CORDEX-Coordinated Output for Regional Evaluations **(**CORDEX-CORE**)** initiative to provide a more focused and resource-efficient set of high-priority RCM simulations across key global domains. CORDEX-CORE use RCMs at a higher horizontal resolution (0.22°) and over two key Representative Concentration Pathways (RCPs), typically RCP2.6 and RCP8.5 with an objective of balancing comprehensive coverage with computational feasibility and ensure consistent outputs across regions (Gutowski et al., 2016; Coppola et al., 2021). For Africa, the CORDEX-CORE outputs are particularly valuable for countries and sub-regions with limited national modelling capacity and importantly, CORDEX-CORE also promotes open data sharing, capacity building, and collaboration between regional institutions and the broader climate modelling community. CORDEX and CORDEX-CORE outputs form the backbone of many regional climate studies, including those assessing impacts on agriculture, water resources, and public health.

1.3 Intra-Seasonal Rainfall Characteristics

It is essential to recognize that the performance of a rainy season is not solely dependent on the overall total rainfall amount, but also on the adequate distribution of rains throughout the season. Failures in rainfall can be manifested as late or early onset and cessation of the season, or short but intense rainfall events separated by prolonged dry spells (Camberlin and Okoola, 2003). The OD of rainfall marks the beginning of a season, though definitions vary among researchers. Several criteria for determining OD varies among regions. They include use of accumulation rainfall, number of rainy days and dry spell periods (Adelekan and Adegebo, 2014; Mugo et al., 2016a). Other models use rainfall data alone (Odekunle et al., 2005) and daily soil water balance (Mugalavai et al., 2012). Models considering dry spells in determining the OD of the rainy season are significant as they reduce the chance of a false start, characterized by early rains followed by long dry spells, and are adaptable to different locations (Sultan and Janicot, 2003). In additional, modifying the length or intensity of the initial wet spell, or the following dry spell, alters the long-

term mean OD date but has minimal impact on inter-annual variability or spatial coherence (Marteau et al., 2009).

Similarly, CD are determined using different methods such as period of days with rainfall accumulation less than a certain threshold for consecutive number of dry days (Adelekan and Adegebo, 2014). Other methods use soil moisture or water balance reaching zero after the OD of the season to determine the end of the season (Taye et al., 2013), and soil water availability dropped to a certain balance of total available water (Mugalavai et al., 2012). The seasonal length (SL) is determined by computing the difference between the cessation day (CD) and the onset day (OD) of the rainy season for each year (Gebremichael et al., 2014; Haleakala et al., 2018).

1.4 Climate Extreme indices

In nature, weather and climate extremes are rare events which happen in the natural climate system (Easterling et al., 2016). For consistency and homogeneity in the determination of climate extreme indices, the joint World Meteorological Organization Commission on Climatology (CCl) and the Climate Variability and Prediction (CLIVAR) Expert Team on Climate Change Detection and Indices (ETCCDI) developed a core set of 27 indices (Zhang et al., 2005; Alexander et al., 2006; Tank et al., 2009; Donat et al., 2013; Easterling et al., 2016). In recent decades, the world has witnessed a significant rise in record-breaking weather and climate events (Lehmann et al., 2015). These extremes including heatwaves, heavy rainfall, droughts, and storms have had wide-ranging impacts on key socio-economic sectors and the environment, including human health and well-being of the community (Tank et al., 2009). Climate extreme indices are used to measure how often and how severely such extreme events occur (Gachon et al., 2005; Sarr et al., 2015). These indices have helped reveal a global increase in both the frequency and intensity of natural disasters, a trend closely linked to climate change and environmental degradation (Adeyeri et al., 2019).
Rainfall indices such as total precipitation due wet day (PRCPTOT) and simple daily rainfall intensity (SDII) help link daily precipitation changes with extreme weather events (Sillmann et al., 2013). Similarly, changes in climate indicators based on daily minimum temperatures tend to be more noticeable than those based on maximum temperatures (New et al., 2000). Temperature extreme indices are essential for quantifying shifts in climate extremes, particularly the frequency of unusually hot or cold days and nights. Globally, there has been a marked decrease in cold nights

(Tn10p) and an increase in warm nights (Tn90p), with some regions experiencing more than a twofold rise, indicating a general upward shift in daily minimum temperatures (Alexander et al., 2006).

1.5 Impacts of rainfall and temperature variability

In Africa, seasonal rainfall changes have serious socio-economic consequences due to the high reliance on rain-fed agriculture (Dunning et al., 2018). Variability in rainfall also affects livestock and crop productivity (Chang'a et al., 2020). Agricultural systems, in particular, are highly sensitive to extremes. Heavy or very heavy rainfall can harm agriculture by causing inundation, delaying planting periods, and increasing the risk of root diseases or crop failure (Posthumus et al., 2009). Changes in rainfall and temperature regimes are also linked to a growing frequency and intensity of drought events, contributing to environmental degradation, infrastructure stress, reduced agricultural productivity, and livestock losses (Li et al., 2021; Uwimbabazi et al., 2022). For agriculture, particularly in regions that rely heavily on rain-fed farming unpredictability of the onset of the rainy season influence agricultural decisions, such as when to prepare land, plant crops, crop choice, pest and disease management and anticipate harvests (Odenkunle, 2004) (Edoga, 2007). These factors help assess whether a particular crop is likely to succeed or fail in a given season (Ngetich et al., 2014).

The changes in diurnal temperature range (DTR), shifts in the frequency of warm or cold tails of extreme temperatures impact crop performance through increased evapotranspiration levels and spread of crop diseases (Machina and Sharma, 2017; Jang and Chun, 2021). In regions highly dependent on farming, climate shocks may trigger population displacement due to water scarcity, crop failure, famine, and food insecurity (Ayugi et al., 2020; Mueller et al., 2020; Bannor et al., 2022). The effects of climate variability are not limited to agriculture. For health sector, increase in DTR elevate the risk of heat-related illnesses, particularly among the elderly and lead to high hospital admission (Jang and Chun, 2021) and may trigger increased incidence of malaria out breaks (Henninger, 2013). The tourism sector is also affected by the changes in extreme temperatures through changes in tourist comfort (Scott and Lemieux, 2010). These growing risks are influencing national planning and policy. By analysing changes in climate extreme indices,

decision-makers can better understand emerging trends and develop informed strategies to safeguard communities, ecosystems, and economies (Zhang et al., 2005; Tank et al., 2009).

1.6 Characteristics of climate in Rwanda

Rwanda is situated in Eastern and Central Africa, positioned between 1°4′ and 2°51′ South latitude and 28°53′ and 30°53′ East longitude, covering a total area of 26,338 square kilometers. From west to east, Rwanda is characterized by diverse topography ranging from highlands in the west and north to the lowlands in the east. Its landscape includes hills valleys and highlands with elevation varying from in Bugarama valley siting at 900 meters to Volcanic region with Karisimbi being the highest peak at 4,507 meters. The central plateau ranges from 1,500 to 2,000 meters while the eastern lowland is dominated by hills with altitudes ranging from 1,000 to 1,500 meters above sea level (Mikova, 2015b). Rwanda's diverse topography influence the rainfall and temperature distribution across the country (Ntwali et al., 2016) (Ngarukiyimana et al., 2017). Low rainfall amounts and high temperatures are observed in low-elevation areas located in the eastern region, and high rainfall amounts and low temperatures are observed in high-elevated areas located northern, western and southwest (Ilunga & Muhire, 2010) (Ogwang, Chen, Li, Gao, et al., 2014) (Ntwali et al., 2016)

Rwanda's rainfall climatology follows the typical bimodal pattern observed in Eastern African region, with two rainy seasons of March-April-May (MAM) commonly known in Kinyarwanda as “Itumba” and September to December (SOND), commonly known in Kinyarwanda as “Umuhindo” and two dry seasons of which one is a short dry season extending from January to February (JF) commonly known in Kinyarwanda as “Urugaryi” and a long dry season spanning the months of June to August (JJA) commonly known in Kinyarwanda as “Impeshyi” (Ntwali et al., 2016) (Siebert, Dinku, Vuguziga, Twahirwa, Kagabo, et al., 2019) (Kazora et al., 2021) (Umutoni et al., 2021) (Sebaziga et al., 2022). The high annual rainfall totals (>1200 mm) are recorded in the areas surrounding the Congo-Nile Trial, Nyungwe National Park in the southwest and the Virunga volcanic mountains in the northern while the eastern lowland record low annual rainfall (<900 mm) (Siebert, Dinku, Vuguziga, Twahirwa, Kagabo, et al., 2019). The peak months for rainfall are April during the MAM and November for the SOND in Rwanda (Muhire et al., 2015) (Ntwali et al., 2016). Similar to rainfall, temperatures across the country vary significantly

with topography. The south-eastern parts of the country in Rusizi valley observes a warmest average temperatures ranging between 23˚C and 24˚C, followed by the eastern lowlands varying between 20˚C to 21˚C. The highlands areas experience lowest temperatures which can drop to around 17˚C and ranges between 17.5˚C to 19˚C in the in the central plateau while the mean annual temperature fluctuates around 20˚C (B. Safari, 2012). Lowest monthly average temperatures are observed in May and November while highest monthly average temperatures are observed in February and August (Ngarukiyimana et al., 2021b).

The climate of Rwanda is predominantly influenced by south-easterly winds, which weaken and shift direction during certain seasons (Siebert, Dinku, Vuguziga, Twahirwa, Kagabo, et al., 2019). During JJA, Rwanda is influenced by the dry Saint Helena and Azores anticyclones, which contribute to dry conditions across the country (Ilunga et al., 2008). In September, the ITCZ begins its passage from the Somalian coast, crossing Lake Victoria where it gains humidity and brings rainfall to Rwanda before moving southward by the end of November. From December to February, the winter monsoon pushes dry and cold air masses from the Arabian Sea over Lake Victoria, gathering humidity that results in light rainfall in Rwanda's highland regions (Ilunga et al., 2004)(Ilunga et al., 2008). Furthermore, a relationship exists between ENSO and rainfall patterns, with El Niño events linked to positive rainfall anomalies (wet years) and La Niña events associated with negative anomalies (dry years) (Ilunga & Muhire, 2010) (Muhire et al., 2015). Normal years typically correspond with negative anomalies in MAM and positive anomalies in SOND (Muhire et al., 2015). Similarly, Indian ocean dipole (IOD) events increase rainfall over Rwanda especially during SOND season (Kazora et al., 2021)(Rusanganwa et al., 2024) (Ingeri et al., 2024).

1.7 Statement of the research problem

Policymakers rely on accurate climate information for effective planning and decision-making (Giorgi et al., 2009; Akinsanola et al., 2015). To advise planning and decision-making, there is a need for a comprehensive assessment of climate variables such as rainfall and temperature (Mikova, 2015b). Rainfall, a critical factor for crop production, is more beneficial when it is evenly distributed rather than experiencing isolated heavy rainfall interrupted by prolonged dry periods (Gitau et al., 2013; Sifer et al., 2016). The performance of agricultural seasons is influenced by

changes in rainfall onset date (OD) and cessation date (CD), which in turn determine the seasonal length (SL) (Odenkunle, 2004). In Rwanda, studies have used station data to study the characteristics and trends of rainfall at both seasonal and annual scales (Henninger, 2013a) and (Muhire et al., 2015). Gridded data, such as those from METEO-RWANDA (Siebert, Dinku, Vuguziga, Twahirwa, & Kagabo, 2019) and the Climate Hazards Group InfraRed Precipitation with Stations (CHIRPS) (Kazora et al., 2021), have been used in previous studies to examine rainfall patterns in Rwanda. However, previous studies in Rwanda have not addressed intra-seasonal rainfall characteristics and their future projections. Understanding the historical and projected changes in rainfall characteristics namely OD, CD, SL and rainy days (RD) is crucial for enhancing agricultural planning and adaptation strategies. Rwanda has recently experienced several weather-related disasters, leading to loss of lives, infrastructure damage, and crop destruction, with an increasing frequency of extreme events (Chang'a et al., 2020). Despite this, there has been limited focus on understanding historical and projected changes in extreme rainfall and temperature indices in Rwanda. To assess changes in climate variables, climate models are employed to simulate future climate conditions under various emission scenarios (Lee et al., 2014). RCMs generate high-resolution climate projections, offering valuable insights into climate change for different global regions. The effectiveness of RCMs depends on their ability to replicate historical observations, as different models can produce varying regional projections even under identical emission scenarios (Giorgi & Francisco, 2000). With Rwanda's vision 2050 and the revised Green Growth and Climate Resilience Strategy, accurate climate projections are essential for implementation. However, there is limited information on the performance of CORDEX-CORE RCMs in simulating Rwanda's climate, which is crucial for projecting future conditions and providing valuable information for strategic planning and decision-making for socio-economic sectors.

1.8 Motivation and Significance of the research

Socio-economic activities heavily depend on rain-fed agriculture and livestock productivity that in turn depend on rainfall availability (Gitau et al., 2013; Dunning et al., 2018; Chang'a et al., 2020). Given that Rwandan farmers practice rain-fed agriculture, the variability in rainfall and temperature both in space and time affects crop production significantly (Kazora et al., 2021).

a. This study:

- Demonstrates that the multi-model ensemble mean provides more reliable simulations of Rwanda's climate than individual models, improving the accuracy of future climate projections for informed decision-making.
- Identifies significant variations and trends in observed rainfall, air temperature, computed rainfall characteristics and extreme climate indices.
- Provides information on future projected changes in rainfall and air temperature patterns, computed extreme climate indices and rainfall characteristics with a tendency toward earlier onset dates, longer rainy seasons, and an increasing number of rainy days. These changes underscore the importance of climate-informed planning in agriculture, water management, and disaster preparedness, offering policymakers critical insights for integrating climate resilience into national development strategies.

b. The findings of this study:

- Could support public and private sector decision-makers in formulating effective policies and funding strategies for climate change adaptation and mitigation.
- May contribute to the implementation of Rwanda's National Environment and Climate Change Policy, Vision 2050, and the Revised Green Growth and Climate Resilient Strategy by providing essential information on current and projected climate changes.
- Could be used as valuable inputs for climate change impact assessments across various socio-economic sectors in Rwanda, including agriculture, health, water resources, energy, disaster management, tourism, economic development, and infrastructure.

1.9 Objectives of the research

The primary objective of this study is to examine the intra-seasonal and seasonal characteristics of rainfall, air temperature and their related extreme indices in Rwanda under changing climate.
To accomplish this, the study has focused on the following specific objectives:

- To assess the performance of CORDEX-CORE RCMs to simulate the climate of Rwanda
- To examine the seasonal characteristics of onset date (OD), cessation dates (CD), seasonal length (SL) and number of rainy days (RD) for both present and future time scales**.**

- Investigate the variability in rainfall and air temperature and their related extreme indices on both present and future time scale.
- To investigate the synoptic features that drive rainfall over Rwanda

1.10 Outline of the thesis

This thesis is organized into nine chapters. Chapter One provides a general introduction to the study, outlining the background, research objectives, and structure of the thesis. Chapter Two evaluates the performance of CORDEX-CORE regional climate models in simulating rainfall variability across Rwanda. Chapter Three investigates historical rainfall variability and trends throughout the country. Chapter Four analyses trends and variability in temperature and associated extreme indices in Rwanda over the past four decades. Chapter Five examines the spatial variability of seasonal rainfall onset, cessation, length, and the number of rainy days. Chapter Six explores observed trends and variability in seasonal extreme rainfall indices, as well as their projected changes under future climate scenarios. Chapter Seven focuses on trends and future projections of seasonal rainfall onset, cessation dates, seasonal length, and rainy days in Rwanda. Chapter Eight analyses both observed and projected changes in seasonal extreme temperature indices across the country. Finally, Chapter Nine presents the main conclusions of the study and outlines potential directions for future research.

1.11 Reference

Adelekan, I. O., & Adegebo, B. O. (2014). Variation in Onset and Cessation of the Rainy Season in Ibadan , Nigeria. *Journal of Science Research*, *13*(January 2014), 13–21.

Adeyeri, O. E., Lawin, A. E., Laux, P., Ishola, K. A., & Ige, S. O. (2019). Analysis of climate extreme indices over the Komadugu-Yobe basin, Lake Chad region: Past and future occurrences. *Weather and Climate Extremes*, *23*(November 2018), 100194. https://doi.org/10.1016/j.wace.2019.100194

Akinsanola, A. A., Ogunjobi, K. O., Gbode, I. E., & Ajayi, V. O. (2015). Assessing the Capabilities of Three Regional Climate Models over CORDEX Africa in Simulating West African Summer Monsoon Precipitation. *Advances in Meteorology*, *2015*.

https://doi.org/10.1155/2015/935431

Alexander, L. V., Zhang, X., Peterson, T. C., Caesar, J., Gleason, B., Klein Tank, A. M. G., Haylock, M., Collins, D., Trewin, B., Rahimzadeh, F., Tagipour, A., Rupa Kumar, K., Revadekar, J., Griffiths, G., Vincent, L., Stephenson, D. B., Burn, J., Aguilar, E., Brunet, M., … Vazquez-Aguirre, J. L. (2006). Global observed changes in daily climate extremes of temperature and precipitation. *Journal of Geophysical Research Atmospheres*, *111*(5), 1–22. https://doi.org/10.1029/2005JD006290

Ayanlade, A., Oluwaranti, A., Ayanlade, O. S., Borderon, M., Sterly, H., Sakdapolrak, P., Jegede, M. O., Weldemariam, L. F., & Ayinde, A. F. O. (2022). Extreme climate events in sub-Saharan Africa: A call for improving agricultural technology transfer to enhance adaptive capacity. *Climate Services*, *27*(December 2021), 100311. https://doi.org/10.1016/j.cliser.2022.100311

Ayugi, B., Tan, G., Rouyun, N., Zeyao, D., Ojara, M., Mumo, L., Babaousmail, H., & Ongoma, V. (2020). Evaluation of meteorological drought and flood scenarios over Kenya, East Africa. *Atmosphere*, *11*(3). https://doi.org/10.3390/atmos11030307

Bannor, F., Magambo, I. H., Mahabir, J., & Tshitaka, J.-L. M. (2022). Interdependence between climate change and migration: Does Agriculture, geography and development level matter in sub-Saharan Africa? *South African Journal of Economics*, 1–20. https://doi.org/10.1111/saje.12343

Camberlin, P., & Okoola, R. E. (2003). The onset and cessation of the "long rains" in eastern Africa and their interannual variability. *Theoretical and Applied Climatology*, *75*(1–2), 43–54. https://doi.org/10.1007/s00704-002-0721-5

Carreras, H., Zanobetti, A., & Koutrakis, P. (2015). Effect of daily temperature range on respiratory health in Argentina and its modification by impaired socio-economic conditions and PM10 exposures. *Environmental Pollution*, *206*, 175–182. https://doi.org/10.1016/j.envpol.2015.06.037

Chang'a, L. B., Kijazi, A. L., Mafuru, K. B., Nying'uro, P. A., Ssemujju, M., Deus, B., Kondowe, A. L., Yonah, I. B., Ngwali, M., Kisama, S. Y., Aimable, G., Sebaziga, J. N., & Mukamana, B. (2020). Understanding the Evolution and Socio-Economic Impacts of the Extreme Rainfall Events in March-May 2017 to 2020 in East Africa. *Atmospheric and Climate Sciences*, *10*(04), 553–572. https://doi.org/10.4236/acs.2020.104029

Coppola, E., Raffaele, F., Giorgi, F., Giuliani, G., Xuejie, G., Ciarlo, J. M., Sines, T. R., Torres-Alavez, J. A., Das, S., di Sante, F., Pichelli, E., Glazer, R., Müller, S. K., Abba Omar, S., Ashfaq, M., Bukovsky, M., Im, E. S., Jacob, D., Teichmann, C., … Rechid, D. (2021). Climate hazard indices projections based on CORDEX-CORE, CMIP5 and CMIP6 ensemble. In *Climate Dynamics* (Vol. 57, Issues 5–6). https://doi.org/10.1007/s00382-021-05640-z

Donat, M. G., Alexander, L. V., Yang, H., Durre, I., Vose, R., Dunn, R. J. H., Willett, K. M., Aguilar, E., Brunet, M., Caesar, J., Hewitson, B., Jack, C., Klein Tank, A. M. G., Kruger, A. C., Marengo, J., Peterson, T. C., Renom, M., Oria Rojas, C., Rusticucci, M., … Kitching, S. (2013). Updated analyses of temperature and precipitation extreme indices since the beginning of the twentieth century: The HadEX2 dataset. *Journal of Geophysical Research Atmospheres*, *118*(5), 2098–2118. https://doi.org/10.1002/jgrd.50150

Dosio, A., Panitz, H. J., Schubert-Frisius, M., & Lüthi, D. (2015). Dynamical downscaling of CMIP5 global circulation models over CORDEX-Africa with COSMO-CLM: evaluation over the present climate and analysis of the added value. *Climate Dynamics*, *44*(9–10), 2637–2661. https://doi.org/10.1007/s00382-014-2262-x

Dunning, C. M., Black, E., & Allan, R. P. (2018). Later wet seasons with more intense rainfall over Africa under future climate change. *Journal of Climate*, *31*(23), 9719–9738. https://doi.org/10.1175/JCLI-D-18-0102.1

Easterling, D. R., Kunkel, K. E., Wehner, M. F., & Sun, L. (2016). Detection and attribution of climate extremes in the observed record. *Weather and Climate Extremes*, *11*, 17–27. https://doi.org/10.1016/j.wace.2016.01.001

Edoga, R. N. (2007). Determination of Length of Growing Season in Samaru Using Different Potential Evapotranspiration Models. *Au J.T.*, *11*(1), 28–35.

Endris, H. S., Omondi, P., Jain, S., Lennard, C., Hewitson, B., Chang'a, L., Awange, J. L., Dosio, A., Ketiem, P., Nikulin, G., Panitz, H. J., Büchner, M., Stordal, F., & Tazalika, L. (2013). Assessment of the performance of CORDEX regional climate models in simulating East African rainfall. *Journal of Climate*, *26*(21), 8453–8475. https://doi.org/10.1175/JCLI-D-12-00708.1

Engelbrecht, F., Adegoke, J., Bopape, M. J., Naidoo, M., Garland, R., Thatcher, M., McGregor, J., Katzfey, J., Werner, M., Ichoku, C., & Gatebe, C. (2015). Projections of rapidly rising surface temperatures over Africa under low mitigation. *Environmental Research Letters*,

10(8). https://doi.org/10.1088/1748-9326/10/8/085004

Fotso-Nguemo, T. C., Vondou, D. A., Tchawoua, C., & Haensler, A. (2017). Assessment of simulated rainfall and temperature from the regional climate model REMO and future changes over Central Africa. *Climate Dynamics*, *48*(11–12), 3685–3705. https://doi.org/10.1007/s00382-016-3294-1

Gachon, P., St-Hilaire, A., Ouarda, T., Nguyen, V. T., Lin, C., Milton, J., Chaumont, D., Goldstein, J., Hessami, M., Nguyen, T.-D., Selya, F., Nadeau, M., Roy, P., Parishkura, D., Major, N., Choux, M., & Bourque, A. (2005). A first evaluation of the strength and weaknesses of statistical downscaling methods for simulating extremes over various regions of eastern Canada. *Environment Canada, Final Report, Montréal, Québec, Canada*, 209.

Gebrechorkos, S. H., Hülsmann, S., & Bernhofer, C. (2019). Long-term trends in rainfall and temperature using high-resolution climate datasets in East Africa. *Scientific Reports*, *9*(1), 1–9. https://doi.org/10.1038/s41598-019-47933-8

Gebremichael, A., Quraishi, S., & Mamo, G. (2014). Analysis of Seasonal Rainfall Variability for Agricultural Water Resource Management in Southern Region , Ethiopia. *Journal of Natural Sciences Research*, *4*(11), 56–80.

Giorgi, F., & Francisco, R. (2000). Uncertainties in regional climate change prediction: A regional analysis of ensemble simulations with the HADCM2 coupled AOGCM. *Climate Dynamics*, *16*(2–3), 169–182. https://doi.org/10.1007/PL00013733

Giorgi, F., & Gutowski, W. J. (2015a). Regional Dynamical Downscaling and the CORDEX Initiative. *Annual Review of Environment and Resources*, *40*(1), 467–490. https://doi.org/10.1146/annurev-environ-102014-021217

Giorgi, F., & Gutowski, W. J. (2015b). Regional Dynamical Downscaling and the CORDEX Initiative. *Annual Review of Environment and Resources*, *40*, 467–490. https://doi.org/10.1146/annurev-environ-102014-021217

Giorgi, F., Jones, C., & Asrar, G. (2009a). Addressing climate information needs at the regional level: the CORDEX framework. *... Organization (WMO) Bulletin*, *November 2008*. http://www.euro-cordex.net/uploads/media/Download_01.pdf

Giorgi, F., Jones, C., & Asrar, G. R. (2009b). Addressing climate information needs at the regional level: the CORDEX framework. *World Meteorological Organization Bulletin*, *58*(3), 175–183. https://doi.org/10.1109/ICASSP.2009.4960141

Gitau, W., Ogallo, L., Camberlin, P., & Okoola, R. (2013). Spatial coherence and potential predictability assessment of intraseasonal statistics of wet and dry spells over Equatorial Eastern Africa. *International Journal of Climatology*, *33*(12), 2690–2705. https://doi.org/10.1002/joc.3620

Goddard, L., & Mason, S. (2002). Sensitivity of seasonal climate forecasts to persisted SST anomalies. *Climate Dynamics*, *19*(7), 619–631. https://doi.org/10.1007/s00382-002-0251-y

Gutowski, J. W., Giorgi, F., Timbal, B., Frigon, A., Jacob, D., Kang, H. S., Raghavan, K., Lee, B., Lennard, C., Nikulin, G., O'Rourke, E., Rixen, M., Solman, S., Stephenson, T., & Tangang, F. (2016). WCRP COordinated Regional Downscaling EXperiment (CORDEX): A diagnostic MIP for CMIP6. *Geoscientific Model Development*, *9*(11), 4087–4095. https://doi.org/10.5194/gmd-9-4087-2016

Haleakala, K., Yue, H., Alam, S., Mitra, R., & Gebremichael, A. I. B. and M. (2018). The evolving roles of intensity and wet season timing in rainfall regimes surrounding the Red Sea. *Environmental Research Letters*, *Ii*, https://doi.org/DOI 10.1088/1748-9326/ac5560.

Henninger, S. M. (2013a). Does the global warming modify the local Rwandan climate? *Natural Science*, *05*(01), 124–129. https://doi.org/10.4236/ns.2013.51A019

Henninger, S. M. (2013b). Local climate changes and the spread of malaria in Rwanda. *Health*, *5*(4), 728–734. https://doi.org/10.4236/health.2013.54096

Huq, S., Reid, H., Konate, M., Rahman, A., Sokona, Y., & Crick, F. (2004). Mainstreaming adaptation to climate change in Least Developed Countries (LDCs). *Climate Policy*, *4*(1), 25–43. https://doi.org/10.1080/14693062.2004.9685508

Ilunga, L., & Muhire, I. (2010). Comparaison des fluctuations des précipitations moyennes annuelles au Rwanda avec les épisodes EL-NINO / LA NINA et les cycles des taches solaires. *Geo-Eco-Trop*, *34*, 75–86.

Ilunga, L., Muhire, I., & Mbaragijimana, C. (2004). Saisons pluviométriques et origine des pluies au Rwanda. *Geo-Eco-Trop*, *28*(1–2), 61–68.

Ilunga, L., Mukingambeho, D., Mugwaneza, A., & Mugiraneza, A. (2008). Probable sowing time in Rwanda. *Geo-Eco-Tro*, 29–36.

Indeje, M., Semazzi, F. H. M., & Ogallo, L. J. (2000). ENSO signals in East African rainfall seasons. *International Journal of Climatology*, *20*(1), 19–46. https://doi.org/10.1002/(SICI)1097-0088(200001)20:1<19::AID-JOC449>3.0.CO;2-0

Ingeri, C., Wen, W., Sebaziga, J. N., Iyakaremye, V., Ekwacu, S., Ayabagabo, P., Twahirwa, A., & Kazora, J. (2024). Potential Driving Systems Associated with Extreme Rainfall across East Africa during October to December (OND) Season 2019. *Journal of Geoscience and Environment Protection*, *12*(07), 25–49. https://doi.org/10.4236/gep.2024.127003

Jang, J. Y., & Chun, B. C. (2021). Effect of diurnal temperature range on emergency room visits for acute upper respiratory tract infections. *Environmental Health and Preventive Medicine*, *26*(1), 1–8. https://doi.org/10.1186/s12199-021-00974-w

Kazora, J., Wen, W., Shahid, S., Ali, M. A., Bilal, M., Habtemicheal, B. A., Iyakaremye, V., Qiu, Z., Almazroui, M., Wang, Y., Joseph, S. N., & Tiwari, P. (2021). Spatiotemporal variability of rainfall trends and influencing factors in Rwanda. *Journal of Atmospheric and Solar-Terrestrial Physics*, *219*(March), 105631. https://doi.org/10.1016/j.jastp.2021.105631

Lee, J. W., Ham, S., Hong, S. Y., Yoshimura, K., & Joh, M. (2014). Future changes in surface runoff over korea projected by a regional climate model under A1B scenario. *Advances in Meteorology*, *2014*. https://doi.org/10.1155/2014/753790

Lehmann, J., Coumou, D., & Frieler, K. (2015). Increased record-breaking precipitation events under global warming. *Climatic Change*, *132*(4), 501–515. https://doi.org/10.1007/s10584-015-1434-y

Li, C., Yang, M., Li, Z., & Wang, B. (2021). How will rwandan land use/land cover change under high population pressure and changing climate? *Applied Sciences*, *11*(12). https://doi.org/10.3390/app11125376

Liebmann, B., Hoerling, M. P., Funk, C., Bladé, I., Dole, R. M., Allured, D., Quan, X., Pegion, P., & Eischeid, J. K. (2014). Understanding recent eastern Horn of Africa rainfall variability and change. *Journal of Climate*, *27*(23), 8630–8645. https://doi.org/10.1175/JCLI-D-13-00714.1

Lobell, D. B., Burke, M. B., Tebaldi, C., Mastrandrea, M. D., Falcon, W. P., & Naylor, R. L. (2008). Prioritizing Climate Change Adaptation Need for Food Security in 2030. *Science*, *319*(February), 607–610. https://doi.org/10.1126/science.1152339

Lyon, B., & Dewitt, D. G. (2012). A recent and abrupt decline in the East African long rains. *Geophysical Research Letters*, *39*(2), 1–5. https://doi.org/10.1029/2011GL050337

Machina, B. M., & Sharma, S. (2017). Assessment of Climate Change Impact on Hydropower Generation : A Case Study of Nigeria. *International Journal of Engineering Technology Science and Research*, *4*(8), 753–762.

Marteau, R., Moron, V., & Philippon, N. (2009). Spatial coherence of Monsoon onset over Western and Central Sahel (1950-2000). *Journal of Climate*, *22*(5), 1313–1324. https://doi.org/10.1175/2008JCLI2383.1

Mikova, K. (2015a). Effect of Climate Change on Crop Production in Rwanda. *Earth Sciences*, *4*(3), 120. https://doi.org/10.11648/j.earth.20150403.15

Mikova, K. (2015b). Effect of Climate Change on Crop Production in Rwanda. *Earth Sciences*, *4*(3), 120. https://doi.org/10.11648/j.earth.20150403.15

Mueller, V., Sheriffc, G., Dou, X., & Gray, C. (2020). Temporary migration and climate variation in eastern Africa. *World Development*, *126*, 104704. https://doi.org/10.1016/j.worlddev.2019.104704

Mugalavai, E. M., Kipkorir, E. C., & Songok, C. K. (2012). *Evaluation of dry spells during sensitive growth stages for maize crop in Western Kenya*. *July*, 1–11.

Mugo, R. M., Ininda, J., & Okoola, R. (2016). Inter Annual Variability of Onset and Cessation of the Long Rains in Kenya. *Journal of Meteorology and Related Sciences*, *9*(region 12), 30–47. https://doi.org/10.20987/jmrs.3.05.2016

Muhire, I., Ahmed, F., & Abutaleb, K. (2015). Relationships between Rwandan seasonal rainfall anomalies and ENSO events. *Theoretical and Applied Climatology*, *122*(1–2), 271–284. https://doi.org/10.1007/s00704-014-1299-4

Mutai, C. C., & Neil., W. M. (2000). East African Rainfall and the Tropical Circulation / Convection on Intraseasonal to Interannual Timescales. *Journal of Climate of Climate*, *13*(22), 3915–3939. https://doi.org/dx.doi.org/10.1175/1520-0442

Mutai, C. C., & Ward, M. N. (2000). East African rainfall and the tropical circulation/convection on intraseasonal to interannual timescales. *Journal of Climate*, *13*(22), 3915–3939. https://doi.org/10.1175/1520-0442(2000)013<3915:EARATT>2.0.CO;2

Nawrotzki, R. J., Hunter, L. M., Runfola, D. M., & Riosmena, F. (2015). Climate change as a migration driver from rural and urban Mexico. *Environmental Research Letters*, *10*(11), 114023. https://doi.org/10.1088/1748-9326/10/11/114023

New, M., Hulme, M., & Jones, P. (2000). Representing twentieth-century space-time climate variability. Part II: Development of 1901-96 monthly grids of terrestrial surface climate. *Journal of Climate*, *13*(13), 2217–2238. https://doi.org/10.1175/1520-0442(2000)013<2217:RTCSTC>2.0.CO;2

Ngarukiyimana, J. P., Fu, Y., Sindikubwabo, C., Nkurunziza, I. F., Ogou, F. K., Vuguziga, F., Ogwang, B. A., & Yang, Y. (2021a). Climate Change in Rwanda: The Observed Changes in Daily Maximum and Minimum Surface Air Temperatures during 1961–2014. *Frontiers in Earth Science*, *9*(March). https://doi.org/10.3389/feart.2021.619512

Ngarukiyimana, J. P., Fu, Y., Sindikubwabo, C., Nkurunziza, I. F., Ogou, F. K., Vuguziga, F., Ogwang, B. A., & Yang, Y. (2021b). Climate Change in Rwanda: The Observed Changes in Daily Maximum and Minimum Surface Air Temperatures during 1961–2014. *Frontiers in Earth Science*, *9*(March), 1–18. https://doi.org/10.3389/feart.2021.619512

Ngarukiyimana, J. P., Fu, Y., Yang, Y., & Ogwang, A. (2017). *Dominant atmospheric circulation patterns associated with abnormal rainfall events over Rwanda , East Africa*. https://doi.org/10.1002/joc.5169

Ngetich, K. F., Mucheru-Muna, M., Mugwe, J. N., Shisanya, C. A., Diels, J., & Mugendi, D. N. (2014). Length of growing season, rainfall temporal distribution, onset and cessation dates in the Kenyan highlands. *Agricultural and Forest Meteorology*, *188*, 24–32. https://doi.org/10.1016/j.agrformet.2013.12.011

Ngigi, S. N., Savenije, H. H. G., Rockström, J., & Gachene, C. K. (2005). Hydro-economic evaluation of rainwater harvesting and management technologies: Farmers' investment options and risks in semi-arid Laikipia district of Kenya. *Physics and Chemistry of the Earth*, *30*(11-16 SPEC. ISS.), 772–782. https://doi.org/10.1016/j.pce.2005.08.020

Nicholson, S. E. (2000). The nature of rainfall variability over Africa on time scales of decades to millenia. *Global and Planetary Change*, *26*(1–3), 137–158. https://doi.org/10.1016/S0921-8181(00)00040-0

Nicholson, S. E. (2017). Climate and climatic variability of rainfall over eastern Africa. *Reviews of Geophysics*, *55*(3), 590–635. https://doi.org/10.1002/2016RG000544

Nikulin, G., Jones, C., Giorgi, F., Asrar, G., Büchner, M., Cerezo-Mota, R., Christensen, O. B., Déqué, M., Fernandez, J., Hänsler, A., van Meijgaard, E., Samuelsson, P., Sylla, M. B., & Sushama, L. (2012). Precipitation climatology in an ensemble of CORDEX-Africa regional climate simulations. *Journal of Climate*, *25*(18), 6057–6078. https://doi.org/10.1175/JCLI-D-11-00375.1

Ntwali, D., Ogwang, B. A., & Ongoma, V. (2016). The Impacts of Topography on Spatial and Temporal Rainfall Distribution over Rwanda Based on WRF Model. *Atmospheric and*

Climate Sciences, *06*(02), 145–157. https://doi.org/10.4236/acs.2016.62013

Nyakwada, W., Ogallo, L. A., & Okoola, R. E. (2009). The Atlantic-Indian Ocean Dipole and Its Influence on East African Seasonal Rainfall. *Journal of Meteorology and Related Sciences*, *3*(October), 21–35.

Odekunle, T. O., Balogun, E. E., & Ogunkoya, O. O. (2005). On the prediction of rainfall onset and retreat dates in Nigeria. *Theoretical and Applied Climatology*, *81*(1–2), 101–112. https://doi.org/10.1007/s00704-004-0108-x

Odenkunle, T. O. (2004). Rainfall and the length of the growing season in Nigeria. *International Journal of Climatology*, *24*(4), 467–479. https://doi.org/10.1002/joc.1012

Oettli, P., & Camberlin, P. (2005). Influence of topography on monthly rainfall distribution over East Africa. *Climate Research*, *28*(3), 199–212. https://doi.org/10.3354/cr028199

Ogega, O. M., Koske, J., Kung'u, J. B., Scoccimarro, E., Endris, H. S., & Mistry, M. N. (2020). Heavy precipitation events over East Africa in a changing climate: results from CORDEX RCMs. *Climate Dynamics*, *55*(3–4), 993–1009. https://doi.org/10.1007/s00382-020-05309-z

Ogwang, B. A., Chen, H., Li, X., & Gao, C. (2014). The influence of topography on East African October to December climate: Sensitivity experiments with RegCM4. *Advances in Meteorology*, *2014*. https://doi.org/10.1155/2014/143917

Ogwang, B. A., Chen, H., Li, X., Gao, C., Prof, T., & Author, C. (2014). *The influence of Topography on East African October to December climate : Sensitivity experiments with RegCM4*. *2014*, 1–27. https://doi.org/doi.org/10.1155/2014/143917

Owiti, Z. (2008). *Linkages between the Indian Ocean Dipole and East African Seasonal Rainfall Anomalies National Council for Science and Technology IGAD Climate Prediction and Applications Centre*. *2*(April), 3–17.

Palmer, P. I. ., Wainwright, C. M., Dong, B., Maidment, R. I., Wheeler, K. G., Gedney, N., Hickman, J. E., Madani, N., Folwell, S. S., Abdo, G., Allan, R. P., Black, E. C. L., Feng, L., Gudoshava, M., Haines, K., Huntingford, C., Kilavi, M., Lunt, M. F., Shaaban, A., & Turner, A. G. (2023). Drivers and impacts of Eastern African rainfall variability. *Nature Reviews Earth and Environment*, *4*(4), 254–270. https://doi.org/10.1038/s43017-023-00397-x

Posthumus, H., Morris, J., Hess, T. M., Neville, D., Phillips, E., & Baylis, A. (2009). Impacts of the summer 2007 floods on agriculture in England. *Journal of Flood Risk Management*, *2*(3), 182–189. https://doi.org/10.1111/j.1753-318X.2009.01031.x

Ramirez-villegas, J., Andrew, J., Dunning, C. M., Allan, R. P., & Black, E. (2017). *Identification of deficiencies in seasonal rainfall simulated by CMIP5 climate models OPEN ACCESS Identification of deficiencies in seasonal rainfall simulated by CMIP5 climate models*.

Rusanganwa, F., Zhang, L., Kazora, J., Sebaziga, J. N., & Ekwacu, S. (2024). Correlation of Rainfall Anomalies in Rwanda from September to December (SOND) with Indian Ocean Dipole (IOD) and El Nino Southern Oscillation (ENSO) Events. *Journal of Geoscience and Environment Protection*, *12*, 115–134. https://doi.org/10.4236/gep.2024.126008

Safari, B. (2012). Trend Analysis of the Mean Annual Temperature in Rwanda during the Last Fifty Two Years. *Journal of Environmental Protection*, *03*(06), 538–551. https://doi.org/10.4236/jep.2012.36065

Safari, B., & Sebaziga, J. N. (2023). Trends and Variability in Temperature and Related Extreme Indices in Rwanda during the Past Four Decades. *Atmosphere*, *14*(9), 1449. https://doi.org/10.3390/atmos14091449

Safari, K. A., Safari, B., Gasore, J., Kipkoech Mutai, B., & Ndakize Sebaziga, J. (2024). Assessing the impact of Land Use Land Cover changes on land surface temperature over Kigali, Rwanda in the past three decades. *Environmental and Sustainability Indicators*, *23*(August). https://doi.org/10.1016/j.indic.2024.100452

Sarr, M. A., Gachon, P., Seidou, O., Bryant, C. R., Ndione, J. A., & Comby, J. (2015). Inconsistent linear trends in Senegalese rainfall indices from 1950 to 2007. *Hydrological Sciences Journal*, *60*(9), 1538–1549. https://doi.org/10.1080/02626667.2014.926364

Scott, D., & Lemieux, C. (2010). Weather and climate information for tourism. *Procedia Environmental Sciences*, *1*(1), 146–183. https://doi.org/10.1016/j.proenv.2010.09.011

Sebaziga, N. J., Safari, B., Ngaina, N. J., Ntwali, D., Mutai, B. K., Safari, A., & Rwema,Michel. (2022). Rainfall variability and trends over Rwanda. *Journal of Climate Change and Sustainability*, *4*(1), 26–34. https://doi.org/10.20987/jccs.04.06.2022

Siebert, A., Dinku, T., Vuguziga, F., Twahirwa, A., & Kagabo, D. M. (2019). Evaluation of ENACTS-Rwanda : A new multi-decade , high- resolution rainfall and temperature data set — Climatology. *International Journal of Climatology*, *January*, 1–17. https://doi.org/10.1002/joc.6010

Siebert, A., Dinku, T., Vuguziga, F., Twahirwa, A., Kagabo, D. M., delCorral, J., & Robertson, A. W. (2019). Evaluation of ENACTS-Rwanda: A new multi-decade, high-resolution rainfall

and temperature data set—Climatology. *International Journal of Climatology*, *39*(6), 3104–3120. https://doi.org/10.1002/joc.6010

Sifer, K., Desta, F. Y., Kassa, A. K., & Quarshi, S. (2016). *Wet and dry spell analysis for decision making in agricultural water management in the eastern part of Ethiopia , West Haraghe*. *August*. https://doi.org/10.5897/IJWREE2016.0650

Sillmann, J., Kharin, V. V., Zhang, X., Zwiers, F. W., & Bronaugh, D. (2013). Climate extremes indices in the CMIP5 multimodel ensemble: Part 1. Model evaluation in the present climate. *Journal of Geophysical Research Atmospheres*, *118*(4), 1716–1733. https://doi.org/10.1002/jgrd.50203

Sillmann, J., Kharin, V. V., Zwiers, F. W., Zhang, X., & Bronaugh, D. (2013). Climate extremes indices in the CMIP5 multimodel ensemble: Part 2. Future climate projections. *Journal of Geophysical Research Atmospheres*, *118*(6), 2473–2493. https://doi.org/10.1002/jgrd.50188

Sultan, B., & Janicot, S. (2003). The West African monsoon dynamics. Part II: The "preonset" and "onset" of the summer monsoon. *Journal of Climate*, *16*(21), 3407–3427. https://doi.org/10.1175/1520-0442(2003)016<3407:TWAMDP>2.0.CO;2

Tank, A. M. G. K., Zwiers, F. W., & Zhang, X. (2009). Guidelines on analysis of extremes in a changing climate in support of informed decisions for adaptation. *Climate Data and Monitoring Rep.WCDMP 72, WMO-TD 1500, 72*, 56.

Taye, M., Zewdu, F., & Ayalew, D. (2013). Characterizing the Climate System of Western Amhara , Ethiopia : A GIS Approach. *American Journal of Research Communication*, *1*(10), 319–355.

Trzaska, S., & Schnarr, E. (2014). A review of downscaling methods for climate change projections. *United States Agency for International Development by Tetra Tech ARD*, *September*, 1–42.

Umutoni, M. A., Japheth, L. P., Lipiki, E. J., Kebacho, L. L., Limbu, P. T. S., & Makula, E. K. (2021). Investigation of the 2016 March to May extreme rainfall over Rwanda. *Natural Hazards*, *108*(1), 607–618. https://doi.org/10.1007/s11069-021-04697-7

Uwimbabazi, J., Jing, Y., Iyakaremye, V., Ullah, I., & Ayugi, B. (2022). Observed Changes in Meteorological Drought Events during 1981–2020 over Rwanda, East Africa. *Sustainability (Switzerland)*, *14*(3). https://doi.org/10.3390/su14031519

Worku, G., Teferi, E., Bantider, A., Dile, Y. T., & Taye, M. T. (2018). Evaluation of regional

climate models performance in simulating rainfall climatology of Jemma sub-basin, Upper Blue Nile Basin, Ethiopia. *Dynamics of Atmospheres and Oceans*, *83*(June), 53–63. https://doi.org/10.1016/j.dynatmoce.2018.06.002

Zhang, X., Aguilar, E., Sensoy, S., Melkonyan, H., Tagiyeva, U., Ahmed, N., Kutaladze, N., Rahimzadeh, F., Taghipour, A., Hantosh, T. H., Albert, P., Semawi, M., Karam Ali, M., Said Al-Shabibi, M. H., Al-Oulan, Z., Zatari, T., Khelet, I. A. D., Hamoud, S., Sagir, R., … Wallis, T. (2005). Trends in Middle East climate extreme indices from 1950 to 2003. *Journal of Geophysical Research Atmospheres*, *110*(22), 1–12. https://doi.org/10.1029/2005JD006181

Chapter 2 Evaluation of CORDEX-CORE regional climate models in simulating rainfall variability in Rwanda

This Chapter reproduces the content of our published paper (https://doi.org/10.1002/joc.7891).

2.1 Introduction

Studies at fine spatial scales are needed to resolve local climate change hot spots within regions (Lobell et al., 2008) and form the basis of a community-led solution that is ideal for smallholder farmers (Ngigi et al., 2005) where downscaling is used to derive finer-resolution information from coarser-scale global climate model (GCM) output (Trzaska and Schnarr, 2014). Other published literature suggests that climate change in Africa will have variable impacts on crops, with both production losses and gains possible (Jarvis et al., 2012). Projected warming and drying may result in a 20% loss in crop yields over Africa in 2050 (Jones and Thornton, 2003). The Fourth Assessment Report of the Intergovernmental Panel on Climate Change (IPCC AR4) predicts that climate change is likely to have a significant effect adverse on agricultural production in many African countries (Boko et al., 2007). The Fifth Assessment Report of the Intergovernmental Panel on Climate Change (IPCC AR5) highlights that there is significant uncertainty about the Sahel though most model projections for the Sahel are slightly towards wetting conditions, while a likely increase in rainfall was observed over parts of central and eastern Africa (Niang et al., 2014). Over East Africa, there is an apparent climate paradox between the recently observed drying trend and model projected increase in rainfall. There is considerable interannual variability in East Africa and uncertainty regarding future precipitation trends in the region (Lyon and Vigaud, 2017). Users of climate information including decision and policymakers rely on the projections of climate change impacts in their decision making (Kim et al., 2014). However, assessing the ability of the regional climate models (RCMs) to simulate the present climate is a key step before their outputs are used for generating the future downscaled projections of the climate of a given region (Endris et al., 2013). The evaluations of the RCMs consist of comparing the generated model outputs with a reference observed data (Endris et al., 2013; Kim et al., 2014). RCMs provide the advantage of high spatial resolution and dynamical downscaling of GCM data (Guo et al., 2018). Given the high computational cost of dynamical downscaling, many collaborative projects are generat- ing dynamically downscaled climate simulations from model intercomparisons and for impact

assessment appli- cations. These projects include the Coordinated Regional Climate Downscaling Experiment (CORDEX) which produces dynamical downscaled climate simulations and archives outputs from a set of RCMs over different regions in the world (Giorgi et al., 2009; Glotter et al., 2014; Mariotti et al., 2014; Giorgi and Gutowski, 2015).

During the last decade, a number of studies have been developed over the African region using the CORDEX RCMs with a spatial resolution of 50 × 50 km (0.44◦). The first study was developed by Nikulin et al. (2012). An ensemble of 10 different RCMs forced by lateral and surface boundary conditions from the European Centre for Medium-Range Weather Forecasts (ECMWF) Interim Re-Analysis (ERA-Interim) was utilized to simulate rainfall over Africa. Model performance was analysed by comparing RCM outputs at different timescales with combinations of observational precipitation data-sets: satellite-based datasets from the Tropical Rainfall Measuring Mission (TRMM-3B42) and the Climate Prediction Center Morphing Technique (CMORPH); satellite-gauge combination datasets from Global Precipitation Climatology Project (GPCP), three gauge-based datasets from the University of Delaware (UDEL), the Climatic Research Unit (CRU) and the Global Precipitation Climatology Centre (GPCC). It was demonstrated that all RCMs simulate the seasonal mean and annual cycle quite accurately, although individual models could exhibit significant biases in some subregions and seasons. A common problem found in the majority of the RCMs was that precipitation starts too early during the diurnal cycle. Generally, the multimodel average was found to outperform any individual RCM simulation, showing biases of similar magnitude to differences across a number of observational datasets.

Other studies focusing on eastern and southern Africa regions have followed. Endris et al. (2013) analysed the performance of the 10 CORDEX RCMs driven by ERA- Interim in simulating eastern African rainfall. Model outputs were compared with gauge-based gridded observational datasets obtained from the GPCC, CRU and GPCP. It was found that most RCMs reasonably simulate the main features of the rainfall climatology over East Africa and also reproduce the majority of regional responses to El Niño-Southern Oscillation (ENSO) and Indian Ocean Dipole (IOD) climate modes. However, significant biases in individual models were observed depending on the sub-region and season. The multimodel ensemble was found to adequately well simulate eastern African rainfall and could therefore be used for the assessment of future climate projections for the region. It is worth noting that rainfall in the eastern African climate is primarily controlled by the seasonal migration of the Inter-tropical Convergence Zone (ITCZ)

of trade winds (Nicholson, 2000). The main drivers of the rainfall interannual variability in East Africa are ENSO and IOD climate modes associated with sea surface temperature (SST) anomalies across the tropical Pacific and Indian Oceans, respectively (Ogallo, 1988; Ogallo et al., 1988; Nicholson and Etekhabi, 1986; Nicholson and Nyenzi, 1990; Simon and Lisa, 2001; Goddard and Mason, 2002; Lyon and DeWitt, 2012), with a significant impact on agriculture and severe consequences on food and social security. Canonically, during the warm phase of ENSO, much of the East Africa region tends to experience wetter than normal conditions because there is typically a teleconnection pattern in the Indian Ocean that enhances convection in the Western Indian Ocean basin (Goddard and Graham, 1999; Black, 2005; Ummenhofer et al., 2009). While this teleconnection pattern is often associated with El Niño events in the Pacific basin, the pattern of sea surface temperature and convection in the Indian Ocean can also act semi-independently, and it is possible to have a warm or positive phase of the IOD (with a similar effect), independent of the ENSO state (Saji et al., 1999). In their study on rainfall over predefined regions in southern Africa, Shongwe et al. (2014) assessed the ability of the 10 CORDEX RCMs driven by the ERA- Interim in capturing monthly rainfall evolution, selected rainfall characteristics and the observed rainfall probability density functions. The ERA-Interim was used as the reference dataset and was completed by GPCP to reduce uncertainties. It was indicated that a majority of the RCMs adequately capture the reference rainfall characteristics and rainfall probability density functions, with a few showing a bias towards excessive light rainfall events. Endris et al. (2016) assessed the ability of two CORDEX RCMs with lateral and surface boundary conditions derived from coupled global climate models (CGCMs), to simulate the teleconnections between tropical sea surface temperatures and rainfall over eastern Africa, and the associated changes in atmospheric circulation patterns over the region. CGCM-driven RCM outputs were compared with ERA-Interim driven RCM outputs. Results from the driving CGCMs were also analysed. The study indicated that the RCMs driven by ERA-Interim (quasi-perfect boundary conditions) successfully capture rainfall teleconnections in most examined regions and seasons. Further, it was shown that most of the errors in simulating the teleconnection patterns come from the driving CGCMs. Luhunga et al. (2016) evaluated the performance of four CORDEX RCMs driven by boundary conditions from three GCMs and ERA-Interim in simulating rainfall and temperature over Tanzania. Model outputs were compared to actual measurements from 22 weather stations. Results indicated that during March-April-May

(MAM) season most of RCMs underestimate the amount of rainfall while during October-November-December (OND) they overestimate. They were found to adequately reproduce the annual cycle of rainfall, the mean climate, the interannual variability and temperature trends. It was recommended the potential use of CORDEX RCMs in simulating rainfall, maxi- mum air temperature and minimum air temperature over Tanzania. Further studies analysing the source of uncertainties were suggested when the same RCM is driven by different GCMs and/or when different RCMs are driven by a same GCM in simulating rainfall and temperature. Kisembe et al. (2018) evaluated the ability of 10 CORDEX RCMs driven by the ERA-Interim to simulate rainfall characteristics over Uganda. Model outputs were compared to two gauge-based gridded datasets (GPCC and CRU) and a satellite-gauge combined dataset from the Climate Hazards Group InfraRed Rainfall and stations (CHIRPS). They found that most models underestimate the annual rainfall over the country. However, the models correctly reproduced the seasonality of precipitation with some differences. The interannual variability of the dry season was well reproduced by the models but not that of the long or the short rainy season, although the ENSO and IOD signals were correctly simulated by most of the models.

In 2016, Gutowski et al. (2016) initiated a new framework, CORDEX-CORE (Coordinated Output for Regional Evaluation). This resulted in a number of studies producing high-resolution climate projections in almost all CORDEX domains (Remedio et al., 2019; Ashfaq et al., 2021; Coppola et al., 2021; Dosio et al., 2021; Giorgi et al., 2021; Gnitou et al., 2021; Sawadogo et al., 2021; Teichmann et al., 2021). Since 2019, CORDEX-CORE (AFR-22) operates for the African domain over an equa- torial domain with a quasi-uniform resolution of approximately 25 × 25 km. The advantage of using increased spatial resolution in RCMs and their potential to repro-duce the local climate in small areas with complex topography have been largely discussed in the literature (Giorgi et al., 2009; Endris et al., 2013; Colmet-Daage et al., 2018).

In a number of CORDEX studies, ECMWF-ERAINT is often used as boundary conditions for assessing the performance of RCMs to simulate observed climate data in a region. Differences observed in RCMs' outputs are due to their formulations (Giorgi et al., 2009; Giorgi and Gutowski, 2015; Sørland et al., 2021). However, for areas with limited station network and varying topography, or areas with small size where the scale of resolution is coarse enough, ECMWF-ERAINT re-analysis may have biases which in return may propagate and amplify into models. In addition, RCMs driven by GCMs to simulate climate observations in a region may be subject to

uncertainties caused by differences in configurations (physics, parameterizations, boundary conditions, numerical schemes) of either RCMs or GCMs or both (Endris et al., 2016; Wu et al., 2020). Studies comparing CORDEX-CORE RCMs driven by GCMs and ECMWF-ERAINT are important in this regard.

This study aims to assess three RCMs, namely CCLM5-0-15, RegCM4-7 and REMO2015, from CORDEX-CORE (AFR-22), in their ability to reproduce rainfall variability in Rwanda for the period 1981–2005. They are forced by boundary conditions from three different global climate models (GCMs), namely MPI-M-MPI- ESM-LR, NCC-NorESM1-M and MOHC-HadGEM2-ES, and the European Centre for Medium-Range Weather Forecasts Reanalysis (ECMWF-ERAINT). Model simulations of daily rainfall displayed on a grid of spatial resolution of 0.22◦ (~25 km) are compared with gridded observational datasets at 0.0375◦ by 0.0375◦ (~4 km) spatial resolution over Rwanda obtained from Rwanda Meteorology Agency for the period 1981–2005. A set of metrics are employed to quantify simulated rainfall pattern discrepancies and deviations from observations.

The study is organized as follows: a brief description of the study area is presented in section 2 followed by section 3 where an explanation of data used from observational and modelled datasets is given (section 3.1) and details on the method employed are given (section 3.2). In section 4, results are presented and discussed. They include spatial distribution of mean climatological seasonal rainfall and bias (section 4.1), spatial correlations (section 4.2), annual cycle (section 4.3), normalized root-mean-square error (section 4.4), trends (section 4.5), Taylor diagrams (section 4.6), inter-annual variability (section 4.7), relation with ENSO and IOD (section 4.8). A conclusion highlighting the results of the study is presented at the end of section 5.

2.2 Study Area

Rwanda is a landlocked country located in central and eastern Africa, bordered by the Democratic Republic of Congo (DRC) to the west, Uganda to the north, Tanzania to the east, and Burundi to the South. Rwanda covers an area of 26,338 km2 and lies between 1◦40 and 2◦510 south, and 28◦530 and 30◦530 east (Figure 2.1). Because of its high altitude, the country has a pleasing moderate and tropical climate. Air temperature in Rwanda varies throughout the year with two maxima and two minima. The two maxima of air temperature occur, respectively, in February and August, while the two minima occur, respectively, in June and in November. The average

temperature for Rwanda is around 20◦C and varies with the topography. The warmest annual average temperatures are found in the eastern plateau (20–21◦C) and the Rusizi valley located in the south-west near the borders with Burundi and Democratic Republic of Congo (23–24◦C), and cooler temperatures are found in higher elevations of the central plateau (17.5–19◦C) and western highlands (<17◦C) (Safari, 2012). Annual rainfall varies across the country due to the complex topography (Ntwali et al., 2016). The highest annual rainfall totals are observed in the belt laying along the Congo-Nile divide from the southwestern high elevations of the Nyungwe National Park to the northwestern volcanic mountainous chain of Virunga (>1,200 mm) and then diminishes towards the eastern plateau (<900 mm). The rainfall climatology of Rwanda exhibits a seasonal bimodality in a year associated with the north–south oscillating migration of the Inter-Tropical Convergence Zone (ITCZ) of trade winds (Siebert et al., 2019). The period of March, April and May corresponds to the long rainy season when the ITCZ moves to the north and the period of October, November and December to the short rainy season when the ITCZ returns to the south. A short dry season occurs from January to February and a long dry season from June to September.

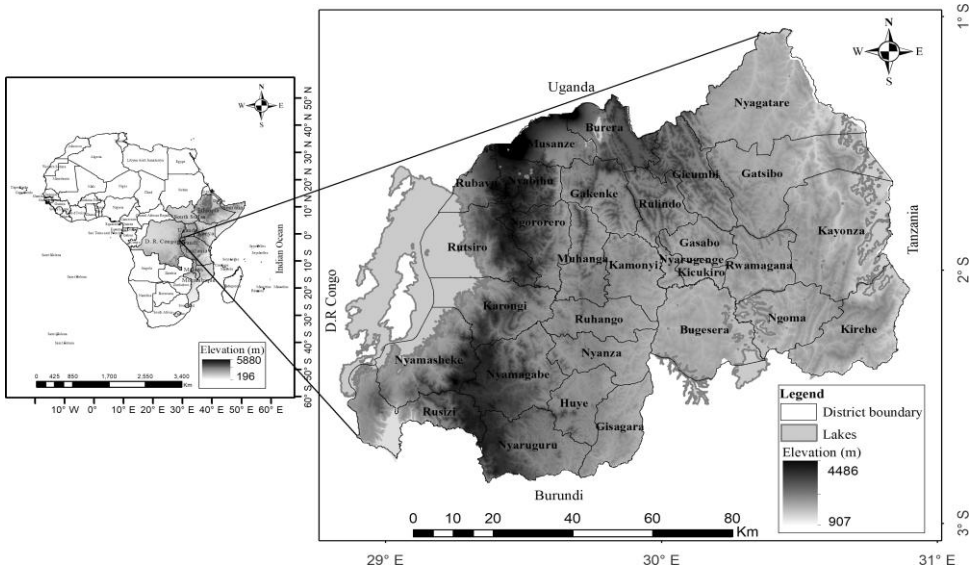

Figure 2. 1: Elevation map of Rwanda showing the locations of districts

During the last years, Rwanda has experienced frequent heavy rainfall causing devastating floods and landslides in the west and north, and episodic droughts in the east. Major floods occurred in 1997, 2001, 2006, 2007, 2008, 2009, 2011, 2012, 2013, 2016 and 2019 and these had major impacts on agriculture, livelihood and especially the economy of the country (David et al., 2011; Muhire et al., 2014; Uwihirwe et al., 2020). As mentioned above, the key factors that influence the

rainfall variability in east African region, where Rwanda is located, include ENSO and IOD. Their influence is modulated by regional circulation systems, topography and large inland water bodies (Thiery et al., 2015). At present, there is no documented study done on the nature of rainfall variability in Rwanda and the underlying causes. A thoroughly analysis of the impact of ENSO and IOD events as well as other climatic factors (variability of global, regional and local atmospheric circulation, ITCZ variability, subtropical cyclones, African Jet Stream, etc.) which may have an impact on rainfall variability in Rwanda is indeed needed. High-resolution simulations are advantageous in studying the climate of Rwanda because of its size and topographic complexity. CORDEX-CORE (AFR-22) RCMs are so far promising tools for researching climate in Rwanda.

2.3 Data and Method

2.3.1 Data

2.3.1.1 Observed data

Historical data from station observations are inadequate on many parts of the world due to sparse or nonexistent observation networks, or limited reporting of recorded observations (Dinku et al., 2018). Rwanda had a large number of active meteorological stations prior to the mid-1990s. However, the number of active stations greatly reduced from around the time of the Genocide Against Tutsi in Rwanda in 1994 and remained very low until about 2010 (Siebert et al., 2019). The Rwanda Mete- orology Agency through the Enhancing National Climate Services (ENACTS) initiative (Dinku et al., 2014; 2017) reconstructed rainfall data by combining station data with bias-adjusted satellite rainfall estimates, and with reanalysis products for the temperature to address temporal and spatial gaps in rainfall and temperature observations in Rwanda (Siebert et al., 2019). Currently, rainfall and temperature data from Rwanda Meteorology Agency are displayed on a grid of spatial resolution of 0.375◦ (~4 km) for the period from 1981 to present for rainfall and 1983 to present for temperature. The datasets collected from Rwanda Meteorology Agency in this study are daily rainfall for the period of 1981 to 2005.

2.3.1.2 CORDEX-CORE (AFR-22) RCMs data

In this study, datasets are obtained from the three regional climate models (RCMs), CCLM5-0-15 (Sørland et al., 2021), RegCM4-7 (Giorgi et al., 2012; 2021; Coppola et al., 2021) and REMO

(Jacob et al., 2012; Remedio et al., 2019) from CORDEX-CORE (AFR-22) forced each by three different global climate models (GCMs), namely MPI-M-MPI-ESM-LR (Giorgetta et al., 2013; Stevens et al., 2013), NCC-NorESM1-M (Bentsen et al., 2013; Iversen et al., 2013), MOHC-HadGEM2-ES and ERA- Interim (Dee et al., 2011), and the European Centre for Medium-Range Weather Forecasts Reanalysis (ECMWF- ERAINT) (Dee et al., 2011). Available CORDEX-CORE (AFR 22) RCM historical dynamically downscaled simu- lations data are for the period 1950–2005, 1970-2005 and 1970–2005 for, respectively, CCLM5-0-15, RegCM4-7 and REMO2015 (https://cordex.org/experiment-guidelines/cordex-core/). Simulations of daily rainfall over Rwanda used in this study are for the same common period from 1981 to 2005 as the observations, are displayed on a grid of spatial resolution of 0.22◦ (~25 km) for evaluation of models' performance. Table 2.1 presents the list of RCMs and driving GCMs/ECMWF-ERAINT used and information on the institutions they belong to as well their descriptions (dynamics, numerical discretization schemes and physical parameterization) and references. The ensemble mean of an RCM driven by different GCMs and the multimodel ensemble mean of different RCM driven by same GCM used in this study are named as follows: CCLM5-0-15_ensemble, RegCM4-7_ensemble and REMO2015_ensemble are, respectively, the ensemble means of CCLM5-0-15, RegCM4-7 and REMO2015 driven by the three GCMs; Mul- timodel ensemble_MPI-M-MPI-ESM-LR, Multimodel ensemble_NCC-NorESM1-M, Multimodel ensemble_NCC-NorESM1-M, Multimodel ensemble_MOHC-HadGEM2.ES and Multimodel ensemble_ECMWF-ERAINT are the multimodel ensemble means of the three RCMs driven, respectively, by MPI-M-MPI-ESM-LR, NCC-NorESM1-M, MOHC-HadGEM2.ES and ECMWF-ERAINT.

Table 2. 1 Information on CORDEX-CORE (AFR-22) RCMs and the driving GCMs/ECMWF-ERAINT used in the study

Information	**AFR-22 CCLM5-0-15**	**RegCM4-7**	**REMO2015**
Institution	Karlsruhe Institute of Technology (KIT), Karlsruhe, Germany in collaboration with the CLM-	Abdus Salam International Centre for Theoretical Physics, Trieste, Italy (ICTP).	Climate Service Center Germany (GERICS), Helmholtz-Zentrum Hereon, Hamburg, Germany

	Community (CLMcom-KIT).		
Horizontal resolution	Horizontal grid spacing of 0.22°x 0.22° (approximately 25x25 km^2) (AFR-22).	Horizontal grid spacing of 0.22°x 0.22° (approximately 25x25 km^2) (AFR-22)	Horizontal grid spacing of 0.22°x 0.22° (approximately 25x25 km^2) (AFR-22)
Projection resolution	Rotated pole 0.22^0.	Rotated Mercator 0.22^0	Rotated pole 0.22^0
Vertical coordinate/levels	Terrain-following height coordinate with 51 levels.	Hybrid sigma-pressure coordinate system with 23 levels.	Hybrid sigma-pressure coordinate system with 27 levels.
Numerical temporal and horizontal discretization	Runge-Kutta time stepping scheme (Wicker and Skamarock, 2002) on a three dimensional Arakawa-C grid (Arakawa and Lamb, 1977).	Numerical discretization described by Grell *et al*. (1994).	Second order finite differences on staggered C-grid Leap-frog with semi-implicit correction and Asselin filter, semi-Lagrangian advection (Robert, 1966; Asselin, 1972).
Time step (s)	120s		120 s
Dynamic framework	Non-hydrostatic for applications from the meso-β to meso-γ scales (Steppeler *et al*., 2003; Doms and Baldauf, 2013; Doms *et al*.,2013).	Hydrostatic dynamical core based on multiple choices of different physics parameterizations (Grell *et al*., 1994; Giorgi *et al*., 2012).	Hydrostatic (Roeckner et. al., 1996; Jacob et al., 2012) based on the dynamics of the German Weather Service weather prediction model

			(Europa Model) and the physics of the ECHAM 4.5 GCM.
Convective scheme	Tiedtke parameterization for convection (Tiedtke, 1989).	Modified-Kuo scheme (Anthes, 1977) Grell scheme (Grell, 1993) with two closure assumptions: Arakawa and Schubert closure (Grell *et al*. (1994), Fritsch and Chappell closure (Fritsch and Chappell, 1980) MIT-Emanuel scheme (Emanuel, 1991; Emanuel and Zivkovic-Rothman, 1999)	Tiedtke parameterization for convection (Tiedtke, 1989) with modifications after Nordeng (1994) and Pfeifer (2006).
Radiation scheme	Ritter and Geleyn (1992).	CCM radiation scheme, NCAR CCM3 (Kiehl *et al*.,1998)	Radiation scheme after Morcrette *et al*. (1986) and Giorgetta and Wild (1995)
Cloud microphysics scheme	Parameterization of precipitation based on four-category scheme that includes cloud water, rain water, snow, and ice	From the European Centre for Medium Weather Forecast's Integrated Forecast System (IFS) (Tiedtke, 1993; Tompkins *et al*.,	Cloud microphysics scheme by Lohmann and Roeckner (1996)

	microphysics Doms *et al*. (2013).	2007; Nogherotto *et al*., 2016)	
Description	**CCLM5-0-15**	**RegCM4-7**	**REMO2015**
Planetary Boundary Layer (PBL) Scheme	Turbulent kinetic energy-based surface transfer and and PBL parameterization (Raschendorfer, 2001).	Holtslag planetary boundary layer scheme (Holtslag *et al*., 1990; Holtslag and Boville, 1993) Coupled by the University of Washington turbulence closure model (Grenier and Bretherton, 2001; Bretherton *et al*., 2004).	Turbulent kinetic energy-based surface transfer and PBL parameterization (Louis, 1979).
Aerosols	Aerosol climatology from Tegen *et al*. 1997).	Chemistry Model. Dust emission parameterizations by Laurent *et al*. (2008) and Alfaro and Gomes (2001).	Aerosols climatology from Pietikäinen *et al*. (2012) based on Tanre *et al*.((1984).

Land surface scheme	TERRA model (Schrodin and Heise, 2001; Schulz *et al*., 2016) Parameterization of Convection (Bechtold *et al*., 2008) ǂ Land-surface models (VEG3D or the Community Land Model (Will *et al*., 2017).	Biosphere- Atmosphere Transfer Scheme-BATS (Dickinson *et al*., 1993; Giorgi *et al*., 2003) The Community Land Model version CLM of NCAR (Oleson *et al*., 2004; Oleson *et al*., 2008, Collins *et al*., 2006).	Based on the surface runoff scheme by Hagemann (2002) and vegetation phenology by (Rechid *et al*., 2009).
Recent reference (s)	Sørland *et al*. (2021)	Giorgi *et al.* (2012) Coppola *et al.* (2021) Giorgi *et al.* (2021)	Jacob *et al*. (2012) Remedio *et al*. (2019) Giorgi *et al*. (2021)
Driving GCM/ Reanalysis/Reference	**Name of RCM driven by GCM/Reanalysis output**		
MPI-M-MPI-ESM-LR Stevens *et al*. (2013) Giorgetta *et al*. (2013)	CCLM5-0-15_MPI-M-MPI-ESM-LR	RegCM4-7_MPI-M-MPI-ESM-LR	REMO2015_MPI-M-MPI-ESM-LR
NCC-NorESM1-M Iversen *et al.* (2013) Bentsen *et al*. (2013)	CCLM5-0-15_NCC-NorESM1-M	RegCM4-7_NCC-NorESM1-M	REMO2015_NCC-NorESM1-M
MOHC-HadGEM2-ES Jones *et al*. (2011)	CCLM5-0-15_MOHC-HadGEM2-ES	RegCM4-7_MOHC-HadGEM2-ES	REMO2015_MOHC-HadGEM2-ES
ECMWF-ERAINT Dee et. al (2011) Hersbach et. al (2020)	CCLM5-0-15_ECMWF-ERAINT	RegCM4-7_ECMWF-ERAINT	REMO2015_ECMWF-ERAINT

Simulation period	1981-2005	1981-2005	1981-2005

2.3.2 Method

2.3.2.1 Interpolation of observed datasets to CORDEX-CORE (AFR-22)

Before using RCMs for climate change studies, it is essential to evaluate their ability of reproducing the observed present climate (Giorgi et al., 2009). Evaluations of RCMs' ability to reproduce climate change projections is gener- ally done, on one side, by interpolating simulated gridded climate variables to the location of weather stations and compare the results with observed station data (Ly et al., 2013; Luhunga et al., 2016). The technique often used is the Inverse Distance Weighted Average interpola- tion method (Hartkamp et al., 1999; Jones, 1999; Ly et al., 2013; Luhunga et al., 2016). RCMs can also be evalu- ated by comparing gridded simulated fields, against gridded datasets of observations. The latest method requires remapping the fields on a common grid (Diaconescu et al., 2015). For remapping on grids with a similar spatial resolution, the bilinear interpolation method (Nikulin et al., 2012; Endris et al., 2013; Kalogno- mou et al., 2013; Gbobaniyi et al., 2014) and the distance- weighted-average interpolation method are commonly used in literature (Eum et al., 2011). The observed datasets from Rwanda Meteorology Agency are displayed on a spa- tial grid of high resolution of 0.0375◦ (∼4 km) much finer than the 0.224◦ (25 km) CORDEX-CORE (AFR-22) grid. For comparison, they are remapped on the same CORDEX-CORE (AFR-22) grid by a bilinear interpolation with the first-order conservative remapping method, using Climate Data Operators (https://code.zmaw.de/projects/ cdo/wiki/Cdo). This interpolation method has been used in other previous CORDEX studies (Nikulin et al., 2012; Kalognomou et al., 2013; Diaconescu et al., 2015).

2.3.2.2 Comparison of observed data to CORDEX-CORE (AFR-22) data

Several techniques have been used in literature for the evaluation of RCMs simulations (Flato et al., 2013; Kim et al., 2014; Dosio et al., 2015). In this study, spatial plots of CORDEX-CORE (AFR-22) RCMs simulated MSR climatology, observed fields and their biases over Rwanda are analysed to assess the overall similarity of the pat- terns and the spatial distribution of the biases. Bias is given by the difference between the CORDEX-CORE (AFR-22) RCM simulated and

observed climatological MSR fields. This bias assessment indicates where the model overestimates (positive/wet bias) or underestimates (negative/dry bias) the observations. Time series of spatially averaged observed and simulated MSR are computed for comparison. After being insured that the series are homogeneous and normal distributed, a Student's t test is carried out at the 5% significance level between series obtained from observations and that obtained from each RCM. The null hypothesis (Ho) is that there is a no significant difference ($p > .05$) between the means of simulated and observed datasets, whereas the alternative hypothesis (Ha) is that there is a significant difference between the two means ($p < .05$). Rainfall annual cycle, interannual variability and trend of MSR rainfall are computed for both observed and simulated data to determine how well the RCMs capture rainfall seasonality in Rwanda. Different metrics are used to test the performance of each CORDEX-CORE (AFR-22) RCM's simulation. They include the mean, variance, standard deviation, standard error, bias, t test, normalized root mean-square error (NRMSE), the Pearson correlation coefficient (r), the Mann–Kendall test for trend analysis (Sneyers, 1990), Theil–Sen's slope estimator (Sen, 1968) and Taylor diagram (Taylor, 2001). They are explained in Data S1, Supporting Information. To assess the performance of the CORDEX-CORE (AFR-22) RCMs in simulating the interannual variability of the mean seasonal rainfall spatial pattern, the spatial variability of Pearson's correlations between observed and simulated MSR anomaly time series are analysed. Time series of standardized anomalies (indices) of spatially averaged observed and simulated MSR over Rwanda are as well analysed for MAM and OND.

2.3.2.3 Relations with ENSO and IOD

In this study, the relations between observed and simulated rainfall and ENSO and IOD are investigated using SST anomalies (indices) over the Pacific Ocean (Trenberth, 1997; Trenberth and Stepaniak, 2001) and over the Indian Ocean (Saji et al., 1999). Averages of SST over eastern tropical Pacific (0–10◦S, 90◦–80◦W) and over equatorial Pacific (5◦N–5◦S, 170◦–120◦W) corresponding, respectively, to Niño1+2 and Niño3.4 regions are obtained from the Earth System Research Laboratory of the National Atmospheric and Oceanic Administration (Huang et al., 2017). El Niño and La Niña phases (warm and cold episodes, respectively) are quantified using Oceanic Niño Indices (ONI) published online by the Climate Prediction Centre (CPC) of the National Oceanic and Atmospheric Administration (NOAA). A 3-month rolling correlation between ENSO and IOD sea surface temperature indices and rainfall indices from observations

and models is applied to the corresponding time series to assess the performance of individual models in reproducing the seasonal relationship between observed rainfall and ENSO and IOD.

2.4 Results and discussion

2.4.1 Spatial distribution of climatological mean seasonal rainfall and bias

Patterns of observed and simulated climatological mean seasonal rainfall (MSR) are presented in Data S2 and S3 for, respectively, MAM and OND. In general, all RCMs repro- duce reasonably well the spatial distribution of observed MSR where higher rainfall is found in the mountainous area of the Congo-Nile divide in the country's western region with decreasing rainfall in the eastern region. Patterns of biases between simulated MSR field and observed MSR field are presented in Data S4 and S5 for, respectively, MAM and OND. Overall, each RCM driven by either GCM or ECMWF-ERAINT indicate similar spatial bias patterns, but with individual model-specific features. However, the heterogeneity of spatial bias patterns creates challenges for interpretation. Therefore, time series of spatially averaged observed and simulated MSR are computed for comparison. Results from the homogeneity test and Jarque-Bera goodness-of-fit test of normality presented in Data S4a and S4b indicate that the obtained series are homogeneous and normally distributed. Figure 2. 2 presents the Box plots of observed and simulated MSR averaged over Rwanda for MAM and OND during the studied period. Table 2. 2 shows the results obtained from a paired Student's t test per- formed at the 5% significance level between the computed time series of spatially averaged observed and simulated MSR for the studied period. During MAM, all models indicate, in general, a dry bias in all parts of the country. All RCMs driven by MPI-M-MPI-ESM-LR indicate a low dry bias [0, −2 mm·day^{-1}] countrywide compared to other RCMs. All RCMs driven by both GCMs and ECMWF- ERAINT present statistically significant ($p < .05$) spatially averaged dry bias except only RegCM4-7_MPI-M-MPI-ESM-LR (0.361 ± 0.289 mm) which shows not significant ($p > 0.05$) wet bias (the first value in the bracket is the spatially average bias and the second value is the standard error for the period of study). RegCM4-7_NCC-NorESM1-M (−1.454 ± 0.194 mm·day^{-1}) presents a more pronounced wet bias in the central region extending from north to the south and relatively low wet and dry bias in the remaining part of the country; RegCM4-7_MOHC-HadGEM2-ES (−2.155± 0.298 mm·day^{-1}) and RegCM4-7_ECMWF-ERAINT (−1.636 ± 0.230 mm·day^{-1}) show a more pronounced dry bias in the central

region extending from north to the south. CCLM5-0-15_NCC- NorESM1-M (−2.437 ± 0.261 mm·day^{-1}), CCLM5-0-15_MOHC-HadGEM2-ES (−2.508 ± 0.222 mm· day^{-1}), CCLM5-0-15_ECMWF-ERAINT (−1.760 ± 0.211 mm·day^{-1}) and CCLM5-0-15_ensemble (−1.975 ± 0.196 mm·day^{-1}) indicate a more pronounced dry bias in the Congo-Nile divide region extending from the southwestern part to the northwestern part of the country. REMO2015_NCC-NorESM1-M (−3.009±0.173 mm·day^{-1}), REMO2015_MOHC-HadGEM2-ES (−2.643±0.181 mm·day^{-1}), REMO2015_ECMWF-ERAINT (−3.112±0.164 mm·day^{-1}) and REMO2015_ensemble (−2.553 ± 0.172 mm·day^{-1}) present a more pronounced dry bias in the Congo-Nile divide region extending to the central plateau and reduced along the coastal part of Lake Kivu. The multimodel ensemble means MME_NCC-NorESM1-M (−2.300±0.194 mm·day^{-1}) and MME_ECMWF-ERAINT (−2.170 ± 0.175 mm·day^{-1}) present a low-to-moderate dry bias with the larger bias values in the central plateau and the north western regions. MME_MOHC-HadGEM2-ES (−2.435 ± 0.222 mm·day^{-1}) presents high dry bias over the whole country. It should be noted that REMO2015 exhibits highest dry biases com- pared to other RCMs when all are driven by same GCM or ECMWF-ERAINT while MME_MPI-M-MPI-ESM-LR (−0.875 ± 0.191 mm·day^{-1}) show lowest dry bias country-wide. During OND, either RegCM4-7 or CCLM5-0-15 driven by any of the three GCMs and their ensemble means indicate a similar wet bias pattern countrywide with reinforced wet conditions in the highest altitude areas of the Congo-Nile divide region extending from the south- western part to the northwestern part of the country and very little wet to dry conditions in the remaining parts. REMO2015 driven by any of the three GCMs and its ensemble indicates, on the contrary, a dry bias pattern countrywide. RegCM4-7 and CCLM5-0-15 driven by ECMWF-ERAINT show a bias pattern with low wet and dry bias here. REMO2015 driven by ECMWF-ERAINT presents a dry bias pattern countrywide. The multimodel ensemble means seem to have a relatively homogeneous spatial distribution of bias (wet or dry) than individual models and their ensembles. RegCM4-7_MPI-M-MPI-ESM-LR (2.676±0.332 mm·day^{-1}), RegCM4-7_NCC-NorESM1-M (2.552±0.381 mm·day^{-1}), RegCM4-7_MOHC-HadGEM2-ES (1.024±0.215 mm·day^{-1}), RegCM4-7_ensemble (2.084±0.195 mm·day^{-1}), CCLM5-0-15_MPI-M-MPI-ESM-LR (2.401±0.403 mm·day^{-1}), CCLM5-0-15_NCC-NorESM1-M (2.133±0.321 mm·day^{-1}), CCLM5-0-15_MOHC-HadGEM2-ES (1.150±0.178 mm·day^{-1}), CCLM5-0-15_ensemble (1.810 ±0.173 mm·day^{-1}) present a statistically significant spatially averaged wet bias; CCLM5-0-15_ECMWF-ERAINT (0.172±0.224 mm·day^{-1}) and RegCM4-7_ECMWF-

ERAINT (−0.318±0.248 mm·day^{-1}) have a spatially averaged low dry bias not statistically significant; REMO2015_MPI-M-MPI-ESM-LR (−1.477±0.177 mm·day^{-1}), REMO2015_NCC-NorESM1-M (−1.524±0.157 mm·day^{-1}), REMO2015_MOHC-HadGEM2-ES (−1.150±0.179 mm·day^{-1}), REMO2015_ensemble (−1.383±0.140 mm·day^{-1}) and REMO2015_ECMWF-ERAINT (−2.256±0.155 mm·day^{-1}) present a statistically significant spatially averaged dry bias. MME_MPI-M-MPI- ESM-LR (1.200±0.199 mm·day^{-1}) and MME_NCC-NorESM1-M (1.054±0.242 mm·day^{-1}) and MME_MOHC-HadGEM2.ES (0.256±0.175 mm·day^{-1}) present statistically significant spatially averaged low wet bias, while MME_ECMWF-ERAINT (−0.801± 0.176 mm·day^{-1}) present statistically significant spatially averaged low dry bias. It is worth noting that CCLM5-0-15_MPI-M-MPI-ESM-LR, CCLM5-0-15_MOHC-HadGEM2-ES. RegCM4-7_MPI- M-MPI-ESM-LR, RegCM4-7_NCC-NorESM1-M, RegCM4-7_RECMWF-ERAINT indicate high values of the variance (>2 mm^2·day^{-1}) (Alfaro and Gomes, 2001) of the spatially averaged MSR, while REMO2015_MPI-M-MPI-ESM-LR, REMO2015_NCC-NorESM1-M, REMO2015_MOHC-HadGEM2-ES, REMO2015_ECMWF-ERAINT, and REMO2015_ensemble indicate low values of the variance (<0.5 mm^2·day^{-1}) (Alfaro and Gomes, 2001) of the spatially averaged MSR.

The homogeneity observed of the spatial distribution of low bias for the multimodel ensemble means during OND is likely due to the cancellation of opposite signed biases across the models. Similar results were reported by Nikulin et al. (2012) and Endris et al. (2013). This makes the multimodel ensemble means outperform the individual models in reproducing the spatial pattern of rainfall during OND. The poor performance of models in representing the rainfall patterns over Rwanda may be due, on one side, to the complex topography which does not make easy the reproduction of related effects by models constrained by their resolution which is still too coerce for a country of small size like Rwanda; on the other side, and importantly, to physical parameterization, timescale and numerical schemes used in the models. The western part of the country, where most of CORDEX-CORE (AFR-22) RCMs have a large magnitude of bias, is dominated by the Congo-Nile divide laying from the south to the north where land surface processes are important because of the presence of large primary forests. In addition, due to the proximity of this area to Lake Kivu, moisture influx and convective phenomena combined with uplifting motion of air due to lake-land breeze, play important role in the production of rainfall in that area during the two rainfall seasons. Studies on East Africa rainfall have linked spatial

distribution of bias in simulated rainfall to the combined effect of physical parameterization and resolution making difficult to suit- ably reproduce all the effects related to complex topography and the African Great Lakes. In their study on simulating climate variability over Lake Victoria Basin in East Africa. Anyah et al. (2006) showed that the up- slope/down-slope flow generated by the mountains east of the Lake Victoria in East Africa and the land-lake breeze circulations play important roles in influencing the intensity of Victoria basin precipitation. Ogwang et al. (2014), studying the influence of topography on East African climate using RegCM4 RCM, has shown that the mean rainfall significantly reduces over the region when topography elevation is reduced. The model showed that when topography over selected high mountains of Kenya, Tanzania and Uganda is reduced to 25%, the mean rainfall is reduced by about 19%. Analysing rainfall with 10 CORDEX RCMs in South Africa, Favre et al. (2016) found that in most models the spatial distribution of biases in annual mean rainfall appears to be linked to orography, where wet biases are quasi-systematic in regions with higher elevation with inversely neutral to dry biases particularly in the coastal fringes. In their study on rainfall over Uganda using the 10 CORDEX RCMs, Kisembe et al. (2018) indicated that most models show wet bias over the highest areas of the region such as the Rwenzori Mountains and the Lendu Plateau located along the Albertine Rift in the west and over the Elgon Mountain in the east. Ntwali et al. (2016) analysing the impact of topography on rainfall over Rwanda using Weather Research and Forecasting (WRF) model identified factors that influence rainfall in the northwestern Congo Nile divide and Virunga mountains region of Rwanda. There are some studies in literature that have shown that increased resolution compared to 25 km (Giorgi et al., 2016; Ban et al., 2021) combined with improved convection parameterization schemes (Prein et al., 2015; Coppola et al., 2020) may provide significant added value especially in high elevated areas. Further studies are therefore needed to better understand the mechanisms governing precipitation in Rwanda in order to reduce the observed gap in the reproduction of the effects relating to its complex topography.

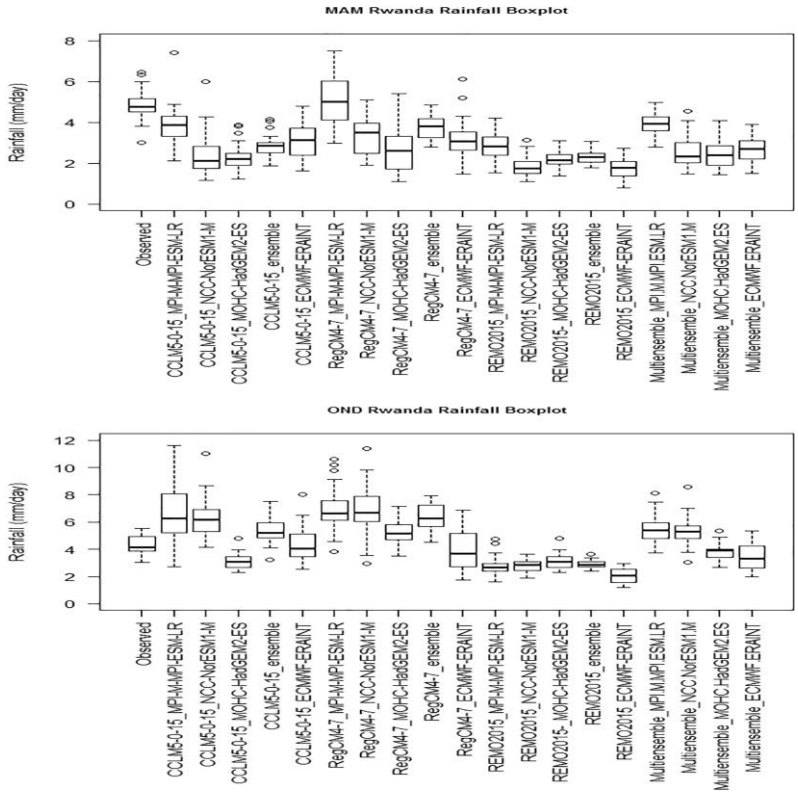

Figure 2. 2 Box plots representing the observed mean daily seasonal rainfall and simulated by different CORDEX CORE (AFR- 22) RCMs driven by different GCMs and ECMWF-ERANT, their ensembles and multi-ensembles for MAM (top) and OND (bottom) averaged over Rwanda for the period 1981–2005

Table 2. 2 Comparison between time series of observed and simulated MSR averaged over Rwanda for the period 1981–2005, during MAM and OND

MAM	X	σ2	p-value	B	SDE
Observation	5.080	0.536			
CCLM5-0-15_MPI-M-MPI-ESM-LR	4.100	1.085	0.000492	−0.980	0.261
CCLM5-0-15_NCC-NorESM1-M	2.643	1.179	9.06E-10	−2.437	0.261
CCLM5-0-15_MOHC-HadGEM2-ES	2.572	0.430	2.16E-11	−2.508	0.222
CCLM5-0-15_ECMWF-ERAINT	3.320	1.293	7.57E-09	−1.760	0.211
CCLM5-0-15_ensemble	3.105	0.291	2.21E-10	−1.975	0.196
RegCM4-7_MPI-M-MPI-ESM-LR	5.441	0.023	0.111732	0.361	0.289
RegCM4-7_NCC-NorESM1-M	3.626	0.961	5.08E-08	−1.454	0.194

RegCM4-7_MOHC-HadGEM2-ES	2.925	0.090	9.15E-08	−2.155	0.298
RegCM4-7_ECMWF-ERAINT	3.444	0.999	1.20E-07	−1.636	0.23
RegCM4-7_ensemble	3.997	0.127	1.65E-06	−1.083	0.18
REMO2015_MPI-M-MPI-ESM-LR	3.073	0.114	1.54E-09	−2.007	0.221
REMO2015_NCC-NorESM1-M	2.071	0.009	2.17E-15	−3.009	0.173
REMO2015-_MOHC-HadGEM2-ES	2.437	0.086	1.03E-13	−2.643	0.181
REMO2015_ECMWF-ERAINT	1.968	0.210	2.86E-16	−3.112	0.164
REMO2015_ensemble	2.527	0.053	1.31E-23	−2.553	0.172
Multiensemble_MPI-M-MPI-ESM-LR	4.205	0.136	6.10E-12	−0.875	0.191
Multiensemble_NCC-NorESM1-M	2.780	0.387	1.84E-16	−2.300	0.194
Multiensemble_MOHC-HadGEM2.ES	2.645	0.074	3.12E-17	−2.435	0.222
Multiensemble_ECMWF-ERAINT	2.910	0.566	5.34E-15	−2.170	0.175
OND	X	σ2	p-value	B	SDE
Observation	4.248	0.523			
CCLM5-0-15_MPI-M-MPI-ESM-LR	6.649	4.966	1.91E-06	6.649	4.966
CCLM5-0-15_NCC-NorESM1-M	6.381	0.885	3.62E-07	6.381	0.885
CCLM5-0-15_MOHC-HadGEM2-ES	3.098	2.232	5.85E-07	3.098	2.232
CCLM5-0-15_ECMWF-ERAINT	4.420	1.757	0.2244672	4.420	1.757
CCLM5-0-15_ensemble	5.376	1.164	4.68E-07	5.376	1.164
RegCM4-7_MPI-M-MPI-ESM-LR	6.924	3.178	1.41E-08	6.924	3.178
RegCM4-7_NCC-NorESM1-M	6.800	3.572	3.18E-07	6.800	3.572
RegCM4-7_MOHC-HadGEM2-ES	5.272	0.899	3.91E-05	5.272	0.899
RegCM4-7_ECMWF-ERAINT	3.930	2.094	0.1058297	3.930	2.094
RegCM4-7_ensemble	6.332	1.087	6.39E-11	6.332	1.087
REMO2015_MPI-M-MPI-ESM-LR	2.771	0.415	7.37E-09	2.771	0.415

REMO2015_NCC-NorESM1-M	2.724	0.220	4.54E-10	2.724	0.220
REMO2015-_MOHC-HadGEM2-ES	3.098	0.321	5.85E-07	3.098	0.321
REMO2015_ECMWF-ERAINT	1.992	0.320	1.07E-13	1.992	0.320
REMO2015_ensemble	2.865	0.132	8.31E-10	2.865	0.132
Multiensemble_MPI-M-MPI-ESM-LR	5.448	1.444	3.99E-05	5.448	1.444
Multiensemble_NCC-NorESM1-M	5.302	0.505	2.59E-05	5.302	0.505
Multiensemble_MOHC-HadGEM2.ES	3.823	0.768	0.209365	3.823	0.768
Multiensemble_ECMWF-ERAINT	3.447	1.033	0.003769	3.447	1.033

Note: Bold values are statistically significant at the 0.05 significance level. X is the mean rainfall (mm·day−1), σ2 is the variance (mm2·day−1) (Alfaro and Gomes, 2001), B is the mean bias (mm·day−1) and SDE is the standard error of the mean bias (mm·day−1).

2.4.2 Spatial correlation of MSR

Spatial correlation between CORDEX-CORE (AFR-22) RCM's simulations and observed datasets are computed to assess the performance of the models in representing the spatial distribution of MSR. Figure 2. 3 represents the magnitude and variability over time of spatial correlations between observed and simulated MSR over Rwanda during MAM and OND. During MAM, almost all RCMs and their ensembles have relatively poor spatial correlations with observations in terms of magnitude, ranging on average between 0.10 and 0.45, and poor consistency. During OND, all RCMs have a level of consistency in reproducing spatial patterns of rainfall which is much better than during MAM. On the average, spatial correlations are between 0.30 and 0.65 with a certain variability. The multimodel ensemble means have better representations than individual models and their ensembles. It is worth noting that in their study on rainfall in East Africa using the 10 CORDEX RCMS with 50 × 50 km (0.44◦) resolution driven by ERA-Interim and observed Global Precipitation Climatology Centre (GPCC) rainfall data as reference, Endris et al. (2013) found that over the southern East Africa (in which Rwanda belongs to), all RCMs and ERA- Interim had nearly same level of consistency in reproducing spatial patterns of rainfall during OND with spatial correlations of closely same range as those found in this study. RegCM4-7 MPI-M MPI-ESM-LR, RegCM4-7 NCC NorESM1-M, RegCM4-7 MOHC

HadGEM2-ES, RegCM4-7 ensemble, RegCM4-7 ECMWF ERAINT, REMO2015 MPI-M MPI-ESM-LR, REMO2015 MOHC HadGEM2-ES, REMO2015 ensemble, and REMO2015 ECMWF ERAINT present low spatial correlations values ($r < 0.40$) during the 1982–1983 and 1997 co-occurrence of the strong El Niño and positive IOD indicating a poor representation of these phenomena. Similarly, CCLM5-0-15 MPI-M MPI-ESM-LR, CCLM5-0-15 MOHC HadGEM2-ES, CCLM5-0-15 ensemble, CCLM5-0-15 ECMWRF ERAINT, REMO2015 MPI-M MPI-ESM-LR, REMO2015 MOHC HadGEMe-ES, REMO2015 ensemble, and REMO2015 ECMWF ERAINT present low spatial correlations values ($r < 0.40$) during the 1988–1989 La Niña. The other models present relatively good spatial correlations values ($r > 0.50$) during that period indicating a good representation of that phenomena. Relatively good spatial correlations values ($r > 0.50$) are shown by all RCMs during the 1994 IOD phase. The multimodel ensemble means have better representations than individual models and their ensembles.

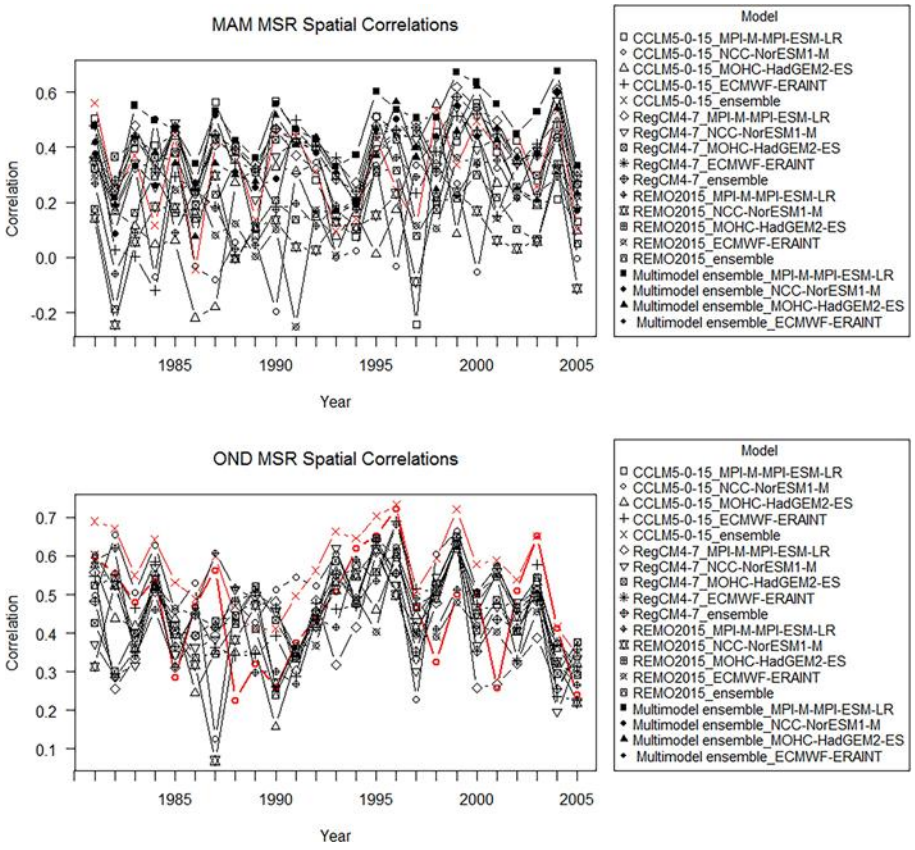

Figure 2. 3 Spatial correlations between mean daily seasonal rainfall simulated by different CORDEX-CORE (AFR-22) RCMs driven by different GCMs and ECMWF-ERANT, their ensembles and multi-ensembles, and observations over Rwanda during MAM (top) and OND (bottom) for the period 1981–2005.

Figure 2. 4 shows the Pearson's correlations between spatially averaged observed and simulated climatological MSR over Rwanda. During MAM, correlations are between 0.10 and 0.70, the multimodel ensemble means have the highest values and REMO015 exhibits the lowest correlation values regardless of the driving GCM or reanalysis compared to other RCMs. In particular, REMO015 driven by NCC-NorESM1-M and MOHC-HadGEM2-ES presents the lowest spatial correlation values. During OND, all RCMs have close spatial correlations that are higher than during MAM, ranging between 0.50 and 0.75. High correlation values (>0.50) indicate a better representation by models of spatially averaged MSR over Rwanda while low correlation values (<0.50) indicate a poor representation. The differences observed between RCMs in reproducing spatial and temporal rainfall pat- tern is likely to be due to model formulation and show how difficult is the representation of large scale phenomena combined with regional and local processes such as the ITCZ, orographic forcing and land-lake breezes influencing precipitation in Rwanda.

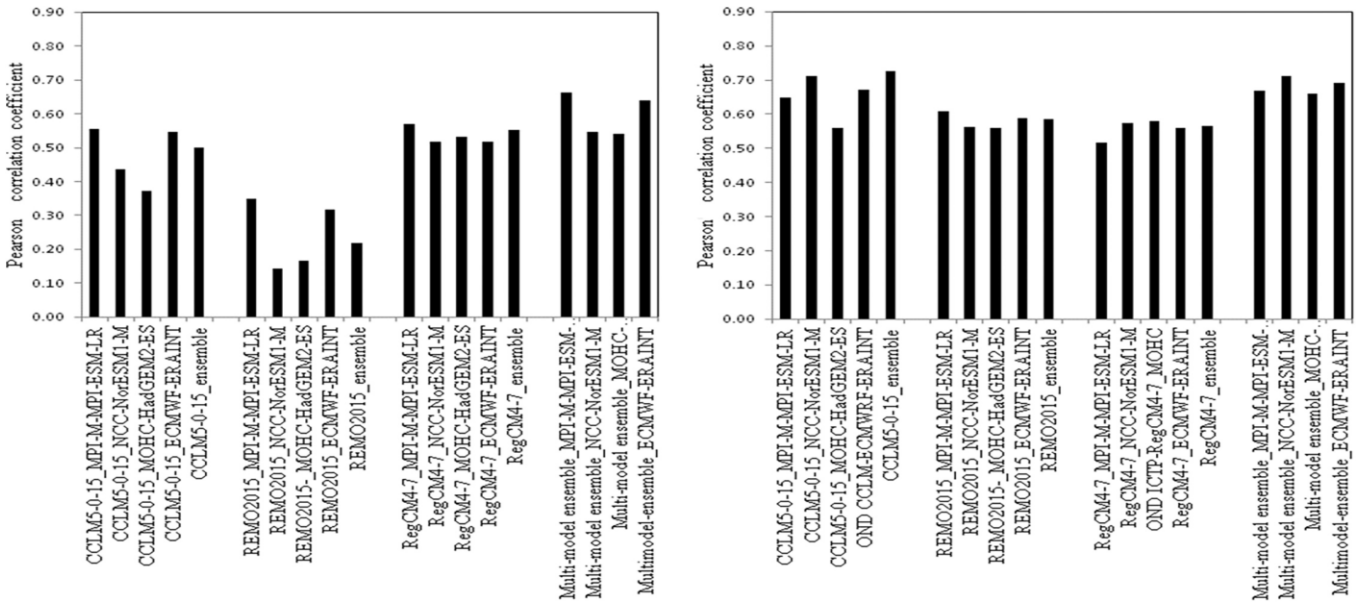

Figure 2. 4 Correlations between spatially averaged over Rwanda of climatological mean daily seasonal rainfall simulated by different CORDEX CORE (AFR-22) RCMs driven by different GCMs and ECMWF-ERANT, their ensembles and multi-ensembles, and observations over Rwanda for MAM (left) and OND (right).

2.4.3 Annual cycle

The annual cycles of observed and simulated rainfall averaged over Rwanda are presented in Data S6. All RCMs, their ensemble and multimodel ensemble means reproduce adequately well the bimodal distributions of the annual cycle. Most models underestimate rainfall during the long rain (March–May), corresponding to the rainfall season of intensive agricultural activities in Rwanda. In contrary, during the short rain (October–November), almost all models exhibit a more pronounced wet bias with the exception of REMO2015 driven by any of the GCMs and their ensemble mean, the multimodel mean of MOHC-HadGEM2-ES and all RCMs driven by ECMWF-ERAINT. Also, it is observed that, in addition to the general wet bias, all RCMs driven by GCMs tends to simulate relatively more rainfall during the short rain season than during the long rain season and this is in opposition with observation. These findings have been indicated previously by Kalognomou et al. (2013) and Kisembe et al. (2018) in their studies on simulating rain- fall over southern Africa and Uganda, respectively, using CORDEX RCMs. An early shift to February–March of the observed April peak of the long rain season is observed for almost all RCMs except only for CCLM5-0-15_MPI- M-MPI-ESM-LR, CCLM5-0-15_ECMWF-ERAINT, RegCM4-7_MPI-M-MPI-ESM-LR and the multimodel ensemble mean of MPI-M-MPI-ESM-LR. It should be noted that CCLM5-0-15, RegCM4-7 and their ensemble models present a large variation during the two rainy sea- sons. The multimodel ensemble mean of MPI-M-MPI- ESM-LR outperforms all individual models.

2.4.4 Normalized root-mean-square error

The spatial patterns of NRMSE between observed and simulate MSR are shown in Data S7 and S8, respectively, for MAM and OND over Rwanda during the studied period. In general, the order of magnitude of the NRMSE for all models is not high, ranging between 0% (0%) and 43% (55%) with a spatial average of 10% (7%) for MAM (OND). However, for MAM, it is spread here and there on the map and it is therefore difficult to interpret its spatial distribution. During OND, the NRMSE is much lower than during MAM and its spatial pattern for each RCM driven by different GCMs and ECMWF-ERAINT seems to be uniformly distributed over the whole country. RegCM4-7 exhibits higher values of NRMSE and this is especially pronounced when driven by MPI-M-MPI-ESM- LR, in the western region near Lake Kivu. CCLM5-0-15 presents a slightly higher error in the eastern region than in the western region except when driven by MPI-M-MPI-ESM-LR where it presents a slightly higher error in the region covering the northwest and the

central plateau. REMO2015_MPI-M-MPI-ESM-LR indicates a high error pattern in the central and western parts of the country but much more pronounced in the southwestern part.

2.4.5 Trends

CORDEX-CORE (AFR-22) RCMs and their ensemble and multimodel ensemble means are analysed with regard to simulating trends of the MSR. Mann-Kendall test for trend analysis and Theil-Sen's slope estimator has been applied to simulated and observed spatial averaged MSR time series over the period 1981-2018. The test has been performed at the significance level α (=0.001, 0.05. 0.01, 0.1). Where the p-value is less than the significance level, the null hypothesis such that no trend exists is rejected and the alternative hypothesis that trend is statistically significant is considered. In the opposite case where the p-value is greater than the significance level, the null hypothesis is accepted, meaning that there is no statistically significant trend. Results are presented in Table 2. 3. During MAM, the observed MSR shows a statistically significant positive trend of 0.045 $mm \cdot day^{-1} \cdot year^{1}$ at 0.05 significance level, while all RCMs do not show any significant trend except for REMO2015_MPI-M-MPI-ESM-LR and REMO2015_ensemble which indicate negative trends of, respectively, -0.050 and -0.017 $mm \cdot day^{-1} \cdot year^{1}$ at 0.05 significance level and at 0.1 significance level. For OND, the observed MSR shows a positive trend of 0.058 $mm \cdot day^{-1} \cdot year^{1}$ at 0.05 significance level, but all RCMs do not show any significant trend. The discrepancy in trends between observed and simulated rainfall has been revealed by several authors and was associated to the difference between RCMs/GCMs formulations specifically to different parameterization of, among others, the hydrological cycle, and the different response to the soil moisture-precipitation feedbacks (Dosio et al., 2015; Dosio and Panitz, 2016; Endris et al., 2016; Wu et al., 2020). Table 2. 1 shows the differences in terms of physical parameterization of each model. More work is needed to deeply understand the mechanisms governing rainfall over east Africa (particularly in Rwanda), and how their physical formulations in models can be improved.

Table 2. 3 Mann-Kendall trend and Theil–Sen's slope estimates in simulated and observed mean seasonal rainfall

Rainfall trend ($mm \cdot day^{-1} \cdot year^{1}$)	MAM		OND	
Time series	Trend	p-value	Trend	p-value
Observed	0.045 (*)	0.0265	0.058 (*)	0.0183

RegCM4-7_MPI-M-MPI-ESM-LR	−0.019 (.)	0.761	0.016 (.)	0.797
RegCM4-7_NCC-NorESM1-M	0.016 (.)	0.528	0.016 (.)	0.691
RegCM4-7_MOHC-HadGEM2-ES	−0.044 (.)	0.216	−0.041 (.)	0.216
RegCM4-7_ECMWF-ERAINT	−0.009 (.)	0.624	0.001 (.)	0.981
RegCM4-7_ensemble	−0.018 (.)	0.315	0.037 (.)	0.726
CCLM5-0-15_MPI-M-MPI-ESM-LR	−0.012 (.)	0.469	0.045 (.)	0.591
CCLM5-0-15_NCC-NorESM1-M	0.029 (.)	0.216	0.017 (.)	0.691
CCLM5-0-15_MOHC-HadGEM2-ES	−0.008 (.)	0.726	−0.067 (.)	0.154
CCLM5-0-15_ECMWF-ERAINT	−0.004 (.)	0.981	−0.007 (.)	0.726
CCLM5-0-15_ensemble	0.005 (.)	0.761	0.004 (.)	0.362
REMO2015_MPI-M-MPI-ESM-LR	−0.050 (*)	0.023	0.010 (.)	0.183
REMO2015_NCC-NorESM1-M	−0.019 (.)	0.252	−0.014 (.)	0.338
REMO2015-_MOHC-HadGEM2-ES	−0.004 (.)	0.761	−0.023 (.)	0.154
REMO2015_ECMWF-ERAINT	−0.020 (.)	0.234	−0.021 (.)	0.154
REMO2015_ensemble	−0.017 (+)	0.053	−0.008 (.)	0.657
Multiensemble_MPI.M.MPI.ESM.LR	−0.173 (.)	0.234	0.127 (.)	0.387
Multiensemble_NCC.NorESM1.M	0.007 (.)	0.981	0.020 (.)	0.907
Multiensemble_MOHC.HadGEM2.ES	−0.140 (.)	0.338	−0.260 (.)	0.123
Multiensemble_ECMWF.ERAINT	−0.093 (.)	0.528	−0.067 (.)	0.657

Note: (***) Trend at $\alpha = 0.001$ significant level; (**) trend at $\alpha = 0.01$ significant level; (*) trend at $\alpha = 0.05$ significant level; (+) trend significant at $\alpha = 0.1$ significant level; (.) no significant trend.

2.4.6 Taylor diagrams

Model simulations of MSR are displayed on Taylor diagrams in order to assess their performance in reproducing both the pattern and the amplitude of the inter-annual deviation from the observation. Figures 2. 5 and 2. 6 present, respectively, for the MSR, the Pearson's spatial correlation, the standard deviation and the amplitude of the centred RMS difference between reference point and simulated fields for each CORDEX-CORE (AFR-22) RCM driven by different GCMs and ECMWF- ERAINT and the corresponding ensemble, and for different

CORDEX-CORE (AFR-22) RCMs driven by same GCM or ECMWF-ERAINT and the corresponding multi- model ensemble mean for MAM and OND. During MAM, CCLM5-0-15 MPI-M MPI-ESM-LR, CCLM5-0-15 NCC NorESM1-M, CCLM5-0-15 ensemble, CCLM5-0-15 ECMWF ERAINT, RegCM4-7 MPI-M MPI-ESM-LR, RegCM4-7 NCC NorESM1-M, RegCM4-7 MOHC HadGEM2-ES, RegCM4-7 ensemble, and RegCM4-7 ECMWF ERAINT have Pearson's spatial correlations with observations ranging between 0.5 and 0.6. However, RegCM4-7_MPI-M-MPI-ESM-LR, RegCM4-7_NCC-NorESM1-M, RegCM4-7_MOHC-HadGEM2-ES, RegCM4-7_ensemble and RegCM4-7_ECMWF-ERAINT show high standard deviations between 1 and 2 mm·day^{-1}, and high amplitude of the centred RMS difference between reference point and simulated fields ranging between almost 1 and 2 mm·day^{-1}. CCLM5-0-15 MPI-M MPI-ESM-LR, CCLM5-0-15 NCC NorESM1-M, CCLM5-0-15 MOHC HadGEM2-ES, and CCLM5-0-15 ECMWF ERAINT have low standard deviation between 0 and 1 mm·day^{-1} and low amplitude of the centred RMS difference between reference point and simulated fields. CCLM5-0-15 MOHC HadGEM2-ES, REMO2015 MPI-M MPI-ESM-LR, REMO2015 NCC NorESM1-M, REMO2015 MOHC HadGEM2-ES, REMO2015 ensemble, and REMO2015 ECMWF ERAINT have Pearson's spatial correlations with observations less than 0.45. The multimodel ensemble means of MPI-M-MPI- ESM-LR and ECMWF-ERAINT have highest Pearson's spatial correlations with observations ranging between 0.60 and 0.65 with standard deviation ranging between 0.5 and 1 mm·day^{-1} and lowest amplitude of the centred RMS difference between reference point and simulated fields, while the multimodel ensemble means of NCC-NorESM1-M and MOHC-HadGEM2-ES have Pearson's spatial correlations with observations ranging between 0.45 and 0.55. with, respectively, standard deviation close to 2 mm·day^{-1} and between 0.5 and 1 mm·day^{-1}.

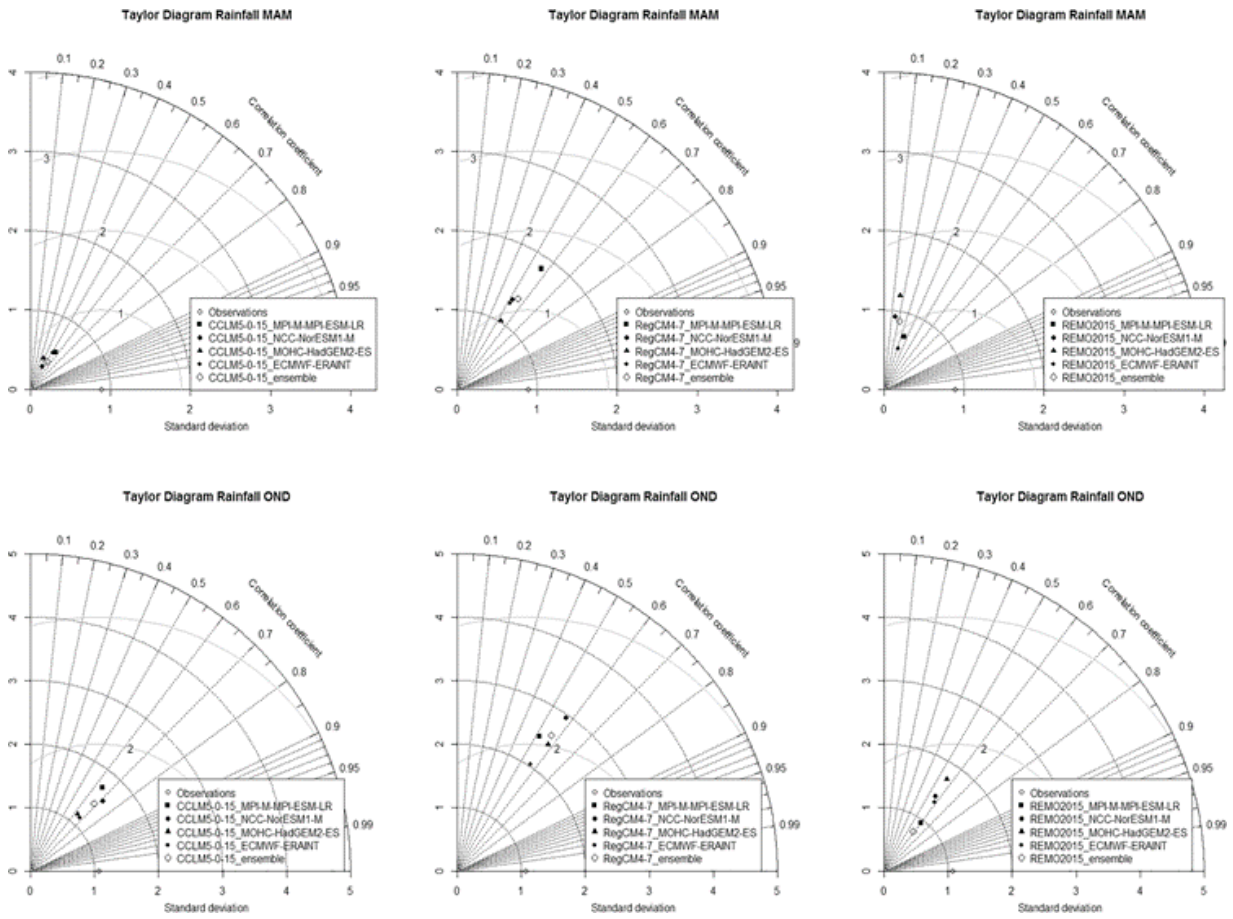

Figure 2. 5 Taylor diagram displaying normalized statistical comparison of mean daily seasonal rainfall simulated by each CORDEX CORE (AFR-22) RCM driven by different GCMs and ECMWF-ERANT, and the corresponding ensemble, with observations over Rwanda during MAM (top) and OND (bottom) for the period 1981-2005.

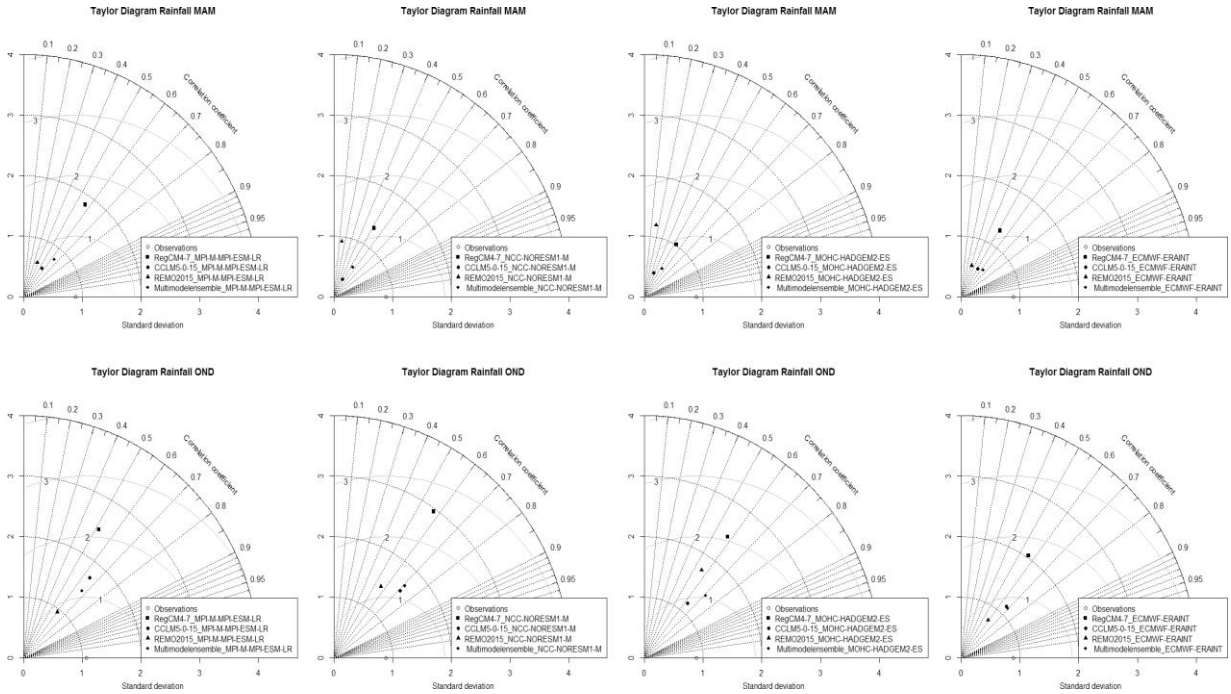

Figure 2. 6 Taylor diagram displaying normalized statistical comparison of mean daily seasonal rainfall simulated by different CORDEX CORE (AFR-22) RCMs driven by same GCM or ECMWF-ERANT, and the corresponding multi-ensemble mean, with observations over Rwanda during MAM (top) and OND (bottom) for the period 1981-2005

The multimodel ensemble means of MPI-M-MPI-ESM-LR and ECMWF-ERAINT have highest Pearson's spatial correlation, lowest standard deviation and lowest amplitude of the centred RMS difference between reference point and simulated field. They per- form better than individual models in reproducing both the pattern and the amplitude of the interannual deviation from the observation. During OND, all models show good Pearson's spatial correlations between 0.50 and 0.75. Similar to what is observed in MAM, RegCM4-7_MPI-M-MPI-ESM-LR, RegCM4-7_NCC-Nor- ESM1-M, RegCM4-7_MOHC-HadGEM2-ES, RegCM4-7_ensemble and RegCM4-7_ECMWF-ERAINT indicate higher standard deviations ranging between 2 and 3 $mm \cdot day^{-1}$ and higher amplitudes of the centred RMS difference between reference point and simulated fields. CCLM5-0-15_MPI-M-MPI-ESM-LR, CCLM5-0-15_NCC- NorESM1-M, CCLM5-0-15_MOHC-HadGEM2-ES and CCLM5-0-15_ECMWF-ERAINT, the multimodel ensemble means of MPI-M-MPI-ESM-LR, NCC- NorESM1-M, MOHC-HadGEM2-ES and ECMWF-ERAINT have Pearson's spatial correlations ranging between 0.60 and 0.75 with low standard deviation between 1 and 2 mm·day−1 and lowest amplitude of the centred RMS

difference between reference point and simulated fields. All these models perform with a few differences better compared to other models in reproducing both the pattern and the amplitude of the interannual deviation from the observation.

A comparison of RCMs driven by each GCM shows that during MAM, when all RCMs are driven by MPI-M- MPI-ESM-LR, the corresponding multimodel ensemble mean presents a relatively higher pattern of Pearson's spatial correlations and lower standard deviation than individual models. It is followed in order by CCLM5-0-15, REMO2015 and RegCM4-7. The same situation prevails when all RCMs are driven by either MOHC-HadGEM2-ES or ECMWF-ERAINT. This is not the case with NCC-NorESM1-M where a model may have higher pattern of correlation than another and the reverse for standard deviation. During OND, when all RCMs are driven by either MPI-M-MPI-ESM-LR or MOHC-HadGEM2-ES or ECMWF-ERAINT, the corresponding multimodel ensemble mean presents higher pattern of Pearson's spatial correlations and lower standard deviation than individual models. It is followed in order by CCLM5-0-15, REMO2015 and RegCM4-7. When all RCMs are driven by NCC-NorESM1-M, CCLM5-0-15 passes in first position and the multimodel ensemble mean of NCC-NorESM1-M in second position.

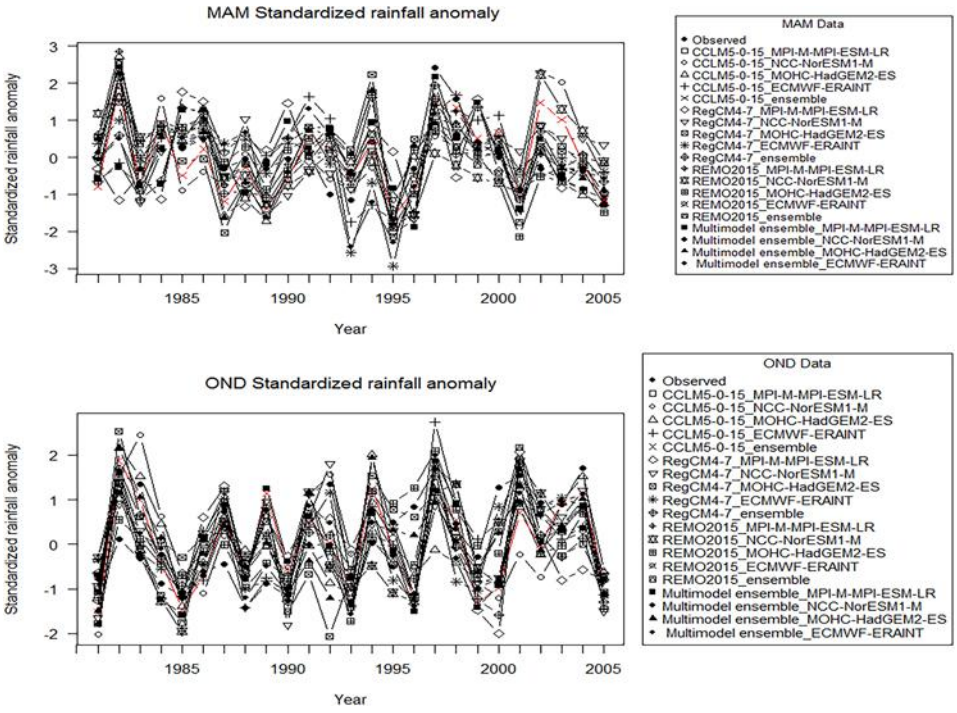

Figure 2. 7 Time series of CORDEX CORE (AFR-22) RCMs driven by different GCMs and ECMWF-ERANT, their ensembles and multi-ensembles, and observed standardized rainfall anomalies over Rwanda for MAM (top) and OND (bottom) during the period 1981–2005.

When comparing the driving GCMs and ECMWF- ERAINT for each RCM, it is found that during MAM, CCLM5-0-15 driven by MPI-M-MPI-ESM-LR presents a relatively higher pattern of Pearson's spatial correlations and lower standard deviation than the when driven by the rest of GCMs or ECMWF-ERAINT. CCLM5-0-15 driven by ECMWF-ERAINT comes in the second position. The same situation prevails for REMO2015. As for RegCM4-7, when driven by MPI-M-MPI-ESM-LR, it has a relatively higher pattern of Pearson's spatial correlations with however higher standard deviation than when driven by other GCMs or ECMWF-ERAINT. When driven by MOHC-HadGEM2-ES, it comes in the second position in terms of Pearson's spatial correlations with lowest standard deviation. During OND, CCLM5-0-15 driven by NCC-NorESM1-M has a relatively higher pat- tern of Pearson's spatial correlations with however high standard deviation. CCLM5-0-15 driven by ECMWF- ERAINT follows in terms of Pearson's spatial correlations with lowest standard deviation. Regarding RegCM4-7, it has highest pattern of Pearson's spatial correlations when driven by MOHC-HadGEM2-ES. RegCM4-7 driven by ECMWF-ERAINT follows in terms of Pearson's spatial correlations with lowest standard deviation. REMO2015 driven by MPI-M-MPI-ESM-LR has a relatively higher pattern of

Pearson's spatial correlations and lower standard deviation than the rest of the driving GCMs or ECMWF-ERAINT.

2.4.7 Interannual variability of the MSR

The spatial variability of Pearson's correlations between observed and simulated seasonal rainfall anomaly time series over Rwanda during the period 1981–2005 are presented in Data S9 and S10 for MAM and OND, respectively. During MAM, all models show low or even negative values of correlations with a heterogeneous spatial distribution. This indicates a poor representation of the spatial distribution of the interannual variability of the MSR by the CORDEX-CORE (AFR-22) RCMs during that season. During OND, all RCMs show an improved pattern of positive correlations but still heterogeneous. CCLM5-0-15_MPI-M-MPI-ESM-LR, RegCM4-7_ECMWF-ERAINT and Multiensemble_ECMWF-ERAINT exhibit spatial distribution of correlations ranging in the intervals [0.30, 0.75]. They indicate a better representation of the spatial distribution of the interannual variability of the MSR during the short rain compared to other models. Time series of CORDEX- CORE (AFR-22) RCMs, their ensembles and multimodel ensemble means and observed standardized anomalies of the spatially averaged MSR over Rwanda is presented in Figure 2. 8 and Table 2. 4 present the correlation coefficients between standardized seasonal rainfall anomalies derived from observational datasets and models. Almost all models are consistent in representing the temporal pat- tern of observed standardized seasonal rainfall anomalies from observations for MAM and OND seasons with slight differences in magnitude. Significant week correlations are observed for CCLM5-0-15_NCC-NorESM1-M (0.39 for MAM, 0.16 for OND), RegCM4-7_MPI-M-MPI-ESM- LR (0.17 for MAM, 0.20 for OND) and REMO2015_NCC-NorESM1-M (0.35 for MAM) indicating poor representation of the MSR interannual variability by those models for the respective seasons. The high rainfall event observed in 1997 is well represented by all models. A similar result was obtained by Endris et al. (2013) and Kisembe et al. (2018) who associated that event to the strong El Niño in phase with positive IOD.

Table 2. 4 Pearson correlation coefficients between standardized rainfall anomalies derived from observations and CORDEX CORE (AFR-22) RCMS, ensembles and multi-ensembles over Rwanda for MAM and OND during the period 1981–2005

Model	MAM	OND

CCLM5-0-15_MPI-M-MPI-ESM-LR	0.51	0.52
CCLM5-0-15_NCC-NorESM1-M	0.39	0.16
CCLM5-0-15_MOHC-HadGEM2-ES	0.73	0.39
CCLM5-0-15_ECMWF-ERAINT	0.67	0.49
CCLM5-0-15_ensemble	0.49	0.70
RegCM4-7_MPI-M-MPI-ESM-LR	0.17	0.20
RegCM4-7_NCC-NorESM1-M	0.64	0.52
RegCM4-7_MOHC-HadGEM2-ES	0.51	0.41
RegCM4-7_ECMWF-ERAINT	0.57	0.42
RegCM4-7_ensemble	0.73	0.65
REMO2015_MPI-M-MPI-ESM-LR	0.89	0.57
REMO2015_NCC-NorESM1-M	0.35	0.57
REMO2015-_MOHC-HadGEM2-ES	0.66	0.81
REMO2015_ECMWF-ERAINT	0.72	0.76
REMO2015_ensemble	0.59	0.38
Multiensemble_MPI-M-MPI-ESM-LR	0.50	0.49
Multiensemble_NCC-NorESM1-M	0.52	0.46
Multiensemble_MOHC-HadGEM2.ES	0.68	0.58
Multiensemble_ECMWF-ERAINT	0.64	0.70

Note: Values in bold are significant at 0.05 significance level.

2.4.8 Relation with ENSO and IOD

Several studies have shown that year to year variations in East African short rain coincide with significant SST anomalies across the tropical Pacific and Indian Oceans associated, respectively, with the ENSO in the eastern Pacific (Ogallo, 1988; Ogallo et al., 1988; Nicholson and Etekhabi, 1986; Mason and Goddard, 2001; Lyon and DeWitt, 2012) and the Indian Ocean Zonal Mode/Dipole (IOZM/IOD) (Goddard and Graham, 1999; Saji et al., 1999; Black, 2005; Ummenhofer et al., 2009). Those anomalies are linked to changes in the Walker circula- tion, regional winds and vertical velocities over East Africa (Hastenrath, 2007; Hastenrath et al., 2010; Mutai et al., 2012; Williams et al., 2012; Nicholson, 2015; Yang et al., 2015). Most of those studies

indicate that in equato- rial East Africa, the warm phase of ENSO (El Niño) is often associated with extreme rainfall causing flooding while on the opposite the cold phase (La Niña) often coincides with extreme drought conditions during the short rain. The predictability of long rain variability in East Africa has been complex and controversial, and attempted explanations have been discussed by several authors (Ogallo et al., 1988; Indeje et al., 2000; Mutai and Ward, 2000; Camberlin and Philippon, 2002; Yang et al., 2014; Nicholson, 2017; MacLeod, 2019). In their study on assessing the 50 km resolution CORDEX RCMs in simulating East African rainfall, Endris et al. (2013) found that most RCMs reproduce the majority of the documented regional responses to large-scale global climate forcing namely ENSO and IOD. Similar conclusions were drawn by Kisembe et al. (2018) in their study on assessing CORDEX RCMs with the same resolution over Uganda.

Due to its geographic location in East Africa, its small size with complex physical features, the rainfall variability of Rwanda is controlled by different factors of different scales. In this study, an investigation is made with the observed rainfall dataset and simulated rainfall dataset from CORDEX-CORE (AFR-22) RCMs to detect a possible association of ENSO and IOD to seasonal rainfall over Rwanda.

Figure 8 presents the seasonal correlations between ENSO and IOD sea surface temperature indices and rainfall indices from observations and CORDEX-CORE (AFR-22) RCMs with their ensemble means and multimodel ensemble means in Rwanda for the period 1981–2005. Two peaks of positive correlations from observations are observed during May–June–July (MJJ) (corresponding to the end of the long rain and the beginning of the long dry seasons) and OND (short rain season), explaining that during El Niño (La Niña) and during positive IOD (negative IOD) phases, prolonged increased (decreased) rainfall is observed during those two periods. This relationship is more pronounced with IOD than the respective ENSO indices. Non-significant low correlation coefficients are observed during MAM (long rain season) and during July–August–September (JAS) (corresponding to the dry season). These results are in conformity with those obtained by Kisembe et al. (2018). It is observed that only the three RCMs driven by ECMWF-ERAINT, the multimodel ensemble means of ECMWF-ERAINT and MPI-M-MPI-ESM-LR follow the pace of the seasonal correlations between observed rainfall indices over Rwanda and ENSO and IOD indices, and therefore reproduce the seasonal relationship of the observed rainfall averaged over Rwanda with both ENSO and IOD. In addition, RegCM4-7_NCC- NorESM1-M

and RegCM4-7_ensemble show a similar shape of correlation for Niño1+2, as well as RegCM4-7_MOHC-HadGEM2-ES and RegCM4-7_ensemble for IOD. High correlation coefficients are observed during OND for all those models which explains the good reproduction of the effect of ENSO and IOD phenomena during this period of the year. The other CORDEX-CORE (AFR-22) RCMs show negative or low positive correlations ranging between −0.3 and 0.3 and erratic shape not following the pace of the seasonal correlations between observed rainfall indices over Rwanda and ENSO and IOD indices and therefore do not reproduce the seasonal relationship of the observed rainfall with both ENSO and IOD.

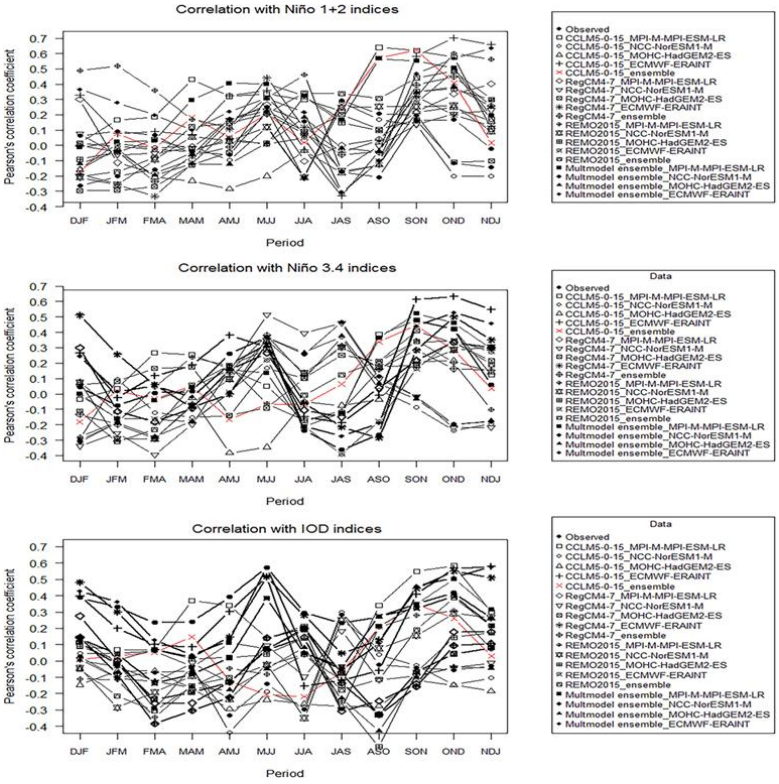

Figure 2. 8 Temporal correlations between Niño1+2 (top), Niño3.4 (middle) and IOD (bottom) indices and rainfall indices from observations and CORDEX CORE (AFR-22) RCMs with their ensemble and multi-ensemble in Rwanda for the period 1981–2005.

2.5 Conclusion

During the last decade, Rwanda has committed to moving towards a green economy and climate resilience pol- icy. A number of policies and strategies related to climate change adaptation and mitigation have been adopted and strategies and plans for their implementation have been put in place (Rwanda, 2006; 2011; 2018; 2019; 2020). This has led the country to a strong economic

growth across various strategic sectors (World Bank, 2019; Africa Development Bank, 2022). However, the current and projected effects of climate change due to human activity amplify the threats caused by rapid population growth, land and water scarcity, food insecurity and limitation of energy resources. These threats constitute the most important factors that can affect the stability of an economy of any developing country (FAO, 2021). In recent years, Rwanda has experienced impacts of climate change manifested by frequent extreme rainfall leading to extensive flooding and landslides in some districts located in high elevated areas of the north and western provinces, a strong variability in duration and frequency of droughts in the low-lying eastern province, and an increased mean temperature. This has caused enormous damage to the natural environment and infrastructure and has resulted in the loss of life and livelihoods (Rwanda Environment Management Authority, 2018).

Understand the mechanisms governing precipitation over Rwanda and predicting future climate to provide information to policy and decision makers, for the formulation of adaptation policies in response to the impacts of climate change, is fundamental for a country whose economy is partly based on rain-fed agriculture.

In this study, the CORDEX-CORE (AFR-22) RCMs have been evaluated in their ability to reproduce rainfall variability in Rwanda for the period 1981–2005. Results from three different RCMs with spatial resolution of 0.22◦ (~25 km), driven by three different GCMs and ERA-Interim for the period 1981–2005, were compared against observational datasets from Rwanda Meteorology Agency. Seasonal climatology pattern and bias, annual cycle, interannual variability and trend of simulated rainfall were analysed. Performances of individual models, their ensemble means and multimodel ensemble means were analysed for the long rain (March-April-May) and the short (October-November-December), by using different metrics. An investigation was made with the observed and simulated rainfall to detect a possible association of ENSO and IOD to seasonal rainfall over Rwanda.

It was found that in general, all RCMS present a spatial distribution of seasonal rainfall biases presenting dry bias during the long rain and, on the contrary, tends to present to some extend wet bias during the short rain. The spatial distribution of seasonal rainfall biases tends to follow the terrain elevation with reinforced dry (wet) bias in high-altitude areas during the long rain (during the short rain). Spatial correlations between observed and simulated mean seasonal rainfall indicate a better consistency in reproducing spatial patterns of rainfall during the short rain than

during the long rain. All RCMs reproduce adequately well the bimodal distributions of the annual cycle, though the GCMs-driven RCMs tend to simulate relatively more rainfall during the short rain season than during the long rain season and this is in opposition with observation. In general, the normalized root-mean-square error between observed and simulated mean seasonal rainfall time series is not as much high during the two seasons. However, it is much lower with spatial pattern tending to be uniformly distributed over the whole country during the short rain while it is heterogeneously distributed during the long rain. A difference is observed in trends where the observed mean seasonal rainfall indicates a positive trend during the two seasons while all RCMs do not show any significant trend. Analysis of Taylor diagrams indicates that the multimodel ensemble means of MPI-M-MPI-ESM-LR and ECMWF-ERAINT perform better than individual RCMs in reproducing both the pattern and the amplitude of the interannual deviation from the observation in both sea- sons. Analysis of the spatial variability of Pearson's correlations between observed and simulated mean seasonal rainfall anomaly time series indicates a poor representation of the spatial distribution of the interannual variability of the mean seasonal rainfall by all CORDEX-CORE (AFR-22) RCMs during the long rain over Rwanda during the period of study. During the short rain, a more improved representation of the spatial distribution of the interannual variability of the mean seasonal rainfall is observed but still heterogeneous. CCLM5-0-15_MPI-M- MPI-ESM-LR, RegCM4-7_ECMWF-ERAINT and Multi-ensemble_ECMWF-ERAINT show a better performance compared to other RCMs. However, it is worth to note that all models are consistent in representing the temporal pattern of observed standardized anomalies of the spatially averaged mean seasonal rainfall during both seasons. The seasonal correlations between observed rainfall anomalies over Rwanda and SST anomalies indi- ces across the tropical Pacific (Niño1+2 and Niño3.4) and Indian Oceans associated, respectively, with the ENSO and the IOD although relatively weak, are reproduced by the three CORDEX-CORE (AFR-22) driven by ECMWF- ERAINT and the multimodel ensemble means of MPI-M- MPI-ESM-LR and ECMWF-ERAINT.

Overall, it has been found that the multimodel ensemble means of MPI-M-MPI-ESM-LR and ECMWF-ERAINT are almost similarly outperforming all individual models over Rwanda for the period of study. Uncertainties affecting the performance of the models in representing the rainfall patterns over Rwanda are likely due, on one side, to the complex topography which does not make easy the reproduction of related effects by models constrained by their resolution which is still too

coerce for a country of small size like Rwanda; on the other side, and importantly, to physical parameterization, timescale and numerical schemes used in the models. It is hoped that with ongoing developments, further work by climate modelers will bring add value when all of those factors are taken into consideration. The analysis of the projections of future climate change in Rwanda using representative concentration pathways (RCP) forcing scenarios will be presented in a forthcoming work. These scenarios provide different pathways of the future climate forcing as a result of human activities (van Vuuren et al., 2011). Boundary conditions will be provided by GCMs used in this study.

2.6 References

African Development Bank. (2022) African Economic Outlook, 2022: Supporting Climate Resilience and a Just Energy Transition in Africa. Abidjan, Côte d'Ivoire: African Development Bank.

Alfaro, S.C. and Gomes, L. (2001) Modeling mineral aerosol produc- tion by wind erosion: emission intensities and aerosol size dis- tributions in source areas. Journal of Geophysical Research, 106, 18075–18084. https://doi.org/10.1029/2000JD900339.

Anthes, R.A. (1977) A cumulus parameterization scheme utilizing a one-dimensional cloud model. Monthly Weather Revue, 105, 270–286. https://doi.org/10.1175/1520-0493(1977)105<0270: ACPSUA>2.0.CO;2.

Anyah, R.O., Semazzi, F.H.M. and Xie, L. (2006) Simulated physical mechanisms associated with multi-scale climate variability over Lake Victoria Basin in East Africa. Monthly Weather Review, 134, 3588–3609. https://doi.org/10.1175/MWR3266.1.

Arakawa, A. and Lamb, V. (1977) Computational design of thebasic dynamical processes in the UCLA general circulation model. In: Chang, J. (Ed.) Methods in Computational Physics: Advances in Research and Applications, Vol. 17. New York, NY: Academic Press, pp. 173–265. https://doi.org/10.1016/B978-0-12-460817-7.50009-4.

Ashfaq, M., Cavazos, T., Reboita, M.S., Torres-Alavez, J.A., Im, E- S., Olusegun, C.F., Alves, L., Key, K., Adeniyi, M.O., Tall, M., Sylla, Mehmood, M.B., Zafar, Q., Das, S., Diallo, I., Coppola, E. and Giorgi, F. (2021) Robust late twenty-first century shift in the regional monsoons in RegCM-CORDEX simulations. Cli-mate Dynamics, 57, 1463–1488. https://doi.org/10.1007/s00382-020-05306-2.

Asselin, R. (1972) Frequency filter for time integrations. Monthly Weather Review, 100, 487–490. https://doi.org/10.1175/1520- 0493(1972)100<0487:FFFTI>2.3.CO;2.

Ban, N., Caillaud, C., Coppola, E., Pichelli, E., Sobolowski, S., Adi- nolfi, M., Ahrens, B., Alias, A., Anders, I., Bastin, S., Belusˇi´c, D., Berthou, S., Brisson, E., Cardoso, R.M., Chan, S.C., Chris- tensen, O.B., Fern´andez, J., Fita, L., Frisius, T., Gasˇparac, G., Giorgi, F., Görgen, K., Haugen, J.E., Hodnebrog, Ø., Kartsios, S., Katragkou, E., Kendon, E. J., Keuler, K., Lavin-Gullon, A., Lenderink, G., Leutwyler, D., Lorenz, T., Maraun, D., Merco- gliano, P., Milovac, J., Panitz, H.-J., Raffa, M., Remedio, A.R., Schär, C., Soares, P.M.M., Srnec, L., Steensen, B. M., Stocchi, P., Tölle, M.H., Truhetz, H., Vergara-Temprado, J., de Vries, H., Warrach-Sagi, K., Wulfmeyer, V. and Zander, M.J. (2021) The first multi-model ensemble of regional climate simulations at kilometer scale resolution. Part I: evaluation of precipitation. Climate Dynamics, 57, 275–302. https://doi.org/10.1007/s00382-021-05708-w.

Bechtold, P., Köhler, M., Jung, T., Doblas-Reyes, F., Leutbecher, M., Rodwell, M., Vitart, F. and Balsamo, G. (2008) Advances in simulating atmospheric variability with the ECMWF model: from synoptic to decadal time-scales. Quarterly Journal of the Royal Meteorological Society, 134, 1337–1351. https://doi.org/10.1002/qj.289.

Bentsen, M., Bethke, I., Debernard, J.B., Iversen, T., Kirkevåg, A., Seland, Ø., Drange, H., Roelandt, C., Seierstad, I.A., Hoose, C. and Kristj´ansson, J.E. (2013) The Norwegian Earth System Model, NorESM1-M—part 1: description and basic evaluation of the physical climate. Geoscientific Model Development, 6, 687–720. https://doi.org/10.5194/gmd-6-687-2013.

Black, E. (2005) The relationship between Indian Ocean sea-surface temperature and East African rainfall. Philosophical Transac- tions: Mathematical, Physical and Engineering Sciences, 363 (1826), 43–47. https://doi.org/10.1098/rsta.2004.1474.

Boko, M., Niang, I., Nyong, A., Vogel, C., Githeko, A., Medany, M., Osman-Elasha, B., Tabo, R. and Yanda, P. (2007) Africa. In: Parry, M.L., Canziani, O.F., Palutikof, J.P., van der Linden, P.J. and Hanson, C.E. (Eds.) Climate Change 2007: Impacts, Adap- tation and Vulnerability. Contribution of Working Group II to the Fourth Assessment Report of the Intergovernmental Panel on Climate Change. Cambridge: Cambridge University Press, pp.433–467.

Bretherton, C.S., McCaa, J.R. and Grenier, H. (2004) A new param- eterization for shallow cumulus convection and its application to marine subtropical cloud-topped boundary layers. Part I: description and 1D results. Monthly Weather Review, 132(4), 864–882.

https://doi.org/10.1175/1520-0493(2004)132<0864: ANPFSC>2.0.CO;2.

Camberlin, P. and Philippon, N. (2002) The East African March– May rainy season: associated atmospheric dynamics and pre- dictability over the 1968–97 period. Journal of Climate, 15 (9), 1002–1019. https://doi.org/10.1175/1520-0442(2002)015<1002:TEAMMR>2.0.CO;2

Collins, W.D., Bitz, C.M., Blackmon, M.L., Bonan, G.B., Bretherton, C.S., Carton, J.A., Chang, P., Doney, S.C., Hack, J.J., Hender-son, T.B., Kiehl, J.T., Large, W.G., Mckenna, D.S., Santer, B.D. and Smith, R.D. (2006) The Community Climate System model version 3 (CCSM3). Journal of Climate, 19, 2122–2143. https://doi.org/10.1175/JCLI3761.1.

Colmet-Daage, A., Emilia, S.-G., Sophie, R., Cécile, L., Valérie, B.E., Pere, Q.-S., Maria, C.L. and Eric, S. (2018) Evaluation of uncer- tainties in mean and extreme precipitation under climate change for northwestern Mediterranean watersheds from high- resolution Med and Euro-CORDEX ensembles. Hydrology and Earth System Sciences, 22, 673–687. https://doi.org/10.5194/hess-22-673-2018.

Coppola, E., Raffaele, F., Giorgi, F., Giuliani, G., Xuejie, G., Ciarlo, J.M., Sines, T.R., Torres-Alavez, J.A., Das, S., di Sante, F., Pichelli, E., Glazer, R., Müller, S.K., Abba Omar, S., Ashfaq, M., Bukovsky, M., Im, E.-S., Jacob, D., Teichmann, C., Remedio, A., Remke, T., Kriegsmann, A., Bülow, K., Weber, T., Bunte- meyer, L., Sieck, K. and Rechid, D. (2021) Climate hazard indi- ces projections based on CORDEX-CORE, CMIP5 and CMIP6 ensemble. Climate Dynamics, 57, 1293–1383. https://doi.org/10.1007/s00382-021-05640-z.

Coppola, E., Sobolowski, S., Pichelli, E., Raffaele, F., Ahrens, B., Anders, I., Ban, N., Bastin, S., Belda, M., Belusic, D., Caldas- Alvarez, A., Cardoso, R. M., Davolio, S., Dobler, A., Fernandez, J., Fita, L., Fumiere, Q., Giorgi, F., Goergen, K., Güttler, I., Halenka, T., Heinzeller, D., Hodnebrog, Ø., Jacob, D., Kartsios, S., Katragkou, E., Kendon, E., Khodayar, S., Kunstmann, H., Knist, S., Lavín-Gullo´n, A., Lind, P., Lorenz, T., Maraun, D., Marelle, L., van Meijgaard, E., Milovac, J., Myhre, G., Panitz, H.-J., Piazza, M., Raffa, M., Raub, T., Rockel, B., Schär, C., Sieck, K., Soares, P. M. M., Somot, S., Srnec, L., Stocchi, P., Tölle, M. H., Truhetz, H., Vautard, R., de Vries, H. and War- rach-Sagi, K. (2020) A first-of-its-kind multi-model convection permitting ensemble for investigating

convective phenomena over Europe and the Mediterranean. Climate Dynamics, 55, 3–34. https://doi.org/10.1007/s00382-018-4521-8.

David, K., Megan, C., Christian, C., Jillian, D., Ryan, H., Robert, M., Mathew, W., Sally, T., Andrew, A.B. and Michael, H. (2011) Green Growth and Climate Resilience National Strategy for Climate Change and Low Carbon Develop- ment. Kigali: Rwanda.

Dee, D., Uppala, S.M., Simmons, A., Berrisford, P., Poli, P., Kobayashi, S., Andrae, U., Balmaseda, M.A., Balsamo, G., Bauer, P., Bechtold, P., Beljaars, A.C., Berg, L.V., Bidlot, J.,Bormann, N., Delsol, C., Dragani, R., Fuentes, M., Geer, A.J., Haimberger, L., Healy, S.B., Hersbach, H., Holm, E.V., Isaksen, L., Kållberg, P.W., Köhler, M., Matricardi, M., McNally, A.P., Monge-Sanz, B., Morcrette, J.J., Park, B., Peubey, C., Rosnay, P.D., Tavolato, C., Thepaut, J. and Vitart, F. (2011) The ECMWF-ERAINT reanalysis: configura- tion and performance of the data assimilation system. Quarterly Journal of the Royal Meteorological Society, 137, 553–597. https://doi.org/10.1002/qj.828.

Diaconescu, E., Gachon, P. and Laprise, R. (2015) On the remap- ping procedure of daily precipitation statistics and indices used in regional climate model evaluation. Journal of Hydrometeorol- ogy, 16, 2301–2310. https://doi.org/10.1175/JHM-D-15-0025.1.

Dickinson, R.E., Henderson-Sellers, A. and Kennedy, P.J. (1993)

Biosphere–atmosphere Transfer Scheme (BATS) version 1e as coupled to the NCAR Community Climate Model. Boulder, CO: University Corporation for Atmospheric Research. Technical report number: NCAR/TN-387+STR. https://doi.org/10.5065/ D67W6959.

Dinku, T., Funk, C., Peterson, P., Maidment, R., Tadesse, T., Gadain, H. and Ceccato, P. (2018) Validation of the CHIRPS satellite rainfall estimates over eastern Africa. Quarterly Journal of the Royal Meteorological Society, 144(1), 292–312. https://doi.org/10.1002/qj.3244.

Dinku, T., Hailemariam, K., Maidment, R., Tarnavsky, E. and Connor, S. (2014) Combined use of satellite estimates and rain gauge observations to generate high-quality historical rainfall time series over Ethiopia. International Journal of Climatology, 34(7), 2489–2504. https://doi.org/10.1002/joc.3855.

Dinku, T., Thomson, M., Cousin, R., del Corral, J., Ceccato, P., Hansen, J. and Connor, S. (2017) Enhancing national climate services (ENACTS) for development in Africa. Climate and Development, 10(7), 664–672. https://doi.org/10.1080/17565529.2017.1405784.

Doms, G. and Baldauf, M. (2013) A description of the nonhydrostatic regional COSMO-model—part I: dynamics and numerics. Offen- bach: COSMO. Technical report. https://doi.org/10.5676/ DWD_pub/nwv/cosmo-doc_5.00_I.

Doms, G., Föster, J., Heise, E., Herzog, H., Mironov, D., Raschendorfer, M., Reinhardt, T., Ritter, B., Schrodin, R., Schulz, J. and Vogel, G. (2013) A description of the nonhydro- static regional COSMO-model-part II: physical parameteriza- tions. Offenbach: COSMO. Technical report. https://doi.org/10. 5676/DWD_pub/nwv/cosmo-doc_5.00_II.

Dosio, A., Jury, M.W., Almazroui, M., Ashfaq, M., Diallo, I., Engel- brecht, F.A., Klutse, N.A.B., Lennard, C., Pinto, I., Sylla, M.B. and Tamoffo, A.T. (2021) Projected future daily characteristics of African precipitation based on global (CMIP5, CMIP6) and regional (CORDEX, CORDEX-CORE) climate models. Climate Dynamics, 57, 3135–3158. https://doi.org/10.1007/s00382-021-05859-w.

Dosio, A. and Panitz, H.J. (2016) Climate change projections for CORDEX Africa with COSMO-CLM regional climate model and differences with the driving global climate models. Climate Dynamics, 46, 1599–1625. https://doi.org/10.1007/s00382-015-2664-4.

Dosio, A., Panitz, H.J., Schubert-Frisius, M. and Lüthi, D. (2015) Dynamical downscaling of CMIP5 global circulation models over CORDEX Africa with COSMO-CLM: evaluation over the present climate and analysis of the added value. Climate Dynamics, 44(9–10), 2637–2661. https://doi.org/10.1007/ s00382-014-2262-x.

Elguindi, N., Bi, X., Giorgi, F., Nagarajan, B., Pal, J., Solmon, F., Rauscher, S., Zakey, A., O'Brien, T., Nogherotto, R. and Giuliani, G. (2017) Regional Climate Model RegCM Reference Manual Version 4.7. Trieste: International Centre for Theoreti- cal Physics.

Emanuel, K.A. (1991) A scheme for representing cumulus convec- tion in large-scale models. Journal of Atmospheric Sciences, 48 (21), 2313–2335. https://doi.org/10.1175/1520-0469(1991) 048<2313:ASFRCC>2.0.CO;2.

Emanuel, K.A. and Zivkovic-Rothman, M. (1999) Development and evaluation of a convection scheme for use in climate models. Journal of Atmospheric Sciences, 56, 1766–1782. https://doi.org/10.1175/1520-0469(1999)056<1766:DAEOAC>2.0.CO;2.

Endris, H.S., Lennard, C., Hewitson, B., Dosio, A., Nikulin, G. and Panitz, H.-J. (2016) Teleconnection responses in multi-GCM driven CORDEX RCMs over eastern Africa. Climate Dynamics, 46, 2821–2846. https://doi.org/10.1007/s00382-015-2734-7.

Endris, H.S., Omondi, P., Jain, S., Lennard, C., Hewitson, B.,Chang, L., Awange, J., Dosio, A., Ketiem, P., Nikulin, G., Panitz, H.-J., Büchner, M., Stordal, F. and Tazalika, L. (2013) Assessment of the performance of CORDEX regional climate models in simulating East African rainfall. Journal of Climate, 26(21), 8453–8475. https://doi.org/10.1175/JCLI-D-12-00708.1.

Eum, H.-I., Gachon, P., Laprise, R. and Ouarda, T. (2011) Evalua- tion of regional climate model simulations versus gridded observed and regional reanalysis products using a combined weighting scheme. Climate Dynamics, 38, 1433–1457. https:// doi.org/10.1007/s00382-011-1149-3.

FAO. (2021) The Impact of Disasters and Crises on Agriculture and Food Security. Rome: FAO. https://doi.org/10.4060/cb3673en.

Favre, A., Philippon, N., Pohl, B., Kalognomou, E.-A., Lennard, C., Hewitson, B., Nikulin, G., Dosio, A., Panitz, H.-J. and Cerezo- Mota, R. (2016) Spatial distribution of precipitation annual cycles over South Africa in 10 CORDEX regional climate model present-day simulations. Climate Dynamics, 46(5–6), 1799–1818. https://doi.org/10.1007/s00382-015-2677-z.

Flato, G., Marotzke, J., Abiodun, B., Braconnot, P., Chou, S.C., Collins, W., Cox, P., Driouech, F., Emori, S., Eyring, V., Forest, C., Gleckler, P., Guilyardi, E., Jakob, C., Kattsov, V., Reason, C. and Rummukainen, M. (2013) Evaluation of climate models. In: Stocker, T.F., Qin, D., Plattner, G.-K., Tignor, M., Allen, S., K., Doschung, J., Nauels, A., Xia, Y., Bex, V. and Midgley, P.M. (Eds.) Climate Change 2013: The Physical Science Basis. Contri- bution of Working Group I to the Fifth Assessment Report of the Intergovernmental Panel on Climate Change. Cambridge: Cambridge University Press, pp. 741–882. https://doi.org/10.1017/CBO9781107415324.020.

Fritsch, J.M. and Chappell, C.F. (1980) Numerical prediction of convectively driven mesoscale pressure systems. Part I: convec- tive parameterization. Journal of Atmospheric Sciences, 37, 1722–1733. https://doi.org/10.1175/1520-0469(1980)037<1722:NPOCDM>2.0.CO;2.

Gbobaniyi, E., Sarr, A., Sylla, M., Diallo, I., Lennard, C., Dosio, A., Dhiédiou, A., Kamga, A., Klutse, N.A.B., Hewitson, B., Nikulin, G. and Lamptey, B. (2014) Climatology, annual cycle and inter-annual variability of precipitation and temperature in CORDEX simulations over West Africa. International Journal of Climatology, 34(7), 2241–2257.

https://doi.org/10.1002/joc.3834.

Giorgetta, M. and Wild, M. (1995) The water vapour continuum and its representation in ECHAM4. Hamburg: Max-Planck Institut für Meteorologie. Technical report number: 162.

Giorgetta, M.A., Jungclaus, J., Reick, C.H., Legutke, S., Bader, J., Böttinger, M., Brovkin, V., Crueger, T., Esch, M., Fieg, K., Glushak, K., Gayler, V., Haak, H., Hollweg, H-D., Ilyina, T., Kinne, S., Kornblueh, L., Matei, D., Mauritsen, T., Mikolaje- wicz, U., Mueller, W., Notz, D., Pithan, F., Raddatz, T., Rast, S., Redler, R., Roeckner, E., Schmidt, H., Schnur, R., Segschneider, J., Six, K.D., Stockhause, K.D., Timmreck, C., Wegner, J., Wid- mann, H., Wieners, K-H., Claussen, M., Marotzke, J. and Ste- vens, B. (2013) Climate and carbon cycle changes from 1850 to 2100 in MPI-ESM simulations for the Coupled Model Intercom- parison Project phase 5. Journal of Advanced Modeling Earth Systems, 5, 572–597. https://doi.org/10.1002/jame.20038.

Giorgi, F., Bi, X. and Qian, Y. (2003) Indirect vs. direct effects of anthropogenic sulfate on the climate of East Asia as simulated with a regional coupled climate-chemistry/aerosol model. Climatic Change, 58, 345–376. https://doi.org/10.1023/A:1023946010350.

Giorgi, F., Coppola, E., Solmon, F., Mariotti, L., Sylla, M.B., Bi, X., Elguindi, N., Diro, G.T., Nair, V., Giuliani, G., Turuncoglu, U. U., Cozzini, S., Güttler, I., O'Brien, T.A., Tawfik, A.B., Shalaby, A., Zakey, A.S., Steiner, A.L., Stordal, F., Sloan, L.C. and Bran- kovic, C. (2012) RegCM4: model description and preliminary tests over multiple CORDEX domains. Climate Research, 52, 7–29. https://doi.org/10.3354/cr01018.

Giorgi, F., Coppola, E., Teichmann, C. and Jacob, D. (2021) Edito- rial for the CORDEX-CORE experiment I special issue. Climate Dynamics, 57, 1265–1268. https://doi.org/10.1007/s00382-021-05902-w.

Giorgi, F. and Gutowski, W.J. (2015) Regional dynamical downscal- ing and the CORDEX initiative. Annual Review of Environment and Resources, 40, 467–490. https://doi.org/10.1146/annurev- environ-102014-021217.

Giorgi, F., Jones, C. and Asrar, G.R. (2009) Addressing climate information needs at the regional level: the CORDEX frame- work. WMO Bulletin, 58(3), 175–183.

Giorgi, F., Torma, C., Coppola, E., Ban, N., Schär, C. and Somot, S. (2016) Enhanced summer convective rainfall at Alpine high elevations in response to climate warming. Nature Geoscience, 9, 584–589. https://doi.org/10.1038/ngeo2761.

Glotter, M., Elliott, J., McInerney, D., Best, N., Foster, I. and Moyer, E. (2014) Evaluating the utility of dynamical downscaling in agricultural impacts projections. Proceedings of the National Academy of Sciences of the United States of America, 111(24), 8776–8781. https://doi.org/10.1073/pnas.1314787111.

Gnitou, G.T., Tan, G., Niu, R. and Nooni, I.K. (2021) Assessing past climate biases and the added value of CORDEX-CORE precipitation simulations over Africa. Remote Sensing, 13, 2058. https://doi.org/10.3390/rs13112058.

Goddard, L. and Mason, S.J. (2002) Sensitivity of seasonal climate forecasts to persisted SST anomalies. Climate Dynamics, 19, 619–631. https://doi.org/10.1007/s00382-002-0251-y.

Grell, G. (1993) Prognostic evaluation of assumptions used by cumulus parameterizations. Monthly Weather Revue, 121, 764– 787. https://doi.org/10.1175/1520-0493(1993)121<0764: PEOAUB>2.0.CO;2.

Grell, G.A., Dudhia, J. and Stauffer, D. (1994) A description of the fifth-generation Penn State/NCAR Mesoscale Model (MM5). Boulder, CO: University Corporation for Atmospheric Research. Technical report number: NCAR/TN-398+STR. https://doi.org/10.5065/D60Z716B.

Grenier, H. and Bretherton, C.S. (2001) A moist PBL parameteriza- tion for large-scale models and its application to subtropical cloud-topped marine boundary layers. Monthly Weather Review, 129(3), 357–377. https://doi.org/10.1175/1520-0493(2001)129<0357:AMPPFL>2.0.CO;2.

Guo, D., Sun, J. and Yu, E. (2018) Evaluation of CORDEX regional climate models in simulating temperature and pre- cipitation over the Tibetan Plateau. Atmospheric and Oceanic Science Letters, 11, 1–9. https://doi.org/10.1080/16742834.2018.1451725.

Gutowski, J.W., Giorgi, F., Timbal, B., Frigon, A., Jacob, D., Kang, H.S., Raghavan, K., Lee, B., Lennard, C., Nikulin, G., O'Rourke, E., Rixen, M., Solman, S., Stephenson, T. and Tangang, F. (2016) WCRP Coordinated Regional Downscaling EXperiment (CORDEX): a diagnostic MIP for CMIP6. Geoscien- tific Model Development, 9, 4087–4095. https://doi.org/10.5194/ gmd- 9-4087-2016.

Hagemann, S. (2002) An Improved Land Surface Parameter Dataset for Global and Regional Climate Models. Hamburg: Max- Planck-Institute for Meteorology. Report number: 336.

Hartkamp, A.D., de Beurs, K., Stein, A. and White, J. (1999) Inter- polation Techniques for Climate Variables. Geographic Informa- tion Systems Series 99-01. Mexico: International Maize and Wheat Improvement Center (CIMMYT).

Hastenrath, S. (2007) Circulation mechanisms of climate anomalies in East Africa and the equatorial Indian Ocean. Dynamics of Atmospheres and Oceans, 43(1–2), 25–35. https://doi.org/10.1016/j.dynatmoce.2006.06.002.

Hastenrath, S., Polzin, D. and Mutai, C. (2010) Diagnosing the droughts and floods in equatorial East Africa during boreal autumn 2005–08. Journal of Climate, 23(3), 813–817. https://doi.org/10.1175/2009JCLI3094.1.

Hersbach, H., Bell, B., Berrisford, P., Hirahara, S., Hor´anyi, A., Muñoz-Sabater, J., Nicolas, J., Peubey, C., Radu, R., Schepers, D., Simmons, A., Soci, C., Abdalla, S., Abellan, X., Balsamo, G., Bechtold, P., Biavati, G., Bidlot, J., Bonavita, M., De Chiara, G., Dahlgren, P., Dee, D., Diamantakis, M., Dragani, R., Flemming, J., Forbes, R., Fuentes, M., Geer, A., Haimberger, L., Healy, S., Hogan, R.J., Ho´lm, E., Janiskov´a, M., Keeley, S., Laloyaux, P., Lopez, P., Lupu, C., Radnoti, G., de Rosnay, P., Rozum, I., Vamborg, F., Villaume, S. and Thépaut, J.-N. (2020) The ERA5 global reanalysis. Quarterly Journal of the Royal Meteorological Society, 146, 1999–2049. https://doi.org/10.1002/qj.3803.

Holtslag, A.A.M. and Boville, B.A. (1993) Local versus nonlocal boundary-layer diffusion in a global climate model. Journal of Climate, 6, 1993. https://doi.org/10.1175/1520-0442(1993)006<1825:LVNBLD>2.0.CO;2.

Holtslag, A.A.M., de Bruijn, E.I.F. and Pan, H.-L. (1990) A high res- olution air mass transformation model for short range weather forecasting. Monthly Weather Revue, 118, 1561–1575. https://doi.org/10.1175/1520-0493(1990)118<1561:AHRAMT>2.0.CO;2.

Huang, B., Thorne, P.W., Banzon, V.F., Boyer, T., Chepurin, G., Lawrimore, J.H., Menne, M.J., Smith, T.M., Vose, R.S. and Zhang, H.M. (2017) Extended reconstructed sea surface temperature, version 5 (ERSSTv5): upgrades, validations, and intercomparisons. Journal of Climate, 30, 8179–8205. https:// doi.org/10.1175/JCLI-D-16-0836.1.

Indeje, M., Semazzi, F.H. and Ogallo, L.J. (2000) ENSO signals in East African rainfall seasons. International Journal of Climatol- ogy, 20(1), 19–46. https://doi.org/10.1002/(SICI)1097-0088(200001)20:1<19::AID-JOC449>3.0.CO;2-0.

Iversen, T., Bentsen, M., Bethke, I., Debernard, J.B., Kirkevåg, A., Seland, O., Drange, H., Kristjansson, J.E., Medhaug, I.,Sand, M. and Seierstad, I.A. (2013) The Norwegian Earth System Model, NorESM1-M-part 2: climate response and sce- nario projections. Geoscientific Model Development, 6, 389-415. https://doi.org/10.5194/gmd-6-389-2013.

Jacob, D., Elizalde, A., Haensler, A., Hagemann, S., Kumar, P., Pod- zun, R., Rechid, D., Remedio, A.R., Saeed, F., Sieck, K., Teich- mann, C. and Wilhelm, C. (2012) Assessing the transferability of the regional climate model REMO to different coordinated regional climate downscaling experiment (CORDEX) regions. Atmosphere, 3, 181–199.

Jarvis, A., Ramirez-Villegas, J., Campo, H., Vanessa, B. and Navarro-Racines, C. (2012) Is cassava the answer to African cli- mate change adaptation? Tropical Plant Biology, 5, 9–29. https://doi.org/10.1007/s12042-012-9096-7.

Jones, C.D., Hughes, J.K., Bellouin, N., Hardiman, S.C., Jones, G.S., Knight, J., Liddicoat, S., O'Connor, F.M., Andres, R.J., Bell, C., Boo, K.-O., Bozzo, A., Butchart, N., Cadule, P., Corbin, K.D., Doutriaux-Boucher, M., Friedlingstein, P., Gornall, J., Gray, L., Halloran, P.R., Hurtt, G., Ingram, W.J., Lamarque, J.-F., Law, R.M., Meinshausen, M., Osprey, S., Palin, E.J., Parsons Chini, L., Raddatz, T., Sanderson, M.G., Sellar, A.A., Schurer, A., Val- des, P., Wood, N., Woodward, S., Yoshioka, M. and Zerroukat, M. (2011) The HadGEM2-ES implementation of CMIP5 centen- nial simulations. Geoscientific Model Development, 4(3), 543–570.

Jones, P.G. and Thornton, P.K. (2003) The potential impacts of climate change on maize production in Africa and Latin America in 2055. Global Environmental Change, 13(1), 51-59. https:// doi.org/10.1016/S0959-3780(02)00090-0.

Jones, P.W. (1999) First- and second-order conservative remapping schemes for grids in spherical coordinates. Monthly Weather Review, 127, 2204–2210. https://doi.org/10.1175/1520-0493(1999).

Kalognomou, E.-A., Lennard, C., Shongwe, M., Pinto, I., Favre, A., Kent, M., Hewitson, B., Dosio, A., Nikulin, G., Panitz, H.-J. and Büchner, M. (2013) A diagnostic evaluation of precipitation in CORDEX models over southern Africa. Journal of Climate, 26, 9477–9506. https://doi.org/10.1175/JCLI-D-12-00703.1.

Kiehl, J.T., Hack, J.J., Bonan, G.B., Boville, B.A., Breigleb, B.P., Williamson, D. and Rasch, P. (1996) Description of the NCAR community climate model (CCM3). Boulder, CO: National Cen- ter for Atmospheric Research. Technical report number: NCAR/TN-420+STR.

Kim, J., Waliser, D., Mattmann, C., Goodale, C., Hart, A., Zimdars, P., Crichton, D., Jones, C., Nikulin, G., Hewitson, B., Jack, C., Lennard, C. and Favre, A. (2014) Evaluation of the CORDEX-Africa multi-RCM hindcast: systematic model errors. Climate Dynamics, 42, 1189–1202. https://doi.org/10.1007/s00382-013-1751-7.

Kisembe, J., Favre, A., Dosio, A., Christopher, L., Sabiiti, G. and Nimusiima, A. (2018) Evaluation of rainfall simulations over Uganda in CORDEX regional climate models. Theoretical and Applied Climatology, 137, 1117–1134. https://doi.org/10.1007/ s00704-018-2643-x.

Laurent, B., Marticorena, B., Bergametti, G., Leon, J. and Mahowald, N. (2008) Modeling mineral dust emissions from the Sahara Desert using new surface properties and soil data-base. Journal of Geophysical Research, 113, D14218.
https://doi. org/10.1029/2007JD009484.

Lobell, D., Burke, M., Tebaldi, C., Mastrandrea, M., Falcon, W. and Naylor, R. (2008) Prioritizing climate change adaptation needs for food security in 2030. Science, 319(5863), 607–610. https://doi.org/10.1126/science.1152339.

Lohmann, U. and Roeckner, E. (1996) Design and performance of a new cloud microphysics scheme developed for the ECHAM general circulation model. Climate Dynamics, 12, 557–572. https://doi.org/10.1007/BF00207939.

Louis, J.F. (1979) A parametric model of vertical Eddy fluxes in the atmosphere. Boundary-Layer Meteorology, 17, 187–202. https:// doi.org/10.1007/BF00117978.

Luhunga, P., Botai, J. and Kahimba, F. (2016) Evaluation of the per- formance of CORDEX regional climate models in simulating present climate conditions of Tanzania. Journal of Southern Hemisphere Earth System Science, 66, 32-54. https://doi.org/10. 22499/3.6601.005.

Ly, S., Charles, C. and Degre, A. (2013) Geostatistical interpolation of daily rainfall at catchment scale: the use of several variogram models in the Ourthe and Ambleve catchments, Belgium. Hydrology and Earth System Sciences, 15, 2259–2274. https://doi.org/10.5194/hess-15-2259-2011.

Lyon, B. and DeWitt, D.G. (2012) A recent and abrupt decline in the East African long rains. Geophysical Research Letters, 39, L02702. https://doi.org/10.1029/2011GL050337.

Lyon, B. and Vigaud, N. (2017) Unraveling East Africa's climate paradox. In: Climate Extremes. Hoboken, NJ: John Wiley & Sons, Inc., pp. 265-281. https://doi.org/10.1002/9781119068020.ch16.

MacLeod, D. (2019) Seasonal forecasts of the East African long rains: insight from atmospheric relaxation experiments. Climate Dynamics, 53, 4505-4520.

Mariotti, L., Diallo, I., Coppola, E. and Giorgi, F. (2014) Seasonal and intraseasonal changes of African monsoon climates in 21st century CORDEX projections. Climatic Change, 125, 53–65. https://doi.org/10.1007/s10584-014-1097-0.

Morcrette, J.J., Smith, L. and Fouquart, Y. (1986) Pressure and tem- perature dependence of the absorption in long wave radiation parameterizations. Beitraege zur Physik der Atmosphaere, 59, 455–469.

Muhire, I., Ahmed, F. and Abutaleb, K. (2014) Relationships between Rwandan seasonal rainfall anomalies and ENSO events. Theoretical and Applied Climatology, 122, 271–284. https://doi.org/10.1007/s00704-014-1299-4.

Mutai, C., Polzin, D. and Hastenrath, S. (2012) Diagnosing Kenya rainfall in boreal autumn: further exploration. Journal of Cli- mate, 25(12), 4323–4329. https://doi.org/10.1175/JCLI-D-11-00414.1.

Mutai, C.C. and Ward, M.N. (2000) East African rainfall and the tropical circulation/convection on intra-seasonal to inter-annual timescales. Journal of Climate, 13(22), 3915–3939. https://doi.org/10.1175/1520-0442(2000)013<3915:EARATT>2.0.CO;2.

Ngigi, S., Savenije, H., Rockström, J. and Gachene, C. (2005) Hydro-economic evaluation of rainwater harvesting and man- agement technologies: Farmers' investment options and risks in semi-arid Laikipia district of Kenya. Physics and Chemistry of the Earth, Parts A/B/C, 30, 772–782. https://doi.org/10.1016/j. pce.2005.08.020.

Niang, I., Ruppel, O.C., Abdrabo, M.A., Essel, A., Lennard, C., Padgham, J. and Urquhart, P. (2014) Africa. In: Barros, V.R., Field, C.B., Dokken, D.J., Mastrandrea, M.D., Mach, K.J., Bilir, T.E., Chatterjee, M., Ebi, K.L., Estrada, Y.O., Genova, R. C., Girma, B., Kissel, E.S., Levy, A.N., MacCracken, S., Mastrandrea, P.R. and White, L.L. (Eds.) Climate Change 2014: Impacts, Adaptation, and Vulnerability. Part B: Regional Aspects. Contribution of Working

Group II to the Fifth Assess- ment Report of the Intergovernmental Panel on Climate Change. Cambridge and New York, NY: Cambridge University Press, pp. 1199–1265.

Nicholson, S.E. (2000) The nature of rainfall variability over Africa on time scales of decades to Millenia. Global and Planetary Change, 26, 137–158. https://doi.org/10.1016/S0921-8181(00)00040-0.

Nicholson, S.E. (2015) Long-term variability of the East African "short rains" and its links to large-scale factors. International Journal of Climatology, 35(13), 3979–3990. https://doi.org/10. 1002/joc.4259.

Nicholson, S.E. (2017) Climate and climatic variability of rainfall over eastern Africa. Reviews of Geophysics, 55, 590–635.

Nicholson, S.E. and Etekhabi, D. (1986) The quasiperiodic behaviour of rainfall variability in Africa and its relationship to the Southern Oscillation. Archives for Meteorology, Geophysics, and Bioclimatology, Series A, 34, 311–348. https://doi.org/10.1007/ BF02257765.

Nicholson, S.E. and Nyenzi, B.S. (1990) Temporal and spatial varability of SST in the tropical Atlantic and Indian oceans. Meteorology and Atmospheric Physics, 42, 1–17. https://doi.org/10.1007/BF01030575.

Nikulin, G., Jones, C., Giorgi, F., Asrar, G., Büchner, M., Cerezo- Mota, R., Christensen, O.B., Déqué, M., Fernandez, J., Hänsler, A., van Meijgaard, F., Samuelsson, P., Sylla, M.B. and Sushama, L. (2012) Precipitation climatology in an ensemble of CORDEX-Africa regional climate simulations. Journal of Climate, 25(18), 6057–6078. https://doi.org/10.1175/JCLI-D-11-00375.1.

Nogherotto, R., Tompkins, A.M., Giuliani, G., Coppola, E. and Giorgi, F. (2016) Numerical framework and performance of the new multiple-phase cloud microphysics scheme in RegCM4.5: precipitation, cloud microphysics, and cloud radiative effects. Geoscientific Model Development, 9, 2533–2547. https://doi.org/10.5194/gmd-9-2533-2016.

Nordeng, T.E. (1994) Extended versions of the convective parametrization scheme at ECMWF and their impact on the mean and transient activity of the model in the tropics. Reading: ECMWF Research Department, European Centre for Medium Range Weather Forecast. Technical report. https://doi.org/10.21957/ e34xwhysw.

Ntwali, D., Ogwang, B. and Ongoma, V. (2016) The impacts of topography on spatial and temporal rainfall distribution over Rwanda based on WRF model. Atmospheric and Climate Sciences, 6, 145–157. https://doi.org/10.4236/acs.2016.62013.

Ogallo, L.J. (1988) Relationships between seasonal rainfall in East Africa and the Southern Oscillation. Journal of Climatology, 8 (1), 31–43. https://doi.org/10.1002/joc.3370080104.

Ogallo, L.J., Janowiak, J.E. and Halpert, M.S. (1988) Teleconnection between seasonal rainfall over East Africa and global sea sur- face temperature anomalies. Journal of the Meteorological Soci- ety of Japan, 66(6), 807–821.

Ogwang, B.A., Chen, H., Li, X. and Gao, C. (2014) The influence of topography on East African October to December climate: sensitivity experiments with RegCM4. Advances in Meteorology, 2014, 143917. https://doi.org/10.1155/2014/143917.

Oleson, K.W., Dai, Y., Bonan, G.B., Bosilovichm, M., Dickinson, R., Dirmeyer, P. and Zeng, X. (2004) Technical description of the Community Land Model (CLM). Boulder, CO: University Cor- poration for Atmospheric Research. Technical report number: NCAR/TN-461+STR. https://doi.org/10.5065/D6N877R0.

Oleson, K.W., Niu, G.-Y., Yang, Z.-L., Lawrence, D.M., Thornton, P. E., Lawrence, P.J., Stöckli, R., Dickinson, R.E., Bonan, G.B., Levis, S., Dai, A. and Qian, T. (2008) Improvements to the Community Land Model and their impact on the hydrologic cycle. Journal of Geophysical Research, 113, G01021. https://doi. org/10.1029/2007JG000563.

Pfeifer, S. (2006) Modeling cold cloud processes with the regional cli- mate model REMO. PhD thesis, University of Hamburg, Ham- burg, Germany.

Pietikäinen, J.P., O'Donnell, D., Teichmann, C., Karstens, U., Pfeifer, S., Kazil, J., Podzun, R., Fiedler, S., Kokkola, H., Birmili, W., O'Dowd, C., Baltensperger, U., Weingartner, E., Gehrig, R., Spindler, G., Kulmala, M., Feichter, J., Jacob, D. and Laaksonen, A. (2012) The regional aerosol-climate model REMO-HAM. Geoscientific Model Development, 5, 1323–1339. https://doi.org/10.5194/gmd-5-1323-2012.

Prein, A.F., Langhans, W., Fosser, G., Ferrone, A., Ban, N., Goergen, K., Keller, M., Tölle, M., Gutjahr, O., Feser, F., Bris- son, E., Kollet, S., Schmidli, J., van Lipzig, N.P.M. and Leung,

R. (2015) A review on regional convection-permitting climate modeling: demonstrations, prospects, and challenges. Reviews of Geophysics, 53, 323–361. https://doi.org/10.1002/2014RG000475.

Raschendorfer, M. (2001) The new turbulence parameterization of LM. COSMO Newsletter, 1, 89–97.

Rechid, D., Raddatz, T.J. and Jacob, D. (2009) Parameterization of snow-free land surface albedo as a function of vegetation phe- nology based on MODIS data and applied in climate modelling. Theoretical and Applied Climatology, 95, 245–255. https://doi.org/10.1007/s00704-008-0003-y.

Remedio, A.R., Teichmann, C., Buntemeyer, L., Sieck, K., Weber, T., Rechid, D., Hoffmann, P., Nam, C., Kotova, L. and Jacob, D. (2019) Evaluation of new CORDEX simulations using an updated Köppen–Trewartha climate classification. Atmosphere, 10(11), 726. https://doi.org/10.3390/atmos10110726.

Ritter, B. and Geleyn, J.F. (1992) A comprehensive radiation scheme for numerical weather prediction models with potential applications in climate simulations. Monthly Weather Revue, 120, 303–325. https://doi.org/10.1175/1520-0493(1992)120<0303:ACRSFN>2.0.CO,2.

Robert, A.J. (1966) The integration of a low order spectral form of the primitive meteorological equations. Journal of the Meteorological Society of Japan, 44(2), 237–245. https://doi.org/ 10.2151/JMSJ1965.44.5_237.

Roeckner, E., Arpe, K., Bengtsson, L., Christoph, M., Claussen, M., Dümenil, L., Esch, M., Giorgetta, M., Schlese, U. and Schulzweida, U. (1996) The atmospheric general circulation model ECHAM-4: model description and simulation of present- day climate, Vol. 218. Hamburg: Max-Planck-Institut für Meteorologie, p. 171. MPI report. https://doi.org/10.17617/2. 1781494.

Rwanda. (2006) National Adaptation Programmes of Action for Cli- mate Change. Kigali: Ministry of Lands, Environment, Forestry, Water and Mines.

Rwanda. (2011) Green Growth and Climate Resilience-National Strategy on Climate Change and Low Carbon Development. Kigali: Ministry of Natural Resources.

Rwanda. (2018) Evaluation of the Green Growth and Climate Resil- ience Strategy

Implementation. Kigali: Ministry of Environment. Rwanda. (2019) National Environment and Climate Change Policy. Kigali: Ministry of Environment.

Rwanda. (2020) Nationally Determined Contribution. Kigali: Ministry of Environment.

Rwanda Environment Management Authority. (2018) Assessment of Climate Change Vulnerability in Rwanda. Kigali: Rwanda.

Safari, B. (2012) Trend analysis of the mean annual temperature in Rwanda during the last fifty-two years. Journal of Environmental Protection, 3, 538–551. https://doi.org/10.4236/jep.2012.36065.

Saji, N.H., Goswami, N., Vinayachandran, P.N. and Yamagata, T. (1999) A dipole mode in the tropical Indian Ocean. Nature, 401 (6751), 360–363. https://doi.org/10.1038/43854.

Sawadogo, W., Reboita, M.S., Faye, A., da Rocha, R.P., Odoulami, R.C., Olusegun, C.F., Adeniyi, M.O., Abiodun, B.J., Sylla, M.B., Diallo, I., Coppola, E. and Giorgi, F. (2021) Current and future potential of solar and wind energy over Africa using the RegCM4 CORDEX-CORE ensemble. Climate Dynamics, 57, 1647–1672. https://doi.org/10.1007/s00382-020-05377-1.

Schrodin, R. and Heise, E. (2001) The multi-layer version of the DWD soil model TERRA-LM. Offenbach: COSMO. Technical report number: 2. https://doi.org/10.5676/DWD_pub/nwv/ cosmo-tr_2.

Schulz, J.-P., Vogel, G., Becker, C., Kothe, S., Rummel, U. and Ahrens, B. (2016) Evaluation of the ground heat flux simulated by a multi-layer land surface scheme using high-quality observations at grass land and bare soil. Meteorologische Zeitschrift, 25, 607–620. https://doi.org/10.1127/metz/2016/0537.

Sen, P.K.J. (1968) Estimates of the regression coefficient based on Kendall's tau. Journal of the American Statistical Association, 63, 1379–1389. https://doi.org/10.2307/2285891.

Shongwe, M., Lennard, C., Liebmann, B., Kalognomou, E.-A., Ntsangwane, L. and Pinto, (2014) An evaluation of CORDEX regional climate models in simulating precipitation over south- ern Africa. Atmospheric Science Letters, 16(3), 199–207. https://doi.org/10.1002/asl2.538.

Siebert, A., Dinku, T., Vuguziga, F., Twahirwa, A., Kagabo, D., del Corral, J. and Robertson, A. (2019) Evaluation of ENACTS- Rwanda; a new multi-decade, high-resolution rainfall and temperature dataset: climatology. International Journal of Climatology, 39, 3104–3120.

https://doi.org/10.1002/joc.6010.

Simon, J.M. and Lisa, G. (2001) Probabilistic precipitation anomalies associated with ENSO. Bulletin of the American Meteorological Society, 82(4), 618–639. https://doi.org/10.1175/1520-0477 (2001)082<0619:PPAAWE>2.3.CO;2.

Sneyers, R. (1990) On the statistical analysis of series of observations. Geneva: World Meteorological Organization. WMO Technical Note 143, WMO No. 415, TP-103.

Sørland, S.L., Brogli, R., Pothapakula, P.K., Russo, E., Van de Walle, J., Ahrens, B., Anders, I., Bucchignani, E., Davin, E.L., Demory, M.-E., Dosio, A., Feldmann, H., Früh, B., Geyer, B., Keuler, K., Lee, D., Li, D., van Lipzig, N.P.M., Min, S.-K., Panitz, H.-J., Rockel, B., Schär, C., Steger, C. and Thiery, W. (2021) COSMO-CLM regional climate simulations in the Coor- dinated Regional Climate Downscaling Experiment (CORDEX) framework: a review. Geoscientific Model Development, 14, 5125–5154. https://doi.org/10.5194/gmd-14- 5125-2021.

Steppeler, J., Doms, G., Schättler, U., Bitzer, H.W., Gassmann, A., Damrath, U. and Gregoric, G. (2003) Meso-gamma scale fore- casts using the non-hydrostatic model LM. Meteorology and Atmospheric Physics, 82, 75–96. https://doi.org/10.1007/s00703-001-0592-9.

Stevens, B., Giorgetta, M., Esch, M., Mauritsen, T., Crueger, T., Rast, S., Salzmann, M., Schmidt, H., Bader, J., Block, K., Brokopf, R., Fast, I., Kinne, S., Kornblueh, L., Lohmann, U., Pincus, R., Reichler, T. and Roeckner, E. (2013) Atmospheric component of the MPI-M earth system model: ECHAM6. Journal of Advances in Modeling Earth Systems, 5, 146–172. https://doi.org/10.1002/jame.20015.

Tanre, D., Geleyn, J.F. and Slingo, J.M. (1984) Results of the introduction of an advanced aerosol-radiation interaction in the ECMWF low resolution global model. In: Aerosols and their Climatic Effects. Hampton, VA: Deepak Publication, pp. 133–177.

Taylor, K. (2001) Summarizing multiple aspects of model performance in a single diagram. Journal of Geophysical Research, 106, 7183–7192. https://doi.org/10.1029/2000JD900719.

Tegen, I., Hollrig, P., Chin, M., Fung, I., Jacob, D. and Penner, J. (1997) Contribution of different aerosol species to the global aerosol extinction optical thickness: estimates from model results. Journal of Geophysical Research, 102, 23895–23915.

https://doi.org/10.1029/97JD01864.

Teichmann, C., Jacob, D., Remedio, A.R., Remke, T., Buntemeyer, L., Hoffmann, P., Kriegsmann, A., Lierhammer, L., Bülow, K., Weber, T., Sieck, K., Rechid, D., Langendijk, G., Coppola, E., Giorgi, F., Ciarlo, J.M., Raffaele, F., Giuliani, G., Xuejie, G., Sines, T., Torres-Alavez, J., Das, S., Di Sante, F., Pichelli, E., Glazer, R., Ashfaq, M., Bukovsky, M., and Im, E.- S. (2021) Assessing mean climate change signals in the global CORDEX-CORE ensemble. Climate Dynamics, 57, 1269–1292. https://doi.org/10.1007/s00382-020-05494-x.

Thiery, W., Davin, E.L., Panitz, H.J., Demuzere, M., Lhermitte, S. and Van Lipzig, N. (2015) The impact of the African Great Lakes on the regional climate. Journal of Climate, 28(10), 4061–4985.

Tiedtke, M. (1989) A comprehensive mass flux scheme for cumulus parameterization in large-scale models. Monthly Weather Revue, 117, 1779–1800. https://doi.org/10.1175/1520-0493(1989)117<1779:ACMFSF>2.0.CO,2.

Tiedtke, M. (1993) Representation of clouds in large-scale models. Monthly Weather Revue, 121, 3040–3061. https://doi.org/10. 1175/1520-0493(1993)121<3040:ROCILS>2.0.CO;2.

Tompkins, A.M., Gierens, K. and Rädel, G. (2007) Ice supersatura- tion in the ECMWF integrated forecast system. Quarterly Jour- nal of the Royal Meteorological Society, 133, 53–63. https://doi.org/10.1002/qj.14.

Trenberth, K.E. (1997) The definition of El Niño. Bulletin of the American Meteorological Society, 78(12), 2771–2777. https://doi.org/10.1175/1520-477(1997)078<2771:TDOENO>2.0.CO;2.

Trenberth, K.E. and Stepaniak, D.P. (2001) Indices of El Niño evo- lution. Journal of Climate, 14, 1697–1701. https://doi.org/10. 1175/1520-0442(2001)0142.0.CO;2.

Trzaska, S. and Schnarr, E. (2014) A Review of Downscaling Methods for Climate Change Projections. Burlington: African and Latin American Resilience to Climate Change (ARCC). Available at: http://www.ciesin.org/documents/Downscaling_CLEARED_000.pdf.

Gupta, A.S., England, M.H. and Reason, C.J. (2009) Contributions of Indian Ocean sea surface temperatures to enhanced East African rainfall. Journal of Climate, 22(4), 993– 1013. https://doi.org/10.1175/2008JCLI2493.1.

Uwihirwe, J., Hrachowitz, M. and Bogaard, T.A. (2020) Landslide precipitation thresholds in Rwanda. Landslides, 17, 2469–2481. https://doi.org/10.1007/s10346-020-01457-9.

van Vuuren, D.P., Edmonds, J., Kainuma, M., Riahi, K., Thomson, A., Hibbard, K., Hurtt, G.C., Kram, T., Krey, V., Lamarque, J.- F., Masui, T., Meinshausen, M., Nakicenovic, N., Smith, S.J., and Rose, S.K. (2011) The representative concentration path- ways: an overview. Climatic Change, 109, 5. https://doi.org/10. 1007/s10584-011-0148-z.

Will, A., Akhtar, N., Brauch, J., Breil, M., Davin, E., Ho- Hagemann, H.T.M., Maisonnave, E., Thürkow, M. and Weiher, S. (2017) The COSMO-CLM 4.8 regional climate model coupled to regional ocean, land surface and global earth system models using OASIS3-MCT: description and performance. Geoscientific Model Development, 10, 1549–1586. https://doi.org/10.5194/gmd-10-1549-2017.

Williams, A.P., Funk, C., Michaelsen, J., Rauscher, S.A., Robertson, I., Wils, T.H.G., Koprowski, M., Eshetu, Z. and Loader, N.J. (2012) Recent summer precipitation trends in the Greater Horn of Africa and the emerging role of Indian Ocean sea surface temperature. Climate Dynamics, 39(9–10), 2307– 2328. https://doi.org/10.1007/s00382-011-1222-y.

World Bank. (2019) Systematic country diagnostic. Washington, DC: World Bank. Report number: 138100-RW. Available at: https:// documents1.worldbank.org [Accessed on 25th June 2019].

Wu, M., Nikulin, G., Kjellström, E., Belusˇi´c, D., Jones, C. and Lindstedt, D. (2020) The impact of regional climate model for- mulation and resolution on simulated precipitation in Africa. Earth System Dynamics, 11, 377–394. https://doi.org/10.5194/esd-11-377-2020.

Yang, W., Seager, R., Cane, M.A. and Lyon, B. (2014) The East Afri- can long rains in observations and models. J. Climate, 27, 7185– 7202. https://doi.org/10.1175/JCLI-D-13-00447.1

Yang, W., Seager, R., Cane, M.A. and Lyon, B. (2015) The annual cycle of East African precipitation. Journal of Climate, 28(6), 2385–2404. https://doi.org/10.1175/JCLI-D-14-00484.1.

Wicker., Louis J., Skamarock, and William, C. (2002) Time-splitting methods for elastic models using forward time schemes. Monthly Weather Review, 130(8), 2088-2097. https://doi.org/10. 1175/1520-0493

Chapter 3 Trends and Variability in Temperature and Related Extreme Indices in Rwanda during the Past Four Decades

This Chapter reproduces the content of our published paper (https://doi.org/10.3390/atmos14091449).

3.1 Introduction

During the last decades, we have observed an increase in the intensity, frequency, and extent of natural disasters and environmental degradation in various places on the Earth. Those effects have been associated with climate change and variability (Brohan et al., 2006; IPCC, 2007; Bouwer, 2011; Comiso et al., 2015; Thomas and López, 2015; IPCC, 2021). According to the recent Sixth Assessment Report (AR6) of the Intergovernmental Panel on Climate Change (IPCC) (IPCC, 2021), a global warming of 1.09 °C has been observed between the Industrial Revolution period up to the present, resulting in climate change and variability. This warming is largely attributed to anthropogenic activities. It is projected that this warming will continue to increase until it reaches an average of 1.5 °C in the 2030s, regardless of how much greenhouse gas emissions rise or fall in the coming decade. Specifically, in East Africa, major cities have witnessed an increase in temperatures that almost double the global warming experienced since pre-industrial times (Engelbrecht et al., 2015; WMO, 2020; East Africa Hazards Watch, 2023). Observations in this region indicate a rapid warming of about 1.9 °C as the maximum temperature and 1.2 °C as the minimum temperature during the period 1979 to 2010 (Gebrechorkos et al., 2019) and a mean temperature increase of 2 °C from 1963 to 2012 (Daron, 2014). During the last years, East Africa has been subject to more recurrent, intense, and prolonged droughts (Russo et al., 2016; Herold et al., 2017; Nashwan and Shahid, 2019; Gebrechorkos et al., 2019; Ayugi et al., 2020; Choi et al., 2023), causing frequent migrations of populations triggered by water scarcity, the drying of crops, famine, and food insecurity (Abebe, 2014; Ayugi et al., 2020; Mueller et al., 2020; Doherty et al., 2022; Bannor et al., 2023). Climate change is likely to affect health in East Africa, resulting in a number of direct and indirect impacts, Malaria being among the greatest threats to human health (Zhou et al., 2004). Particularly in Rwanda, a study by Safari, (2012) indicated that during the period of 1958 to 2010, the annual mean temperature in Kigali City increased by 0.0455 °C/year. This was suggested to be associated with a possible urbanization and growing population. Another

study by Safari (2010) showed that in 2004, water levels decreased considerably, resulting in a reduction in power generation. Rwanda's low-lying eastern region has recently seen a rise in mean temperature, statistically significant unpredictability in the duration and frequency of droughts causing environmental and infrastructure damage, and a loss of crop output and livestock (Li et al., 2021; Uwimbabazi et al., 2022). The northwestern high-elevated area has experienced an increased potential for Malaria disease (Loevinsohn, 1994; Henninger, 2013; Maniragaba et al., 2018). The strong variability in temperature has affected crop production, impacting the economy of the country (Lydie, 2016; Hunter et al., 2020).

Most studies using observational temperature have focused on changes in mean values. Recent studies have shown that extreme temperatures have major impacts on important socio-economic sectors such as agriculture, power generation and consumption, and human health (Easterling et al., 2000; Meehl et al., 2000; Walther et al., 2002). In accordance with the definition of climate extreme by the authors of (Lal et al., 2012), air temperature is "extreme" when it reaches or is higher (lower) than an assumed threshold value corresponding to a tolerance limit (Revadekar et al., 2012). Assessing changes in extremes requires objectively defining and quantifying the various types of extremes in weather parameters. The World Meteorological Organization (WMO) Commission for Climatology Expert Team on Climate Change Detection, Monitoring and Indices (ETCCDMI) has played an important role in developing a number of relevant indices and enabling their global analyses via regional participation (Caesar et al., 2006; Diaz and Murnane, 2008; Rettie et al., 2023). Statistical studies of extreme temperature indices are important for the analysis of their frequency of occurrence, spatial distribution, and duration (Diaz and Murnane, 2008).

Studies in regions other than Africa based on observational data have analyzed the frequencies of warm and cold events and have indicated that warm extremes are increasing and cold extremes are decreasing (Caesar et al., 2006; Rettie et al., 2023). Analyzing station data over East Africa during the period of 1967-2009, Ngaina and Mutai, (2013) found that the maximum temperature extremes increased while minimum temperature extremes decreased with a statistically significant rise in the number of warm days and warm nights and a decrease in the number of cold days and cold nights. The space-time pattern of the observed changes was found to be not well organized. Similar results were obtained by Omondi et al., (2014) studying the changes in temperature extremes over the Greater Horn of Africa region during the period of 1961-2010. A study by Ngarukiyimana et al., (2021) on Rwanda during the period of 1961-2014 has indicated that the minimum temperature

increased at a faster rate than the maximum temperature, resulting in the decrease in the diurnal temperature range in the northern region of the country. In their study, Cheng et al., (2014) and Lei et al., (2020) have shown that the decrease in the diurnal temperature range has caused impacts on the health of the population.

Understanding climate change impacts is needed to inform policy and decision makers for the formulation of policies on mitigation and adaptation. The integration of these policies into strategies and implementation plans of key economic sectors of the country is important to ensure stability and sustainable development (Bastin et al., 2019). So far, Rwanda has implemented a multitude of policy initiatives. Nevertheless, several challenges and needs still remain in regard to comprehending the underlying mechanism of climate change and variability, as well as their repercussions on crucial sectors of the economy, including agriculture, health, water resources, infrastructure, and energy (Rwanda, 2006; Rwanda, 2011; Rwanda, 2018; Rwanda, 2019; (Clay and King, 2019; Rwanda, 2020; Trevor, 2021; Kim et al., 2022; Rwanda, 2022). Further needs include minimizing uncertainties in seasonal forecasting, improving methodologies and tools for climate change monitoring and detection (WMO, 2004; White et al., 2013; STAP, 2017), and vulnerability and adaptation assessment (FAO, 2018). To this end, objective information derived from meteorological data is required.

Therefore, this present study intends to analyze trends and variabilities of minimum, maximum, and mean temperatures as well as extreme temperature indices using high-resolution daily gridded data (5 km) over Rwanda for the period of 1983 to 2022. This work is organized into the following sections. Section one outlines the characteristics of the study area, data, and methodology; section two presents the results and discussion, while the conclusion and recommendations are indicated in the third section.

3.2 Materials and Methods

3.2.1 Study Area

Rwanda is part of the East Africa region with total area of 26,338 km^2, where land area is about 24,950 km^2 (94.7%), and inland lakes cover about 1390 km^2 (5.3%) (Figure 3.1). Agricultural land covers 14,020 km^2 (59%) of total country land. The hydrological network comprises numerous lakes, rivers, and associated wetlands. The topography of Rwanda is complex, ranging from high to lowland areas, with a mixture of mountains, hills, and valleys. Rwanda has five climate types

(Henninger, 2013): The first is the savanna type located in the East-Rwandan dry and hot lowland zone lying from the border with neighboring Tanzania in the east and stretching gradually from east to west and spreading beyond the surrounding area of the capital, Kigali City. The second is the temperate type located in the central highlands zone with elevation that increases from east to west. In that area, rainfall also increases markedly following the elevation. The third is the humid mountain climate type covering southern Rwanda area, especially around the Nyungwe National Park located on the Congo-Nile Divide. The fourth is the dry mountain climate type found in the Virunga National Park, located in the volcanic mountains of northern region. The fifth is Kivu-sea climate type along the coastal ridge of Lake Kivu, where land-lake wind circulation interacts with high evaporation rates prevailing on Lake Kivu to create amounts of rainfall on the western bridge of the Congo-Nile watershed, thus making it a distinct regional climate system.

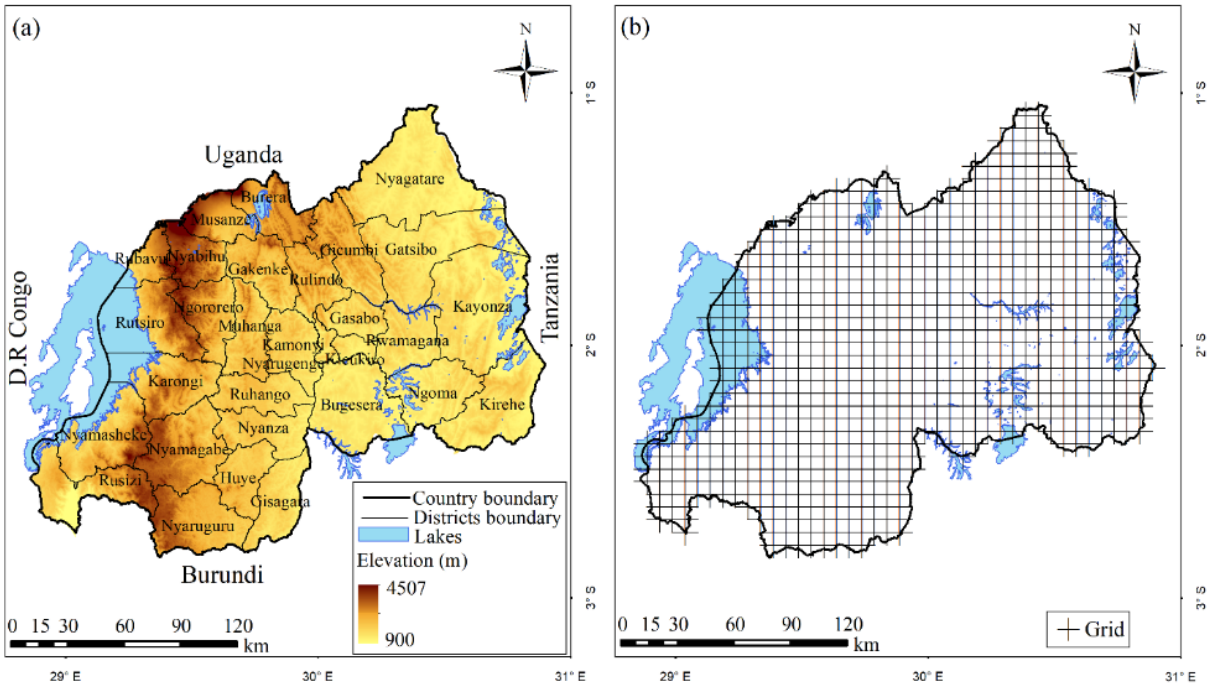

Figure 3. 1 The elevation map of Rwanda (a) and the grid covering the study area (b).

The country experiences four seasons: the short dry season (January–February, JF), the long rain season (March-April–May, MAM), the long dry season (June-July-August, JJA), and the short rain season (September-October-November-December, SOND). In general, maximum and minimum temperatures decrease gradually with topography from the eastern to the western parts of the country in all seasons. The average temperature for Rwanda is around 20°C and varies with

the topography. The warmest annual average temperatures are found in the eastern plateau (20-21°C) and south-eastern valley of Rusizi (23-24°C) in the south-west, and cooler temperatures are found in higher elevations of the central plateau (17.5-19 °C) and high-lands (<17 °C) in the north and north-west.

According to Fifth National Population and Housing Census held in 2022 (National Institute of Statistics of Rwanda, 2023), the country's population is 13,246,394, which corresponds to an annual growth rate of 2.3% between 2012 and 2022. Men represent 48.5% of the population, while women represent 51.5%. The population accessing improved drinking water is 79%, while 12% have access to safely managed water drinking services. In total, 72.1% of Rwandans live in rural areas, while 27.9% live in urban areas. In 2022, GDP at current market prices was estimated at RWF 13,716 billion. Services sector contributed 47% of GDP, agriculture sector contributed 25% of the GDP, and industry sector contributed 21% of GDP, while 7% was attributed to adjustment for taxes and fewer subsidies on products.

Despite the recent experience that the East African region has known and knows today, the impacts of climate change have not spared Rwanda (Herold et al., 2017) (Nashwan & Shahid, 2019)(Choi et al., 2023). The country has committed to undertake adaptation and mitigation measures to the greatest extent possible for vulnerable communities. However, to achieve this, it is necessary to have objective information from scientifically analyzed meteorological observations. With the development that Rwanda has experienced during last decades after 1994 Genocide Against the Tutsi, meteorological services have significantly increased their capacity and the number of active meteorological stations covering the whole country. This enabled us to undertake an initiative, via collaboration with experts, of displaying observed meteorological data on a grid of 5 km resolution (Dinku et al., 2014; Siebert et al., 2019). The resulting gridded data set consisted of a combination of quality controlled station data with satellite data for rainfall and reanalysis data for temperature to fill the gaps. Such development has motivated researchers to undertake some studies on climate change in Rwanda.

3.2.2 Data and Methods

3.2.2.1 Data

Gridded data sets of the maximum and minimum temperatures covering the period from 1983 to 2022 at a spatial resolution of 0.05 degrees (~5 km) were provided by the Rwanda Meteorology

Agency (METEO-RWANDA). They can be accessed online at https://www.meteorwanda.gov.rw. They were reconstructed in Meteo Rwanda following the methodology described by Dinku et al., (2014) and Siebert et al., (2019). A quality control (homogeneity test, missing data, and outliers) was first carried out on temperature data from 66 Rwandan weather stations. To address temporal and spatial gaps in the data time series, a combination with bias-adjusted Japanese 55-year reanalysis project (JRA55) was then performed.

3.2.2.2 Methods

Extreme Temperature Indices

Five extreme temperature indices (Table 3. 1) were computed based on the methodology provided by Expert Team on Climate Change Detection and Indices (ETCCDI) (Karl et al., 1999; Tank et al., 2009; Zhang et al., 2011). Percentile-based threshold indices were computed for each calendar day using data for consecutive 5-day moving windows centered on that calendar day (Zhang and Yang, 2004) from the 1991-2020 base period. The computation of extreme temperature indices and their corresponding thresholds was carried out using RClimDex v1.0 base package (Zhang and Yang, 2004).

Table 3. 1 List of extreme temperature indices used in this study.

Index	Description	Definition	Unit	Reference
DTR	Diurnal temperature range	Annual mean difference between daily maximum and minimum temperature	°C	(Folland et al., 2001)
Tn10p	Cold nights	Number of days in a year with minimum temperature below a threshold corresponding to 10th percentile of daily minimum temperature distribution in the 1991–2020 baseline period.	days/year	(Karl et al., 1999; Tank et al., 2009; Zhang et al., 2011)

Tx10p	Cold days	Number of days in a year with maximum temperature below a threshold corresponding to 10^{th} percentile of daily maximum temperature distribution in the 1991–2020 baseline period.	days/year	(Karl et al., 1999; Tank et al., 2009; Zhang et al., 2011)
Tn90p	Warm nights	Number of days in a year with minimum temperature above a threshold corresponding to 90^{th} percentile of daily minimum temperature distribution in the 1991-2020 baseline period.	days/year	(Karl et al., 1999; Tank et al., 2009; Zhang et al., 2011)
Tx90p	Warm days	Number of days in a year with maximum temperature above a threshold corresponding to 90^{th} percentile of daily maximum temperature distribution in the 1991-2020 baseline period.	days/year	(Karl et al., 1999; Tank et al., 2009; Zhang et al., 2011)

- ***The Mann–Kendall (MK) Trend Test and Theil–Sen's Slope Estimator (TSS)***

The non-parametric Mann-Kendall test and the Theil-Sen's slope estimator approach is widely used as trend tests as well as for estimation of magnitudes of trends in hydrology and climate time series (Sneyers, 1990; Safari, 2012; Tan et al., 2015). They have been recommended by the World Meteorological Organization (WMO) owing to their compatibility with non-normalized data as well as missing values (Sneyers, 1990).

- *The Mann–Kendall test*

Let $(x_1, y_1), (x_2, y_2), \dots, (x_n, y_n)$ be a set of joint observations from two random variables X and Y respectively, such that all the values of the couple (x_i, y_i) are unique. Kendall's rank correlation measures the strength of monotonic association between the vectors X and Y.

The Mann-Kendall test statistic is calculated from the sum of the signs (+ or −) of the slopes. The statistic *S* called Kendall score is expressed as

$$S = \sum_{k=1}^{n-1} \sum_{j=k+1}^{n} sign(x_j - x_k) \quad (1)$$

where n is the length of the sample, x_k and x_j are from $k = 1, 2, \dots, n-1$ and $j = k + 1, 2, \dots, n$, and the $sign(x_j - x_k)$ is an indicator function that takes on the values 1, 0, or −1, as indicated below:

$$sign(x_j - x_k) = \begin{cases} +1 \; if \; (x_j - x_k) > 0 \\ 0 \; if \; (x_j - x_k) = 0 \\ -1 \; if \; (x_j - x_k) < 0 \end{cases} \quad (2)$$

If $n \geq 10$, the statistic S is approximately normally distributed with the mean $(S) = 0$, and the variance of S can be obtained as follows:

$$var(S) = \frac{n(n-1)(2n+5) - \sum_{j=1}^{p} t_j(t_j - 1)(2t_j + 5)}{18} \quad (3)$$

where p is the number of ties in the series, and t_j is the number of data points in the j^{th} tied group. For trend test, the variable *Y* can be time. The presence of statistically significant trend is evaluated using the Z value. This statistic is used to test the null hypothesis such that no trend exists. The standardized test statistic *Z* is given via

$$Z = \begin{cases} \frac{S-1}{\sqrt{var(S)}}, if \; S > 0 \\ 0, \qquad if \; S = 0 \\ \frac{S+1}{\sqrt{var(S)}}, if \; S < 0 \end{cases} \quad (4)$$

The trend is said to be increasing (decreasing) if Z is positive (negative). To test for either increasing or decreasing monotonic trends with confidence level α, the null hypothesis H_0 is rejected if $|Z| > Z_{(1-\alpha/2)}$, where $Z_{(1-\alpha/2)}$ is the corresponding value of $p = \alpha/2$, following the

standard normal cumulative distribution tables, and represents the standard normal deviates, and p is the significant level for the test.

- *Autocorrelation*

The presence of positive or negative autocorrelation in the time series may increase the possibility of detecting trends while there is no trend and vice versa (Hamed and Rao, 1998; Serrano et al., 1999; Yue et al., 2003k; Novotny and Stefan, 2007). The existence of positive autocorrelation in the series can lead the Mann-Kendall test to a conclusion of the presence of trend in the series, while it may not be always true. On the other hand, the existence of negative autocorrelation in the series can lead to the opposite.

The coefficient of autocorrelation ρ_k of a discrete time series for lag-*k* is obtained following the formula adopted by Datta and Das, (2019) as follows:

$$\rho_k = \frac{\sum_{i=1}^{n-k}(x_i - \bar{x})(x_{i+k} - \bar{x}_{i+k})}{\left[\sum_{i=1}^{n-k}(x_i - \bar{x})^2 \mathrm{x} \sum_{i=1}^{n-k}(x_{i+k} - \bar{x}_{i+k})^2\right]^{\frac{1}{2}}} \quad (5)$$

- *The Modified Mann–Kendall (MMK) test*

A modified Mann-Kendall test was proposed by Ahmed et al., (2017) to take into consideration the influence of autocorrelation in data, which is often ignored. A correction is brought to the variance of *S* (Yue et al., 2003; Taxak et al., 2014; Mahrt, 2014; Das et al., 2022), which is replaced by

$$var^*(S) = var(S)\frac{n}{n_k^*} \quad (6)$$

where $\frac{n}{n_k^*}$ represents a correction due to the autocorrelation in the data and is given via

$$\frac{n}{n_k^*} = 1 + \frac{2}{n(n-1)(n-2)}\sum_{i=1}^{n-1}(n-i)(n-i-1)(n-i-2)\rho_k \quad (7)$$

where n is the actual number of observations, n_k^* represents the effective number of observations to account for the autocorrelation in the data, and ρ_k is the autocorrelation function of the ranks of the observations. As the non-significant values of ρ_k can badly affect the precision of the variance of S, and thus, only significant ρ_k values are opted to estimate $\frac{n}{n_k}$ (Mondal et al., 2012). In this method, the autocorrelation*s* ρ_k between ranks of the observations have been calculated from the respective time series after subtracting from the time series an estimate of Sen's slope (described

below) from the data. The Mann-Kendall test was then applied with the corrected variance $var^*(S)$.

- *Theil–Sen slope estimator*

In a case where a linear trend exists in a time series, the slope or magnitude of that trend can be detected using a simple non-parametric procedure first developed by Theil (Sen, 1968) and later modified by Sen (Theil, 1992). Sen's slope has the advantage over the slope of regression, in the sense that gross data series errors and outliers do not affect it much. The slope is determined to be the mean of all pair-wise slopes for any pair of points in the dataset. The following equation is used to estimate each individual slope:

$$Q_{ij} = \frac{x_j - x_i}{j - i}, j > i \text{ , for } i = 1,2, \dots, N \quad (8)$$

If in the time series, there are n values of Q_{ij}, estimates of the slope will be $N = n(n-2)/2$. The slope of the Sen Estimator is the mean slope of such N values of pair-wise slopes. The Sen's slope is obtained using

$$Q = \text{Median}\left(\frac{x_j - x_i}{j - i}\right), j > i, \text{for } i = 1,2, \dots, N \quad (9)$$

$$Q = \begin{cases} Q_{\left\lceil \frac{N+1}{2} \right\rceil} & if\ n\ is\ odd \\ \frac{1}{2}\left(Q_{\frac{N}{2}} + Q_{\left\lfloor \frac{N+2}{2} \right\rfloor}\right) & if\ n\ is\ even \end{cases} \quad (10)$$

Positive value of Q indicates an upward or increasing trend and a negative value of Q gives a downward or decreasing trend in the time series.

In this present study, trends were computed at each grid point for time series of maximum temperature, minimum temperature, and extreme temperature indices using the Modified Mann-Kendall non-parametric rank statistic test (Chechin et al., 2019) and the Theil-Sen (TS) estimator approach (Allabakash and Lim, 2022) for, respectively, trend analysis and slope estimation. Trends were computed at the scale of a year and then converted at a scale of decade for analysis. Significant trends were considered at confidence level $\alpha = 0.05$. The standard deviation was computed at each grid for time series of respective indexes to represent their variabilities. They were computed and then analyzed at annual scale for the period of study. In climate studies, spatial interpolation is important for local analysis by Geographic Information Systems (GIS). Two different methods are commonly used: the Kriging method and Inverse Distance Weighted (IDW)

method (Weber and Englund, 1992, Weber and Englund, 1994). Kriging method is a geostatistical interpolation method that takes into consideration the distance and the degree of variation between known data points when estimating values at neighboring unknown locations. IDW uses a linear weighted combination of known data points, taking into account the distance, i.e., giving more weight to a closer data point and less weight to distant one. The advantage of Kriging interpolation method to IWD is that it is statistically optimal interpolator for dense and well spatially distributed data (Setianto and Triandini, 2015). However, IWD interpolation method may be preferred over Kriging for sparse data. In this present study, maps were generated using Kriging interpolation method for spatial interpolation with the ArcGIS10 software. Spatially aggregated mean maximum temperature, minimum temperature, and extreme temperature indices were computed by taking simple arithmetic averages of respective indexes for all grids, and their trends were further analyzed.

3.3 Results

3.3.1 Spatial Distributions of Long-Term Mean of Tx, Tn, and T

Figure 3. 2 presents the spatial distribution of the long-term mean of Tx, Tn, and T over Rwanda during the period of 1983-2022. In general, Tx, Tn, and T decrease gradually with topography from the eastern to the western parts of the country in all seasons. Tx and T have maximum values during the JJA and JF seasons and minimum values during MAM and SOND. Tn has the lowest value during JJA and the highest value during MAM.

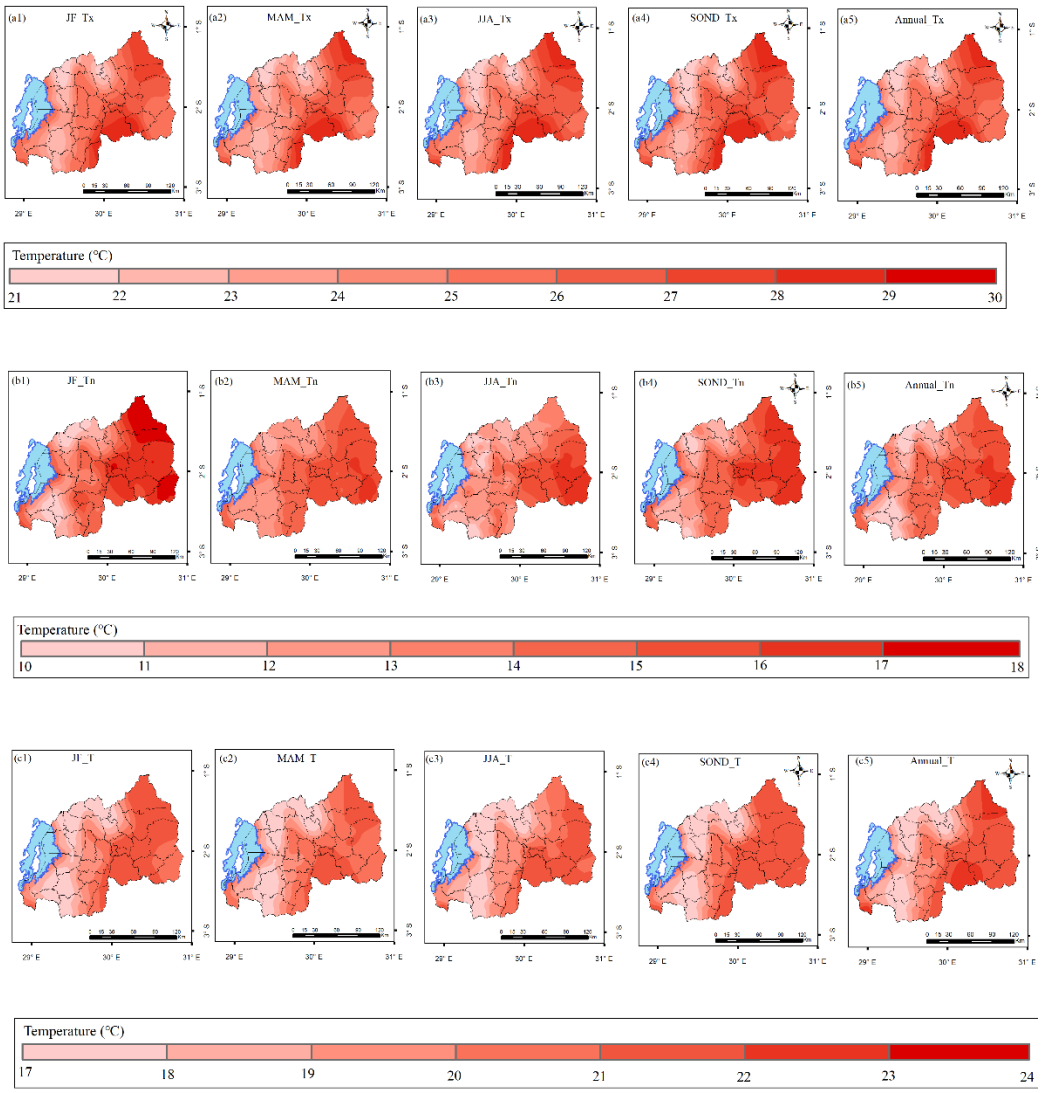

Figure 3. 2 Spatial distribution of long-term mean of Tx, Tn, and T over Rwanda during the period of 1983–2022 expressed in °C. Tx for JF (a1), Tx for MAM (a2), Tx for JJA (a3), Tx for SOND (a4), Tx for mean annual (a5),Tn for JF (b1), Tn for MAM (b2), Tn for JJA (**b3**), Tn for SOND **(b4),** Tn for mean annual (**b5**), T for JF (**c1**), T for MAM (**c2**), T for JJA (**c3**), T for SOND (**c4**), T for mean annual (**c5**), (Computed from the data used in this study, obtained from Rwanda Meteorology Agency).

3.3.2 Trends of Temperatures

Figure 3. 3 presents the spatial distribution of trends Tx, Tn, and T over Rwanda during the period of 1983–2022 expressed in °C/decade for seasons and the annual average. In general, temperatures

decrease gradually with topography from the eastern to the western parts of the country in all seasons. The analysis of the spatial distribution of the trends of temperatures indicates that for Tx, the southeastern (Kirehe District) and the southwestern (Nyamasheke and Rusizi Districts) present the highest but moderate statistically significant positive trend (0.24–0.40 °C/decade) during JJA and SOND. During MAM, the southeastern part of the country (Kirehe District) indicates statistically significant high positive trends (0.40–0.56 °C/decade). For Tn, statistically high significant positive trends (0.48–0.64 °C/decade) are observed during SOND across the country. No statistically significant trend is observed for the annual mean of Tn. As for T, statistically significant high positive trends (0.24–0.40 °C/decade) are observed over the southeastern part of the country (Kirehe District) during MAM and over the southwestern (Nyamasheke and Rusizi Districts) and southern of the eastern region (Bugesera and Ngoma Districts) during SOND. Statistically significant increasing trends are observed for spatially averaged Tn during JJA (0.17 °C/decade) and SOND (0.20 °C/decade) as well for T during SOND (0.16 °C/decade).

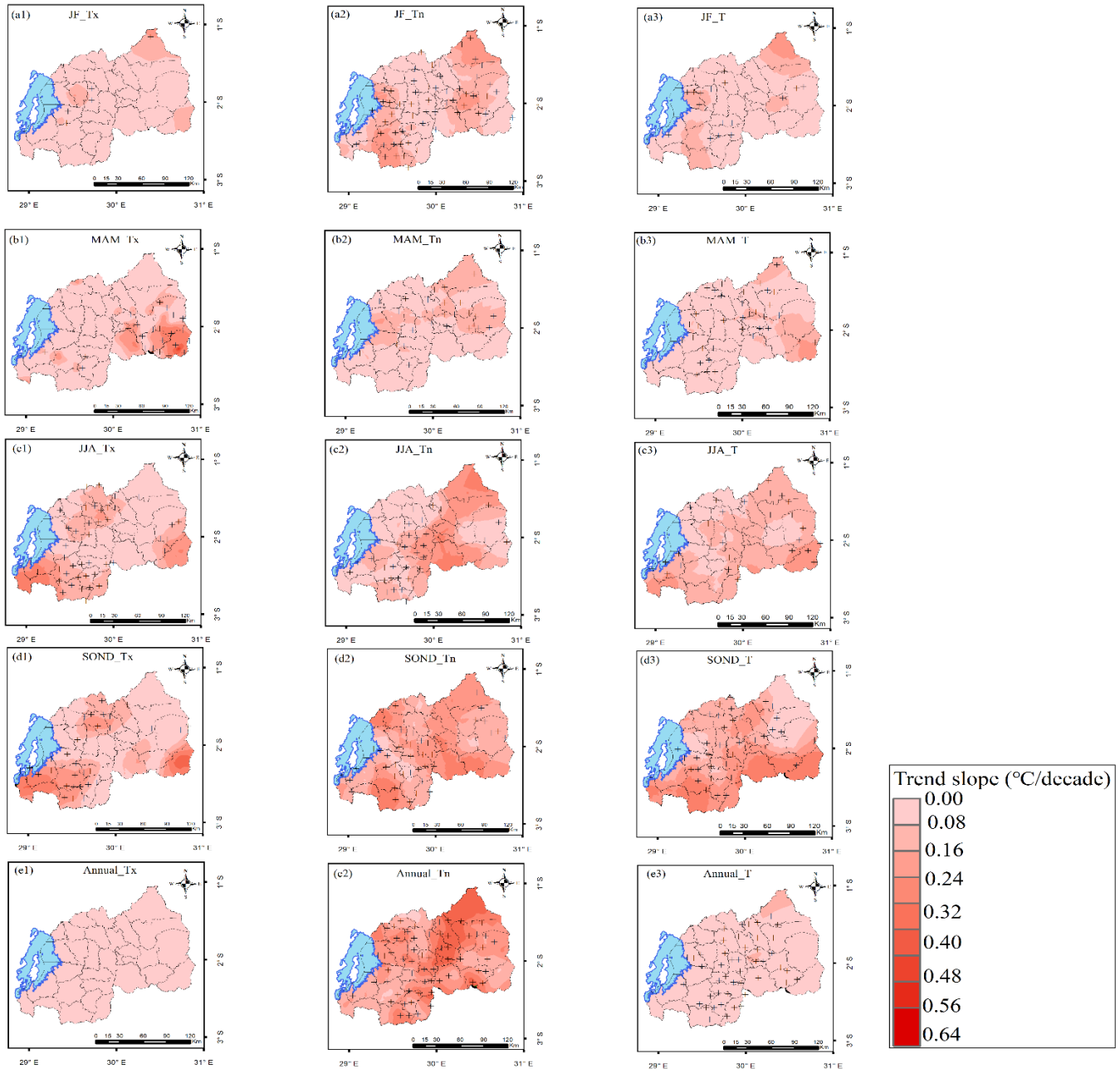

Figure 3. 3 Spatial distribution of trends for Tx, Tn, and T over Rwanda during the period of 1983–2022 expressed in °C/decade. Tx for JF (a1), Tn for JF (a2), T for JF (a3), Tx for MAM (b1), Tn for MAM (b2), T for MAM (b3), Tx for JJA (c1), Tn for JJA (**c2**), T for JJA (**c3**), Tx for SOND (**d1**), Tn for SOND (**d2**), T for SOND (**d3**), mean annual Tx (**e1**), mean annual Tn (**e2**), and mean annual T (**e3**). Trend slope in °C/decade (obtained by multiplying by 10 the computed trend slope in °C/year using the MMK method). Areas with statistically significant positive trends are

indicated with + sign, and areas with statistically significant negative trends are indicated with − sign.

Table 3. 2 presents the trends of spatially averaged Tx, Tn, and T for JF, MAM, JJA, SOND, and mean annual during the period of 1983–2022. Statistically significant increasing trends are observed for spatially averaged Tn during JJA (0.17 °C/decade) and SOND (0.20 °C/decade) as well for T during SOND (0.16 °C/decade).

Table 3. 2 Trends of spatially averaged Tx, Tn, and T during JF, MAM, JJA, SOND, and mean annual over Rwanda during the period of 1983–2022 expressed in °C/decade.

Tn					
Season	**Z**	**Tau**	**Sen's Slope**	***p*-Value**	**Significance**
JF	0.456	0.051	0.000	0.648	**No**
MAM	0.949	0.105	0.007	0.342	**No**
JJA	2.444	0.269	0.017	0.015	Yes
SOND	2.538	0.279	0.020	0.011	Yes
ANNUAL	2.063	0.227	0.013	0.039	Yes
Tx					
Season	Z	tau	Sen's Slope	*p*-value	Significance
JF	−1.133	−0.126	−0.010	0.257	No
MAM	1.358	0.150	0.013	0.174	No
JJA	−1.535	−0.169	−0.010	0.125	No
SOND	1.367	1.367	0.010	0.172	No
ANNUAL	0.188	0.022	0.000	0.851	No
T					
Season	Z	tau	Sen's Slope	*p*−value	Significance
JF	−0.281	−0.032	0.000	0.779	No
MAM	1.217	0.135	0.008	0.224	No
JJA	1.280	0.141	0.005	0.201	No
SOND	2.839	0.312	0.016	0.005	Yes
ANNUAL	1.708	0.187	0.007	0.088	No

Figure 3. 4 indicates the decadal differences in Tx for JF, MAM, JJA, SOND, and annual mean with reference to the period of 1983–1992.

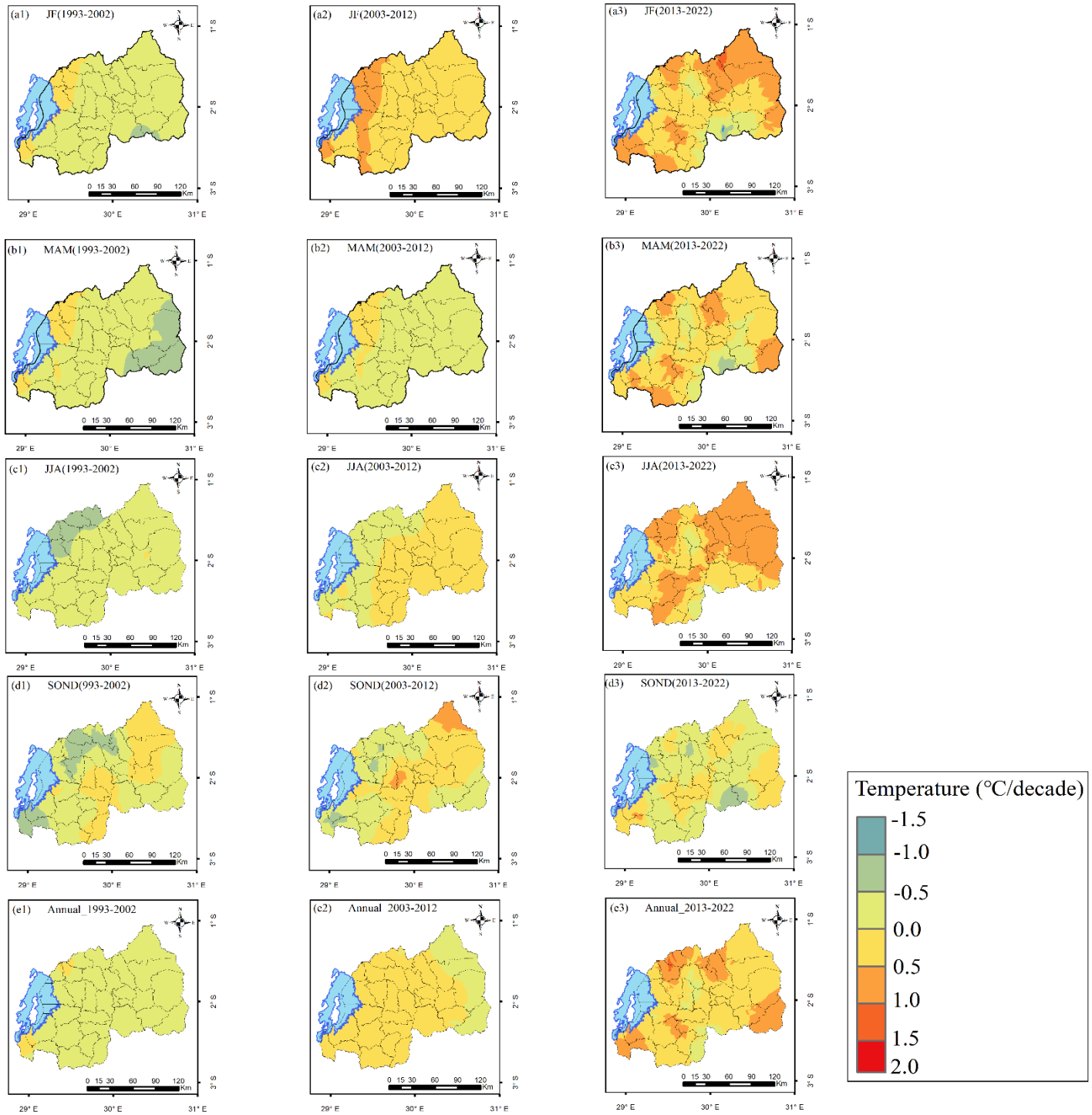

Figure 3. 4 Decadal differences of Tx for JF, MAM, JJA, SOND, and the annual mean with reference to the period of 1983-1992. Tx for JF (1993–2002) (a1), Tx for JF (2003–2012) (a2), Tx

for JF (2013-2022) (a3), Tx for MAM (1993-2002) (b1), Tx for MAM (2003-2012) (b2), Tx for MAM (2013-2022) (b3), Tx for JJA (1993-2002) (c1), Tx for JJA (2003-2012) (c2), Tx for JJA (2013-2022) (c3), Tx for SOND (1993-2002) (d1), Tx for SOND (2003-2012) (d2), Tx for SOND (2013-2022) (d3), annual Tx (1993-2002) (e1), annual Tx (2003-2012) (e2), and for annual Tx (2013-2022) (e3).

Figure 3. 5 indicates the decadal differences of Tn for JF, MAM, JJA, SOND, and annual mean with reference to the period of 1983–1992. During the second decade (1993–2002), the JF season shows a general reduction in Tn countrywide. The northeastern part shows a lower decrease (−0.5–0.0 °C) compared to the remaining parts of the country (−1.0–−0.5 °C). Increases in Tn (0.0–1.0 °C) are seen in many areas during MAM, JJA, and the year. During SOND, increases in Tn (1.0–1.5 °C) are observed in most parts of the country. The same range of increase is observed over the eastern part during the JJA season. During the third decade (2003–2012), relatively low increases in Tn (0.0–0.5 °C) are observed countrywide during JF season. During MAM, increases in Tn (0.5–1.0 °C) are observed in many parts of the country, while low increases ([0.0, 0.5] °C) are observed in the southeastern part. During JJA, increases in Tn (0.5–1.0 °C) are observed in many parts of the country, while low increases (0.0–0.5 °C) are observed in the western areas. During the SOND season, most parts of the country experienced increases in Tn (1.0–1.5 °C), while an increase of 0.5–1.0 °C was observed over the southwestern region. Annually, increases in Tn (0.5–1.0 °C) are found in all parts of the country. During the fourth decade (2013–2022), increases in Tn (0.5–1.0 °C) were observed over the central eastern and central western parts, while increases in Tn ([0.1, 1.5] °C) were observed over the remaining parts of the country. During MAM, increases in Tn (0.5–1.0 °C) are observed over the central eastern part, while there were increases in Tn (1.5–2.0 °C) in the remaining parts of the country. During JJA, it is observed that increases in Tn (2.5–3.0 °C) in the central plateau extend to the western highland, while increases in Tn (2.0–2.5 °C) are observed in the remaining parts of the country. During SOND, increases in Tn (3.0–3.5 °C) are observed countrywide. On an annual basis, increases in Tn (0.5–1.0 °C) are observed over the central eastern and central western parts, while increases in Tn (1.0–1.5 °C) are observed in the remaining parts of the country.

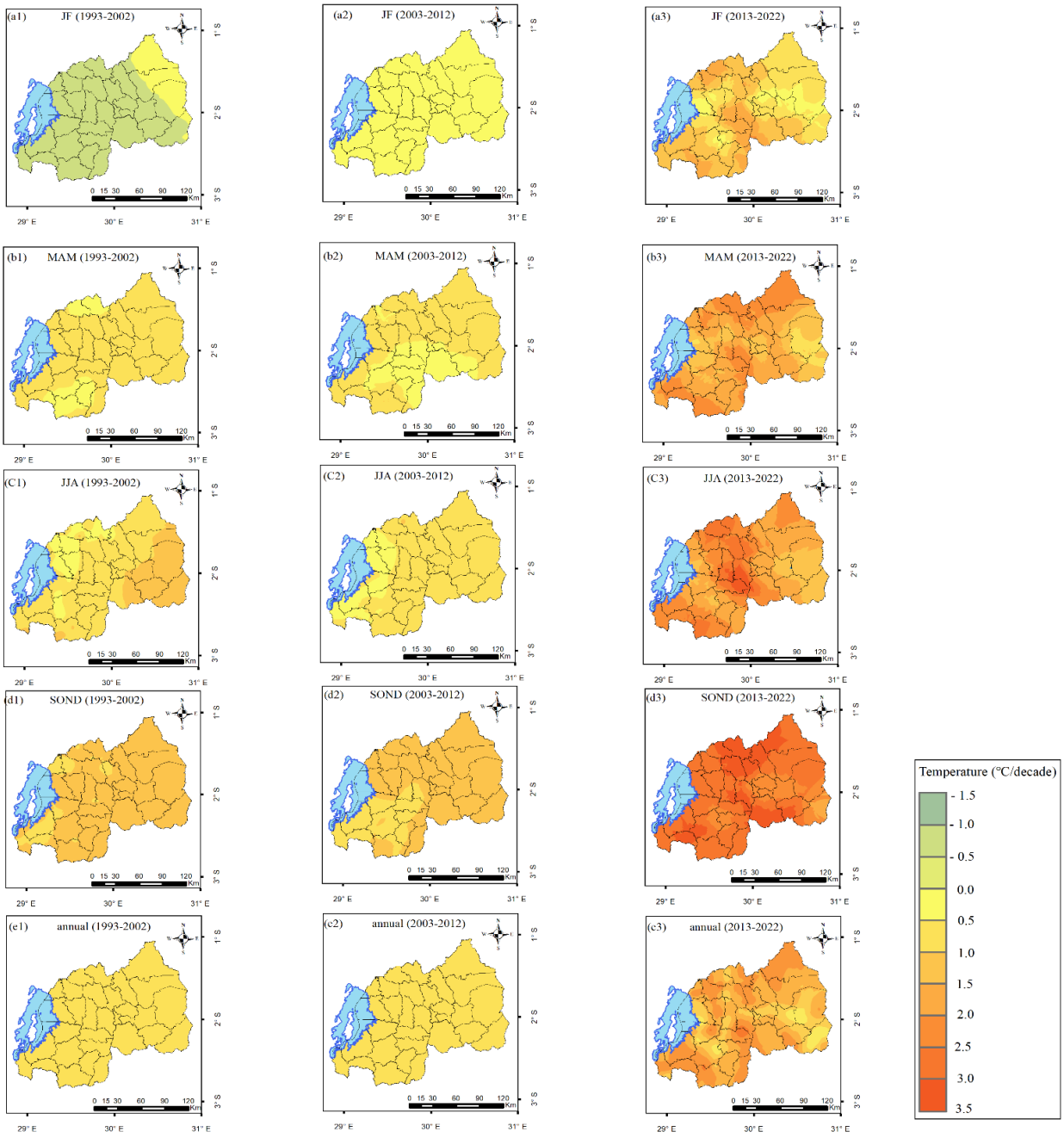

Figure 3. 5 Decadal differences of Tn for JF, MAM, JJA, SOND, and the annual mean with reference to the period of 1983-1992. Tn for JF (1993-2002) (a1), Tn for JF (2003-2012) (a2), Tn for JF (2013-2022) (a3), Tn for MAM (1993-2002) (b1), Tn for MAM (2003-2012) (b2), Tn for MAM (2013-2022) (b3), Tn for JJA (1993-2002) (c1), Tn for JJA (2003-2012) (c2), Tn for JJA (2013-2022) (c3), Tn for SOND (1993-2002) (d1), Tn for SOND (2003-2012) (d2), Tn for SOND (2013-2022) (d3), annual Tn (1993-2002) (e1), annual Tn (2003-2012) (e2), and annual Tn (2013-2022) (e3).

Figure 3. 6 indicates the decadal differences in T for JF, MAM, JJA, SOND, and annual mean with reference to the period of 1983-1992.

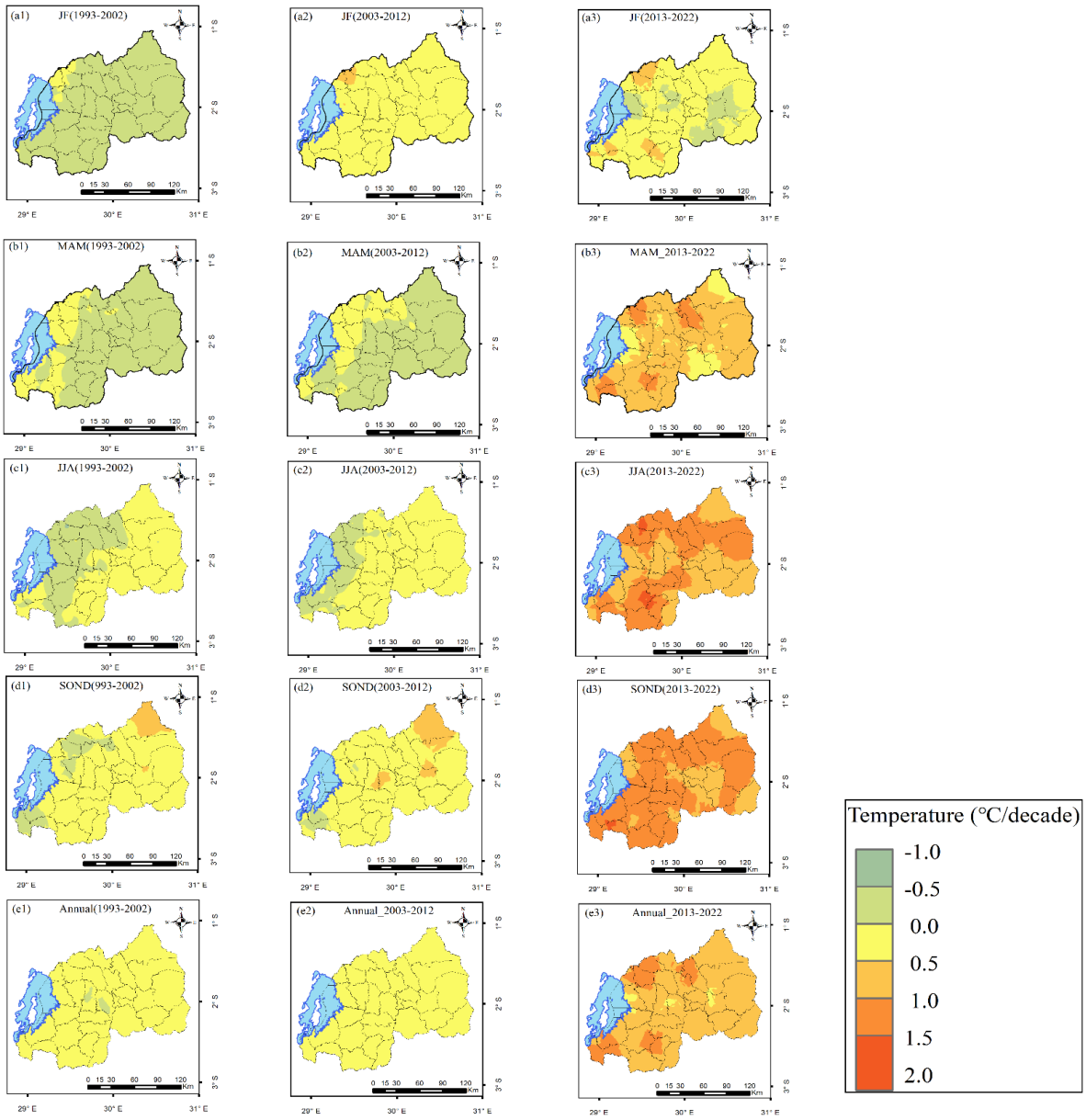

Figure 3. 6 Decadal differences of T for JF, MAM, JJA, SOND, and the annual mean with reference to the period of 1983-1992. T for JF (1993-2002) (a1), T for JF (2003-2012) (a2), T for JF (2013–2022) (a3), T for MAM (1993-2002) (b1), T for MAM (2003-2012) (b2), T for MAM (2013–2022) (b3), T for JJA (1993-2002) (c1), T for JJA (2003-2012) (c2), T for JJA (2013-2022) (c3), T for SOND (1993-2002) (d1), T for SOND (2003-2012) (d2), T for SOND (2013-2022) (d3), annual T (1993-2002) (e1), annual T (2003-2012) (e2), and annual T (2013-2022) (e3).

3.3.3 Spatial Distributions of Long-Term Mean of DTR, Tn10p, Tx10p, and Tn90p

Figure 3. 7 indicates the spatial distribution of the long-term mean of DTR, Tn10p, Tx10p, Tn90p, and Tx90p over Rwanda for the period of 1983-2022. For DTR (Figure 7a), four distinguished parts are observed: the northwestern region (10.5-11 °C), the part extending from the south to the southeastern region (11.5-12.0 °C), the south-central parts of the country (12.0-12.5 °C), and the remaining parts of the country (11.0-11.5 °C). For Tn10p (Figure 7b), three distinguished parts are observed: the extreme western region ([7, 8] days/year), the part extending from the south to central parts (9-10 days/year), and the remaining parts of the country (8–9 days/year). For Tx10p (Figure 7c), two distinguished parts are observed: the south, central, and extreme eastern parts (10–11 days/year) and the remaining parts of the country (9–10 days/year). For Tn90p (Figure 7d), two distinguished parts are observed: the central eastern and southeastern (9–10 days/year) and the remaining parts of the country (7–8 days/year). For Tx90p (Figure 7e), two distinguished parts are observed: the southern and northeastern (10–11 days/year) and the remaining parts of the country (9–10 days/year).

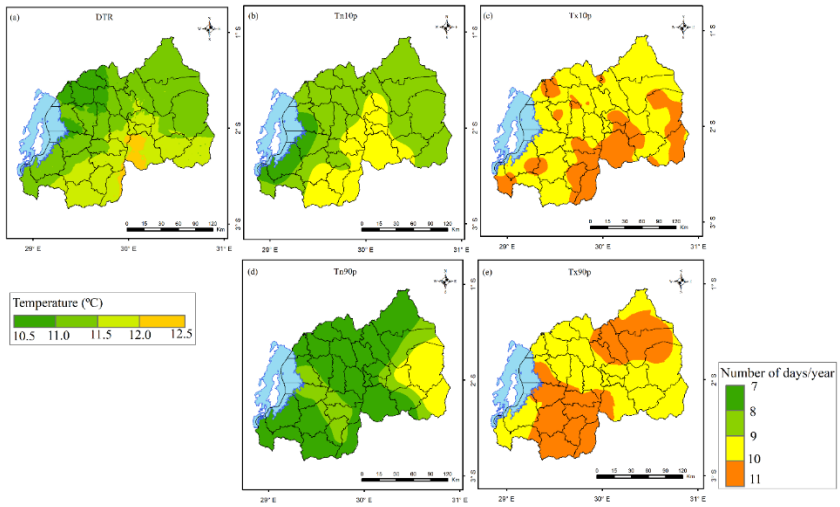

Figure 3. 7 Spatial distribution of long-term mean of DTR (a) expressed in °C, Tn10p (b); Tx10p (c); Tn90p (d); and Tx90p (e) expressed in days over Rwanda for the period 1983–2022. Legend is common for Tn10p, Tn90p, Tx10p, and Tx90p

3.3.4 Trends of Extreme Indices

Figure 3. 8 indicates the spatial distribution of trends of DTR, Tn10p, Tx10p, Tn90p, and Tx90p. Overall, a statistically significant decrease in DTR is observed in most parts of the country except

the eastern region and small parts of the western region. The central part (Kigali City and Gicumbi Districts) extended to the northeastern part of the country (Nyagatare District) and exhibits the highest decrease (−0.2–0.0 °C/decade) of DTR. Tn10p presents statistically significant negative trends over the whole country except in a narrow band along the Congo-Nile Divide. The central part of the country (Kigali City, Rulindo, and Gicumbi Districts) has the highest decrease (−2–0 days/decade) of Tn10p. Tn90p presents statistically significant positive trends in most parts of the country. The central part (Kigali City, Kamonyi, Ruhango, Bugesera, and Gicumbi District) extended to the northeastern part (Nyagatare and Gatsibo District), the southern part (Huye, Nyaruguru and Nyamagabe Districts), and the northwestern part of the country (Rubavu, Nyabihu, Musanze and Burera Districts), which presented a high increase (2–3 days/decade) in Tn90p. Tx10p exhibits positive trends over the whole country. Statistically significant high positive trends (1–3 days/decade) are observed on one side in the south-central eastern (Gisagara, Nyanza, and Bugesera Districts) and central eastern parts (Rwamagana District) and on the other side in some portions of the southeastern parts of the country (Kirehe, Kayonza, and Ngoma Districts). Tx90p exhibits over the whole country positive trends. Statistically significant high positive trends (2–3 days/decade) are observed in the western highland (Muhanga, Ngororero, Rutsiro, Rubavu, Nyabihu Musanze, and Gakenke Districts) and central parts of the eastern region (Rwamagana, Ngoma, Kayonza and Kirehe Districts).

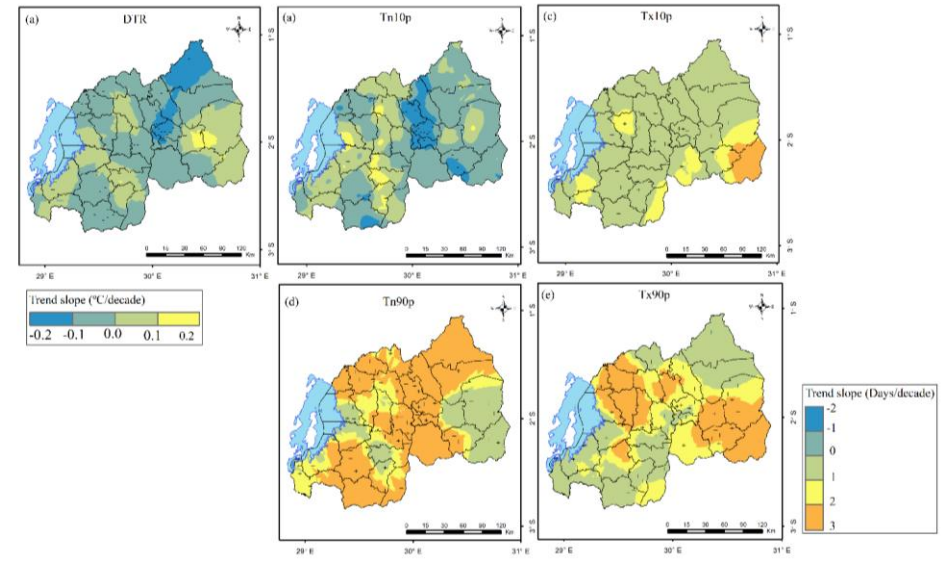

Figure 3. 8 Spatial distribution of trends of DTR (a) expressed in °C/decade, Tn10p (b); Tx10p (c); Tn90p (d); and Tx90p (e) expressed in days/decade over Rwanda during the period of 1983-2022. “Trend slope in °C/decade (obtained by multiplying by 10 the computed trend slope in

°C/year by the MMK method) for DRT" and "Trend slope in Days/decade (obtained by multiplying by 10 the computed trend slope in Days/year by the MMK method) for Tn10p, Tn90p, Tx10p, and Tx90p". Areas with statistically significant positive trends are indicated with + sign, and areas with statistically significant negative trends are indicated with − sign. Legend is common for Tn10p, Tn90p, Tx10p, and Tx90p.

Table 3. 3 presents the spatially averaged trends of DTR, Tn10p, Tx10p, Tn90p, and Tx90p. Spatially averaged DTR shows a statistically significant decreasing trend (−0.14 °C/decade), while spatially averaged Tn90p, Tx10p and Tx9p show statistically significant increase trends (0.62, 0.84, and 1.28 days/decade).

Table 3. 3 Trends of spatially averaged DTR(a) (°C/year) and Tn10p(b); Tx10p(c); Tn90p(d); and Tx90p(e) (days/year) over Rwanda during the period of 1983–2022.

Season	**Z**	**Tau**	**Sen's Slope**	***p*-Value**	**Significance**
DTR	−2.307	0.255	−0.014	0.021	Yes
Tn10p	−0.851	0.095	−0.049	0.395	No
Tn90p	1.317	0.146	0.062	0.029	Yes
Tx10p	2.342	0.259	0.084	0.019	Yes
Tx90p	2.552	0.282	0.128	0.011	Yes

Figure 3. 9 indicates the DTR for various decades of this present study**.** Overall, the first three decades (Figure 9a–c) show high values compared to the fourth decade (Figure 9d). The western region, the southeastern region, and small parts of the northern region show low values of DTR (8–10 °C) for all decades. The south-central eastern and northeastern parts indicate high values of DTR (13–16 °C). The remaining parts of the country present moderate values of DTR (10–13 °C).

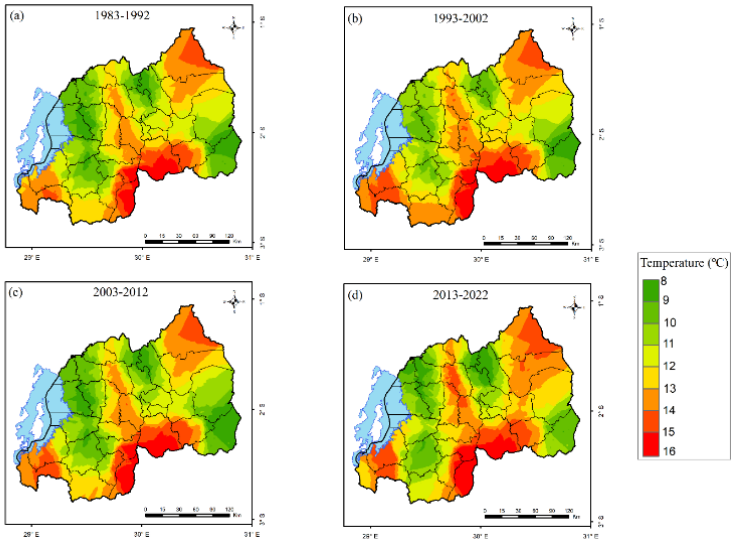

Figure 3. 9 Decadal spatial distribution of DTR expressed in °C over Rwanda for the period of 1983–2022. The first decade (1983–1992) (a), the second decade (1993–2002) (b), the third decade (2003–2012) (c), and the fourth decade (2013–2022) (d).

Figure 3. 10 presents Tn10p for various decades of this present study. During the first decade (Figure 10a), high values (12–14 days/year) are observed in the central region. The southwestern, northwestern highlands, central plateau, and eastern region indicate relatively high values (10–12 days/year). Moderate values (8–10 days/year) are observed over the central and western highlands, while the remaining parts of the country experienced low values (4–6 days/year). During the second and third decades (Figure 10b, c), respectively, the central, southern, and northwestern parts experienced relatively low values (6–8 days/year), while the remaining parts of the country observed low values (4–6 days/year). During the fourth decade (Figure 10d), central parts and a few areas of the southwestern region exhibited low values (4–6 days/year). The southwestern, northwestern, and central parts experienced relatively low values (6–8 days/year), while the remaining parts of the country observed relatively high values (10–12 days/year).

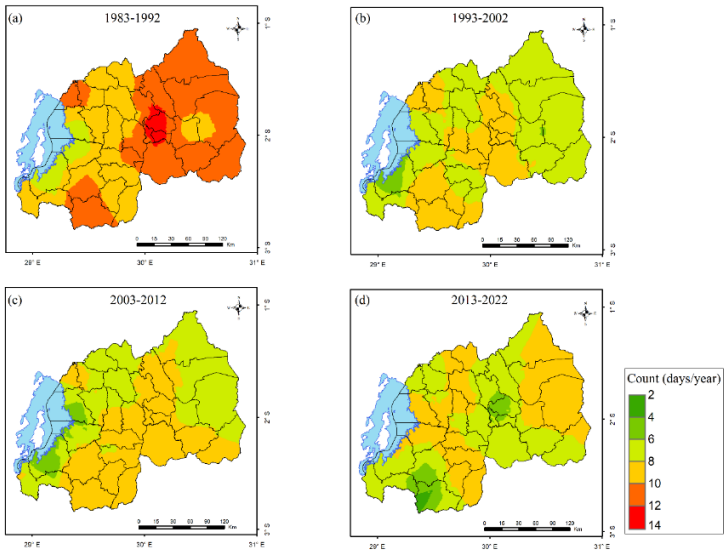

Figure 3. 10 Decadal spatial distribution of Tn10p expressed in day/year over Rwanda for the period of 1983–2022. The first decade (1983–1992) (a), the second decade (1993–2002) (b), the third decade (2003–2012) (c), and the fourth decade (2013–2022) (d).

Figure 3. 11 presents Tx10p for various decades of this present study. During the first decade (Figure 11a), low values (6–8 days/year) are observed in the southeastern and few parts of the northern highland. The remaining parts of the country experience relatively low values (8–10 days/year). During the second and third decades (Figure 11b,c), respectively, the central eastern and northern regions experienced moderate values (10–12 days/year). The remaining parts of the country observed relatively moderate values (12–14 days/year). During the fourth decade (Figure 11d), high values (14–16 days/year) are observed over the southeastern and southwestern parts. The remaining parts of the country experienced moderate values (10–12 days/year).

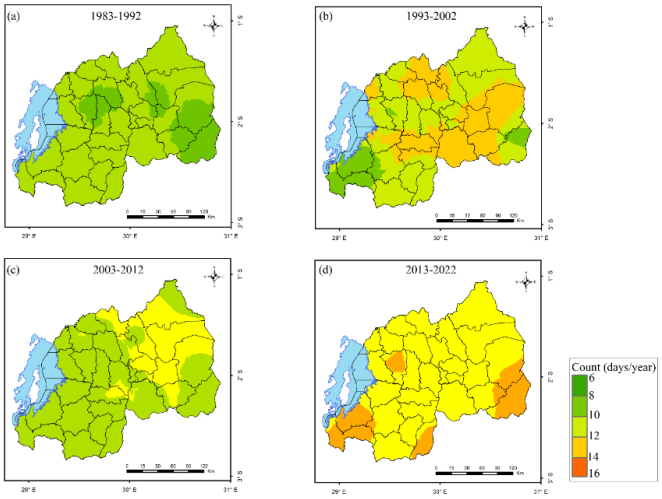

Figure 3. 11 Decadal spatial distribution of Tx10p expressed in day/year over Rwanda for the period of 1983–2022. The first decade (1983–1992) (a), the second decade (1993–2002) (b), the third decade (2003–2012) (c), and the fourth decade (2013–2022)) (d).

Figure 3. 12 indicates Tn90p for various decades of this present study. During the first decade (Figure 12a), low values (2–4 days/year) are observed over southwestern and northeastern parts. Relatively low values (4–6 days/year) are observed over the central plateau and northern western highland. The remaining parts of the country experience relatively moderate values (6–8 days/year). During the second decade (Figure 12b), relatively high values (10–12 days/year) are observed over the central eastern and central western parts. Many parts of the country experienced moderate values (8–10 days/year), while low values (2–4 days/year) are observed over the southwestern parts of the country. During the third decade (Figure 12c), moderate values (8–10 days/year) are shown over the central eastern and central western parts. Many parts of the country experienced relatively moderate values (6–8 days/year), while low values (2–4 days/year) are observed over the southwestern part of the country. During the fourth decade (Figure 12d), high values (12–14 days/year) are observed over the northern, central, and northeastern regions. The remaining parts of the country observed relatively high values (10–12 days/year).

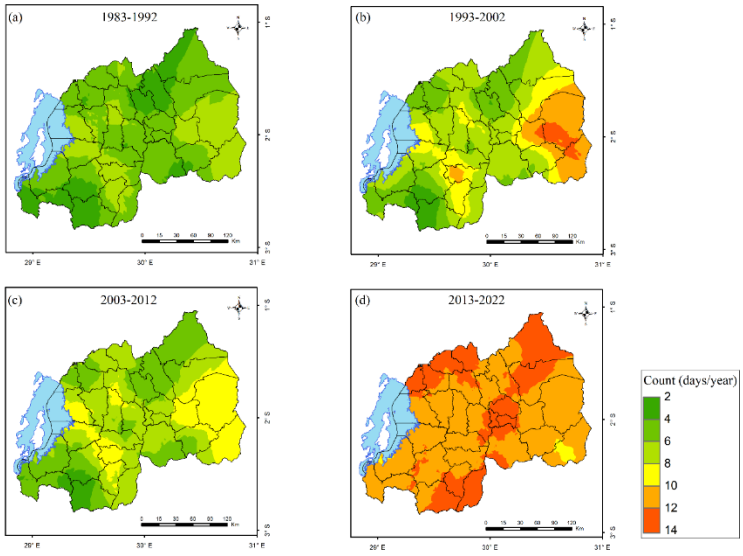

Figure 3. 12 Decadal spatial distribution of Tn90p expressed in day/year over Rwanda for the period of 1983–2022. The first decade (1983–1992) (a), the second decade (1993–2002) (b), the third decade (2003–2012) (c), and the fourth decade (2013–2022) (d).

Figure 3. 13 indicates Tx90p for various decades of this present study. The first decade (Figure 13a) exhibited homogeneous spatial distributions (8–10 days/year) countrywide. During the second decade (Figure 13b), the southwestern region indicates relatively low values (8–10 days/year), while the remaining parts of the country show low values (6–8 days/year). For the third decade (Figure 13c), relatively low values (8–10 days/year) are observed over the southeastern and extreme southwestern. The remaining parts of the country exhibit moderate values (10–12 days/year). During the fourth decade (Figure 13d), high values (14–18 days/year) are observed over the central eastern, southeastern, and highly elevated areas of the western and northern region, while the remaining parts of the country experienced moderate values (10–12 days/year).

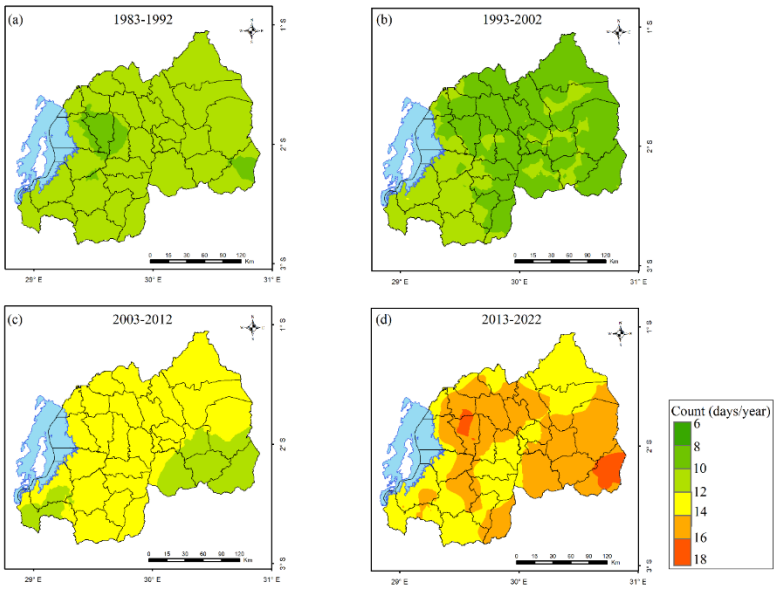

Figure 3. 13 Decadal spatial distribution of Tx90p expressed in day/year over Rwanda for the period of 1983–2022. The first decade (1983–1992) (a), the second decade (1993–2002) (b), the third decade (2003–2012) (c), and the fourth decade (2013–2022) (d).

Figure 3. 14 indicates the decadal differences of DTR, Tn10p, Tx10p, Tn90p, and Tx90p. The decadal difference in DTR and Tn10p indicate decreasing patterns for all decades, while Tn90p and Tx10p show increasing patterns for all decades. During the second decade (1993–2002), it was found that for DTR (Figure 14a1), the extreme eastern parts of the country showed the highest decrease (−1.0–−0.8 °C/decade). The eastern region extending to the central part of the country presents a moderate decrease of −0.6–−0.4 °C/decade. The areas surrounding the Congo-Nile Divide indicate a very low decrease (−0.2–0 °C/decade), while the remaining parts of the country low decrease (−0.4–−0.2 °C/decade). For Tn10p (Figure 14b1), the eastern part of the country has the highest decrease (−4–−3 days/decade). The western, southern, and northern parts of the country show a low decrease (−2–0 days/decade), while the remaining parts of the country present a moderate decrease (−3–−2 days/decade). For Tn90p (Figure 14c1), the eastern parts of the country have the highest increase (4–5 days/decade). The central plateau shows a moderate increase (2–4 days/decade), while the remaining parts of the country present a low increase (0–2 days/decade). For Tx10p (Figure 14d1), the southwestern and extreme northwestern present very low increases (0–2 days/decade). The central part extending to the western of the eastern region indicates a moderate increase (3–4 days/decade), while in the remaining parts of the country, low increases

(2–3 days/decade) are observed. As for Tx90p (Figure 14e1), a relatively low decrease (−2–0 days/decade) is observed in the northern, central plateau, and the eastern parts of the country, while a relatively low increase (0–2 days/decade) is observed in the remaining parts of the country. During the third decade (2003–2012), it is found for DTR (Figure 14a2) that a low decrease (−0.4–0.2 °C/decade) is observed over the eastern parts of the country, while the remaining parts of the country have very low decrease (−0.2–0 °C/decade). For Tn10p (Figure 14b2), the western, southern, and northern parts of the country have a low decrease (−2–0 days/decade). A high decrease (−4–−3 days/decade) is observed over northwestern and extreme eastern, while the remaining parts of the country indicate a moderate decrease (−3–−2 days/decade). For Tn90p (Figure 14c2), the southwestern, northwestern northeastern, and south-central parts of the country present low increases (0–2 days/decade), while the remaining parts of the country show a moderate increase (2–3 days/decade). For Tx10p (Figure 14d2), a few areas of the eastern region present a low increase (2–3 days/decade), while the remaining parts of the country show a very low increase (0–2 days/decade). As for Tx90p (Figure 14e2), the southwestern, south-central, and eastern parts of the country present low increases (0–2 days/decade), while the remaining parts of the country experienced moderate values (2–4 days/decade). During the fourth (2013–2022) decade, (Figure 14a3), a high decrease (−1.0–−0.8 °C/decade) is observed over the southeastern, south-central extending to small areas of central and northern parts of the country, while the remaining parts of the country exhibit moderate decrease (−0.6–−0.4 °C/decade). For Tn10p (Figure 14b3), the whole country shows a low decrease (−2–0 days/decade). For Tn90p (Figure 14c3), the central plateau has a moderate value increase (3–4 days/decade), while the remaining parts of the country experienced a moderate increase (2–3 days/decade). For Tx10p (Figure 14d3), high increases (4–5 days/decade) are observed over the extreme southeastern parts of the country. The central parts of the southern and western regions, the northern highland, and the western parts of the eastern region indicate low increases (2–3 days/decade), while the remaining parts of the country observed moderate values (3–4 days/decade). As for Tx90p (Figure 14e3), the southeastern region extending to the central part and the northern highland present a high increase (4–6 days/decade), while the remaining parts of the country indicated a moderate increase (2–4 days/decade).

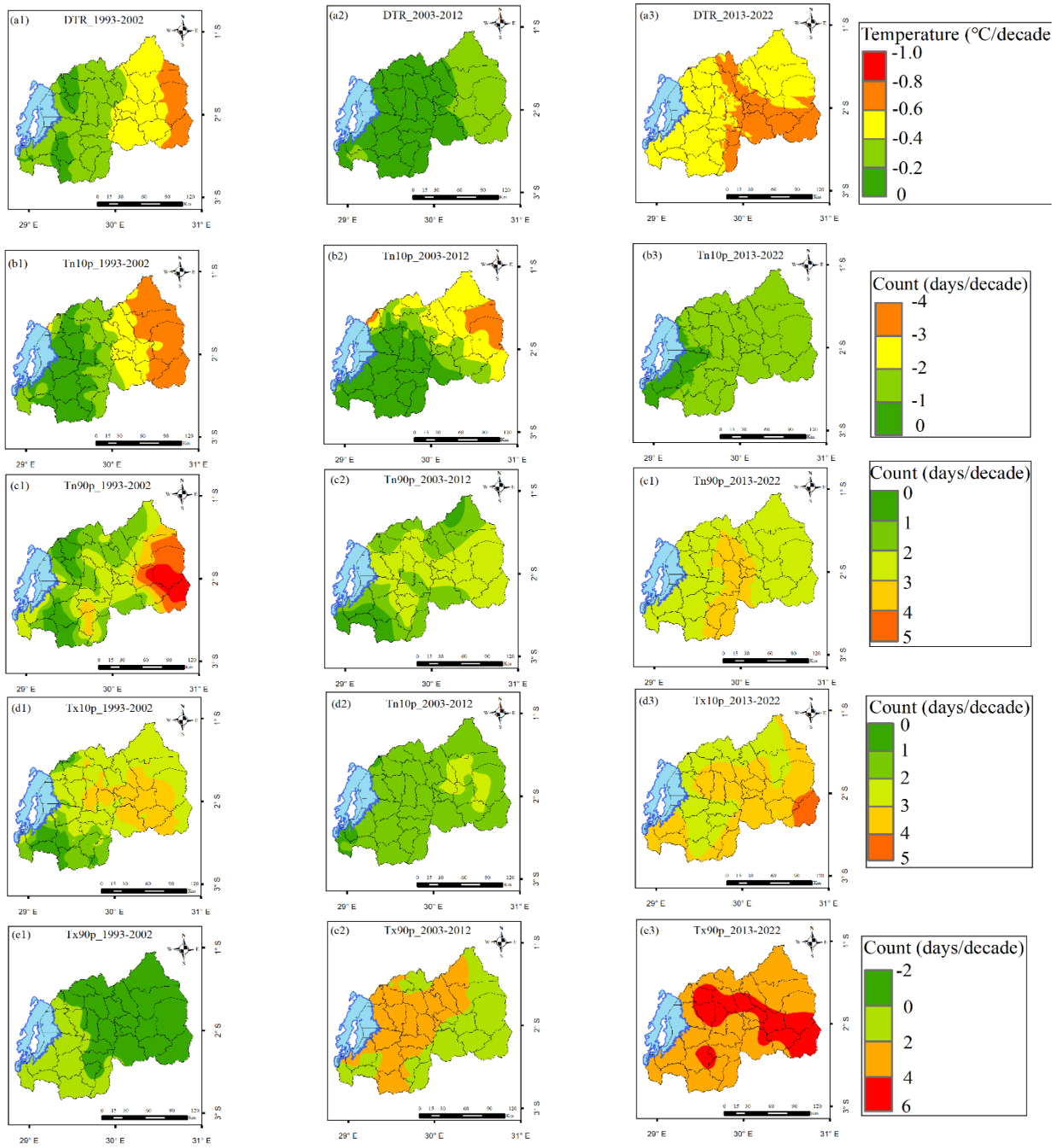

Figure 3. 14 Spatial distribution of decadal differences of DTR, Tn10p, Tx10p, Tn90p and Tx90p. DTR for the second decade (1993-2002) (a1), DTR for the third decade (2003-2012) (a2), DTR for the fourth decade (2013-2022) (a3). Tn10p for the second decade (1993-2002) (b1), Tn10p for the third decade (2003-2012) (b2), Tn10p for the fourth decade (2013-2022) (b3). Tn90p for the second decade (1993-2002) (c1), Tn90p for the third decade (2003-2012) (c2), and Tn90p for the fourth decade (2013-2022) (c3). Tx10p for the second decade (1993-2002) (d1), Tx10p for the

third decade (2003-2012) (d2), and Tx10p for the fourth decade (2013-2022) (d3). Tx90p for the second decade (1993-2002) (e1), Tx90p for the third decade (2003-2012) (e2), and Tx90p for the fourth decade (2013-2022) (e3). Legend is common for each extreme temperature index for all decades.

3.3.4 *Variability in Temperatures and Extreme Indices*

Figure 3. 15 presents the spatial distributions of temporal variability of Tx, Tn, and T for JF, MAM, JJA, and SOND and the annual mean over Rwanda. In general, Tx represents the highest variability compared to Tn. Tx shows statistically significant high variability (1.4–1.6 °C) over the eastern and northwestern highlands in all seasons, except JJA. The two regions are important for the economy of the country as they constitute areas of intense agricultural activity. Tn country presents statistically significant high variability (1.2–1.4 °C) in the southwestern part of the country during all seasons, while it presents statistically significant high variability (1.0–1.2 °C) in the northeastern part of the country during JF and JJA seasons. The annual means of Tx and Tn indicate no statistically significant high value of variability is observed over the whole country. T shows that no statistically significant variability is observed for all seasons and the annual mean.

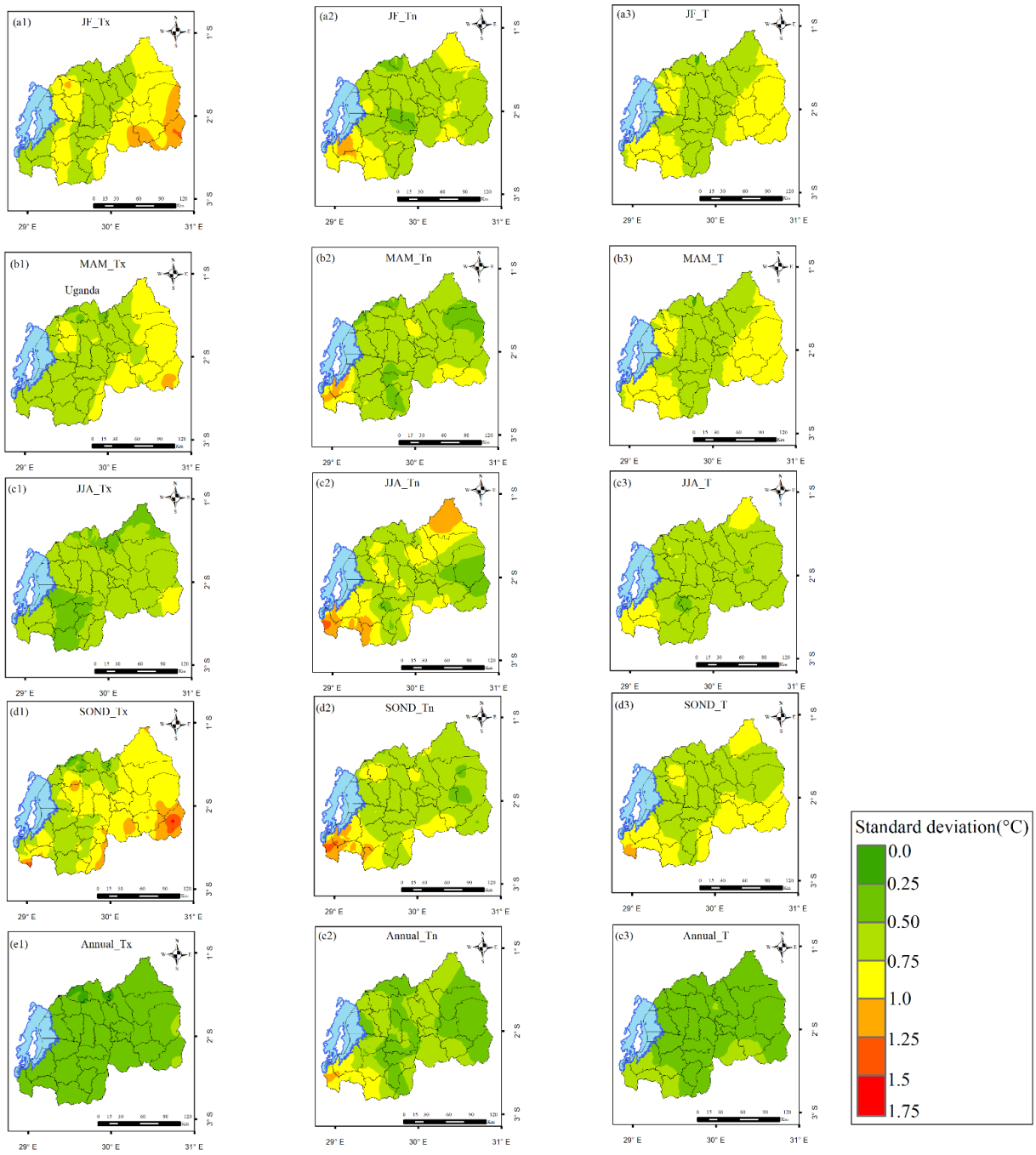

Figure 3. 15 Spatial variability of Tx, Tn, and T over Rwanda during the period of 1983–2022 expressed in terms of standard deviation in °C. Tx for JF (a1), Tn for JF (a2), T for JF (a3), Tx for MAM (b1), Tn for MAM (b2), T for MAM (b3), Tx for JJA (c1), Tn for JJA (c2), T for JJA (c3), Tx for SOND (d1), Tn for SOND (d2), T for SOND (d3), mean annual Tx (e1), mean annual Tn (e2), and mean annual T (e3).

Figure 3. 16 presents the spatial variability of DTR, Tn10p, Tx10p, Tn90p, and Tx90p. DTR shows statistically significant high variability (1.25–1.75 °C) in the southwestern parts compared to the south-central eastern part and a few areas of the northern highland (0.75–1.25 °C), while the remaining parts of the country indicate the lowest variability (0.25–0.75 °C). Tn10p shows higher variability ([5–7] days) than Tx10p (2–3 days), Tn90p (4–5 days), and Tx90p (3–4 days), especially in the area covering the central, south-western, south-central, and northwestern parts of Rwanda.

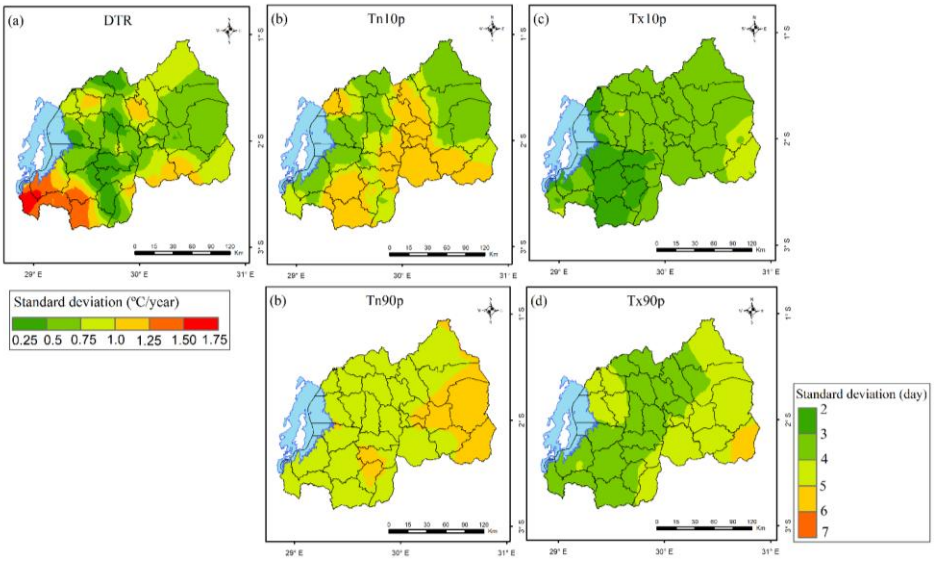

Figure 3. 16 Spatial variability expressed in terms of standard deviation for DTR (a) in °C/year, Tn10p (b); Tx10p (c); Tn90p (d); and Tx90p (e) in days/year over Rwanda during the period of 1983–2022. Legend is common for Tn10p, Tn90p, Tx10p, and Tx90p.

3.4 Projected changes in seasonal temperatures

Figure 3 17 presents the spatial distribution of projected changes in seasonal mean maximum temperature for 2026-2060 and 2066-2100 period. For all seasons, maximum temperature is projected to increase throughout the century with more magnitude under RCP8.5 than RCP2.6 emission scenarios. During JF, for the 2026-2060 period, under RCP2.6**,** a greater increase in Tx of (**[2, 3] °C**) is projected in the eastern and south-western areas of the country, while the remaining areas are expected to increase by **(**[1, 2] °C**).** Under RCP8.5**,** Tx is projected to increase by ([1, 2] °C) in the southern, south-eastern, and north-western areas, and by ([2, 3] °C) in other regions. For the 2066-2100 period, under RCP2.6, the north-eastern and south-western regions are projected to

increase by ([1, 2] °C), the south-central and northern highlands are projected to decrease ([-1, 0] °C), while the remaining areas are expected to increase by ([0, 1] °C). Under RCP8.5, Tx in the south-western and north-eastern areas is projected to increase by ([2, 3] °C), while the remaining areas are expected to increase by ([1, 2] °C).

During MAM, for the 2026-2060 period, under RCP2.6, Tx is projected to increase by ([0, 1] °C) in the northern and south-western regions and decrease by ([-2, -1] °C) in the remaining areas. Under RCP8.5, it is projected to decrease by ([-1, 0] °C) in the south-central region and increase by ([0, 1] °C) in other areas. For the 2066-2100 period, under RCP2.6, Tx is projected to increase by ([0, 1] °C) in the northern and south-western regions and decrease by ([-1, 0] °C) in the remaining areas. Under RCP8.5, a projected increase of ([2, 3] °C) is expected in the northern and south-western regions, and an increase of ([1, 2] °C) in the remaining areas.

For JJA, during the 2026-2060 period, under RCP2.6, Tx is projected to increase by ([2, 3] °C) in the north-western highlands and in the eastern parts of the country, while the remaining areas are expected to increase by ([1, 2] °C). Under RCP8.5, Tx is projected to increase by ([3, 4] °C) in some areas of the eastern and north-western regions, and by ([1, 2] °C) in other areas. For the 2066-2100 period, under RCP2.6, Tx is projected to increase by ([2, 3] °C) in the north-western highlands and by ([1, 2] °C) in the remaining areas of the country, while under RCP8.5, it is expected to increase by ([3, 4] °C) across the entire country.

During SOND, for the 2026-2060 period, under RCP2.6, Tx is projected to increase by ([0, 1] °C) across the entire country. Under RCP8.5, it is projected to increase by ([1, 2] °C) in the southern and northern highlands, and by ([0, 1] °C) in the remaining areas. For the 2066-2100 period, under RCP2.6, Tx is projected to decrease by ([-1, 0] °C) in the central and north-eastern regions, and increase by ([1, 2] °C) in the remaining areas. Under RCP8.5, Tx in the central and north-eastern regions is projected to increase by ([1, 2] °C), while in the remaining areas it is projected to increase by ([2, 3] °C).

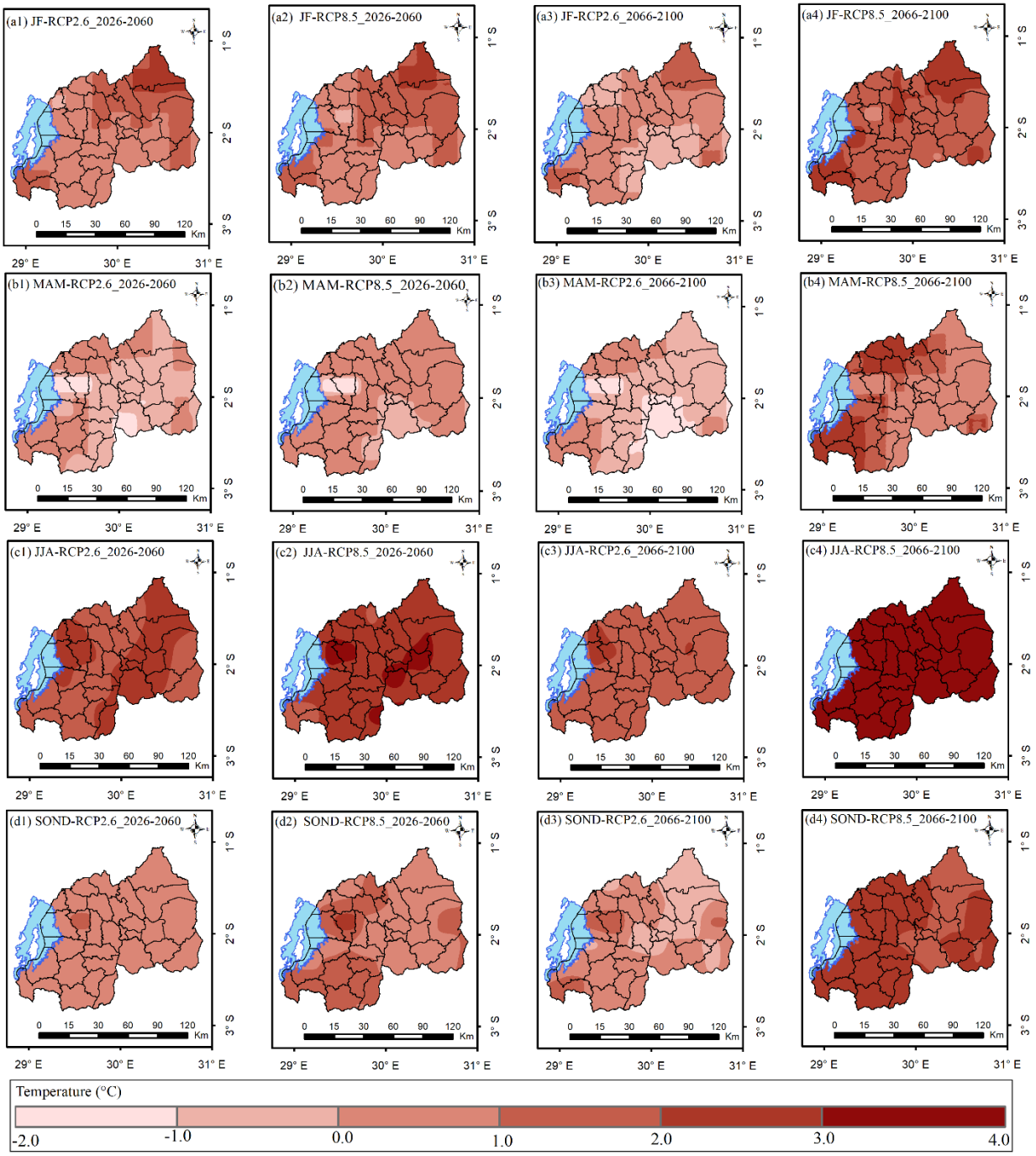

Figure 3. 17**:** Spatial distribution of projected changes seasonal mean maximum temperature (Tx) for January-February (JF, a_1-a_4), March-April-May (MAM, b_1-b_4), June-July-August (JJA, c_1-c_4) and September-October-November-December (SOND, d_1-d_4) for 2026-2060 and 2066-2100 period.

Figure 3 18 presents the spatial distribution of projected changes in seasonal mean minimum temperature for 2026-2060 and 2066-2100 period. For all seasons, minimum temperature is

projected to increase throughout the century, with larger increases expected under RCP8.5 compared to RCP2.6. During JF, for the 2026-2060 period, under RCP2.6, a greater increase in Tn of ([3, 4] °C) is projected in the south-western, ([2, 3] °C) in the south-central, extreme northern highland and in few areas of the central while an increase of ([0, 1] °C) is projected in north-eastern and ([1, 2] °C) in remaining areas. Under RCP8.5, Tn is projected to increase by ([1, 2] °C) in the north-eastern and by ([2, 3] °C) in other regions. For the 2066-2100 period, under RCP2.6, Tn in the north-eastern is projected to increase by ([0, 1] °C), in the south-central and western highlands by ([1, 2] °C), while the remaining areas are expected to increase by ([2, 3] °C). Under RCP8.5, Tn in the south-western and south-central areas is projected to increase by ([3, 4] °C), while the remaining areas are expected to increase by ([2, 3] °C).

During MAM, for the 2026-2060 period, under RCP2.6, Tn is projected to increase by ([3, 4] °C) in the south-western, ([2, 3] °C) in the north-eastern and by ([1, 2] °C) in the remaining areas. Under RCP8.5, it is projected to increase ([3, 4] °C) in the south-western ([0, 1] °C) in the south-eastern and by ([2, 3] °C) in other areas. For the 2066-2100 period, under RCP2.6, Tn is projected to increase by ([3, 4] °C) in the south-western, ([2, 3] °C) in the north-eastern and by ([1, 2] °C) in the remaining areas. Under RCP8.5, a projected increase of ([3, 4] °C) is expected in the north-eastern and south-western and ([2, 3] °C) in the remaining areas.

For JJA, during the 2026-2060 period, under RCP2.6, Tn is projected to increase by ([2, 3] °C) in the north-western highlands, south-western and north-eastern, by ([0, 1] °C) in south-eastern, while the remaining areas are expected to increase by ([1, 2] °C). Under RCP8.5, Tn is projected to increase by ([3, 4] °C) in some areas of the north-eastern, south-western and north-western regions, by ([1, 2] °C) in other south-eastern and by ([2, 3] °C) in other areas. For the 2066-2100 period, under RCP2.6, Tn is projected to increase by ([2, 3] °C) in the north-western highlands, north-eastern and south-western, by ([0, 1] °C) in the south-eastern and by ([1, 2] °C) in the remaining areas of the country, while under RCP8.5, it is expected to increase by ([2, 3] °C) in the south-eastern few areas of the northern and southern region and by ([3, 4] °C) in the remaining areas of the country.

During SOND, for the 2026-2060 period, under RCP2.6, Tn is projected to increase by ([3, 4] °C) in south-western and by ([2, 3] °C) in remaining areas. Under RCP8.5, it is projected to increase by ([2, 3] °C) in the central and eastern regions and by ([3, 4] °C) in the remaining areas. For the 2066-2100 period, Tn is projected to increase by ([3, 4] °C) in south-western and by ([2, 3] °C) in

remaining areas under RCP2.6. Under RCP8.5, it is projected to increase by ([2, 3] °C) in the central parts of the country and by ([3, 4] °C) in the remaining areas of the country.

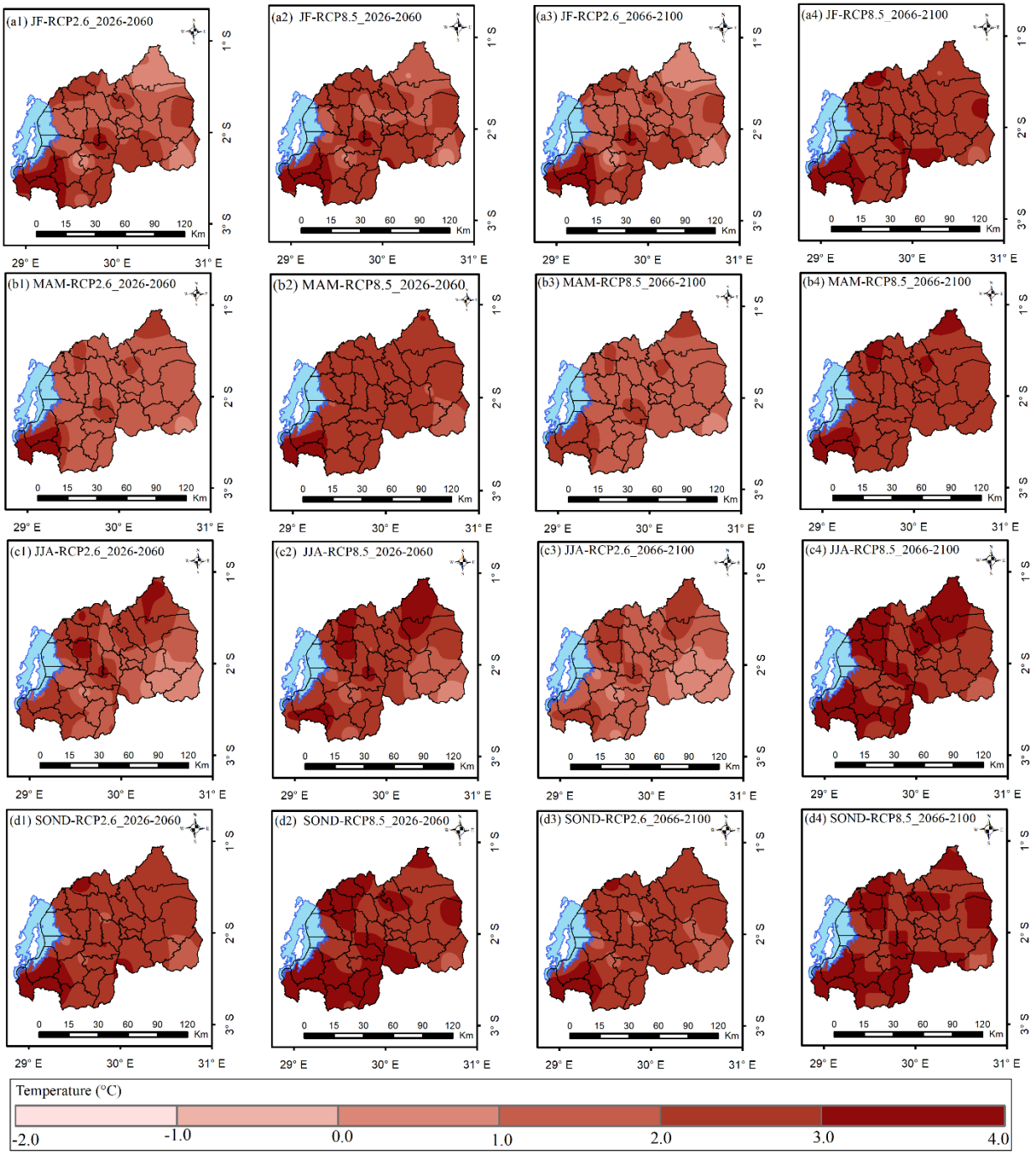

Figure 3. 18**:** Spatial distribution of projected changes seasonal mean minimum temperature (Tn) for January-February (JF, a_1-a_4), March-April-May (MAM, b_1-b_4), June-July-August (JJA, c_1-c_4) and September-October-November-December (SOND, d_1-d_4) for 2026-2060 and 2066-2100 period.

Figure 3 19 presents the spatial distribution of projected changes in seasonal mean temperature for 2026-2060 and 2066-2100 period. Mean temperatures are projected to rise in all seasons throughout the century, with greater increases anticipated under RCP8.5 than under RCP2.6. During JF, for the 2026-2060 period, under both RCP2.6 and RCP8.5, a greater increase in T of ([2, 3] °C) is projected in the south-western, ([1, 2] °C) in remaining areas. For the 2066-2100 period, under RCP2.6, T in the south-eastern and few areas of the eastern is projected to increase by ([0, 1] °C), while the remaining areas are expected to increase by ([2, 3] °C). Under RCP8.5, T is projected to increase by ([3, 4] °C) country wide. During MAM, for the 2026-2060 period, T in the northern and south-western is projected to increase by ([1, 2] °C) under RCP2.6 and by ([2, 3] °C) under RCP8.5, while remaining areas are projected to experience an increase of ([0, 1] °C) under both RCP2.6 and RCP8.5. For the 2066-2100 period, under RCP2.6, T is projected to increase by ([0, 1] °C) country wide while under RCP8.5, it is projected to increase by ([1, 2] °C) in south-eastern and by ([2, 3] °C) in the remaining areas.

For JJA, during the 2026-2060 period, under RCP2.6, T is projected to increase by ([1, 2] °C) in the south-eastern and southern and by ([2, 2] °C) in the remaining areas of the country. Under RCP8.5, T is projected to increase by ([2, 3] °C) in some areas of the north-eastern, and north-western and by ([1, 2] °C) in other areas. For the 2066-2100 period, under RCP2.6, T is projected to increase by ([1, 2] °C) in the north-western highlands and in north-eastern while in the remaining areas of the country, T is projected to increase by ([0, 1] °C), Under RCP8.5, it is expected to increase by ([3, 4] °C) in the south-western and northern regions and by ([1, 2] °C) in the remaining areas of the country. During SOND, for the 2026-2060 period, under both RCP2.6 and RCP8.5, T is projected to increase by ([2, 3] °C) in south-western and north-western and by ([1, 2] °C) in remaining areas. For the 2066-2100 period, T is projected to increase by ([2, 3] °C) in south-western and by ([1, 2] °C) in remaining areas under RCP2.6. Under RCP8.5, it is projected to increase by ([3, 4] °C) in the south-western parts of the country and by ([2, 3] °C) in the remaining areas of the country.

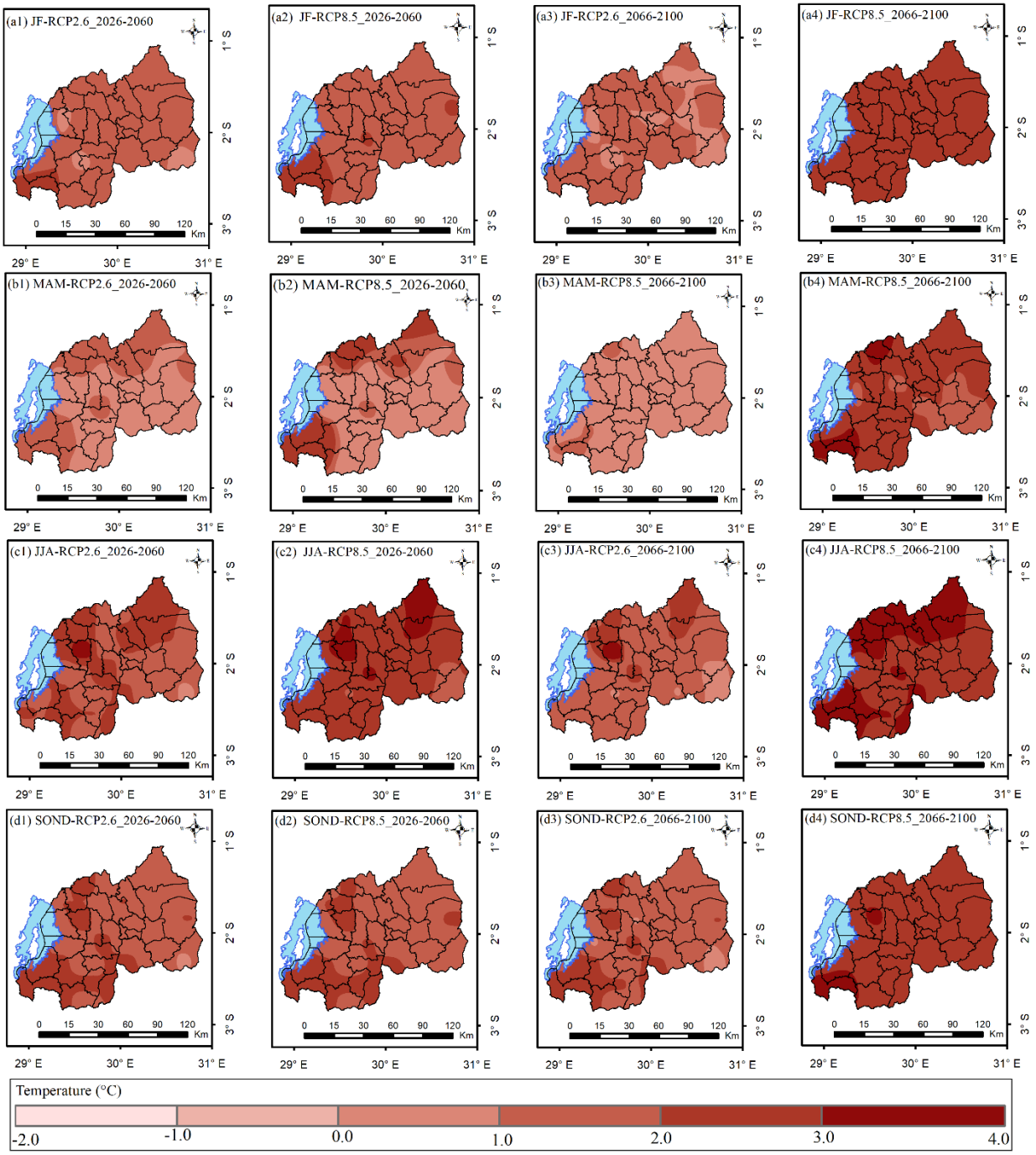

Figure 3. 19**:** Spatial distribution of projected changes seasonal mean temperature (T) for January-February (JF, a_1-a_4), March-April-May (MAM, b_1-b_4), June-July-August (JJA, c_1-c_4) and September-October-November-December (SOND, d_1-d_4) for 2026-2060 and 2066-2100 period.

Figure 3 20 presents the country averaged observed and projected seasonal maximum temperature changes for over Rwanda. For JF season, maximum temperature increase is expected under RCP8.5 than under RCP2.6. Under RCP2.6, an increase of 0.5 to 1.5 °C is expected for 2026-2066 period while a slight increase by 0.5 to 1°C is expected during 2066-2100 period. Under RCP8.5, temperature is expected to increase by about 0.5 to 2°C for the 2026-2060 period and about 2.5 to 4.5 °C during the period 2066-2100. For MAM season, an increase of 1 to 1.5°C is expected under RCP2.6 and 1.5 to 2.5 °C under RCP8.5 during the period 2026-2060. Moving towards the end of the century (2066-2100), temperature is expected to reduce by 0.5 to 1°C under RCP2.6 while under RCP8.5, it is expected to rise by 3.5-4°C. For JJA season, temperature is expected to increase by 1 to 3°C under RCP2.6 and 2 to 3.5°C under RCP8.5 during 2026-2060 period. During 2066-2100 period, an increase of 1.5 to 2.5 is projected under RCP2.6 and 3-5°C under RCP8.5. For SOND season, an increase of 0.5 to 1.5°C is expected under RCP2.6 and 1-2°C under RCP8.5 during 2026-2060 period. Towards the end of the century (2066-2100), a projected increase by 1 to 2.5°C is expected under RCP2.6 and 2.5 to 4°C under RCP8.5.

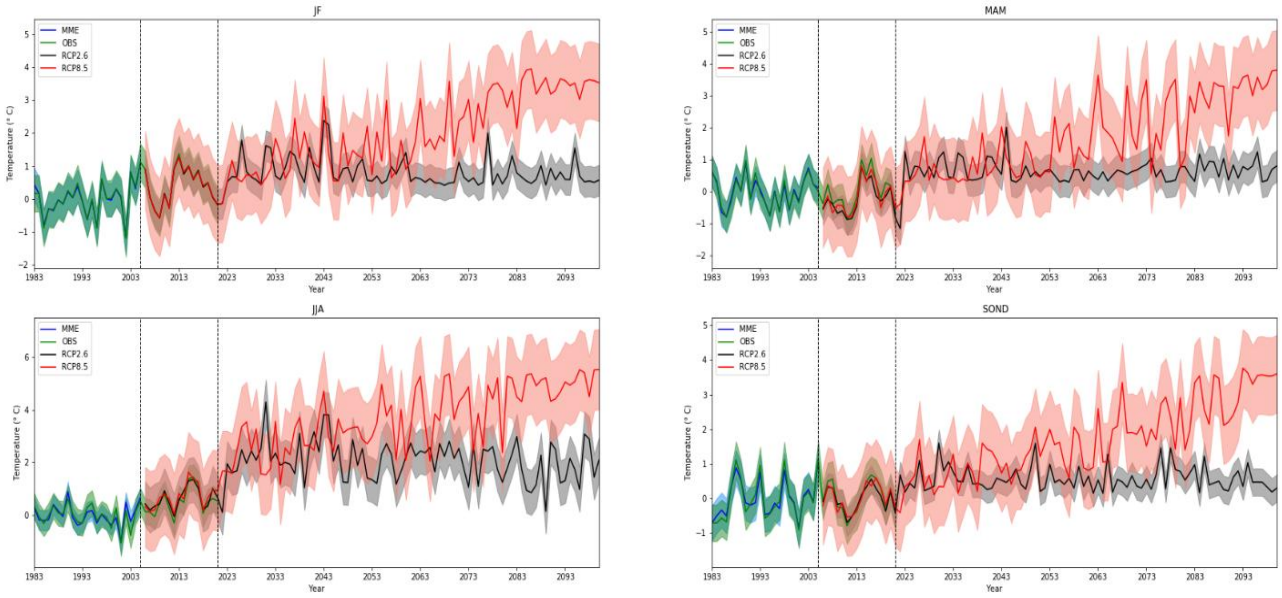

Figure 3. 20**:** The country averaged observed and projected maximum temperature changes for January-February (JF), March-April-May (MAM), June-July-August (JJA) and September-October-November-December (SOND) over Rwanda for 1983-2100 period.

Figure 3 21 presents the country averaged observed and projected seasonal maximum temperature changes for over Rwanda. For JF season, minimum temperature is expected to increase under

RCP8.5 than under RCP2.6. During 2026-2060 period, increase of 1.5 to 2.5 °C is expected under RCP2.6 and 2.5 to 4°C under RCP8.5. During 2066-2100 period, a projected increase of 1.5 to 2.5°C is expected under RCP2.6 and 3 to 4°C under RCP8.5. For MAM season, an increase of 1.5 to 2.5°C is expected under RCP2.6 and 2 to 3.5 °C under RCP8.5 during the period 2026-2060. During 2066-2100 period, a projected increase by 1.5-2.5°C is expected under RCP2.6 while under RCP8.5, it is expected to rise by 3 to 4°C. For JJA season, temperature is expected to increase by 1.5 to 2.5°C under RCP2.6 and 2 to 3.5°C under RCP8.5 during 2026-2060 period. During 2066-2100 period, an increase of 1.5 to 2.5 is projected under RCP2.6 and 3 to 4°C under RCP8.5. For SOND season, an increase of 2.5 to 3°C is expected under RCP2.6 and 3 to 4°C under RCP8.5 during 2026-2060 period. During 2066-2100 period, a projected increase by 2 to 3°C is expected under RCP2.6 and 3 to 4°C under RCP8.5.

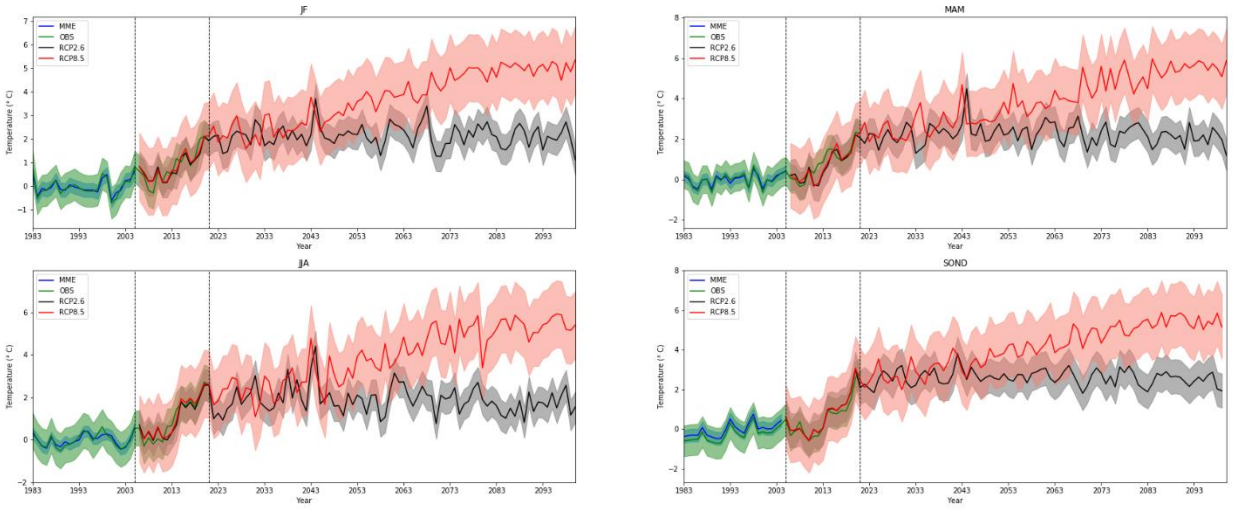

Figure 3. 21**:** The country averaged observed and projected minimum temperature changes for January-February (JF), March-April-May (MAM), June-July-August (JJA) and September-October-November-December (SOND) over Rwanda for 1983-2100 period.

Figure 3 22 presents the country averaged observed and projected seasonal mean temperature changes for over Rwanda. For JF season, minimum temperature is expected to increase under RCP8.5 than under RCP2.6. During 2026-2060 period, increase of 1 to 2 °C is expected under RCP2.6 1.5 to 2.5°C under RCP8.5. During 2066-2100 period, a projected increase of 1 to 1.5°C is expected under RCP2.6 and 3 to 4°C under RCP8.5. For MAM season, an increase of 0.5 to 1.5°C is expected under RCP2.6 and 1.5 to 2.5 °C under RCP8.5 during the period 2026-2060. During 2066-2100 period, a projected increase by 1 to 1.5°C is expected under RCP2.6 while

under RCP8.5, it is expected to rise by 3 to 5°C. For JJA season, temperature is expected to increase by 1.5 to 2°C under RCP2.6 and 2 to 3.5°C under RCP8.5 during 2026-2060 period. During 2066-2100 period, an increase of 1.5 to 2.5 is projected under RCP2.6 and 3 to 4°C under RCP8.5. For SOND season, an increase of 1 to 2°C is expected under RCP2.6 and 1.5 to 2.5°C under RCP8.5 during 2026-2060 period. During 2066-2100 period, a projected increase by 1 to 2°C is expected under RCP2.6 and 3 to 4°C under RCP8.5.

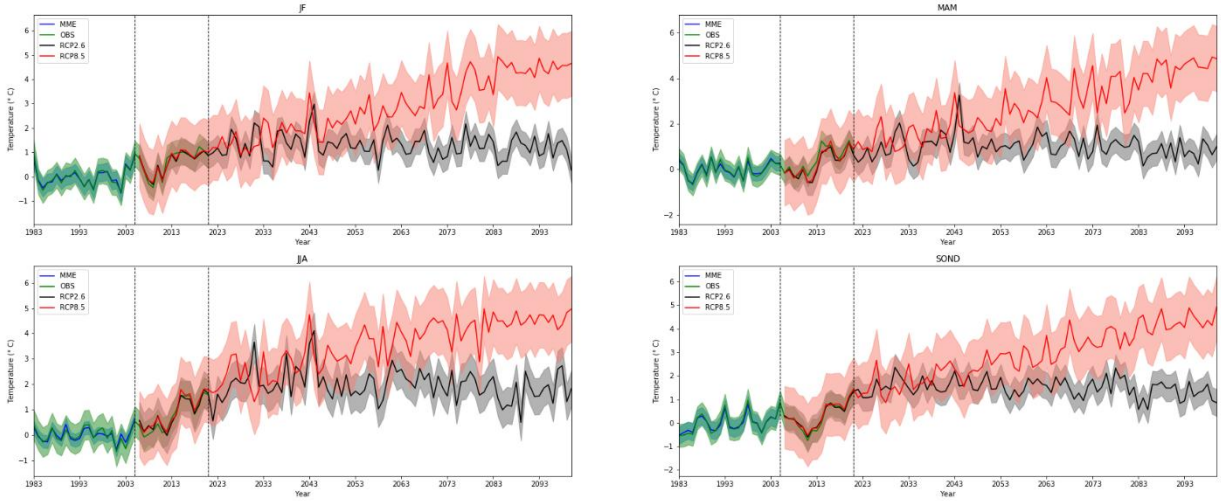

Figure 3. 22**:** The country averaged observed and projected mean temperature changes for January-February (JF), March-April-May (MAM), June-July-August (JJA) and September-October-November-December (SOND) over Rwanda for 1983-2100 period.

3.5 Discussion

Overall, temperatures decrease gradually with topography from the eastern to the western parts of the country in all seasons. Variations in temperature are primarily due to changes in cloud cover, rainfall, humidity, and winds. Temperatures follow the annual seasonal cycle. The difference in temperature between day and night is the maximum during JF and JJA and the minimum during MAM and SOND. The seasons of MAM and SOND correspond to the periods of crop growth. During those periods, statistically significant high positive trends of T were observed over some areas of great agricultural activity. Such an increase in T can affect crop production in the affected area by altering plant respiration rates and responses to biotic stressors (Das et al., 2022).

Some studies have associated the higher rate of Tn compared to that of Tx with soil conditions, radiative cooling, and surface layer stability during the night (Ahmed et al., 2017; Chechin et al.,

2019). The warming of surface temperature was linked to human-induced Greenhouse Gases (Weber and Englund, 1992; Weber and Englund, 1994; Allabakash and Lim, 2022; Setianto and Triandini, 2015; Lu et al., 2022). In East Africa, the variability of temperature is in general associated with natural internal variability such as the El Nino Southern Oscillation as well as the Inter-decadal Pacific Oscillation (Gu and Adler, 2013; Lyon, 2014; Dai, 2016). In particular, the increased surface air temperature has led to the recently observed extreme dry events in the years of 2016 and 2017 over Rwanda. Rising temperatures may lead to increased evapotranspiration levels (Bunyasi, 2012; Machina and Sharma, 2017), impacting the water resources by decreasing water discharge, resulting in reduced hydropower generation (Kachaje et al., 2016). In addition, it may intensify the drought conditions, leading to severe impacts on agricultural activities (Uwimbabazi et al., 2022). The observed strong variability of temperature over the eastern and northwestern highlands of Rwanda has negatively impacted the economy of the country as they constitute areas of intense agricultural activity (Hunter et al., 2020).

Extreme temperature indices were found to be not coherent. The results obtained from country averages are in line with previous studies conducted over the East Africa region with the exception of Tx10p, which increases in Rwanda instead of decreasing (Ngaina and Mutai, 2013; Omondi et al., 2014; Mekasha et al., 2014; Kachaje et al., 2016; Owoyesigire et al., 2016; Chang'a et al., 2017; Gebrechorkos, 2018; East Africa Hazards Watch, 2023). The decrease in DTR has been observed in many parts of the world and was shown to be mainly related to the increase in Tn (Easterling et al., 1997; Vose et al., 2005). The changes in extreme temperature indices have been associated with the variation in convective rainfall events, cloud cover, increase in minimum temperature, or decrease in maximum temperature (Camberlin, 2017; DIKE et al., 2019; (Zhou et al., 2009). Several studies have revealed that the increase in DTR may affect human health by causing cardiovascular diseases and chronicle respiratory, resulting in low and high respiratory infections (King'uyu et al., 2000; Lim et al., 2012; Wang et al., 2013; Cheng et al., 2014; Carreras et al., 2015; Zheng et al., 2016; Wang et al., 2020; Jang and Chun, 2021). Zhou et al, (2004) and Meinshausen et al., (2009) have related changes in cold nights, cold days, warm nights, and warm days to climate change brought by human activities, including urbanization and industrialization, producing greenhouse gases (Hu et al., 2015; Marigi et al., 2016; Chen and Dirmeyer, 2020; Lu et al., 2021). The increase in warm nights, cold days, and warm days affects crop growth (Mekasha et al., 2014; Leng et al., 2015; Sheffield et al., 2012) and can influence the development and

outbreak of new crop diseases (Jang and Chun, 2021). Jang and Chun Jang and Chun (2020) have indicated that the rise in warm nights and warm days could induce significant impacts on sectors such as the energy necessitating high water for cooling, water supply by increasing freshwater need, and transportation by distortion of roads. The increase in temperature and drying conditions have resulted in increased drought in many places of the Earth (Khodzhimetov, 1997; Agutu et al., 2017; Mutsotso et al., 2018; REMA, 2019; Polong et al., 2019; Kew et al., 2021; IPCC, 2021; Yannick and Randriamarolaza, 2023). During the last years, East Africa has experienced more recurrent, intense, and longer-lasting drought events (Russo et al., 2016; Agutu et al., 2017; Herold et al., 2017; Nashwan and Shahid, 2019; Gebrechorkos et al., 2019; Ayugi et al., 2020; Choi et al., 2023), causing damage to infrastructure, water scarcity, drying of crops, famine, and food insecurity, leading to the frequent migrations of populations (Abebe, 2014; Ayugi et al., 2020; Mueller et al., 2020; Doherty et al., 2022; Bannor et al., 2023). Recent observations have indicated that the eastern and southeastern parts of Rwanda have been experiencing rainfall deficits, resulting in severe droughts alternated by prolonged moderated drought. This made those areas vulnerable to water inaccessibility and food insecurity (Lydie, 2016; Ayugi et al., 2020; Uwimbabazi et al., 2022).

This study analyzed the trends and variability in the maximum, minimum, and mean temperatures and their associated extreme indices, as they have an impact on important key sectors of the economy such as agriculture, health, water resources, infrastructure, and energy. Another method of investigation recently developed can be used for comparison, such as the Innovative Trend Analysis methodology (Alashan, 2020; Birpınar et al., 2023). The results obtained will be useful in future studies to make a quantitative analysis of the effects of these trends and variables on these sectors. The obtained information will be useful in helping policy makers and decision makers integrate appropriate factors, taking into account mitigation and adaptation to climate change in planning for all sectorial levels.

3.6 Conclusion

In this present study, an analysis of the trends and variabilities of the maximum, minimum, and mean temperatures and their associated extreme indices was performed using the Modified Mann–Kendall test and the Theil-Sen estimator and the standard deviation, respectively. Statistically significant ($\alpha = 0.05$) positive trends were observed for spatially averaged minimum temperature

in JJA and SOND and for spatially averaged mean temperature in SOND. The maximum temperature presented higher variability than the minimum temperature and mean temperature countrywide. Diurnal temperature range and cold nights indicated a statistically significant (α = 0.05) decrease over the country, while warm days, cold days, and warm nights showed a statistically significant ($\alpha = 0.05$). The diurnal temperature range showed a statistically significant ($\alpha = 0.05$) high variability in the southwestern parts compared to the remaining parts of the country. Cold nights show higher variability than cold days, warm nights, and warm days, especially in the area covering the central, south-western, south-central parts, and the northwestern part of Rwanda. These obtained results will be useful in future studies to make a quantitative analysis of the effects of these trends and variabilities on those sectors. They will serve to inform the community and policy decision making to take objective measures to prevent the impact of temperature increase and its variability on important economic sectors.

Some future directions of research can be mentioned: (i) investigate changes using other methods, i.e., Innovative Trend Analysis methodology recently developed (Alashan, 2020; Birpınar et al., 2023) for comparison and (ii) recognize that drought is another effect of climate change in Rwanda. Some studies have recently been conducted on the East African region to determine the variability and trends in factors related to drought (Lobell and Field, 2007; Christiansen et al., 2011; Pita-Díaz and Ortega-Gaucin, 2020). Further studies are still needed to investigate those factors to understand the effect of climate warming.

3.7 References

Abebe, M. A. (2014). Climate Change, Gender Inequality, and Migration in East Africa. *Washington Journal of Environmental Law & Policy*, *4*(1), 104–140.

Agutu, N. O., Awange, J. L., Zerihun, A., Ndehedehe, C. E., Kuhn, M., & Fukuda, Y. (2017). Assessing multi-satellite remote sensing, reanalysis, and land surface models' products in characterizing agricultural drought in East Africa. *Remote Sensing of Environment*, *194*, 287–302. https://doi.org/10.1016/j.rse.2017.03.041

Ahmed, K., Shahid, S., Ali, R. O., Harun, S. Bin, & Wang, X. J. (2017). Evaluation of the performance of gridded precipitation products over balochistan province, pakistan. *Desalination and Water Treatment*, *79*(August), 73–86. https://doi.org/10.5004/dwt.2017.20859

Alashan, S. (2020). Combination of modified Mann-Kendall method and Şen innovative trend

analysis. *Engineering Reports*, *2*(3), 1–13. https://doi.org/10.1002/eng2.12131

Allabakash, S., & Lim, S. (2022). Anthropogenic influence of temperature changes across East Asia using CMIP6 simulations. *Scientific Reports*, *12*(1), 1–14. https://doi.org/10.1038/s41598-022-16110-9

Ayugi, B., Tan, G., Rouyun, N., Zeyao, D., Ojara, M., Mumo, L., Babaousmail, H., & Ongoma, V. (2020). Evaluation of meteorological drought and flood scenarios over Kenya, East Africa. *Atmosphere*, *11*(3). https://doi.org/10.3390/atmos11030307

Bannor, F., Magambo, I. H., Mahabir, J., & Tshitaka, J. M. (2023). Interdependence between climate change and migration: Does agriculture, geography, and development level matter in sub-Saharan Africa? *South African Journal of Economics*, *91*(2), 141–160. https://doi.org/10.1111/saje.12343

Bastin, J. F., Clark, E., Elliott, T., Hart, S., Van Den Hoogen, J., Hordijk, I., Ma, H., Majumder, S., Manoli, G., Maschler, J., Mo, L., Routh, D., Yu, K., Zohner, C. M., & Crowther, T. W. (2019). Correction: Understanding climate change from a global analysis of city analogues. *PLoS ONE*, *14*(10), 1–13. https://doi.org/10.1371/journal.pone.0224120

Birpınar, M. E., Kızılöz, B., & Şişman, E. (2023). Classic trend analysis methods' paradoxical results and innovative trend analysis methodology with percentile ranges. *Theoretical and Applied Climatology*, *153*(1–2), 1–18. https://doi.org/10.1007/s00704-023-04449-6

Bouwer, L. M. (2011). Have disaster losses increased due to anthropogenic climate change? *Bulletin of the American Meteorological Society*, *92*(1), 39–46. https://doi.org/10.1175/2010BAMS3092.1

Brohan, P., Kennedy, J. J., Harris, I., Tett, S. F. B., & Jones, P. D. (2006). Uncertainty estimates in regional and global observed temperature changes: A new data set from 1850. *Journal of Geophysical Research Atmospheres*, *111*(12), 1–21. https://doi.org/10.1029/2005JD006548

Bunyasi, M. (2012). Vulnerability of Hydro-Electric Energy Resources in Kenya Due to Climate Change Effects: The Case of the Seven Forks Project. *Journal of Agriculture and Environmental Sciences*, *1*(1), 36–49. www.aripd.org/jaes

Caesar, J., Alexander, L., & Vose, R. (2006). Large-scale changes in observe daily maximum and minimum temperatures: Creation and analysis of a new gridded data set. *Journal of Geophysical Research Atmospheres*, *111*(5). https://doi.org/10.1029/2005JD006280

Camberlin, P. (2017). Temperature trends and variability in the Greater Horn of Africa:

interactions with precipitation. *Climate Dynamics*, *48*(1–2), 477–498. https://doi.org/10.1007/s00382-016-3088-5

Carreras, H., Zanobetti, A., & Koutrakis, P. (2015). Effect of daily temperature range on respiratory health in Argentina and its modification by impaired socio-economic conditions and PM10 exposures. *Environmental Pollution*, *206*, 175–182. https://doi.org/10.1016/j.envpol.2015.06.037

Chang'a, L. B., Kijazi, A. L., Luhunga, P. M., Ng'ongolo, H. K., & Mtongor, H. I. (2017). Spatial and Temporal Analysis of Rainfall and Temperature Extreme Indices in Tanzania. *Atmospheric and Climate Sciences*, *07*(04), 525–539. https://doi.org/10.4236/acs.2017.74038

Chechin, D. G., Makhotina, I. A., Lüpkes, C., & Makshtas, A. P. (2019). Effect of wind speed and leads on clear-sky cooling over Arctic sea ice during polar night. *Journal of the Atmospheric Sciences*, *76*(8), 2481. https://doi.org/10.1175/JAS-D-18-0277.1

Chen, L., & Dirmeyer, P. A. (2020). Distinct Impacts of Land Use and Land Management on Summer Temperatures. *Frontiers in Earth Science*, *8*(June), 1–12. https://doi.org/10.3389/feart.2020.00245

Cheng, J., Xu, Z., Zhu, R., Wang, X., Jin, L., Song, J., & Su, H. (2014). Impact of diurnal temperature range on human health: a systematic review. *International Journal of Biometeorology*, *58*(9), 2011–2024. https://doi.org/10.1007/s00484-014-0797-5

Choi, Y. W., Campbell, D. J., & Eltahir, E. A. B. (2023). Near-term regional climate change in East Africa. *Climate Dynamics*, *61*(1–2), 961–978. https://doi.org/10.1007/s00382-022-06591-9

Christiansen, D. E., Markstrom, S. L., & Hay, L. E. (2011). Impacts of climate change on the growing season in the United States. *Earth Interactions*, *15*(33), 1–17. https://doi.org/10.1175/2011EI376.1

Clay, N., & King, B. (2019). Smallholders' uneven capacities to adapt to climate change amid Africa's 'green revolution': Case study of Rwanda's crop intensification program. *World Development*, *116*, 1–14. https://doi.org/10.1016/j.worlddev.2018.11.022

Comiso, J. C., Perez, G. J. P., & Stock, L. V. (2015). Enhanced pacific ocean sea surface temperature and its relation to typhoon haiyan. *Journal of Environmental Science and Management*, *18*(1), 1–10. https://doi.org/10.47125/jesam/2015_1/01

Dai, A. (2016). Future Warming Patterns Linked to Today's Climate Variability. *Scientific*

Reports, *6*(November 2015), 6–11. https://doi.org/10.1038/srep19110

Daron, J. D. (2014). Regional Climate Messages: East Africa. Scientific report from the CARIAA Adaptation at Scale in Semi-Arid Regions (ASSAR) Project. *Scientific Report from the CARIAA Adaptation at Scale in Semi-Arid Regions (ASSAR) Project*, 1–30.

Das, S., Datta, P., Sharma, D., & Goswami, K. (2022). Trends in Temperature, Precipitation, Potential Evapotranspiration, and Water Availability across the Teesta River Basin under 1.5 and 2◦ C Temperature Rise Scenarios of CMIP6. *Atmosphere*, *13*(6), 1–22. https://doi.org/10.3390/atmos13060941

Datta, P., & Das, S. (2019). Analysis of long-term seasonal and annual temperature trends in North Bengal, India. *Spatial Information Research*, *27*(4), 475–496. https://doi.org/10.1007/s41324-019-00250-8

Diaz, H. F., & Murnane, R. J. (2008). The significance of weather and climate extremes to society: An introduction. *Climate Extremes and Society*, *9780521870*, xiii–xvi. https://doi.org/10.1017/CBO9780511535840.002

DIKE, V. N., LIN, Z., WANG, Y., & NNAMCHI, H. (2019). Observed trends in diurnal temperature range over Nigeria. *Atmospheric and Oceanic Science Letters*, *12*(2), 131–139. https://doi.org/10.1080/16742834.2019.1570688

Dinku, T., Hailemariam, K., Maidment, R., & Connor, S. (2014). Combined use of satellite estimates and rain gauge observations to generate high-quality historical rainfall time series over Ethiopia. *International Journal of Climate Climatology*, *2504*(November 2013), 2489–2504. https://doi.org/10.1002/joc.3855

Doherty, A., Pearce, M., Calow, R., Daoust, G., Higazi, A., Burgin, L., & Osborne, R. (2022). Climate risk report for the East Africa region. *Met Office*, *ODI*, *FCDO*. http://www.uneca.org/acpc/publications

East Africa Hazards Watch. (2023). *Cities Warming*. https://eahazardswatch.icpac.net/map/use/ (accessed on 26 June 2023)

Easterling, D. R., Horton, B., Jones, P. D., Peterson, T. C., Karl, T. R., Parker, D. E., Salinger, M. J., Razuvayev, V., Plummer, N., Jamason, P., & Folland, C. K. (1997). Maximum and minimum temperature trends for the globe. *Science*, *277*(5324), 364–367. https://doi.org/10.1126/science.277.5324.364

Easterling, D. R., Meehl, G. A., Parmesan, C., Changnon, S. A., Karl, T. R., & Mearns, L. O.

(2000). Climate extremes: Observations, modeling, and impacts. *Science*, *289*(5487), 2068–2074. https://doi.org/10.1126/science.289.5487.2068

Engelbrecht, F., Adegoke, J., Bopape, M. J., Naidoo, M., Garland, R., Thatcher, M., McGregor, J., Katzfey, J., Werner, M., Ichoku, C., & Gatebe, C. (2015). Projections of rapidly rising surface temperatures over Africa under low mitigation. *Environmental Research Letters*, *10*(8). https://doi.org/10.1088/1748-9326/10/8/085004

FAO. (2018). Tracking Adaptation in Agricultural Sectors: Climate change adaptation indicators. In *Tracking Adaptation in Agricultural Sectors. Food and Agriculture Organization of the United Nations Rome*. https://doi.org/10.18356/87fe25de-en

Folland, C. K., Karl, T. R., Christy, J. R., Clarke, R. A., Gruza, G. V., Jouzel, J., Mann, M. E., Oerlemans, J., Salinger, M. J., & Wang, S.-W. (2001). Climate Change 2001: The Scientific Basis. Contribution of Working Group I to the Third Assessment Report of the Intergovernmental Panel on Climate Change. *Cambridge University Press, Cambridge, United Kingdom and New York, NY, USA, 881pp.* https://doi.org/10.1016/S1058-2746(02)86826-4

Gebrechorkos, S. H. (2018). Changes in temperature and precipitation extremes in Ethiopia , Kenya and Tanzania. *International Journal of Climatology*, *June 2018*, 18–30. https://doi.org/10.1002/joc.5777

Gebrechorkos, S. H., Hülsmann, S., & Bernhofer, C. (2019). Long-term trends in rainfall and temperature using high-resolution climate datasets in East Africa. *Scientific Reports*, *9*(1), 1–9. https://doi.org/10.1038/s41598-019-47933-8

Gu, G., & Adler, R. F. (2013). Interdecadal variability/long-term changes in global precipitation patterns during the past three decades: Global warming and/or pacific decadal variability? *Climate Dynamics*, *40*(11–12), 3009–3022. https://doi.org/10.1007/s00382-012-1443-8

Hamed, K. H., & Rao, A. R. (1998). A modified Mann-Kendall trend test for autocorrelated data. *Journal of Hydrology*, *204*, 182–196. https://doi.org/10.1200/jco.2018.36.15_suppl. 522

Henninger, S. M. (2013a). Does the global warming modify the local Rwandan climate? *Natural Science*, *05*(01), 124–129. https://doi.org/10.4236/ns.2013.51A019

Henninger, S. M. (2013b). Local climate changes and the spread of malaria in Rwanda. *Health*, *5*(4), 728–734. https://doi.org/10.4236/health.2013.54096

Herold, N., Alexander, L., Green, D., & Donat, M. (2017). Greater increases in temperature

extremes in low versus high income countries. *Environmental Research Letters*, *12*(3), 10–13. https://doi.org/10.1088/1748-9326/aa5c43

Hu, W., Zhou, W., & He, H. (2015). The effect of land-use intensity on surface temperature in the dongting lake area, China. *Advances in Meteorology*, *2015*. https://doi.org/10.1155/2015/632151

Hunter, R., O., C., Coldrey, K., Cronin, K., & New, M. (2020). Research Highlights – Climate Change and Future Crop Suitability in Rwanda. *University of Cape Town, South Africa, Undertaken in Support of Adaptation for Smallholder Agriculture Programme' (ASAP) Phase 2. International Fund for Agricultural Development (IFAD), Rome.*, 3–6. https://www.ifad.org/documents/38714170/42164624/climate_analysis_rwanda.pdf

IPCC. (2007). Climate Change 2007: Synthesis Report. Contribution of Working Groups I, II and III to the Fourth Assessment Report. In *Intergovernmental Panel on Climate Change [Core Writing Team,Pachauri, R.K and Reisinger, A. (eds.)]. IPCC, Geneva, Switzerland, 104 pp*. https://doi.org/10.1256/004316502320517344

IPCC. (2021a). Climate Change 2021: The Physical Science Basis. Contribution of Working Group I to the Sixth Assessment Report of the Intergovernmental Panel on Climate Change [Masson-Delmotte, V., P. Zhai, A. Pirani, S.L. Connors, C. Péan, S. Berger, N. Caud, Y. Chen, . In *Cambridge University Press, Cambridge, United Kingdom and New York, NY, USA, 2391 pp. doi:10.1017/9781009157896.*

IPCC. (2021b). Climate Change 2021 The Physical Science Basis Summary for Policymakers Working Group I Contribution to the Sixth Assessment Report of the Intergovernmental Panel on Climate Change. In *Climate Change 2021: The Physical Science Basis.*

Jang, J. Y., & Chun, B. C. (2021). Effect of diurnal temperature range on emergency room visits for acute upper respiratory tract infections. *Environmental Health and Preventive Medicine*, *26*(1), 1–8. https://doi.org/10.1186/s12199-021-00974-w

Kachaje, O., Kasulo, V., & Chavula, G. (2016). The potential impacts of climate change on hydropower: An assessment of Lujeri micro hydropower scheme, Malawi. *African Journal of Environmental Science and Technology*, *10*(12), 476–484. https://doi.org/10.5897/ajest2016.2209

Karl, T., Nicholls, N., & Ghazi, A. (1999). CLIVAR/RCOS/WMO Workshop on Indices and Indicators for Climate Extremes. *Climate Change*, *42*, 3–7.

Kew, S. F., Philip, S. Y., Hauser, M., Hobbins, M., Wanders, N., Jan Van Oldenborgh, G., Van Der Wiel, K., Veldkamp, T. I. E., Kimutai, J., Funk, C., & Otto, F. E. L. (2021). Impact of precipitation and increasing temperatures on drought trends in eastern Africa. *Earth System Dynamics*, *12*(1), 17–35. https://doi.org/10.5194/esd-12-17-2021

Khodzhimetov, T. A. (1997). Measuring devices for monitoring parodontium resistance and endurance towards chewing load. *Biomedical Engineering*, *31*(1), 56–58. https://doi.org/10.1007/BF02365970

Kim, S. K., Marshall, F., & Dawson, N. M. (2022). Revisiting Rwanda's agricultural intensification policy: benefits of embracing farmer heterogeneity and crop-livestock integration strategies. *Food Security*, *14*(3), 637–656. https://doi.org/10.1007/s12571-021-01241-0

King'uyu, S. M., Ogallo, L. A., & Anyamba, E. K. (2000). Recent trends of minimum and maximum surface temperatures over Eastern Africa. *Journal of Climate*, *13*(16), 2876–2886. https://doi.org/10.1175/1520-0442(2000)013<2876:RTOMAM>2.0.CO;2

Lal, P. N., Mitchell, T., Aldunce, P., Auld, H., Mechler, R., Miyan, A., Romano, L. E., Zakaria, S., Dlugolecki, A., Masumoto, T., Ash, N., Hochrainer, S., Hodgson, R., Islam, T. U., Mc Cormick, S., Neri, C., Pulwarty, R., Rahman, A., Ramalingam, B., … Wilby, R. (2012). National systems for managing the risks from climate extremes and disasters. In *Managing the Risks of Extreme Events and Disasters to Advance Climate Change Adaptation: Special Report of the Intergovernmental Panel on Climate Change* (Vol. 9781107025). https://doi.org/10.1017/CBO9781139177245.009

Lei, L., Bao, J., Guo, Y., Wang, Q., Peng, J., & Huang, C. (2020). Effects of diurnal temperature range on first-ever strokes in different seasons: A time-series study in Shenzhen, China. *BMJ Open*, *10*(11), 1–8. https://doi.org/10.1136/bmjopen-2019-033571

Leng, G., Tang, Q., & Rayburg, S. (2015). Climate change impacts on meteorological, agricultural and hydrological droughts in China. *Global and Planetary Change*, *126*, 23–34. https://doi.org/10.1016/j.gloplacha.2015.01.003

Li, C., Yang, M., Li, Z., & Wang, B. (2021). How will rwandan land use/land cover change under high population pressure and changing climate? *Applied Sciences (Switzerland)*, *11*(12). https://doi.org/10.3390/app11125376

Lim, Y. H., Hong, Y. C., & Kim, H. (2012). Effects of diurnal temperature range on cardiovascular

and respiratory hospital admissions in Korea. *Science of the Total Environment*, *417–418*, 55–60. https://doi.org/10.1016/j.scitotenv.2011.12.048

Lobell, D. B., & Field, C. B. (2007). Global scale climate-crop yield relationships and the impacts of recent warming. *Environmental Research Letters*, *2*(1). https://doi.org/10.1088/1748-9326/2/1/014002

Loevinsohn, M. E. (1994). Climatic warming and increased malaria incidence in Rwanda. *The Lancet*, *343*(8899), 714–718. https://doi.org/10.1016/S0140-6736(94)91586-5

Lu, C., Sun, Y., & Zhang, X. (2022). Anthropogenic Influence on the Diurnal Temperature Range since 1901. *Journal of Climate*, *35*(22), 3583–3598. https://doi.org/10.1175/JCLI-D-21-0928.1

Lu, Y., Yue, W., & Huang, Y. (2021). Effects of land use on land surface temperature: A case study of Wuhan, China. *International Journal of Environmental Research and Public Health*, *18*(19). https://doi.org/10.3390/ijerph18199987

Lydie, M. (2016). Droughts and Floodings Implications in Agriculture Sector in Rwanda: Consequences of Global Warming. *Nature*, *11*(tourism), 13. https://www.intechopen.com/books/advanced-biometric-technologies/liveness-detection-in-biometrics

Lyon, B. (2014). Seasonal drought in the Greater Horn of Africa and its recent increase during the March-May long rains. *Journal of Climate*, *27*(21), 7953–7975. https://doi.org/10.1175/JCLI-D-13-00459.1

Machina, B. M., & Sharma, S. (2017). Assessment of Climate Change Impact on Hydropower Generation : A Case Study of Nigeria. *International Journal of Engineering Technology Science and Research*, *4*(8), 753–762.

Mahrt, L. (2014). Stably stratified atmospheric boundary layers. *Annual Review of Fluid Mechanics*, *46*, 23–45. https://doi.org/10.1146/annurev-fluid-010313-141354

Maniragaba, A., Muse, S. G., Benjamin, M. N., & Kato, N. J. (2018). Impact of Climate Variation on Malaria Incidence in Rwandan Highland. *East African Journal of Science and Technology*, *8*, 75–76.

Marigi, S. N., Njogu, A. K., & Githungo, W. N. (2016). Trends of Extreme Temperature and Rainfall Indices for Arid and Semi-Arid Lands of South Eastern Kenya. *Journal of Geoscience and Environment Protection*, *04*(12), 158–171.

https://doi.org/10.4236/gep.2016.412012

Meehl, G. A., Karl, T., Easterling, D. R., Changnon, S., Pielke, R., Changnon, D., Evans, J., Groisman, P. Y., Knutson, T. R., Kunkel, K. E., Mearns, L. O., Parmesan, C., Pulwarty, R., Root, T., Sylves, R. T., Whetton, P., & Zwiers, F. (2000). An Introduction to Trends in Extreme Weather and Climate Events: Observations, Socioeconomic Impacts, Terrestrial Ecological Impacts, and Model Projections * . *Bulletin of the American Meteorological Society*, *81*(3), 413–416. https://doi.org/10.1175/1520-0477(2000)081<0413:aittie>2.3.co;2

Meinshausen, M., Meinshausen, N., Hare, W., Raper, S. C. B., Frieler, K., Knutti, R., Frame, D. J., & Allen, M. R. (2009). Greenhouse-gas emission targets for limiting global warming to 2°C. *Nature*, *458*(7242), 1158–1162. https://doi.org/10.1038/nature08017

Mekasha, A., Tesfaye, K., & Duncan, A. J. (2014). Trends in daily observed temperature and precipitation extremes over three Ethiopian eco-environments. *International Journal of Climatology*, *34*(6), 1990–1999. https://doi.org/10.1002/joc.3816

Mondal, A., Kundu, S., & Mukhopadhyay, A. (2012). RAINFALL TREND ANALYSIS BY MANN-KENDALL TEST: A CASE STUDY OF NORTH-EASTERN PART OF CUTTACK DISTRICT, ORISSA. *International Journal of Geology, Earth and Environmental Sciences*, *2*(1), 70–78. http://www.cibtech.org/jgee.htm

Mueller, V., Sheriff, G., Dou, X., & Gray, C. (2020). Temporary migration and climate variation in eastern Africa. *World Development*, *126*, 104704. https://doi.org/10.1016/j.worlddev.2019.104704

Mutsotso, R. B., Sichangi, A. W., & Makokha, G. O. (2018). Spatio-Temporal Drought Characterization in Kenya from 1987 to 2016. *Advances in Remote Sensing*, *07*(02), 125–143. https://doi.org/10.4236/ars.2018.72009

Nashwan, M. S., & Shahid, S. (2019). Spatial distribution of unidirectional trends in climate and weather extremes in Nile river basin. *Theoretical and Applied Climatology*, *137*(1–2), 1181–1199. https://doi.org/10.1007/s00704-018-2664-5

National Institute of Statistics of Rwanda. (2023). *Main Indicators: 5th Rwandan Population and Housing Census (PHC)); National Institute of Statistics of Rwanda: Kigali, Rwanda*.

Ngaina, J., & Mutai, B. (2013). Observational evidence of climate change on extreme events over East Africa. *Global Meteorology*, *2*(1), 2. https://doi.org/10.4081/gm.2013.e2

Ngarukiyimana, J. P., Fu, Y., Sindikubwabo, C., Nkurunziza, I. F., Ogou, F. K., Vuguziga, F.,

Ogwang, B. A., & Yang, Y. (2021). Climate Change in Rwanda: The Observed Changes in Daily Maximum and Minimum Surface Air Temperatures during 1961–2014. *Frontiers in Earth Science*, *9*(March). https://doi.org/10.3389/feart.2021.619512

Novotny, E. V., & Stefan, H. G. (2007). Stream flow in Minnesota: Indicator of climate change. *Journal of Hydrology*, *334*(3–4), 319–333. https://doi.org/10.1016/j.jhydrol.2006.10.011

Omondi, P. A. o., Awange, J. L., Forootan, E., Ogallo, L. A., Barakiza, R., Girmaw, G. B., Fesseha, I., Kululetera, V., Kilembe, C., Mbati, M. M., Kilavi, M., King'uyu, S. M., Omeny, P. A., Njogu, A., Badr, E. M., Musa, T. A., Muchiri, P., Bamanya, D., & Komutunga, E. (2014). Changes in temperature and precipitation extremes over the Greater Horn of Africa region from 1961 to 2010. *International Journal of Climatology*, *34*(4), 1262–1277. https://doi.org/10.1002/joc.3763

Owoyesigire, B., Mpairwe, D., Ericksen, P., & Peden, D. (2016). Trends in variability and extremes of rainfall and temperature in the cattle corridor of Uganda. *Uganda Journal of Agricultural Sciences*, *17*(2), 231. https://doi.org/10.4314/ujas.v17i2.8

Pita-Díaz, O., & Ortega-Gaucin, D. (2020). Analysis of anomalies and trends of climate change indices in Zacatecas, Mexico. *Climate*, *8*(4). https://doi.org/10.3390/cli8040055

Polong, F., Chen, H., Sun, S., & Ongoma, V. (2019). Temporal and spatial evolution of the standard precipitation evapotranspiration index (SPEI) in the Tana River Basin, Kenya. *Theoretical and Applied Climatology*, *138*(1–2), 777–792. https://doi.org/10.1007/s00704-019-02858-0

REMA. (2019). Assessment of climate change vulnerability in Rwanda. *Rwanda Environment Management Authority, Kigali*.

Rettie, F. M., Gayler, S., Weber, T. K. D., Tesfaye, K., & Streck, T. (2023). Comprehensive assessment of climate extremes in high-resolution CMIP6 projections for Ethiopia. *Frontiers in Environmental Science*, *11*(May), 1–18. https://doi.org/10.3389/fenvs.2023.1127265

Revadekar, J. V., Kothawale, D. R., Patwardhan, S. K., Pant, G. B., & Rupa Kumar, K. (2012). About the observed and future changes in temperature extremes over India. *Natural Hazards*, *60*(3), 1133–1155. https://doi.org/10.1007/s11069-011-9895-4

Russo, S., Marchese, A. F., Sillmann, J., & Immé, G. (2016). When will unusual heat waves become normal in a warming Africa? *Environmental Research Letters*, *11*(5). https://doi.org/10.1088/1748-9326/11/5/054016

Rwanda. (2006). *National Adaptation Programmes of Action for Climate Change. Kigali: Ministry of Lands, Environment, Forestry, Water and Mines*. *December*.

Rwanda. (2011). *Green Growth and Climate Resilience-National Strategy on Climate Change and Low Carbon Development. Kigali: Ministry of Natural Resources. October*, 100. http://repository.ubn.ru.nl/bitstream/handle/2066/135304/135304.pdf?sequence=1#page=8

Rwanda. (2018). *Evaluation of the Green Growth and Climate Resilience Strategy Implementation. Kigali: Ministry of Environment*. *October*.

Rwanda. (2019). *National Environment and Climate Change Policy*. *June*, 31.

Rwanda. (2020). *Rwanda's revised Nationally Determined Contributions - NDCs*. *November*.

Rwanda. (2022). Revised Green Growth and Climate Resilience: National Strategy for Climate Change and Low Carbon Development. *Kigali, Rwanda*.

Safari, B. (2010). A review of energy in Rwanda. *Renewable and Sustainable Energy Reviews*, *14*(1), 524–529. https://doi.org/10.1016/j.rser.2009.07.009

Safari, B. (2012). Trend Analysis of the Mean Annual Temperature in Rwanda during the Last Fifty Two Years. *Journal of Environmental Protection*, *03*(06), 538–551. https://doi.org/10.4236/jep.2012.36065

Sen, P. K. (1968). Estimates of the Regression Coefficient Based on Kendall's Tau. *Journal of the American Statistical Association*, *63*(324), 1379–1389. https://doi.org/10.1080/01621459.1968.10480934

Serrano, A., Mateos, V. L., & García, J. A. (1999). Trend analysis of monthly precipitation over the Iberian Peninsula for the period 1921-1995. *Physics and Chemistry of the Earth, Part B: Hydrology, Oceans and Atmosphere*, *24*(1–2), 85–90. https://doi.org/10.1016/S1464-1909(98)00016-1

Setianto, A., & Triandini, T. (2015). Comparison of Kriging and Inverse Distance Weighted (Idw) Interpolation Methods in Lineament Extraction and Analysis. *Journal of Applied Geology*, *5*(1), 21–29. https://doi.org/10.22146/jag.7204

Sheffield, J., Wood, E. F., & Roderick, M. L. (2012). Little change in global drought over the past 60 years. *Nature*, *491*(7424), 435–438. https://doi.org/10.1038/nature11575

Siebert, A., Dinku, T., Vuguziga, F., Twahirwa, A., Kagabo, D. M., delCorral, J., & Robertson, A. W. (2019). Evaluation of ENACTS-Rwanda: A new multi-decade, high-resolution rainfall and temperature data set—Climatology. *International Journal of Climatology*, *39*(6), 3104–

3120. https://doi.org/10.1002/joc.6010

Sneyers, R. (1990). On the Statistical Analysis of Series of Obervations. *WMO Technical Note 143; WMO No. 415, TP-103;World Meteorological Organization: Geneva, Switzerland*.

STAP. (2017). *Strengthening Monitoring and Evaluation of Climate Change Adaptation: A STAP Advisory Document*. https://www.thegef.org/sites/default/files/publications/STAP_CCA_ME_complete_synthesis.pdf

Tan, C., Yang, J., & Li, M. (2015). Temporal-spatial variation of drought indicated by SPI and SPEI in Ningxia Hui Autonomous Region, China. *Atmosphere*, *6*(10), 1399–1421. https://doi.org/10.3390/atmos6101399

Tank, A. M. G. K., Zwiers, F. W., & Zhang, X. (2009). Guidelines on analysis of extremes in a changing climate in support of informed decisions for adaptation. *Climate Data and Monitoring Rep.WCDMP 72, WMO-TD 1500, 72*, 56.

Taxak, A. K., Murumkar, A. R., & Arya, D. S. (2014). Long term spatial and temporal rainfall trends and homogeneity analysis in Wainganga basin, Central India. *Weather and Climate Extremes*, *4*, 50–61. https://doi.org/10.1016/j.wace.2014.04.005

Theil, H. (1992). A Rank-Invariant Method of Linear and Polynomial Regression Analysis. In: Raj, B., Koerts, J. (eds) Henri Theil's Contributions to Economics and Econometrics. *Advanced Studies in Theoretical and Applied Econometrics*, *23*(1950), 1397–1412.

Thomas, V., & López, R. (2015). Global Increase In Climate-Related Disasters. *ADB Economics Working Paper Series, No. 466, Asian Development Bank (ADB), Manila, Https://Hdl.Handle.Net/11540/5274*, *466*, 1–33.

Trevor, M. L. (2021). The Impacts of Climate Change: A Comprehensive Study of Physical, Biophysical, Social and Political Issues. *Amsterdam, The Netherlands*, 547–557. https://doi.org/https://doi.org/10.1016/C2019-0-04893-5

Unger, J. (2004). Intra-urban relationship between surface geometry and urban heat island: Review and new approach. *Climate Research*, *27*(3), 253–264. https://doi.org/10.3354/cr027253

Uwimbabazi, J., Jing, Y., Iyakaremye, V., Ullah, I., & Ayugi, B. (2022). Observed Changes in Meteorological Drought Events during 1981–2020 over Rwanda, East Africa. *Sustainability (Switzerland)*, *14*(3). https://doi.org/10.3390/su14031519

Vose, R. S., Easterling, D. R., & Gleason, B. (2005). Maximum and minimum temperature trends

for the globe: An update through 2004. *Geophysical Research Letters*, *32*(23), 1–5. https://doi.org/10.1029/2005GL024379

Walther, G., Post, E., Convey, P., Menzel, A., Parmesank, C., Beebee, T. J. C., Fromentin, J., I, O. H., & Bairlein, F. (2002). Ecological response to recent climate cnahge. *Nature*, *416*, 389–395.

Wang, M. Z., Zheng, S., He, S. L., Li, B., Teng, H. J., Wang, S. G., Yin, L., Shang, K. Z., & Li, T. S. (2013). The association between diurnal temperature range and emergency room admissions for cardiovascular, respiratory, digestive and genitourinary disease among the elderly: A time series study. *Science of the Total Environment*, *456–457*, 370–375. https://doi.org/10.1016/j.scitotenv.2013.03.023

Wang, Z., Zhou, Y., Luo, M., Yang, H., Xiao, S., Huang, X., Ou, Y., Zhang, Y., Duan, X., Hu, W., Liao, C., Zheng, Y., Wang, L., Xie, M., Tang, L., Zheng, J., Liu, S., Wu, F., Deng, Z., … Ran, P. (2020). Association of diurnal temperature range with daily hospitalization for exacerbation of chronic respiratory diseases in 21 cities, China. *Respiratory Research*, *21*(1), 1–10. https://doi.org/10.1186/s12931-020-01517-7

Weber, D. D., & Englund, E. J. (1994). Evaluation and comparison of spatial interpolators II. *Mathematical Geology*, *26*(5), 589–603. https://doi.org/10.1007/BF02089243

Weber, D., & Englund, E. (1992). Evaluation and comparison of spatial interpolators. *Mathematical Geology*, *24*(4), 381–391. https://doi.org/10.1007/BF00891270

White, J. W. C. ;, Alley, R. B. ;, Archer, D. E. ;, Barnosky, A. D. ;, Dunlea, E. ;, Foley, J. ;, Fu, R. ;, Holland, M. M. ;, Lozier, M. S. ;, Schmitt, J. ;, Smith, L. C. ;, Sugihara, G. ;, Thompson, D. W. J. ;, Weaver, A. J. ;, & Wofsy, S. C. (2013). Abrupt Impacts of Climate Change: Anticipating Surprises. *Washington, DC: The National Academies Press*.

WMO. (2004). *REPORT OF THE CCl/CLIVAR EXPERT TEAM ON CLIMATE CHANGE DETECTION, MONITORING AND INDICES (ETCCDMI)*. *WMO-TD No. 1205*, 24–26. http://www.wmo.int/pages/prog/wcp/wcdmp/documents/WCDMP-54_000.pdf

WMO. (2020). *World Meteorological Organization Commission for Climatology. State of the Climate in Africa 2019. World Meteorological Organisation, Geneva. Report WMO-No.1253, 37p*.

Yannick, L., & Randriamarolaza, A. (2023). *Extreme temperatures detection and attribution related to external forcing in Madagascar*. *May 2022*, 3907–3924.

https://doi.org/10.1002/joc.8065

Yue, S., Pilon, P., & Phinney, B. (2003). Canadian streamflow trend detection: Impacts of serial and cross-correlation. *Hydrological Sciences Journal*, *48*(1), 51–63. https://doi.org/10.1623/hysj.48.1.51.43478

Zhang, X., Alexander, L., Hegerl, G. C., Jones, P., Tank, A. K., Peterson, T. C., Trewin, B., & Zwiers, F. W. (2011). Indices for monitoring changes in extremes based on daily temperature and precipitation data. *Wiley Interdisciplinary Reviews: Climate Change*, *2*(6), 851–870. https://doi.org/10.1002/wcc.147

Zhang, X., & Yang, F. (2004). RClimDex requires the base package of R and graphic user interface TclTk. *Climate Research Branch Environment Canada Downsview, Ontario Canada*, 1–23.

Zheng, S., Wang, M., Li, B., Wasng, S., He, S., Yin, L., Shang, K., & Li, T. (2016). Gender, age and season as modifiers of the effects of diurnal temperature range on emergency room admissions for cause-specific cardiovascular disease among the elderly in Beijing. *International Journal of Environmental Research and Public Health*, *13*(5), 1–15. https://doi.org/10.3390/ijerph13050447

Zhou, G., Minakawa, N., Githeko, A. K., & Yan, G. (2004). Association between climate variability and malaria epidemics in the East African highlands. *Proceedings of the National Academy of Sciences of the United States of America*, *101*(8), 2375–2380. https://doi.org/10.1073/pnas.0308714100

Zhou, L., Dai, A., Dai, Y., Vose, R. S., Zou, C. Z., Tian, Y., & Chen, H. (2009). Spatial dependence of diurnal temperature range trends on precipitation from 1950 to 2004. *Climate Dynamics*, *32*(2–3), 429–440. https://doi.org/10.1007/s00382-008-0387-5

Chapter 4 Rainfall variability and trends over Rwanda

This Chapter reproduces the content of our published paper (https://doi.org/10.20987/jccs.04.06.2022).

4.1 Introduction

Bimodal rainfall patterns occur across the majority of East Africa, including Rwanda. (Mutai and Neil, 2000; Schreck and Semazzi, 2004; Ilunga; Muhire, 2010). Many countries in African rely on seasonal rainfall for domestic and agricultural purposes (Challinor *et al*., 2007). Variability in rainfall has an impact on agricultural productivity, which changes crop productivity (Mahmudul *et al,* 2011; Ochieng *et al.,* 2016). Since the economy of Sub-Saharan African (SSA) countries is hinged on the agricultural sector, rainfall variability will have various effects on farming activities and other socio-economic that contribute to the development of the country. Precipitation patterns over East Africa region are largely controlled by the movement of the Inter-Tropical Convergence Zone (ITCZ) (Okoola, 1999), Sea Surface Temperature (SST), the convergence of Saint Helena Anticyclones from the South Atlantic Ocean and Mascarene Anticyclones from the Indian Ocean (Indeje *et al*., 2000; Ilunga *et al*., 2004; Kizza *et al*., 2009; Gitau *et al*., 2013).

Over East Africa EL-Niño enhances the probability of being unusually wet during the short rains while the long rains remain largely unaffected (Indeje *et al*., 2000; Nicholson *et al*., 2001; Schreck and Semazzi, 2004; Hastenrath and Polzin, 2004; Ilunga and Muhire, 2010; Muhire *et al*., 2015). The positive (negative) phases of the Indian Ocean dipole (IOD) results in an increased (decreased) rainfall over the EA with a strong connection during El Niño/La Niña years (Owiti, 2008). The EA rainfall variability is also linked with the Madden-Julian Oscillation (MJO) with a higher association to the west of the region (Peter. *et al.,* 2008). Research findings have indicated that rainfall in the EA is characterized by immense rainfall variation over short distances. Annual mean rainfall over most parts of the EA ranges between 800 and 1200mm in wet seasons (Nicholson, 2017) even though some areas can receive much more rainfall due to highlands particularly in the western and northern parts of the region. In sub-Saharan Africa during the past few decades, smart agriculture has become more prevalent, especially in regions where literature suggests that climatic variability and change will have an impact on agricultural productivity and food security in the absence of adequate interventions. (Zougmoré *et al.,* 2018).

Several researches have been made with aim of understanding the behaviour and trend of rainfall in Rwanda. The use of limited data was demonstrated by many researchers (Henninger, 2013; Muhire and Ahmed, 2014; Muhire *et al.,* 2015a; Muhire *et al.,* 2015b; Mohammed *et al*., 2016; Ntirenganya 2018). In the recent past, the study to understand the climatology of Rwanda has been made using gridded data (Asher *et al.*, 2019); however, rainfall variability and its associated trend was not a subject of this study. Recent research by Kazora *et al.,* (2021) attempted to understand the behavior of rainfall and associated circulation anomalies using Climate Hazards Category Infrared Precipitation with Stations (CHIRPS) rainfall data. It is important to understand the rainfall variability and associated trends in Rwanda using a high quality and complete dataset. This study aims at identifying the nature of rainfall variability over Rwanda on seasonal and annual timescale by assessing the spatial and temporal characteristics in the historical rainfall to depict its current variability and trends in the country. The findings from the study will inform decision-makers and policy-makers of the necessity to integrate climate variability and climate change information into developing policies and to formulate strategies that support different economic sectors such as industries, services and agriculture among others.

4.2 Materials and Methods

4.2.1 Study Area

Rwanda, is known as land of thousand hills, landlocked country located in East Africa, between 1°4′ and 2°51′ South; 28°53′ and 30°53′ east and covers an area of 26,338 km^2. Rwanda is bordered by Tanzania to the East, Uganda to the North, Democratic Republic of Congo to the West, and Burundi to the South (Figure 4. 1). Diverse climate patterns characterizing the country into complex topographical features. These include the highland areas located in the northwest and successive hills and valleys over the central plateau while the low land areas are the dominant features over the eastern parts of the country. The Crest Congo Nile delineates the western highlands and the central plateau while several mountains predominately occupy the northern region of the country. Due to the complex topography, mean annual rainfall varies geographically across the country (Ntwali *et al*., 2016) with the south-western and north-western highland areas of the country receiving high amount of rainfall while the eastern region receives a low amount of rainfall (Ilunga and Muhire, 2010; Ntwali *et al.,* 2016). Rwanda experiences two major rainy

seasons in a year, March to May (MAM) rainy season (locally referred to as 'Itumba') and September to December (SOND) rainy season ('Umuhindo' in local term). A short dry season (commonly known as 'Urugaryi') occurs from January to February (JF) while and a long dry season (kwown as 'Impeshyi' in local language) extends from June to August (JJA) (Muhire *et al.,* 2015a; Siebert *et al*., 2019) with the two monthly rainfall peaks being April and November for MAM and SOND rainy seasons respectively (Ntwali *et al.,* 2016; Muhire *et al.,* 2015b).

Rwanda exhibits six climatic zones from eastern to western parts of the country based on annual rainfall and temperature distribution. The dry and hot lowland climate zone extending from the east of the Southern Province to the Eastern Province of the country. The temperate climate zone of the central highlands with an elevation increasing from east to west, and a less temperature fluctuation separating the southern Rwanda humid mountain climate zone situated south of the Congo-Nile watershed extending to the Volcano National Park in the northern region of the country with the northern mountain ranges exhibiting mountainous climatic zone. The fifth climatic zone is the Lake Kivu sea climate zone extending from Rubavu to Bugarama in the southern parts of Lake Kivu and the last is the Kigali urban climate (Henninger, 2013). Large scale systems that influence the climate of Rwanda, include dry Saint Helena and Azores anticyclones. These systems influence drie conditions over the country during June to August (Ilunga *et al.,* 2004; Ilunga *et al.,* 2008; Kizza *et al.,* 2009). The ITCZ movement southwards, passing over the trough of Lake Victoria and Congo Air mass enhances the rain over Rwanda, before reaching its southernmost location by the end of November. During the short dry season (December to February), northern winter monsoon pushes dry and cold air masses from the Arabian Sea over Lake Victoria and induces little rainfall in the highland regions of the country (Ilunga *et al.,* 2004; Kizza *et al.,* 2009). The mean rainfall significantly reduces when topography reduces (Ntwali *et al.,* 2016).

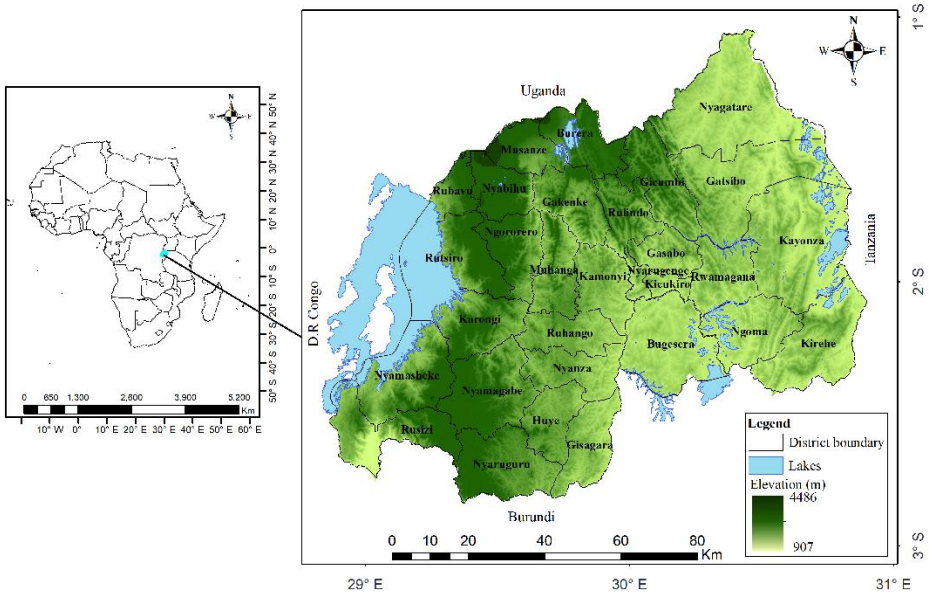

Figure 4. 1 Geographical location of Rwanda, topographic features and the meteorological station location

1.1.2 Data

The daily gridded rainfall dataset which was accumulated to monthly, seasonal and annual total were obtained from Rwanda Meteorology Agency (Meteo Rwanda) with a spatial resolution 0.0375 degrees (~ 4km) for the period of 1981 and 2017. Twelve synoptic stations were chosen for the graphical analysis and seventy-two climatological stations were added to the synoptic stations for spatial analysis. The generation of the gridded dataset improves the accessibility of meteorological data in areas with no or sparse observation resulting from silent weather stations especially during periods of political instability and recovery. This dataset was generated by merging quality-controlled observed data with satellite rainfall estimates data from Tropical Applications of Meteorology using SATellite (TAMSAT). More information on the generation of the dataset is found in (Siebert *et al.*, 2019).

4.2.3 Methods

Methods of spatial and temporal analysis were employed to evaluate the degree of rainfall variability and its related trend over Rwanda. A graphical method was used to analyse the temporal variability of rainfall. This method's benefit is that it enables immediate visual examination of whether a trend is present in each time series. Mann–Kendall (MK), a nonparametric rank-based

test was employed under this study to test the statistical significance of the observed trends where positive values show an upward slope while a downward slope is indicated by a negative value (Safari, 2012; Nsubuga *et al*., 2014; Ongoma *et al*., 2017).

$S = \sum_{i=1}^{n-1} \sum_{j=i+1}^{n} sgn(x_j - x_i)$ (1)

In equation (1) sgn is the sign function and x_i and x_j are the sequential data values n is the number of data points. $sgn(x_j - x_i) = \begin{cases} 1 & \text{if } x_i - x_j > 0, \\ 0 & \text{if } x_i - x_j = 0, \\ -1 & \text{if } x_i - x_j < 0. \end{cases}$ (2)

Under the null hypothesis if no trend, the statistic in (2) follows an approximately normal distribution with mean zero and variance.

$\sigma_S^2 = \frac{n(n-1)(2n+5) - \sum_{k=1}^{m} t_k(t_k-1)(2t_k+5)}{18}$ (3)

In equation (3) $m\ is$ the number of is tied groups and $t_k$is the number of data points in the group k. When the sample size $n \geq 10$, the statistical test Z is computed using equation (4)

$Z = \begin{cases} \frac{S-1}{\sigma_S} & \text{if } S > 0, \\ 0 & \text{if } S = 0, \\ \frac{S+1}{\sigma_S} & \text{if } S < 0. \end{cases}$ (4)

To compute the change magnitude in rainfall, the Theil–Sen's slope estimator (Theil, 1950 and Sen, 1968) was employed at 95% significance level.

$T_i = \frac{(x_k - x_j)}{j-k}$, $j \neq k$, (5)

From equation (5), x_j and x_k are the data values for j and k times of a period$(j > k)$. For a time series x having observations, there is a possible $N = n\,(n-1)/2$ values of T_i that can be computed. According to Sen's method, slope estimator Q_i is thus the median of these N values of T_i.

$Q_i = \begin{cases} T_{(N+1)/2} & for\ N\ odd\ observations \\ \frac{1}{2}\left(T_{N/2} + T_{(N+1)/2}\right) & for\ N\ even\ obesvations. \end{cases}$

The examination of spatial variability of rainfall at annual and seasonal timescale was done by using the coefficient of variation (CV) which measures the degree of variability in a dataset. The results from seasonal mean rainfall distribution, trend magnitude and coefficient of variation were

presented spatially using ArcGIS that provided spatial maps, thus these methods enabled us to understand how rainfall varies spatially across the country.

4.3 Results

4.3.1 Rainfall distribution

The climatological distribution of monthly, seasonal and annual mean rainfall over Rwanda were analysed to understand the spatial distribution and their corresponding patterns over the country. The distribution in monthly mean rainfall shows that rainfall over Rwanda follows a bimodal pattern with MAM and SOND being the rainy seasons. It is also clear that JJA is the long dry season while from JF is a short dry season. On a monthly basis, rainfall is observed over Rwanda through the year which may be an indication of a potential for activities relying on rainfall for their performance (Figure 4. 2).

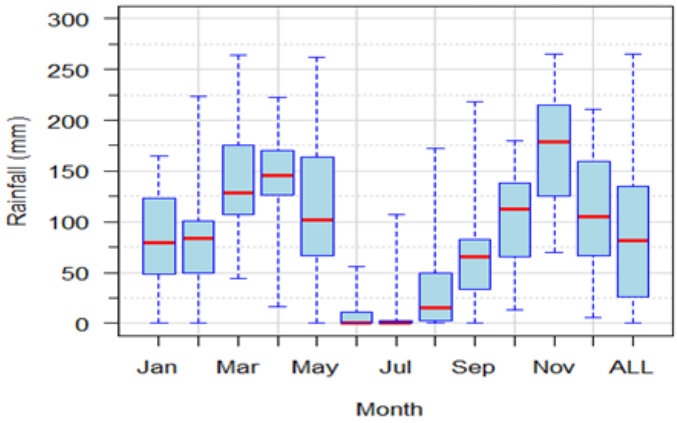

Figure 4. 2 A box-and-whiskers plot showing the amount of rain each month over Rwanda (1981-2010). Data from the second and third quartiles are shown as boxes. First and fourth quartiles are shown by whiskers. The median value for each month is shown by the red line.

The mean rainfall distribution presented in Figure 4. 3 indicated a non-homogeneous pattern over different regions of the country. During MAM, analysis of rainfall distribution shows a low amount of rainfall over the eastern parts of the country (Kirehe, Ngoma and Kayonza, eastern part of Bugesera, southern of Rwamagana, southern parts of Gatsibo district extending to the central parts and southern parts of Kigali City) increasing towards the north-eastern parts of the country over the central and northern parts of Gatsibo and Nyagatare districts, along the central parts of the country and the areas bordering Lake Kivu in the western parts of the country. The highland region

in the areas surrounding the Crest Congo Nile extending to the Nyungwe National Park and the surrounding areas (Nyamagabe and Nyaruguru Districts) of the southern province, Volcano National Park, , north-western region in the areas of Ngororero, Nyabihu and Rutsiro districts surrounding Gishwati National Park and over northern parts (Gicumbi, Burera, Gakenke and Musanze districts) revealed higher amount of rainfall which may be attributed mainly to the influence of the topography.

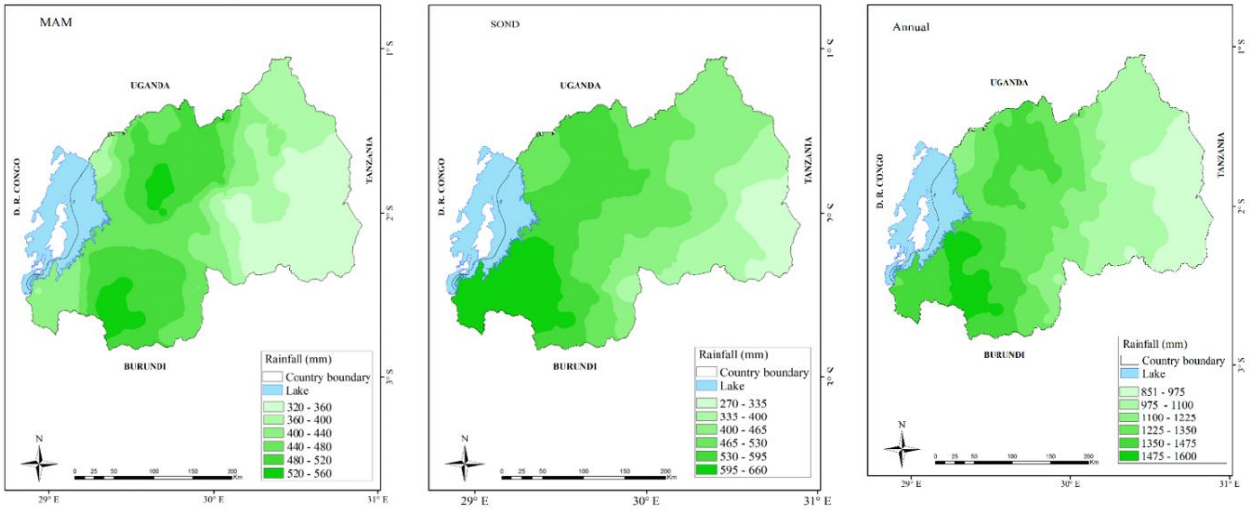

Figure 4. 3 Rwanda's rainfall distribution in space from March to May (left), September to December (center) and mean yearly rainfall (right) from 1981-2017.

The mean rainfall distribution during SOND rainy season showed higher amount of rainfall in the south-western parts (areas around Kamembe extending to Nyungwe National Park, Nyamagabe and Nyaruguru) areas bordering Lake Kivu except the areas over Gisenyi-Aero and north-western Rutsiro, the highland region along Crest Congo Nile, Volcano National Park and northern highlands of Burera, Musanze, Gakenke and Ngororero extending to the north-western highland of Muhanga district. A lower amount of rainfall was obtained over the eastern parts of the country (Kirehe, Ngoma and Kayonza, Eastern part of Bugesera, Akagera National Park and north-eastern parts of Gisagara district increasing towards western of Rwamagana, central and north-western Bugesera, Gatsibo and Nyagatare district extending to the Central plateau (Kigali City and central part of the southern region) (Figure 4. 3). The spatial distribution of annual mean rainfall shows a low rainfall in the eastern lowlands (Kirehe, Kayonza, areas around Akagera National Park and the south-eastern parts of Gatsibo District) increasing towards the central, north-eastern and central plateau. Higher rainfall was observed over the south-western parts of the southern region in the

areas surrounding Nyungwe National Park extending along the western, northern and north-western highlands of the country. Highland region along Crest Congo Nile extending to the Nyungwe National Park, Volcano National Park, south-western parts (Rubona, Nyamagabe and Kamembe), areas over north-western parts (Gakenke, Gicumbi, Burera and Musanze districts) areas received a high amount of rainfall reducing towards the central parts of the country (Figure 4. 3).

4.3.2 Rainfall variability

The coefficient of variation during the MAM showed that the areas to the extreme eastern region of the country (Kirehe district), the central region (northern Rwamagana extending to south-western of Gatsibo bordering southern Gicumbi and the south-eastern parts of the southern region of the country (Huye and Gisagara) exhibited more pronounce rainfall variability indicating less reliability to rainfall over the area. The central and north-eastern parts of the eastern areas extending to the central region of the country (Kigali city, Kamonyi, Ruhango Nyanza, southern region of Muhanga) registered a less pronounced variability while the south-western and northern highland areas of the country showed less variability (high reliability) during MAM rainfall season (Figure 4. 4). During the SOND season, a more pronounced variability in rainfall was observed in the areas of south-eastern parts of the dry and hot lowland climate zone (Kirehe District). A considerable magnitude of rainfall variability was registered over Kigali City, the central-eastern parts towards the areas around Akagera National Park and the extreme South-eastern parts of the southern region reducing towards the north-eastern parts and the central areas of the southern region. The western region in the areas bordering Lake Kivu and Nyungwe National Park extending to the northern highland and the areas around the Volcano National Park revealed a lower variability in rainfall (Figure 4. 4). Spatial distribution of the annual coefficient of variation indicated a higher rainfall variation over Kigali City, the central-eastern part (Rwamagana, Gatsibo, northern Kayonza and southern part of Nyagatare) reducing towards the southern and extreme northern parts of the eastern region and the south-eastern extending to the central parts of the Southern province of the country. The lower annual rainfall variation over the western parts of the country in the areas bordering Lake Kivu extending to the highland areas of the country in the areas bordering Nyungwe National Park, Crest Congo Nile and the Volcano National Park areas over the northern and north-western highland of the country was observed (Figure 4. 4). The spatial distribution in seasonal and annual mean rainfall results indicated that the western and the northern

highlands receive higher amounts of rainfall reducing towards the central and low amount of rainfall over the low land thus confirming the results of (Ntwali *et al*., 2016).

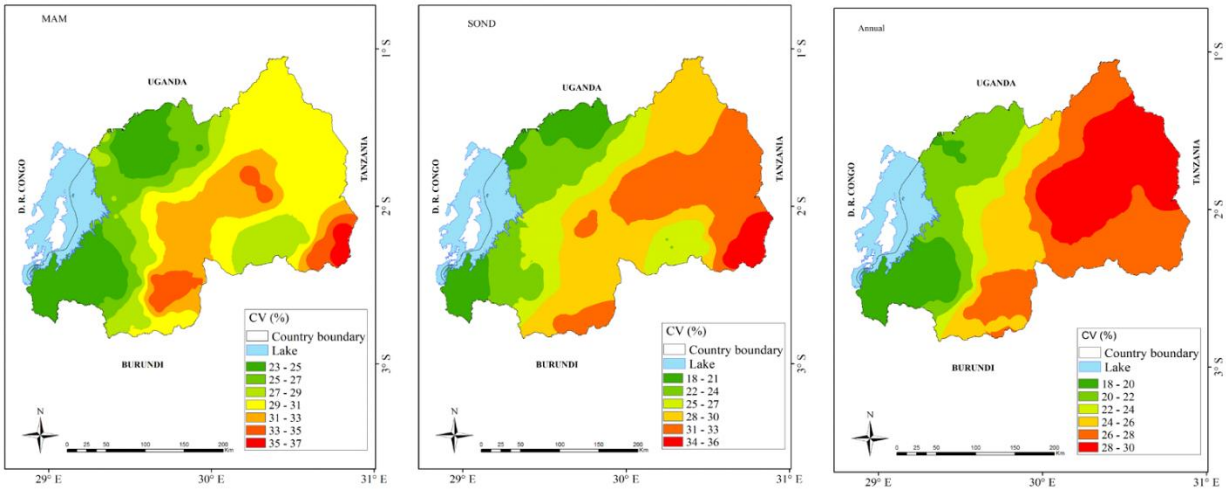

Figure 4. 4 Rwanda's rainfall variability distribution in space from March to May (left), September to December (center) and yearly rainfall variability (right) from 1981-2017.

4.3.3 Trend analysis

The temporal variability results obtained using graphical and statistical methods indicated non-homogeneous characteristics during the annual and the seasonal time scale. The corresponding slope and significance test results are presented in the sub-section below. The graphical trend results indicated a decreasing trend during the MAM season for the twelve stations (Figure 4. 5). During the SOND season, five stations out of twelve registered a decreasing trend while seven stations out of twelve indicated an increasing trend (Figure 4. 6). On an annual timescale, only three out of twelve stations namely Kawangire, Nyagatare and Gisenyi-Aero revealed an increasing trend while the rest of the stations had decreasing trends (Figure 4. 7). The trend results obtained using the statistical method indicated a non-homogeneity during both the annual and seasonal time scales. The results from most stations revealed that the MAM season has decreasing rainfall trends except Nyagatare station which indicated a non-significant increase. The eleven stations with decreasing trends included Kigali-Aero located in Kigali City, Byimana, Rubona-Colline and Gikongoro Met located in the southern parts. In the northern areas, the stations of Ruhengeri-Aero and Byumba registered decreasing trends. The stations located in the Eastern Province showed decreasing trends over Kawangire and Kibungo-Kazo respectively. The stations located in the Western region (Kamembe-Aero, Gisenyi-Aero and Rubengera) show a decrease of

3.3 mm year^{-1}, 1.3 mm year^{-1} and 1.8 mm year^{-1} corresponding to 5.7%, 15.5% and 5.8% respectively. During the SOND rainy season, a significant increasing trend of 3.1 mm year^{-1} corresponding to 4.3% was revealed over Gisenyi-Aero station located in the Western region. Other stations located in Western (Kamembe-Aero and Rubengera), Kigali City (Kanombe-Aero), northern areas (Ruhengeri-Aero) and North-eastern parts of the country (Nyagatare) had non-significant decreasing trends. Non-significant increasing trends were observed over stations located in the southern parts of the country (Byimana, Rubona-Colline and Gikongoro Met). The same was observed for stations located over eastern parts (Kawangire and Kibungo-Kazo stations) and northern parts (Byumba station).

On the annual timescale, three stations out of twelve stations namely Kawangire and Nyagatare located in the eastern region as well as Gisenyi-Aero located in north-western parts of the country revealed non-significant increasing trends. A significant decreasing trend was observed over the south-western parts (Kamembe-Aero) of 9.1 mm year^{-1} corresponding to -6.7%. Out of twelve stations, eight stations registered a non-significant decreasing trend. The stations located in the Southern Province (Byimana, Rubona-Colline and Gikongoro-Met) registered decreasing trends. Over the northern parts (Byumba Met and Ruhengeri-Aero stations) also revealed decreasing trends. In the eastern parts, a decreasing trend of 1.6 mm year^{-1} corresponding to 4.2% was observed over Kibungo-Kazo station as well as Kigali-Aero station located in Kigali city which revealed a negative slope of 4 mm year^{-1} corresponding to 6.7% (Table 4. 1).

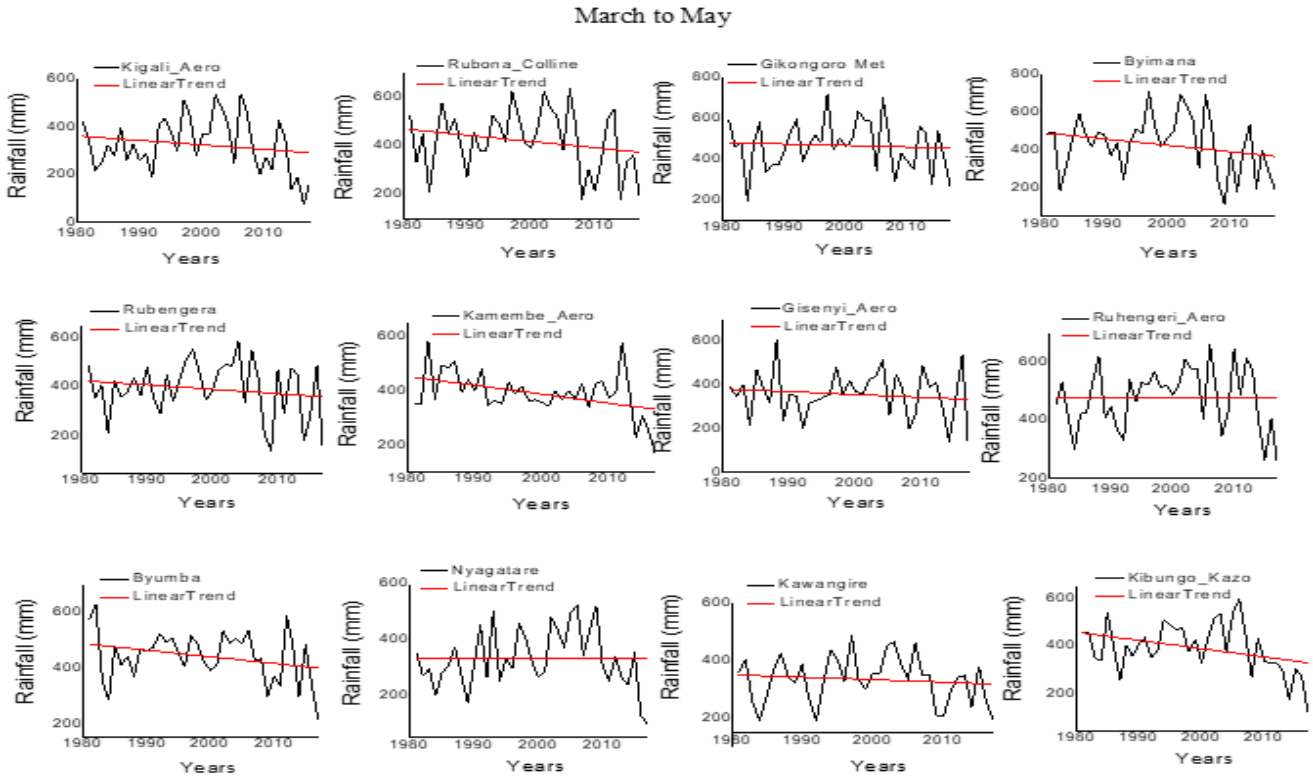

Figure 4. 5 Temporal variability and trends of March to May seasonal rainfall over selected stations in Rwanda (1981-2017).

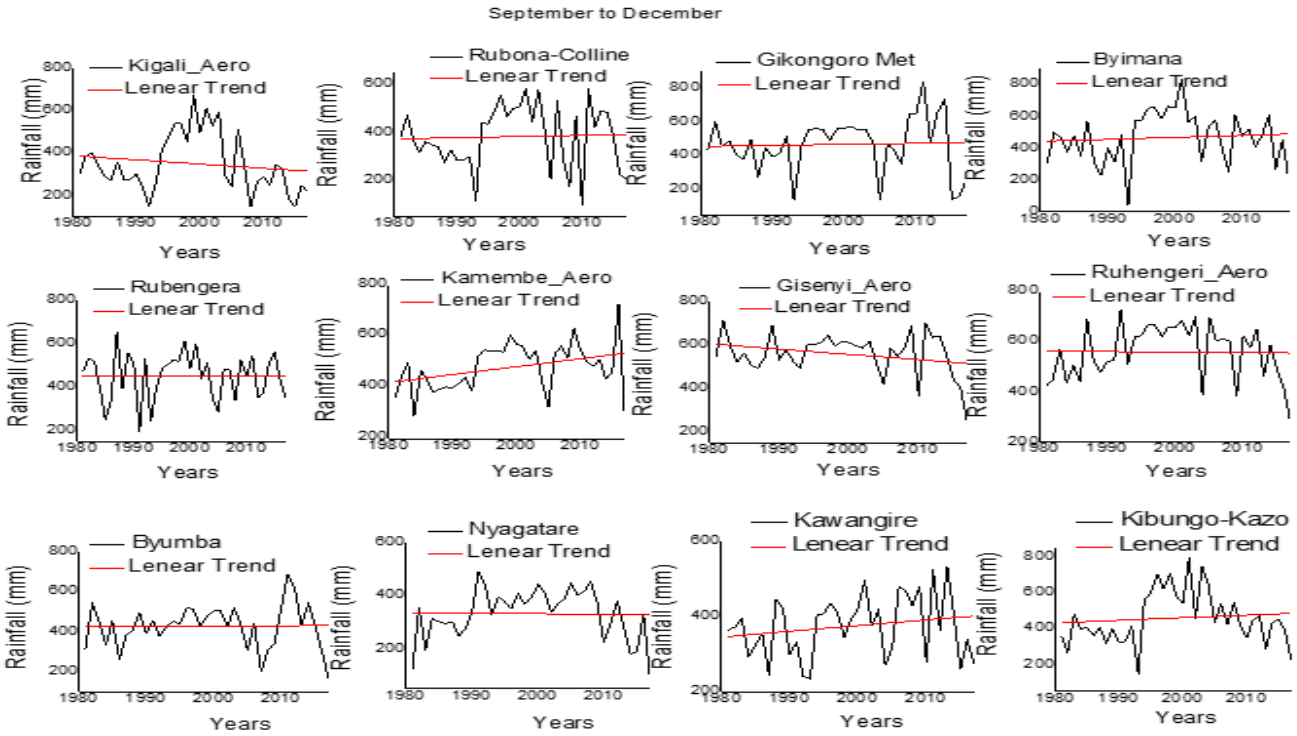

Figure 4. 6 Temporal variability and trends of September to December seasonal rainfall over selected stations in Rwanda (1981-2017).

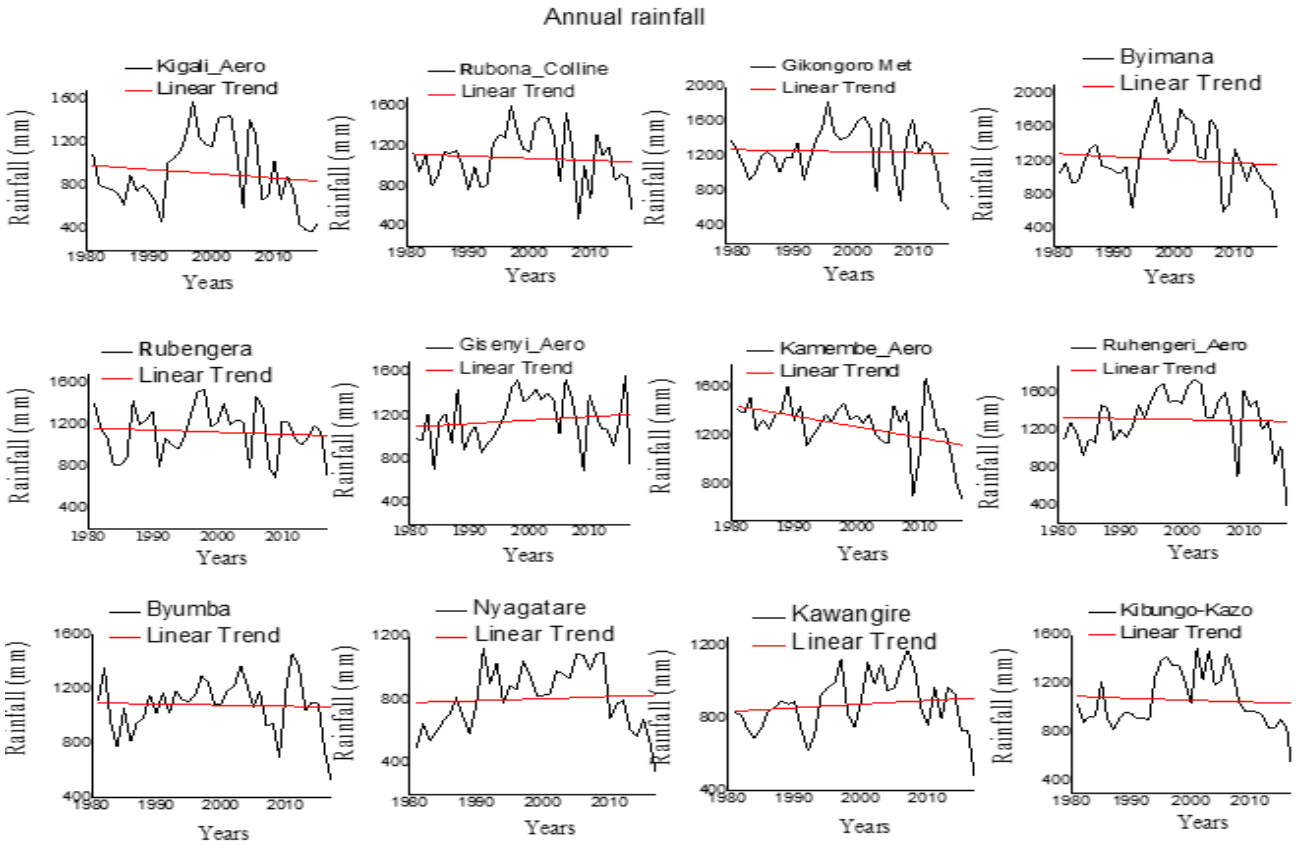

Figure 4. 7 Temporal variability and linear trends of annual rainfall over selected stations in Rwanda (1981-2017)

Table 4. 1 Statistical characteristics of rainfall for the 12 stations for March-April- May (MAM) and September-October-November- December (SOND) where, CV (coefficient of variation), Z (Mann Kendal trend, (-) decreasing and (+) increasing), S (significance of trend at 90% (+) and at 95% (*)), Q (Sen's slope, mm year^{-1}), and T (trend, %/year) in the period 1981 to 2017 over Byimana (BMN), Byumba Met (BYM), Kamembe-Aero (KMB), Kigali-Aero (KGL), Kawangire (KGR), Ruhengeri-Aero (RHR), Kibungo-Kazo (KNK), Nyagatare(NGT), Gikongoro-Met(GRM), Gisenyi-Aero (GSN), Rubengera(RGR) and Rubona-Colline (RNC) respectively.

Time	Station		BYN	BYM	KMB	KGL	KGR	RHR	KNK	NGT	GRM	GSN	RGR	RNC
Annual	Mean		1222	1082	1336	1115	878	1332	1063	1014	1395	1168	1319	1132
	CV		24	24	20	27	28	20	25	26	20	21	20	25
	Trend	Z	-	-		-	+	-	-	+	-	+	-	-
		S			*									
		Q	-3.7	-0.8	-9.1	-4	2.4	-1.9	-1.6	1.3	-1.2	3.2	-1.9	-2.1

		T	-3.1	-8.5	-6.7	-6.7	8.5	-10.1	-4.2	6.5	-3.7	3.6	-1.8	-1.3
MAM	Mean		472	441	408	327	335	478	363	382	515	386	453	497
	CV		31	28	23	32	29	23	27	30	26	28	27	33
	Trend	Z	-	-	-	-	-	-	-	-	-	-	-	-
		S							*			+		
		Q	-3.4	-0.3	-3.3	-1.9	-1	-0.9	-3.5	0.5	-0.7	-1.3	-1.8	-2.6
		T	-9.7	-19.8	-5.7	-13.4	-31.1	-17.7	-9.8	3.2	0.3	-15.5	-5.8	0.7
SOND	Mean		466	426	617	499	373	558	350	432	545	480	561	445
	CV		31	25	20	32	32	18	32	30	25	20	24	29
	Trend	Z	+	+	-	-	+	-	+	-	+	+	-	+
		S										*		
		Q	1.22	0.17	-2.41	-1.97	1.51	-0.21	1.48	-0.2	0.61	3.1	-0.5	0.48
		T	9.9	1.5	-17.4	-23.9	16	-8.8	12	-12	2.2	4.3	-8.2	1.4

The spatial rainfall trend during the MAM showed a decline in the South-eastern region extending to the central parts and Kigali City. The areas of the south-western bordering Lake Kivu and Nyungwe National Park revealed an increasing trend reducing towards the southern region in the areas along Crest Congo Nile extending to the northern highlands and north-western region of the country (Figure 4. 6). A decreasing rainfall trend during the SOND season was revealed over Kigali City and the north-eastern region in the areas of the Nyagatare district extending to the northern parts of the country surrounding the Volcano National Park increasing in the Western and Southern areas with a peak increasing in the areas around Lake Kivu extending to the lowland of Bugarama (Figure 4. 6). On the annual time scale, a decreasing trend over the southern side of the Eastern province, the central plateau extending to the northern highlands towards the areas of the Volcano National Park increasing to the central and south-western parts of the western region bordering the Lake Kivu areas and the south-eastern areas of the Southern region of the country was indicated on an annual basis. The areas around Nyungwe National Park, the central and north-eastern parts of eastern region extending to the Akagera National Park registered an increase in trend (Figure 4. 6). The spatial trend analysis indicated a decreasing trend over Kigali City and the central parts during both annual and seasonal timescales extending to the eastern, southern and North-western parts with an increasing trend over the south-western parts during the long rain and through the year. The results obtained for the long rain season confirmed the results obtained by

(Nahayo *et al.*, 2018; Sebaziga *et al.*, 2020) while the results obtained during the short rain season and through the year contradicted the results of (Ntirenganya, 2018) which indicated that there is no visible trend. The difference in results may be due to the temporal resolution type of data used in the previous study.

The rainfall trend results obtained in this study during MAM season confirm the results of other researchers within the region (Funk *et al*., 2008; Williams and Funk, 2011; Lyon and Dewitt, 2012; Yang *et al*., 2014) who have indicated that on longer timescales, total precipitation received during the MAM season has declined in recent decades. The results however contradicted the results obtained by Mohammed *et al*., (2016) which indicated a non-significant trend in rainfall records ranging from 1964 to 2010. The disparities in the results may be attributed to extended periods of meteorological data gaps. Only Kigali Airport meteorological station provided almost complete dataset of continuous records from 1964 to 2010 and it was selected to be the reference rain gauge in filling missing data at other rainfall gauges which were not located in the same climatic zone. Rainfall decline over the regions has been attributed to the changes in the sea surface temperatures (SSTs) in the south-central Indian Ocean (Funk *et al*., 2008) and western Pacific Ocean (Lyon and Dewitt, 2012; Yang *et al*., 2014) which favour a local increase in precipitation, with the ensuing latent heating changing regional wind and moisture flow patterns and lowering precipitation during East Africa's lengthy rainy season (Williams and Funk, 2011).

During the short rains, a decreasing trend over Kigali City and the central plateau was noticed while the rest of the country registered an increasing trend with a higher increase in the areas surrounding NNP and the north-western parts of the country. The results obtained during the SOND season confirms the results of (Mutai and Neil., 2000; Schreck and Semazzi, 2004; Ummenhofer *et al*., 2009). It was further indicated that over East Africa, the warming of sea surface temperature anomalies in the western equatorial Indian Ocean dominates the enhanced short rainy season, with the eastern cold pole of the tropical IOD playing a less significant role. (Ummenhofer *et al*., 2009). Seasonally, the ENSO teleconnection influence is most evident during short rainy season. (Mutai and Neil., 2000; Schreck and Semazzi, 2004).

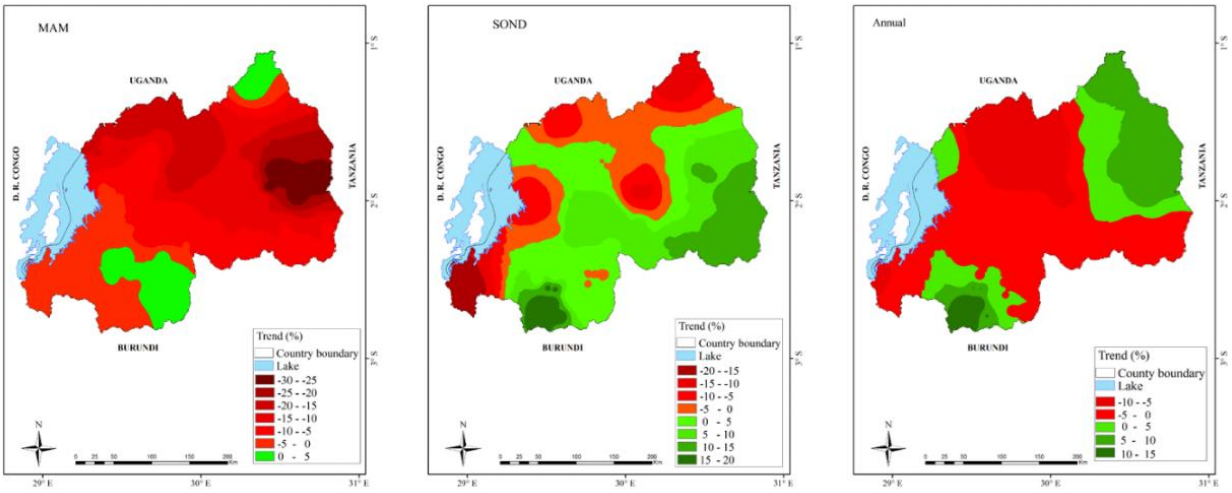

Figure 4. 8 Rwanda's spatial distribution of rainfall trend from March to May (left), September to December (center) and annual rainfall trend (right) from 1981-2017.

4.4 Projected changes in seasonal rainfall

Figure 4.9 presents the spatial distribution of projected changes in seasonal mean rainfall for 2026-2060 and 2066-2100 period. During MAM, for the 2026-2060 period, rainfall is projected to decrease across the entire country, with the south-western, north-western, and south-eastern regions experiencing the largest reductions of ([-300, -200] mm). The remaining regions are expected to see reductions of ([-100, 0] mm) under both RCP2.6 and RCP8.5, with greater magnitudes projected under RCP8.5 than under RCP2.6. For 2066-2100 period, under RCP2.6, the south-central is projected to experience an increase in rainfall ([0, 100] mm) while the remaining areas are projected to experience and reduce rainfall of ([-200, -100]) in north-western highland and south-western and by ([-100, 0]) in other areas. Under RCP8.5, rainfall is projected to reduce ([-100, 0] mm) in the south-western, northern-western and south-eastern and increase in remaining areas ([0, 100] mm) with the extreme south-central projected to reduce by (-200, -100] mm).

During SOND, for the 2026-2060 period, under RCP2.6, rainfall is projected to decrease by ([-100, 0] mm) in some areas of the south-eastern and north-eastern regions, increase by ([0, 100] mm) in the eastern region, and by ([100, 200] mm) in the south-western and northern highlands, while the remaining areas are projected to increase by ([200, 300] mm). Under RCP8.5, rainfall is expected to increase by ([0, 100] mm) in eastern areas, while other areas are projected to experience increases of ([200, 300] mm). For the 2066-2100 period, under RCP2.6, rainfall is

projected to decrease by ([-100, 0] mm) in some areas of the south-eastern and north-eastern regions, increase by ([0, 100] mm) in the eastern region, south-western and few areas of the northern highland and by ([100, 200] mm) in the southern and northern areas, while in the central plateau is expected to receive more increase rainfall ([200, 300] mm). Under RCP8.5, rainfall is expected to increase by ([0, 100] mm) in south-western, ([100, 200] mm) in extreme south-eastern, north-eastern and the western, while other areas are projected to experience increases of ([200, 300] mm).

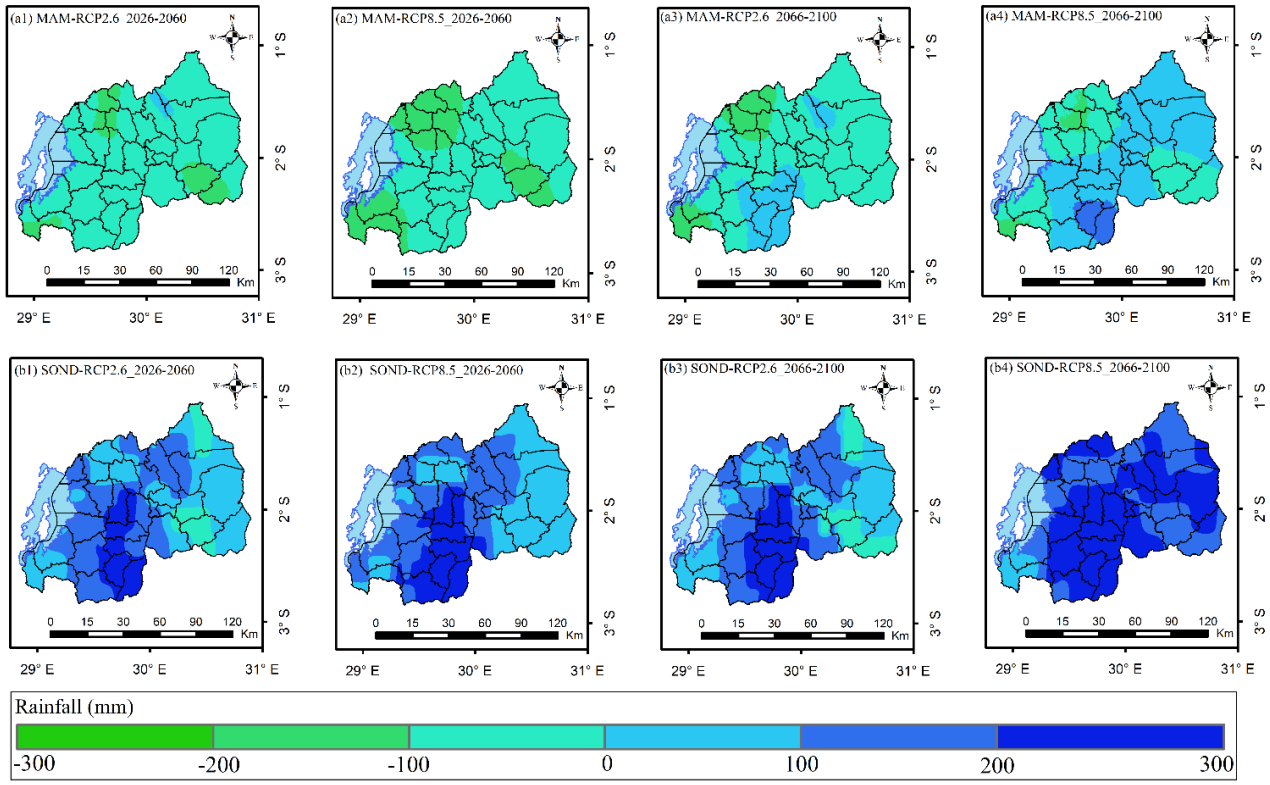

Figure 4. 9 Spatial distribution of projected changes in seasonal mean rainfall March-April-May (MAM, a_1-a_4) and September-October-November-December (SOND, b_1-b_4) for 2026-2060 and 2066-2100 period.

Figure 4.10 presents the country averaged observed and projected seasonal rainfall changes over Rwanda. The projected mean rainfall during JF season, indicates more variability and shows more reduction under RCP8.5 than RCP2.6. For MAM, a general reduction in rainfall is evident. The period of 2026-2066 shows more reduction with high magnitude under RCP2.6 than RCP8.5. Moving to the end of the century, RCP8.5 shows more rainfall reduction compared to RCP2.6. During the JJA season, a reduction in rainfall is seen throughout the entire period with comparable

reduction magnitude under both RCP2.6 and RCP8.5 emission scenarios. For SOND season, a general increase in rainfall is projected under both RCP2.6 and RCP8.5 emission scenarios. However, high rainfall increase is expected under RCP8.5 than RCP8.5.

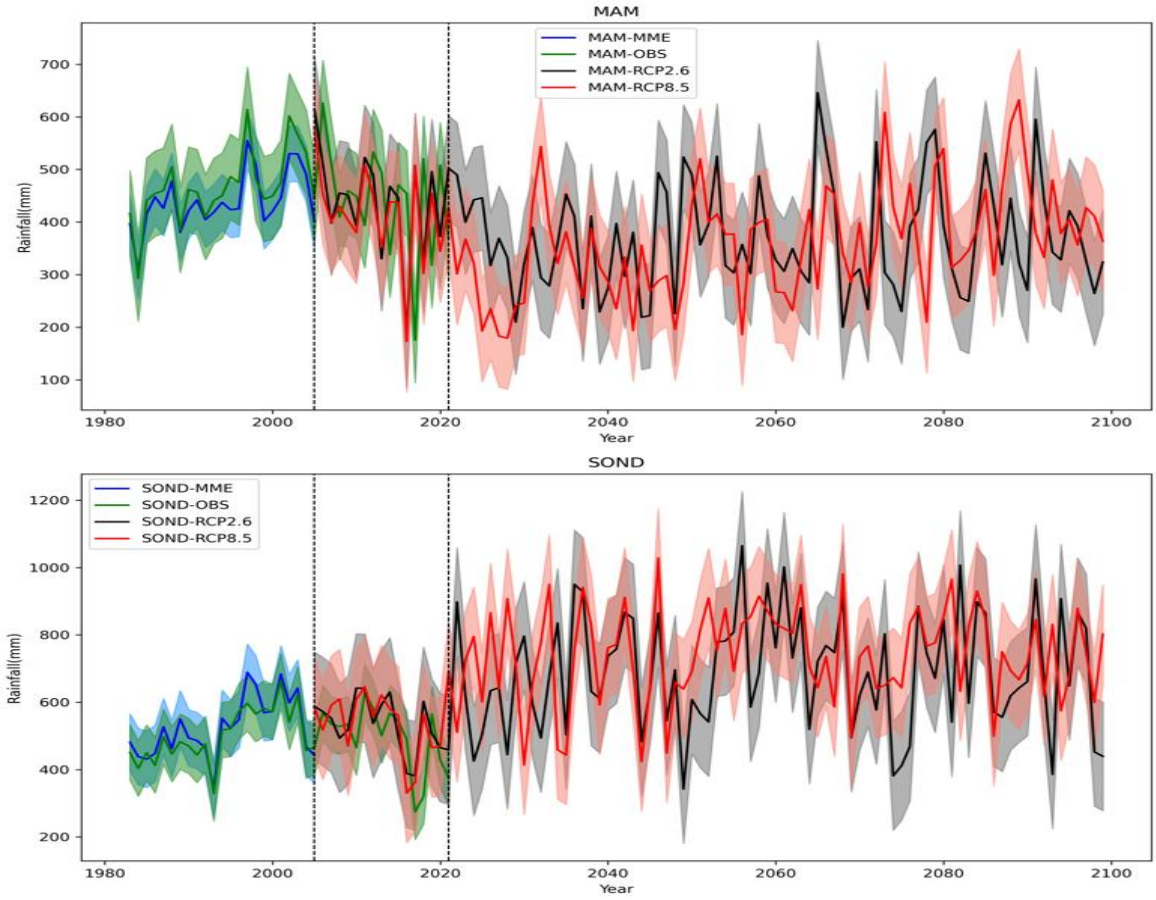

Figure 4. 10 The country averaged observed and projected rainfall changes for March-April-May (MAM) and September-October-November-December (SOND) over Rwanda for 1983-2100 period.

4.5 Conclusion

In this study, we investigated the temporal variability and trend in rainfall from the year 1981 to 2017 over Rwanda for twelve synoptic rainfall stations using graphical and statistical methods. To carry out spatial analysis, seventy-two rainfall stations were considered in addition to the twelve synoptic stations. Sen's slope estimator and the Mann-Kendall techniques were employed to identify trends and gauge the size of changes, while the variability analysis involved calculating the coefficient of variation. The results indicated a higher variability in annual rainfall over Kigali City, central and

eastern Rwanda whereas lower variation in the western parts of Rwanda. A significant decrease in rainfall of 9.1 mm year^{-1} was observed over the southern parts corresponding to -6.7%. During the long rain season, a high variability over the extreme eastern parts, central and the southern region of the country was revealed whereas a low variability was registered over northern highland with a significant decreasing slope of 3.5 mm year^{-1} corresponding to -9.8%. During the short dry season, lower variability was registered over the north-western high land and the western region while pronounced variability was observed over the south-eastern parts of the dry and hot lowland climatic zone. A significantly increasing rainfall of 3.1 mm year^{-1} corresponding to 4.3% was revealed over the western part while the remaining stations revealed a non-uniform trend. The results obtained under this study will improve policy-making and suggest policy implications. Because the country relies mainly on rain fed agriculture, the resulting variability and trend results may serve as the basis for proper planning, increasing areas under small scale irrigation with best water harvesting techniques, encouraging agronomic practices that improve the soil water holding capacity such as mulching, agroforestry, use of organic manure, crop rotation, minimum tillage, cover crops/plants and zero grazing, introduction of drought resistant crops and varieties should be envisaged as adaptation measures and climate smart agriculture practices as a strategy for mitigation measures. It is also important to note a non-homogeneity in the obtained results which may indicate a need for further refinement of climate zoning over the country.

4.6 References

Challinor, A., Wheeler, T., Garforth, C., Craufurd, P. and A. Kassam, 2007: Assessing the vulnerability of food crop systems in Africa to climate change. *Clim. change*, 83(3) 381–399.https://doi.org/10.1007/s10584-007-9249-0

Funk, C., Dettinger, M.D., Michaelsen, J.C., Verdin, J.P., Brown, M.E., Barlow, M. and A. Hoell, 2008: Warming of the Indian Ocean threatens eastern and southern African food security but could be mitigated by agricultural development. *PNAS*, 105(32) 11081–11086. https://doi.org/10.1073/pnas.0708196105

Gitau, W., Ogallo, L., Camberlin, P. and R. Okoola, 2013: Spatial coherence and potential predictability assessment of intraseasonal statistics of wet and dry spells over Equatorial Eastern Africa. *Int. J. Climatol.*, 33(12) 2690–2705.https://doi.org/10.1002/joc.3620

Hastenrath, S. and D. Polzin, 2004: Dynamics of the surface wind field over the equatorial Indian

Ocean. *Q. J. R. Meteorol. Soc.*, 130(597) 503–517.https://doi.org/10.1256/qj.03.79

Henninger, S.M., 2013: Does the global warming modify the local Rwandan climate? *Nat. Sci*, 5(1) 124–129.https://doi.org/10.4236/ns.2013.51A019

Ilunga, L. and Muhire, I., 2010: Comparaison des fluctuations des précipitations moyennes annuelles au Rwanda avec les épisodes EL-NINO / LA NINA et les cycles des taches solaires. *Geo-Eco-Trop*, 34(June) 75–86.

Ilunga, L., Muhire, I. and Mbaragijimana, C. (2004) Saisons pluviométriques et origine des pluies au Rwanda. *Geo-Eco-Trop*, 28(1–2) 61–68.

Ilunga, L., Mukingambeho, D., Mugwaneza, A. and Mugiraneza, A., 2008: Dates probables des semailles au Rwanda. *Geo-Eco-Tro*, 29–36.

Indeje, M., Semazzi, F.H.M. and Ogallo, L.J., 2000: ENSO signals in East African rainfall seasons. *Int. J. Climatol.*, 20(1) 19–46. https://doi.org/10.1002/(SICI)1097-0088(200001)20:1<19::AID-JOC449>3.0.CO;2-0

Kazora J., Wang W., Shamsuddin S. Arfan A.Md., Muhammad B., Birhanu A. H., Iyakaremye V. Zhongfeng Q., Mansour A., Yu W., Sebaziga N.J, Pravash T. 2021: Spatiotemporal variability of rainfall trends and influencing factors in Rwanda. JASTP. https://doi.org/10.1016/j.jastp.2021.105631

Kizza, M., Rodhe, A., Xu, C., Ntale, H.K. and Halldin, S., 2009: Temporal rainfall variability in the Lake Victoria Basin in East Africa during the twentieth century. *Theor. Appl. Climatol.*,119–135. https://doi.org/10.1007/s00704-008-0093-6

Lyon, B. and Dewitt, D.G., 2012: A recent and abrupt decline in the East African long rains. *Geophys. Res. Lett.*, 39 L02702,1–5. https://doi.org/10.1029/2011GL050337

Mahmudul Alam, Mohd Ekhwan bin Toriman, Chamhuri Siwar and Basri Talib, 2011: Rainfall Variation and Changing Pattern of Agricultural Cycle. *Am. J. Environ. Sci 7(1),82-89.* https://doi.org/10.3844/ajessp.2011.82.89.

Mohammed, H., Jean, C.K. and Ahmad, W.A., 2016: Projections of precipitation, air temperature and potential evapotranspiration in Rwanda under changing climate conditions. *Afr. J. Environ. Sci. Technol*, 10(1) 18–33. https://doi.org/10.5897/AJEST2015.1997

Muhire I, Ahmed F (2014) Spatio-temporal trend analysis of precipitation data over Rwanda. *South Afr Geogr J.* https://doi.org/10.1080/03736245.2014.924869

Muhire, I., Ahmed, F. and Abutaleb, K., 2015a: Relationships between Rwandan seasonal rainfall

anomalies and ENSO events. *Theor. Appl. Climatol.;* 122(1) 1-14. https://doi.org/10.1007/s00704-014-1299-4

Muhire, I., Ahmed, F. and Abutaleb, K., 2015b: Spatio-temporal variations of rainfall erosivity in Rwanda. J. Soil Sci. Environ. Manage, 6(4) 72–83. https://doi.org/10.5897/JSSEM14. 0452.

Mutai, C.C. and Neil., W.M., 2000: East African Rainfall and the Tropical Circulation / Convection on Intraseasonal to Interannual Timescales. *J. Clim*, 13(22) 3915–3939. https://doi.org/10.1175/1520-0442(2000)013<3915:EARATT>2.0.CO;2

Nahayo, L., Habiyaremye, G., Kayiranga, A., Kalisa, E., Mupenzi, C. and Nsanzimana, D.F., 2018: Rainfall variability analysis and its impact on crop production in Rwanda. *A.J. Soc. Sci. Res.* 4(1) 9–15.

Nicholson, S.E., 2017: Climate and climatic variability of rainfall over eastern Africa. *Rev. Geophys*, 55(3) 590–635. https://doi.org/10.1002/2016rg000544

Nicholson, S.E., Leposo, D. and Grist, J., 2001: The relationship between El Niño and drought over Botswana. *J. Clim.*, 14(3) 323–335. https://doi.org/10.1175/1520-0442(2001)014<0323:trbeno>2.0.co;2

Nsubuga, F.W., Olwoch, J.M. and Rautenbach, H., 2014: Variability properties of daily and monthly observed near-surface temperatures in Uganda: 1960-2008. *Int. J. Climatol.*, 34(2) 303–314. https://doi.org/10.1002/joc.3686

Ntirenganya, F., 2018: Analysis of Rainfall Variability in Rwanda for Small-scale Farmers Coping Strategies to Climate Variability. *EAJST,* 8(1) 75-96.

Ntwali, D., Ogwang, B.A. and Ongoma, V., 2016: The Impacts of Topography on Spatial and Temporal Rainfall Distribution over Rwanda Based on WRF Model. *Atmos.Clim.Sci.*, 06(02) 145–157. https://doi.org/10.4236/acs.2016.62013.

Ochieng.J, Kirimi. L, Mathenge. M, 2016: Effects of climate variability and change on agricultural production: The case of small-scale farmers in Kenya. *NJAS-WAGEN J LIFE SC 77, 71–78*

Okoola, R.E., 1999a: A diagnostic study of the eastern Africa monsoon circulation during the Northern Hemisphere spring season. *Int.J. Climatol.*, 19(2) 143–168. https://doi.org/10.1002/(sici)1097-0088(199902)19:2<143::aid-joc342>3.0.co;2-u

Ongoma, V., & Chen, H., 2016: Temporal and spatial variability of temperature and precipitation over East Africa from 1951 to 2010. *Meteorol. Atmos. Phys.*, 129(2), 131 144. https://doi.org/10.1007/s00703-016-0462-0

Owiti, Z., 2008: Linkages between the Indian Ocean Dipole and East African Seasonal Rainfall Anomalies. *J.K.MS*, 2(1) 3–17.

Peter. O., Laban. O., Raphael. O., Herry., H. and Mathewe., W., 2008: East African Rainfall Variability Associated with the Madden-Julian Oscillation. *J.K.MS*, 2(2) 105–114.

Safari, B., 2012: Trend Analysis of the Mean Annual Temperature in Rwanda during the Last Fifty-Two Years. *JEP*, 3(6)538-551. https://doi.org/10.4236/jep.2012.36065

Schreck, C. J., & Semazzi, F. H. M., 2004: Variability of the recent climate of eastern Africa. *Int. J. Climatol.*, 24(6), 681–701. https://doi.org/10.1002/joc.1019

Sebaziga, N.J., Ntirenganya, F., Tuyisenge, A. and Iyakaremye, V., 2020: A Statistical Analysis of the Historical Rainfall Data over Eastern Province in Rwanda. *EAJST* 10(1) 33–52.

Sen, P.K., 1968: Estimates of the Regression Coefficient Based on Kendall's Tau. J*ASA*, 63 (324) 1379–1389. https://doi.org/10.2307/2285891

Siebert, A., Dinku, T., Vuguziga, F., Twahirwa, A. and Kagabo, D.M., 2019: Evaluation of ENACTS-Rwanda: A new multi-decade, high- resolution rainfall and temperature data set — Climatology. *Int. J. Climatol.,* 39(6) 1–17. https://doi.org/10.1002/joc.6010

Theil, H., 1950: A rank-invariant method of linear and polynomial regresion analysis, II. *Proc. Kon. Ned. Akad.,* 53 521–525.

Ummenhofer, C.C., Gupta, A. Sen, England, M.H. and Reason, C.J.C., 2009: Contributions of Indian Ocean sea surface temperatures to enhanced East African rainfall. *J. Clim.*, 22(4) 993–1013. https://doi.org/10.1175/2008JCLI2493.1

Williams, A.P. and Funk, C., 2011: A westward extension of the warm pool leads to a westward extension of the Walker circulation, drying eastern Africa. *Clim Dyn*, 37(11–12) 2417–2435. https://doi.org/10.1007/s00382-010-0984-y

Yang, W., Seager, R., Cane, M. A., & Lyon, B., 2014: The East African Long Rains in Observations and Models. *J.Clim.,* 27(19), 7185–7202. https://doi.org/10.1175/jcli-d-13-00447.1

Zougmoré, R.B., Partey, S.T., Ouédraogo, M., Torquebiau, E. and Campbell, B.M., 2018: Facing climate variability in sub-Saharan Africa: analysis of climate-smart agriculture opportunities to manage climate-related risks. *Cah. Agric.*, 27(3) 34001. https://doi.org/10.1051/cagri/2018019

Chapter 5 Spatial Variability of Seasonal Rainfall Onset, Cessation, Length and Rainy Days in Rwanda

This Chapter reproduces the content of our published paper (https://doi.org/10.1007/s00704-024-05086-3).

5.1 Introduction

The effects of climate change on agriculture are unevenly distributed across the world and are caused by changes in temperature, precipitation and atmospheric carbon dioxide levels due to global climate change (Sovacool et al. 2021, Pope et al. 2022). For countries that practice rain fed agriculture, changes in seasonal precipitation regimes greatly impact crop productivity (Tubiello et al. 2007, Liu and Allan 2013, Lipiec et al. 2013). This affects farmer's ability to rely on their knowledge of the seasonality such as timing and ending of the rainy season which reduces the time that crops have to complete their growth cycle (Linderholm 2006). Extremely wet conditions can delay planting or harvesting, leading to complete crop failure and yield losses rendering workers jobless (Kristjanson et al., 2012, Warren et al. 2015) and exacerbating the pre-existing poverty conditions leading to famine and malnutrition (Adejuwon 2006). Even though irrigation of crops is able to reduce the impacts of lower rainfall and higher temperatures on yields, using water resources for irrigation has downsides and is expensive (Connor et al. 2012). The agriculture sector, which is the backbone of the Rwandan economy and the means of subsistence for communities, is impacted by the irregularities in the country's rainfall (Mupenzi et al. 2011). The study of drought characteristics in Rwanda revealed that there are non-significant trends in annual and seasonal rainfall (Uwimbabazi et al. 2022). The study on climate change effects on food security in Rwanda indicated that irregularity in the rainfall affects crop cultivation and the onsets and offsets of the rainfall patterns are no longer reliable (Rwanyiziri and Rugema 2013). Irregular rainfalls and a shift in the rainy seasons that occurred in 2002 were to be blamed for the poor performance of crop output in that year (Mikova, 2015). Rwanda is a country with a high agricultural potential for both subsistence and profitable farming. Onset and cessation days and seasonal length of rainy season are critical factors in farming practices in relation to the harvest anticipated and preparation of agricultural activities (Odenkunle 2004, Dunning et al. 2017). The difficulties in the choice of the crop type, diversity and planning for sowing period result from yearly variation of onset day (OD), cessation day (CD) and the seasonal length (SL) as well as

existence of dry spells within the rainy season (Mugalavai et al., 2008). The amount of rainfall, the start and duration of the rainy season and the rate of evapotranspiration are all important elements that affect how much water plants need. These variables function as predictors of a crop's climatic adaptability and likelihood of success or failure in a particular growing season (Ngetich et al. 2014). The seasonal OD and CD depends on the rainfall with OD being more variable than the CD of the season (Camberlin et al., 2009). The need to understand the characteristics of the rain has become subject of discussion since the community livelihoods depend on climate-sensitive activities (Adelekan and Adegebo, 2014) where knowledge of changes in rainfall at the local level is imperative for agricultural planning and sustainable food production (Laux et al. 2008). The OD and CD of rainfall season are significantly vital to countries depending largely on rain-fed agriculture (Adelekan and Adegebo, 2014) and are central characteristics of rainfall distribution since these are more closely linked with precipitation effectiveness which is more important to the growing season than annual rainfall totals (Ati et al., 2002) Odekunle et al. 2005). Besides that OD, SL and CD of seasonal rainfall vary in space and time (Odenkunle, 2004) and their understanding is paramount due to the risk related to early/late onset or cessation days to facilitate effective agricultural practice and management to reduce the risk of crops fail to mature leading to little or no harvest at the end of the season (Dodd and Jolliffe, 2001) Sultan and Janicot 2003). The variability in the SL demands the application of agricultural management practices to improve production (Jena et al., 2019). Studies conducted over Ruteete Subcounty in Uganda indicated that farmers rely on their past experiences and traditional approaches to determine the OD and CD of the rainy season (Nyakaisiki et al., 2019), although there is need to determine OD and CD empirically (Adelekan, 2019). Determination of the starting and ending of the rainy season can be challenging (Omotosho et al., 2000). The inconsistency in OD determination method was indicated where local patterns are not in cycle with variation of global factors that influence rainfall in the area(Marteau et al., 2009). Over the Indonesian Maritime Continent, a flexible driest period has been used to determine the onset day of the rainy season (Ferijal et al. 2022). Different methods have been used in West Africa to determine OD. They include: i) cumulative rainfall (Dodd and Jolliffe 2001, Marteau et al. 2009 Amekudzi et al. 2015), ii) rainfall model (Wati et al., 2019), iii) rainfall-evapotranspiration relation model (Edoga, 2007) Sobowale et al. 2016, Gebremedhin et al. 2023), iv) percentage cumulative mean rainfall model (Guenang and Mkankam Kamga, 2012) Amekudzi et al. 2015), v) wind shear model (Edoga, 2007) and vi) five consecutive days

(Sobowale et al., 2016). Over the Eastern and equatorial African, other methods are found, including i) rainfall accumulation (Camberlin and Okoola 2003, Tesfaye and Walker 2004, Segele and Lamb 2005, Mesay Abebe 2006, Mugalavai et al. 2008, Recha et al. 2012, Mugo et al. 2016), ii) percentage cumulative mean rainfall model (Recha et al. 2012, Haleakala et al. 2018), iii) daily climatology (Diem and Sung 2018), iv) five consecutive rainfalls (Egeru et al. 2014, Mugo et al. 2016, Haleakala et al. 2018, Omay et al. 2023), and v) pentad rainfall (Kijazi and Reason 2012). Like OD, CD of the rainy season has been defined using different methods by different authors. Those include the use of i) water balance method (Tesfaye and Walker 2004, Mesay Abebe 2006, Taye et al. 2013), ii) rainfall accumulation and dry spell (Egeru et al. 2014, Haleakala et al. 2018), iii) soil water balance (Getahun et al. 2016), iv) day after starting of the season for which no rain occurs over a period of time (Mugalavai et al. 2008), v) percentage cumulative mean rainfall model (Mugo et al., 2016). The SL was defined as the difference between the CD and OD (Mugalavai et al. 2008, Gebremichael et al. 2014, Haleakala et al. 2018).

Numerous studies have shown that models building on rainfall data alone in determining the OD and CD are more efficient due to that rainfall totals have a direct connection as the cycle trigger, since it represents minimum water availability to carryout sowing operations compared to other related factors (Ati et al. 2002, Odenkunle 2004, Laux et al. 2008, Amekudzi et al. 2015). It was also indicated that the use of rainy days criteria yields rainfall OD and CD that are more realistic than those obtained using rainfall amount alone (Odekunle et al. 2005). In the humid areas, the determination of OD of rains based on five consecutive days is considered more satisfactory (Odekunle 2006). The criteria of using dry spell occurrence in the determination of OD of seasonal rainfall, reduces the chance of a false start of rain characterized by early rainfall followed by long dry spells and also offer flexibility concerning the characterization of the start of rains for diverse locations (Sultan and Janicot 2003). In addition, the determination of OD by combining different methods to come up with hybrid method was considered as effective due to the mixture of factors that influence rainfall onset (Ati et al. 2002). Rainfall characteristics in Rwanda have been the subject of several recent studies (Muhire et al. 2015, Ntwali et al. 2016, Siebert et al. 2019, Kazora et al. 2021, Umutoni et al. 2021, Umuhoza et al. 2021, Zhou et al. 2021, Safari et al. 2022, Sebaziga et al. 2022, Uwimbabazi et al. 2022, Sebaziga et al. 2023) with a converging result indicating a general variation in seasonal and annual total rainfall. Rainfall OD and CD, SL and rainy day (RD) are crucial for crop production and food security in Rwanda yet scantily

documented. The objective of this study is to analyze the spatial patterns and variabilities of Seasonal Rainfall Onset Days (OD), Cessation Days (CD), Seasonal Length (SL), and Number of Rainy Days (RD) in Rwanda using an observational data set from 1983-2021. After the introduction, the paper is organized as follows: section one provides a brief description of materials and methods (study area, data and methods), results are presented in section two followed by discussion in section three, while the conclusion is presented in the fourth section.

5.2 Materials and methods

5.2.*1 Study Area*

Rwanda is located in Eastern and Central Africa and lies between 1°4′ and 2°51′ South, and 28°53′ and 30°53′ East with a total 26,338 km^2. The total agricultural land is 14,020 km^2 (59%) of total country land. In the third quarter of 2023, the Gross Domestic Product (GDP) at current market prices in Rwanda was estimated at Frw 4,249 billion. This was contributed by services sector (46%), agriculture sector (25%), industry sector (21%) and adjustment for taxes and subsidies (7%)(National institute of Statistics of Rwanda 2023a). The Fifth National Population and Housing Census (National Institute of Statistics of Rwanda 2023b) shows that the total population of Rwanda is 13,246,394 with an annual growth rate of 2.3%. This population is distributed around the country with 72.1% and 27.9% of total population live, respectively, in rural and urban areas**.** Among this population, women represent 51.5% and men represent 48.5% of the population**.**

The topography of Rwanda is complex, spanning from highland to lowland regions with a mixture of mountains, hills, and valleys with elevations ranging from 900 m to 4507 m. The Congo Nile Ridge overlaying Lake Kivu dominates the country's western side and is between 2500 and 3000 meters high, while volcanic area, the highest of which is Karisimbi at 4507 meters, rule the country's northern part. The eastern lowland area is dominated by hills with an altitude ranging from 1000 to 1500 m, the central plateau displays a relief of hills with an altitude range between 1500 m and 2000 m while the 900-meter-high characterizes the southwestern lowland of Bugarama valley (Mikova 2015). Rwanda presents six climate zones from the eastern to western (Henninger 2013)**.** These are the savanna zone located in the East-Rwandan dry and hot lowland zone, the temperate zone of the central highland found in the central highlands region, the south-rwanda humid mountain climate zone covering southern Rwanda, around the Nyungwe National Park and Congo-Nile Trial, the north-rwanda dry mountain climate zone located in the Virunga National Park, in the volcanic mountains of northern region, urban climate of Kigali and Kivu-sea climate

zone locate along the coastal ridge of Lake Kivu. The western part of the nation, which has more mountains and higher elevations, is typically cooler and wetter than the eastern part, which is lower and flatter (Siebert et al. 2019). Rwanda's rainfall climatology clearly displays the seasonal bimodality common to the East Africa area. It experiences four distinct seasons, of which two are wet and the other two are dry. March through May (MAM) and September through December (SOND) are rainy seasons, January through February (JF) and June through August (JJA) are dry months (Muhire et al. 2015, Siebert et al. 2019, Kazora et al., 2021, Umutoni et al. 2021, Sebaziga et al. 2022) with April and November being the monthly rainfall peak, respectively, for both rainy seasons (Muhire et al. 2015, Ntwali et al. 2016).The season fits the country's climatology and agricultural methods despite the unequal seasonal duration. Although the timing of sowing and harvest varies by cultivation for various crops, this seasonal division of the year is most consistent with the larger harvests in May and December (Siebert et al. 2019). Rwanda's climate is mainly influenced by the migration from south to north and vis-versa of the Intertropical Convergence Zone (ITCZ) as well as high pressure systems such as the Mascarene, Saint Helena, Azores and Arabian Ridge (Siebert et al. 2019). Regional factors such as the Lake Victoria and Congo air masses combined with topography also play an important role (Kizza et al. 2009; Ntwali et al. 2016; Ngarukiyimana et al. 2017; Zhou et al. 2021). Some recent studies have shown that large-scale factors such as the El Niño Southern Oscillation (ENSO) and the Indian Ocean Dipole (IOD) can also influence to some extent the climate of Rwanda (Ilunga and Muhire, 2010; Muhire et al. 2015; Kazora et al., 2021; Safari et al. 2022).

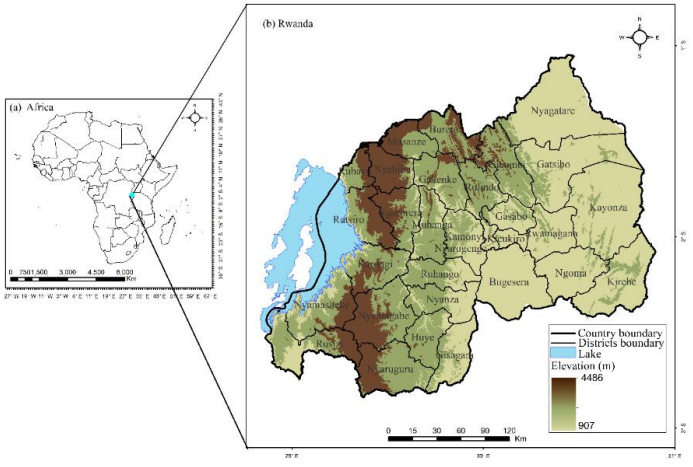

Figure 5. 1 Geographical location of Rwanda in Africa (a), Administrative and elevation map of Rwanda (b).

Different studies have classified Rwanda into different climate zones. Ilunga and Muhire (2010) classified Rwanda into four climatic regions based on the data from 1961 to 1990. These regions were: i) Lake Kivu border zone, ii) Congo Nile crest, iii) central plateau, and iv) eastern lowland. The method of subdivision into climatic zones used here has the disadvantage of using only rainfall data and on few weather stations. A subsequent study by Henninger (2013) using data from 1996 to 2011 divided Rwanda into six climatological zones. These are: i) the Lake Kivu climate zone, ii) the south-Rwanda humid mountain climate zone, iii) the north-Rwanda dry mountain climate zone, iv) the temperate climate zone of the central highland, v) the urban climate zone of Kigali and vi) the East-Rwandan dry and hot lowland climate zone. This study has the advantage of having used rainfall and temperature data from a larger number of climatological stations, however the time series were over a short period. In the present study, the classification of climatic zones in Rwanda uses rainfall and temperature data that are currently available over a longer period and distributed on a grid of high resolution. K-mean clustering method is applied to identify near homogeneous zones (Atanabe, 2010; Singh and Gill, 2013; Pitri et al., 2018; Sriadhi et al., 2020; Biabiany et al., 2020 ; Wickramasinghe et al., 2022). Those are namely: i) the Lake Kivu climate zone, located to the coast of Lake Kivu,; ii) the mountain forest climate zone, located on the southern and southwestern parts of Nyungwe National Park; iii) the mountain climate zone, located in the area over Congo-Nile divide extended to the mountain areas of the northern volcanoes highland; iv) the temperate climate zone of the central highlands that encompasses the central mountainous part extended from the southern region to the northern region; v) the central plateau climate zone located between the temperate climate zone of the central highlands in the west and vi) the eastern low land climate zone in the eastern part of the country.

In comparison with the study of Henninger (2013), the new subdivision shows that the pre-existing mountain climate zone was including the actual mountain forest climate zone. In addition, a new zone, the central plateau extended from the south to the north, is separated from the pre-existing temperate zone of the central highlands.

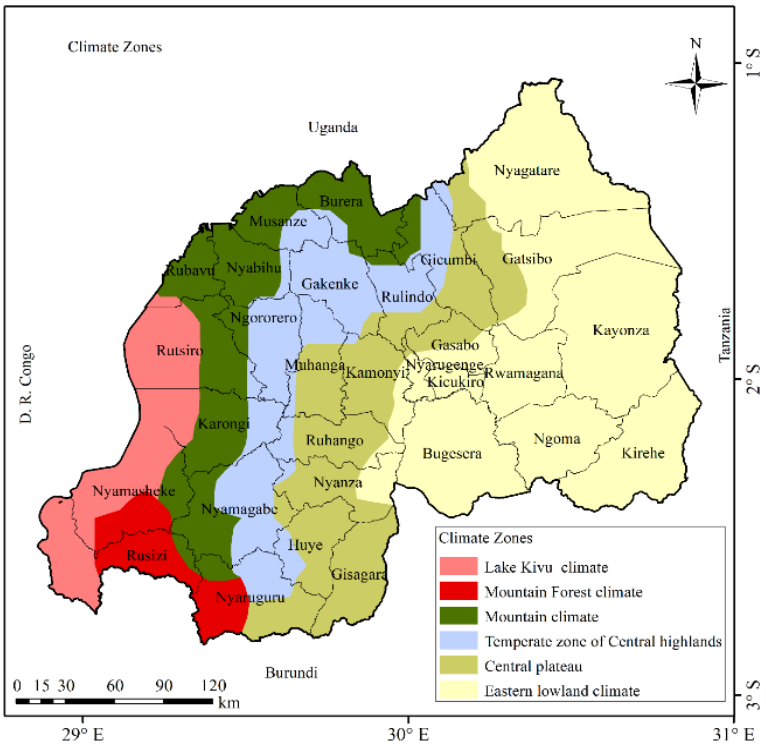

Figure 5. 2 The new climatic classification of Rwanda, based on data from 1983-2021.

5.2.*1* Data

The present study uses daily rainfall, maximum and minimum temperature obtained from Rwanda Meteorology Agency ranging from 1983 to 2021. Rainfall and temperature data are displayed on a grid with a spatial resolution of 4km (0.0375°) and 5km (0.05°) respectively. The reconstruction process followed the methodology detailed by Dinku et al. (2014) and Siebert et al. (2019). Quality control procedures were applied to observed rainfall and temperature datasets, as outlined by Safari et al. (2022) and Safari and Sebaziga (2023). Both rainfall and temperature were then remapped to a consistent spatial resolution using a bilinear interpolation method, as described in Nikulin et al., (2012), Endris et al., (2013), and Kalognomou et al., (2013).

Time series of SST over eastern tropical Pacific (0–10ºS, 90º–80ºW) and over equatorial Pacific (5ºN–5ºS, 170º–120ºW) corresponding, respectively, to Niño1+2 and Niño3.4 regions were retrieved online from the Physical Science Laboratory (PSL) of the National Oceanic and Atmospheric Administration (NOAA) website: https://psl.noaa.gov/data/timeseries/. Warm and cold periods are based on a threshold of +/- 0.5ºC.

Time series of Indian Ocean Dipole index (DMI/IOD) indices were retrieved from Climate Prediction Centre (CPC) of NOAA website: https://www.cpc.ncep.noaa.gov/products/international/ocean_monitoring/IODMI/. Positive and negative periods are based on a threshold of +/- 0.4^{o}C.

5.2.*2 Methods*

To compute the onset day (OD) of seasonal rainfall, the start of counting was defined as February for the long rain season (LR) and September for short rain season (SR). The following steps (or criteria) were proceeded: the first step was to consider a period of five consecutive days accumulating at least 25mm (Adelekan and Adegebo 2014, Mugo et al. 2016); the second step consisted in considering if the first day and at least two other days of that period of five days not having rainfall less than 1mm (Laux et al. 2007, Camberlin et al. 2009, Haleakala et al. 2018); the third step was to considerer, if after the fifth day of the selected period no dry period (rainfall less than 1 mm) of seven days or more occurred in the following thirty days (Recha et al. 2012, Adelekan and Adegebo 2014). The criteria of using 1mm was considered to define the number of rainy day (RD) (Camberlin et al. 2009, Haleakala et al. 2018) and this was adopted because rainfall amounts less than one millimeter usually increases the noise (Moron et al. 2006). The potential evapotranspiration (PET) is key criteria for the agricultural practices and decision-making. Computation of ET requires numerous meteorological parameters such solar radiation, wind, temperature, rainfall and humidity as inputs. The commonly used method is the Penman–Monteith method where data are available (Droogers and Allen 2002, Valipour 2015, Awal et al. 2020). Different studies have shown that the modified Hargreaves approach has the advantage of being free of the inherent drawbacks of the Thornthwaite technique, and its results are comparatively near to the widely recognized Penman-Monteith equation of the Food and Agriculture Organization (Grandgirard et al., 2002; Hargreaves and Allen, 2003; Beguería et al., 2014; Awal et al., 2020). In the present study, we have opted to use the modified Hargreaves method, which uses temperature (maximum, minimum and mean temperatures) and rainfall in evaluating the evapotranspiration (Stern and Cooper 2011, Valipour 2015).

According to the modified Hargreaves approach, the potential evapotranspiration is expressed as follows:

$$PET = 0.00102R_a(T_{max} - T_{min} - 0.0123R)^{0.76}(T + 17), \quad (1)$$

where PET is the potential evapotranspiration (mm day−1), R_a is the extraterrestrial radiation (MJm^2day-1), T_{max} is the maximum air temperature (∘C), T_{min} is the minimum air temperature (∘C) and T is the average daily air temperature (∘C).

As for the cessation day (CD) of the rainy season, it was defined as any day when accumulated ten days rainfall is less than half of the corresponding PET (Kijazi and Reason 2012). Once the OD and CD of the rainy season have been computed, the seasonal length (SL) was calculated by subtracting, for each year, the day at which the rain begin from the day at which rain end (Edoga 2007, Mugalavai et al. 2008, Gebremichael et al., 2014, Haleakala et al., 2018). To understand the variability in rainfall, OD, CD, SL and RD, coefficient of variation measure was used where high values denote more disperse and lower values indicate less spread out of data (Barde and Barde 2012).

Table 5. 1 Summary of studied rainfall characteristics

Characteristic	Definition	Units	Reference
Seasonal Rainfall Onset Day (OD)	(i) To consider period of five consecutive days accumulating at least 25mm;	Number (of the day starting with the first day of the calendar year)	Adelekan and Adegebo 2014, Mugo et al. 2016
	(ii) then to consider the first day and at least two other days of that period of five days not having rainfall less than 1mm;		Laux et al. 2007, Camberlin et al. 2009, Haleakala et al. 2018
	(iii) the onset day is then the day after the fifth day of the selected period with no dry		Recha et al. 2012, Adelekan and Adegebo 2014.

	period (rainfall less than 1 mm) of seven days or more occurred in the following thirty days.		
Seasonal Rainfall Cessation Day(CD)	Number of the day when accumulated ten days rainfall is less than half of the corresponding PET	Number (of the day starting with the first day of the calendar year)	Kijazi and Reason 2012
Seasonal Rainfall Length (SL)	The difference between Seasonal Rainfall Cessation day and Seasonal Rainfall Onset Day	Number (of days)	(Edoga, 2007) Mugalavai et al. 2008, Gebremichael et al., 2014, Haleakala et al., 2018
Number of Seasonal Rainfall Rainy days (RD)	Any day that receives rainfall greater or equal to 1mm.	Number (of days)	Camberlin et al. 2009, (Moron et al., 2006); Haleakala et al. 2018

The Pearson's correlation coefficient (r) allows measuring the level of association between the rainfall characteristics and the seasonal rainfall. A correlation coefficient of 1 denotes positive linear relation, -1 denotes a negative linear relationship while a correlation coefficient equal to 0.0 represents no association between the two variables (Luhunga *et al*., 2016).

$$r = \frac{\frac{1}{n}\sum_{t=1}^{n}(R_i - R)(C_i - C)}{\sqrt{\frac{1}{n}\left[\sum_{t=1}^{n}(R_i - R)^2\right]\left[\sum_{t=1}^{n}(C_i - C)^2\right]}} \quad (2)$$

where R_i and C_i are the rainfall and rainfall characteristics, and R and C are the mean rainfall and mean rainfall characteristics.

Time series of standardized anomalies of seasonal rainfall intensity (RI index), onset day (OD index), cessation day (CD index), length (SL index), number of rainy days (RD index), mean seasonal sea surface temperature (SST) for Niño 1+2 (Niño 1+2 index) and Niño 3.4 (Niño 3.4 index) were computed for each season as bellow:

$$A = (x_i - \bar{x}) \,/\, \sigma \,,\; i = 1, \ldots, N \qquad (3)$$

where x_i corresponds to a rainfall characteristics (OD, CD, SL, RD) or mean seasonal SST of a year i, N is the number of years, $\bar{x}$ is the mean of (x_i), A is the corresponding anomaly or index and $\sigma$is the standard deviation defined as:

$$\sigma = \sqrt{\frac{(x_i - \bar{x})^2}{n-1}} \qquad (4)$$

5.3 Results

Figure 5. 3 presents the long term mean of onset day (OD) and, cessation day (CD) for LR and SR. It is observed that the seasonal rainfall starts early over southwestern and northwestern parts of the country and later over the eastern parts of the country. This explains a West to East (W-E) progression of seasonal rainfall commencement. For LR (Fig. 3a), the OD ranges between 19 February and 27 March while for SR (Figure 3b), the OD ranges from 11 September to 22 November. During the LR, a mean OD ranging between 19 February and 9 March are observed over the south-western region bordering the Lake Kivu and the Nyungwe National Park, over areas along Congo Nile Trail, the highland of the southern region and the areas over the northwestern highland extending to Virunga National Park. The areas over the central plateau and the eastern region extending to Akagera National Park show a mean OD ranging between 9 March and 27 March. For SR, a mean OD ranging from 11 September to 18 October is shown over the southwestern region, southeastern of the Lake Kivu, areas surrounding Nyungwe National Park, northern parts of the country over Virunga National Park extending to the northwestern, southern region and the areas towards the Congo Nile Trail. The mean OD ranging between 18 October and 22 November is observed over the central plateau and the eastern region in the areas surrounding Akagera National Park.

As opposed to OD which show a W-E progression, the CD starts early over the eastern and later over the western which shows an East-West (E-W) progression. For LR (Fig. 3c), the mean CD ranges between 14 May and 30 May while for SR (Figure 2d), mean CD ranging between 15 December and 8 January. During the LR, a mean CD ranging between 14 May and 22 May is observed over the eastern region, central plateau and south-central parts of the country. The western parts of the country extending to the eastern side of Lake Kivu, the northern and southern

regions, and areas lying on Congo Nile Trail and Nyungwe National Park observed a mean CD ranging between 22 May and 30 May. During the SR (Fig. 3d), the eastern lowland, central plateau, northern highland and south-central parts of the country indicate a mean CD ranging between 15 December and 27 December. The southern, western and northern regions, and areas surrounding Nyungwe National Park and Congo Nile Trail show a mean CD ranging between 27 December and 8 January.

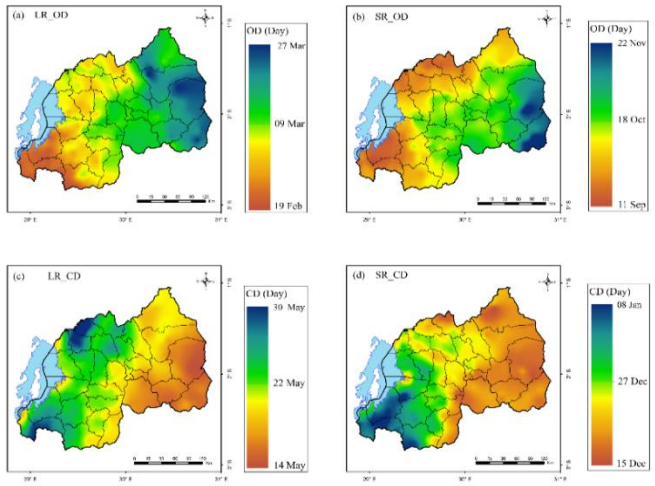

Figure 5. 3 Long term mean of (a): onset day (OD) for LR (b) onset day (OD) for SR, (c) cessation day (CD), for LR and (d) cessation day (CD) for SR using observation data from 1983 to 2021.

Figure 5. 4 presents the long-term mean of seasonal length (SL) and number of rainy days (RD) for LR and SR. The SL increases from east to west showing short SL over the eastern and extended SL over the western parts of the country. The mean SL for LR (Fig. 4a) ranges between 55 to 99 days while the mean SL for SR (Fig. 4b) ranges between 46 to 116 days. During the LR, the southwestern and northern highlands indicate a mean SL range between 77 and 99 days, which reduces towards the central highlands. A mean SL ranging between 55 and 77 days is observed over the eastern and central parts of the country. During the SR, a mean SL ranging from 81 to 116 days is observed over the southwestern and northern highland and reduces towards the central highland, south-central and northeastern parts of the eastern lowland region. The central eastern parts of the country indicated a mean SL ranging between 46- 81 days.

The mean RD (Fig. 4c) ranges between 24 and 68 days for LR while for SR (Fig. 4d), it ranges between 24 and 74 days. During the LR, the central plateau, the south-central region and the eastern lowland region observed a mean RD ranging between 24-48 days while the western

bordering Lake Kivu, areas surrounding Nyungwe National Park, the Congo Nile Trail region extending to the northwest, northern highland and Virunga National Park indicated a mean RD in the range of 48 to 68 days. For SR, the mean RD ranging between 24 and 49 days is shown over the central and south-eastern parts of the eastern region which increase towards the northeastern part, south-central and central parts of the country while the central plateau, southern and northern highland extending to Virunga National Park, areas surrounding Congo Nile Trail region and over the southwestern are bordering Nyungwe National Park and Lake Kivu shown a mean RD in the range of 49 to 74 days.

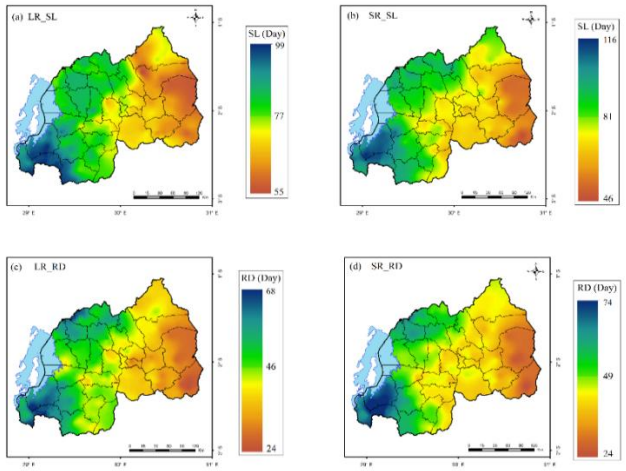

Figure 5. 4 Long-term mean of: (a) seasonal length (SL), for LR, (b) seasonal length (SL) for SR, (c) number of rainy days (RD) for LR and (d) number of rainy days (RD) for SR, using observation data from 1983 to 2021.

Figure 5. 5 presents the spatial coefficient of variation of onset days (ODV) and cessation days (CDV) for LR and SR. The spatial variability in OD for LR (Fig. 5a) ranges between 9 and 34 % while during the SR (Fig. 5b), it ranges between 5 and 11 %. The southwestern parts of the country indicated low ODV while the eastern parts shown high ODV. During the LR, the southwestern part bordering Lake Kivu, Nyungwe National Park and Congo Nile Trail shown a coefficient of variation ranging between 9 and 21.5 % increasing towards the central plateau and north-eastern parts of the country while eastern and extreme northern parts indicated a coefficient of variation ranging between 21.5 and 34 %. For SR, the extreme eastern parts of the eastern lowland region show a ODV ranging between 8 and 11% reducing towards the western, northern, Congo Nile Trail region, south-central and north-eastern, while the south-western parts of the country indicated a

ODV ranging between 5 and 8%. For CD, the SR shows lower magnitude of variation in the offset days compared to that of the LR. The CDV during LR (Fig. 5c) ranges from 2 to 7 % while for SR (Fig. 5d), CDV varies between 1 and 5 %. For LR, CDV ranging between 4.5 and 7 % is indicated over the southwestern part bordering coastal areas of the Lake Kivu, areas around Nyungwe National Park and northwestern highland which reduces towards the central plateau, southern and northern while a CDV ranging between 2 and 4.5 % is shown over the south-central and south-eastern and central parts of the eastern region. During the SR, a CDV ranging between 3 and 5 % is indicated over the areas around Congo Nile Trail, Nyungwe National Park, the western part bordering coastal areas of the Lake Kivu, over the southern, northern, northwestern highland and central plateau while the areas surrounding Virunga National Park, south-central and eastern parts of the country indicated a CDV ranging between 1 and 3 %.

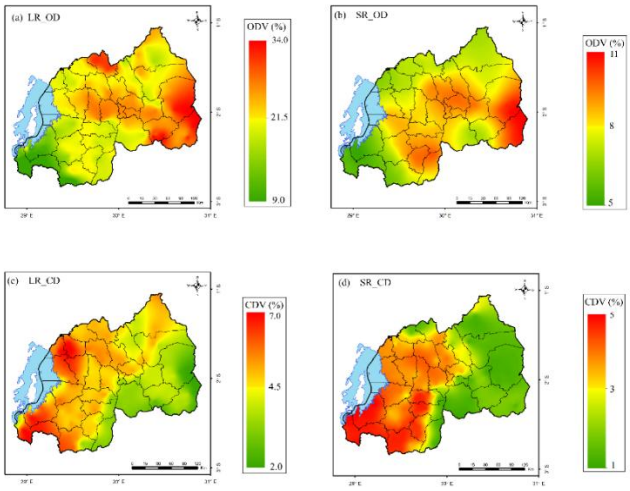

Figure 5. 5 Coefficient of variation of: (a) onset day (ODV) for LR, (b) onset day(ODV) for SR, (c) cessation day (CDV) for LR and (d) cessation day (CDV) for SR using observation data from 1983 to 2021.

Figure 5. 6 presents the spatial coefficients of variation of seasonal length (SLV), and number of rainy days (RDV) for LR and SR. Both the LR and SR show a non-uniform variability of the SL. The SLV during LR **(**Fig. 6a) ranges between 10 and 35 % while for SR (Fig. 6b), it ranges between 15 and 31 %. During the LR, the south-western side extending to coastal areas of Lake Kivu, areas near Nyungwe National Park and few areas of the northern region show a SLV ranging between 10 and 22.5 %) while the eastern region, central plateau, northern highland in the region surrounding Virunga National Park, areas lying to the Congo Nile Trail extending to southern and the western parts of the country indicate a SLV ranging between 22.5 and 35 %. For the SR, the

south-western, south-central and the eastern lowland region indicate a SLV ranging between 15 and 23 % while the central plateau, northern and north-western highland of the country shown a SLV ranging between 23 and 31 %).

For RD, the RDV ranges between of 17 and 32 % for the LR and varies between13 to 38 % for the SR. High variability is observed over the eastern and central parts of the country during the LR while the southern, western and northern regions of the country shown high variation during the SR. For the LR (Fig. 6c), the RDV ranging between 17 and 24.5 % is shown over the south-western and north-western highland increasing towards the north-western highland, southern and central plateau while the south-central, central and eastern parts of the country indicated a coefficient of variation ranging between 24.5 and 32 %. For the SR (Fig. 6d), the south-central and eastern parts of the country indicate a RDV ranging between 13 and 25.5 % while the rest of the country shown a RDV ranging between 25.5 and 38 %.

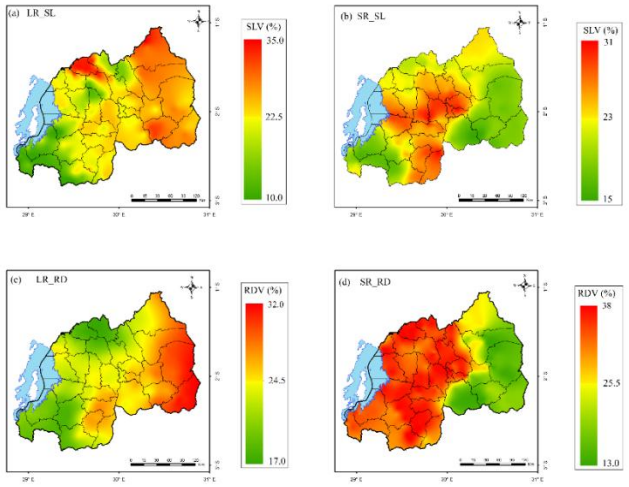

Figure 5. 6 Coefficients of variation of: (a) seasonal length (SLV) for LR, (b) seasonal length (SLV) for SR, (c) number of rainy days (RDV) for LR and (d) number of rainy days (RDV) for SR (d), using observation data from 1983 to 2021.

Figure 5. 7 presents time series of seasonal rainfall intensity (RI), onset days (OD), cessation days (CD), seasonal length (SL) and number of rainy days (RD) during the long rains season (MAM) and the short rains season (SOND) rainy seasons. For the long rains season, years with above than average rainfall are 1988, 1997, 2002, 2003, 2004, 2015, 2018, 2020, while years with bellow than average rainfall are 1984, 1992, 2008, 2011, 2014, 2017, 2019, 2021. Early ODs were observed in 1988, 1990, 2002, 2004, 2007, 2018 and 2020, and late ODs n 1983, 1994, 1998, 2015 and 2017. Early CDs were observed in 1983, 1985, 1999, 2013, 2014, 2016 and 2017, and late CDs in 1987,

1998, 2002, 2003, 2006, 2008, 2009 and 2012. Shorter SLs were observed in 1983, 1984, 1992, 1994, 1998, 2014, 2015 and 2017, and longer in 1987, 1990, 2002, 2007 and 2018. Few RDs were observed in 1983, 1984, 1992, 1994, 1998 and 2014, and in 1988, more RDs 1997, 2002, 2004, 2007, 2015 and 2018. For the short rains season years with above than average rainfall are 1996, 1997, 1998, 199, 2000, 2001, 2003, 2006, 2011, 2012, 2014, 2015, 2019, while years with bellow than average rainfall are 1983, 1984, 1986, 1993, 2010, 2017, 2018, 2020, 2021. Early ODs were observed in 1998, 2001, 2011, 2019 and 2021and late ODs in 1984, 1989, 1993, 1996, 2010, 2017 and 2018. Early CDs were observed in 1988, 2008, 2010, 2016, 2017 and 202, and late CDs in 1996, 1997, 1999, 2002, 2006, 2009. Shorter SLs were observed in in 1984, 1993, 1996, 2010 and 2017, and longer SL in 1997, 2002, 2009, 2011 and 2019. Few RDs were observed in in 1984, 1993, 2010, 2017, 2018 and 2021, and more RDs in 1997, 1999, 2001, 2002, 2003, 2006, 2011 and 2019.

For the long rains season the correlations between rainfall intensity and the rainfall characteristics are r_{ODLR}=-0.51 for onset day, r_{CDLR}=0.36 for cessation day, r_{SLLR}=0.57 for seasonal length and r_{RDLR}=0.65 for number of rainy days. For the short rains season the correlations between rainfall intensity and the rainfall characteristics are r_{ODSR} -0.49 for onset day, r_{CDSR}=0.54 for cessation day, r_{SLSR}=0.70 for seasonal length, r_{RDSR}=0.80 for number of rainy days.

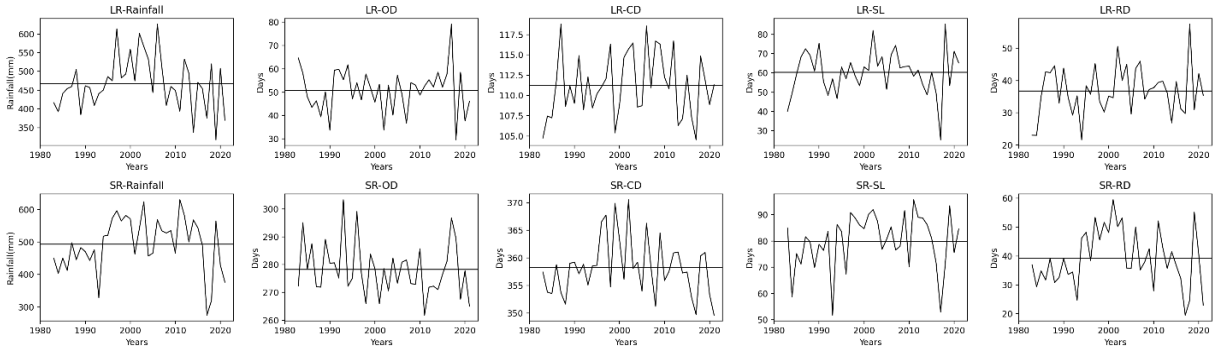

Figure 5. 7 Time series of seasonal rainfall intensity (RI), onset days (OD), cessation days (CD), seasonal length (SL) and number of rainy days (RD) during March-April-May (MAM) and September-October-November-December (SOND) over Rwanda from 1983 to 2021. Horizontal line indicates the mean value.

Figure 5. 8 presents time series of standardized anomalies of seasonal rainfall intensity, onset day, cessation day, length, number of rainy days, SST for Niño 1+2 and Niño 3.4, and the Indian Ocean Dipole Mode Index for the long rains season over Rwanda during the period 1983-2021. The

observed 1983 very strong El Niño in both Nino 1+2 (Niño 1+2 index=2.93) and Nino 3.4 (Niño 3.4 index=1.85) coinciding with a strong negative IOD (IOD index=-0.64) was associated with a bellow than average rainfall (417 mm<468 mm, RI index=-0.46). This long rains season was characterized by late onset day (65, OD index=1.46), early cessation day (105, CD index=-1.68), short seasonal length (40 days, SL index=-1.83) and few rainy days (23 days, RD index=-1.85), compared to the mean onset day (51), mean cessation day (111), mean seasonal length (60 days) and mean rainy days (37 days), respectively. During 1998, the observed very strong El Niño in both Niño 1+2 (Niño 1+2 index=2.54) and Niño 3.4 (Niño 3.4 index=1.56) with however a very weak IOD (IOD index=-0.04) were associated with an above than average rainfall (483 mm>468 mm, RI index=0.32). This year corresponds to a long rains season with heavy rains, floods and landslides associated with a shift of the season with late onset day (58, OD index=0.74), late cessation day (116, CD index=1.32), short seasonal length (58 days, SL index=-0.17) and few rainy days (33 days, RD index=-0.44). The year 2015 was characterized with a very strong El Niño in both Niño 1+2 (Niño 1+2 index=0.84) and Niño 3.4 (Niño 3.4 index=1.23) with also a very weak IOD (IOD index=0.09) with a relatively above than average rainfall (475 mm>468 mm, RI index=0.18). This long rains season was characterized by late onset day (52, OD index=0.14), late cessation day (112, CD index=0.32, short seasonal length (60 days, SL index=-0.005) and more rainy days (40 days, RD index=0.38), compared to the mean onset day (51), mean cessation day (111), mean seasonal length (60 days) and mean rainy days (37 days), respectively. Correlations coefficients between onset day index and Niño 1+2 index (r=0.39) and onset day index and IOD index (0.39) are relatively good.

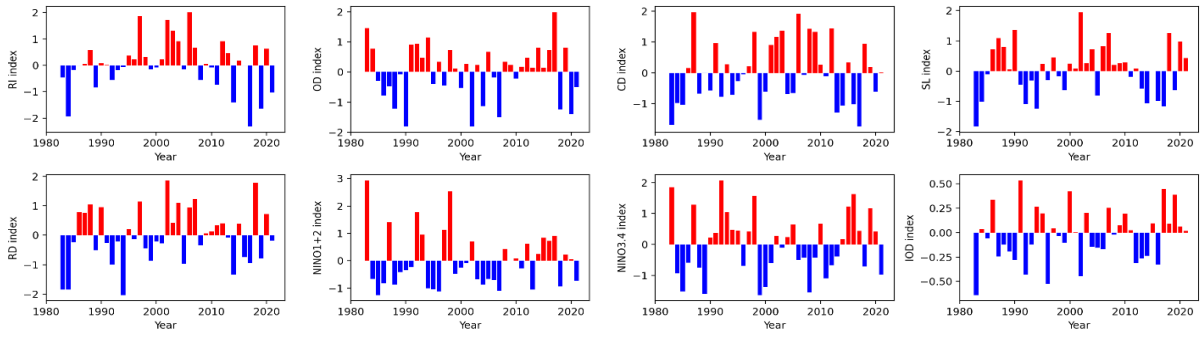

Figure 5. 8 Time series of standardized anomalies of seasonal rainfall intensity (RI index), onset day (OD index), cessation day (CD index), length (SL index), number of rainy days (RD index), SST for Niño 1+2 (Niño 1+2 index) and Niño 3.4 (Niño 3.4 index), and the Indian Ocean Dipole

Mode Index (IOD index) for the short rains season (LR) over Rwanda during the period 1983-2021.

Figure 5. 9 presents time series of standardized anomalies of seasonal rainfall intensity, onset day, cessation day, length, number of rainy days, SST for Niño 1+2 and Niño 3.4, and the Indian Ocean Dipole Mode Index for the short rains season over Rwanda during the period 1983-2021. The observed strong 2010 negative IOD (IOD index-0.91) coupled with a strong La Niña in Niño 1+2 (Niño 1+2 index=-1.21) and Niño 3.4 (Niño 3.4 index=-1.51), caused a less than average rainfall (465mm<493 mm RI index=-0.39). Late onset day (287, OD index=0.79), early cessation day (356, CD index=-0.46), short seasonal length (70 days, DL index=-1.18) and few rainy days (28 days, RD index=-0.95) were observed. The strong positive IOD (IOD index=1.44) which occurred in 2019 corresponded to weak El Niño for Niño3.4 (Niño 3.4 index=0.45) and La Niña for Niño 1+2 (Niño 1+2 index=-0.34). It was observed an above than average rainfall (565 mm>493 mm, RI index=0.77) with early onset day (268, OD index=-1.14), late cessation day (361, CD index=0.53), long seasonal length (93 days, SL index=1.67) and more rainy days (55 days, RD index=1.31). Correlations coefficients between cessation day index and Niño 3.4 index (r=0.38) and cessation day index and IOD index (0.31) are relatively good.

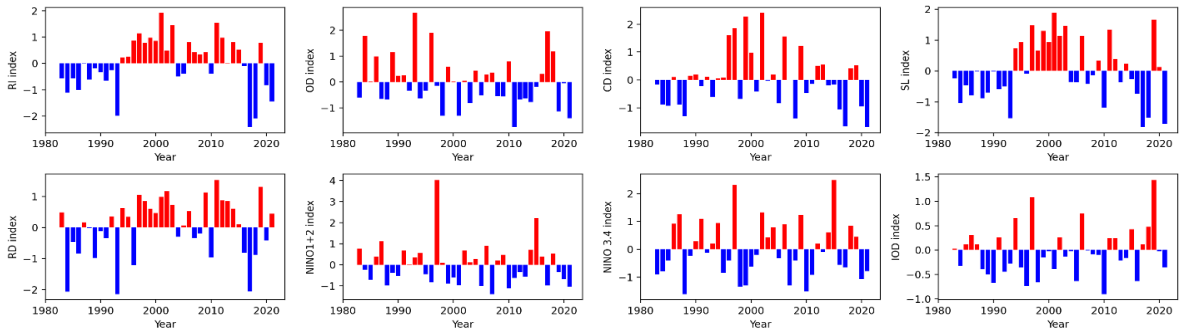

Figure 5. 9 Time series of standardized anomalies of seasonal rainfall intensity (RI index), onset day (OD index), cessation day (CD index), length (SL index), number of rainy days (RD index), SST for Niño 1+2 (Niño 1+2 index) and Niño 3.4 (Niño 3.4 index, and the Indian Ocean Dipole Mode Index (IOD index) for the short rains season (SR) over Rwanda during the period 1983-2021.

5.4 Discussion

The obtained results suggest an existence of the west to east propagation in onset day and east to west gradient of cessation for both seasons in Rwanda, and shorter seasonal length and fewer rainy days over the eastern lowland than the western and northern highland of Rwanda. The observed spatial pattern of mean onset day, cessation day, seasonal length and number of rainy days tend to follow the spatial distribution of the seasonal rainfall with early onset day, late cessation day, higher seasonal length and more rainy days observed in the west than in the east of Rwanda. This is in accordance with the results of Siebert et al. (2019) showing that the areas receiving more rainfall tend to have higher frequency of rainy days. The observed mean onset dates over the eastern region of Rwanda are comparable to those obtained by Ndomba (2010) over Pangani River Basin in Tanzania which indicated the onset day ranging between early March and end March for the long rain and mid-October to mid-November for the short rain. The study on probable sowing time in Rwanda using rainfall from 1960-1990 for the short rain season (Ilunga et al. 2008) indicated that rainfall start at the end of September over Congo Nile Trial and northern highland and between end September and early November in the eastern lowland. These results are in line with results obtained in the present study where in particular the eastern lowland shows later onset day. Results from this study indicate that the onset has a prime role in the long rain season as it exhibits a strong spatial coherence and a large variability. Analysis of the correlations between the rainfall characteristics and the rainfall intensity, for the long rains and the short rains seasons, indicates that the onset days are independent to rainfall intensity, while the cessation days are weakly dependent to rainfall intensity, but more dependent for the short rains season. The seasonal length and the number of rainy days are strongly dependent to rainfall intensity, but more dependent in short rains seasons. In their study over the Equatorial East Africa, Camberlin et al. (2009), found that in the long rains, the onset and cessation days are independent of the number of rain days and the daily rainfall intensity while in the short rain season they are more strongly inter-related. Some studies have indicated the influence of large-scale phenomena on the seasonal rainfall onset and cessation days in East Africa. In their study over Tanzania, Kijazi and Reason (2005) indicated that , reduced rainfall during La Niña years tends to be connected with a late onset and, consequently, a shorter than average rainfall season, while higher rainfall over the north coast during El Niño years was linked to an earlier onset and longer than usual rainy season. A recent

study by Yonah et al. (2023) indicated that there were significant positive patterns for correlation between onset with dry spell and IOD and Niño 3.4 indices in northern and northeastern Kenya and over the Tanzania's Indian Ocean northern coast. The study showed also that there was an inter-annual relationship between onset dates with dry spell and IOD and Niño 3.4 indices.

Investigations done in the present study indicate that large-scale systems influence the studied rainfall characteristics in Rwanda. Results show that Inter-annual relationship between onset days and Niño 1+2 and IOD indices shows a relatively good correlation coefficient for long rains season. Correlations between cessation days and Niño 3.4 and IOD indices are also relatively good for short rains season. IOD has more influence on rainfall characteristics during the short rain season than during the long rains season. El Niño has a strong impact on long rains by bringing heavy rains and flooding over short periods. These results motivate further studies needed for an in-depth analysis of to what extent these large-scale systems may influence the spatial pattern and variability of the in-situ rainfall characteristics.

For country practicing rain-fed agricultural, crop production is harmed by rainfall variability, delayed onset, early termination, and dry spells throughout the growing season (Nicholson et al. 2000, Sivakumar et al. 2005, Kipkorir et al. 2007, Mugalavai et al. 2008, Kumi et al., 2023). Areas with expected early arrival of the rainy would be suitable for crops with long growing season. This would mitigate the influences of climate change on crops at numerous stages of development (Sivakumar et al. 2005). In addition, if the commencement of the season is followed by protracted dry spells, there is a chance of total seedling failure (Kipkorir et al. 2007). Likewise, areas with short growing season would favor early maturing plants to avoid the risk related with delayed commencement and early termination which limit the agricultural growing period, leading to low crop output and hurting subsistence farmers' food security (Mugalavai et al. 2008). This paper addresses the potential contributions of climatology to agricultural planning and development.

To put the study's results into practice, climate scientists, agricultural extension personnel, and farmers must work together. This Synergy can be achieved through implementation of agro-meteorological forecasting (World Meteorological Organization 2012) and generation of weather advisories (Nicholson et al. 2000, Ati et al. 2002, World Meteorological Organization 2012, Oyekale 2015, Chengula and Nyambo 2017, Agyekum et al. 2022). Integration of climate information into agricultural practices enable farmers to better decide and plan their seasonal cropping activities (Chengula and Nyambo 2017, Nyang'au et al. 2021). This may include growing

crops with long growing season length if the commencement of the rains is early or crops with short growing length in the case of late onset day (Mugalavai et al. 2008).

5.5 Conclusion

This study investigates the spatial patterns and variabilities of seasonal rainfall onset day, cessation day, seasonal length and number of rainy days in Rwanda for the long rain season and the short rain season using observational data set from 1983-2021. Patterns of the onset of the rain season show a West to East progression while withdraw of the rain indicated an East to West progression. Early onset and late cessation days were observed over the southwestern and the northwestern parts of the country for both seasons. The eastern parts of the country showed late onset and early withdraw of the rainy for the two seasons. Longer seasonal length and more number of rainy days were observed over the western, northern and southern parts of the country while short season length and fewer rainy days were indicated over eastern lowland region. Relatively high variability in OD were observed over the northwest, central plateau and eastern regions for long rain. Seasonal length shows high variability over the northern and eastern regions for LR and over the southcentral and central plateau regions for short rain. The eastern region experienced relatively moderate variability in the number of rainy days during the long rain season, and over the western, northern, southern, and central plateau regions during the short rain season. The findings derived from this research will help farmers, policy and decision-making for appropriate adaptation and mitigation strategies and policies. Some potential study avenues are as follows: (i) investigate various criteria of determining the onset and cessation days of a rainy season and their variabilities; (ii) assessment of dry spells occurrence during the growing season; (iii) assessing atmospheric circulation anomalies associated with changes in onset and cessation days of the rainy season; (iv) analysing the influence of large-scale systems on the spatial pattern and variability of rainfall characteristics and (v) modeling the statistical distribution of onset and cessation days.

5.6 References

Adejuwon, J. (2006). Food Security , Climate Variability and Climate Change in Sub Saharan West Africa. *AIACC Final Report No.AF 23*, 1–156.

Adelekan, I. O. (2019). Local knowledge of climatic conditions and agricultural activities in southwestern nigeria, *J. Sc. Res.,2009*.

Adelekan, I. O., and Adegebo, B. O. (2014). Variation in Onset and Cessation of the Rainy Season in Ibadan , Nigeria. *J. Sci. Res.*, *13*(2014), 13–21.

Agyekum, T. P., Antwi-Agyei, P., and Dougill, A. J. (2022). The contribution of weather forecast information to agriculture, water, and energy sectors in East and West Africa: A systematic review. *Front. Envir. Sci.*, *10*, 1–14. https://doi.org/10.3389/fenvs.2022.935696

Amekudzi, L., Yamba, E., Preko, K., Asare, E., Aryee, J., Baidu, M., and Codjoe, S. (2015). Variabilities in Rainfall Onset, Cessation and Length of Rainy Season for the Various Agro-Ecological Zones of Ghana. *Climate*, *3*(2), 416–434. https://doi.org/10.3390/cli3020416

Atanabe, M. A. W. (2010). Application of Cluster Analysis to Climate Model Performance Metrics. *J. Appl. Meteorol. Climatol.*, 50 (*2004)*, 1666–1675. https://doi.org/10.1175/2011JAMC2643.1

Ati, O. F., Stigter, C. J., and Oladipo, E. O. (2002). A comparison of methods to determine the onset of the growing season in Northern Nigeria. *Int. J. Climatol.*, *22*(6), 731–742. https://doi.org/10.1002/joc.712

Awal, R., Habibi, H., Fares, A., and Deb, S. (2020). Estimating reference crop evapotranspiration under limited climate data in West Texas. *J. Hydrol.: Reg. Stud, 28*(2019), 100677. https://doi.org/10.1016/j.ejrh.2020.100677

Barde, P., and Barde, M. (2012). What to use to express the variability of data: Standard deviation or standard error of mean? *Perspect. Clin. Res.*, *3*(3), 113. https://doi.org/10.4103/2229-3485.100662

Beguería, S., Vicente-Serrano, S. M., Reig, F., and Latorre, B. (2014). Standardized precipitation evapotranspiration index (SPEI) revisited: Parameter fitting, evapotranspiration models, tools, datasets and drought monitoring. *Int. J. Climatol.*, *34*(10), 3001–3023. https://doi.org/10.1002/joc.3887

Biabiany, E., Bernard, D. C., Page, V., and Paugam-moisy, H. (2020). Computers and Geosciences Design of an expert distance metric for climate clustering : The case of rainfall in the Lesser Antilles. *Comput. Geosci.*, 145(2020),104612. https://doi.org/10.1016/j.cageo.2020.104612

Camberlin, P., Moron, V., Okoola, R., Philippon, N., and Gitau, W. (2009). Components of rainy seasons' variability in Equatorial East Africa: Onset, cessation, rainfall frequency and intensity. *Theor.Appl. Climatol.*, *98*(3–4), 237–249. https://doi.org/10.1007/s00704-009-0113-1

Camberlin, P., and Okoola, R. E. (2003). The onset and cessation of the ‘“ long rains ”’ in eastern Africa and their interannual variability. *Theor.Appl. Climatol.*,*54*(1–2), 43–54. https://doi.org/10.1007/s00704-002-0721-5

Chengula, F., and Nyambo, B. (2017). Dissemination of agricultural weather forecasts under weather and climate variability: a case of the smallholder farmers in Moshi rural District, Tanzania. *IJ AEE*, *3*(1), 048–057. www.premierpublishers.org,

Connor, J. D., Schwabe, K., King, D., and Knapp, K. (2012). Irrigated agriculture and climate change: The influence of water supply variability and salinity on adaptation. *Ecol. Econ. 77*, 149–157. https://doi.org/10.1016/j.ecolecon.2012.02.021

Diem, J. E., and Sung, H. S. (2018). Rainfall Characteristics and Trends — and the Role of Congo Westerlies — in the Western Uganda Transition Zone of Equatorial Africa From 1983 to 2017. *J. Geophys. Res. Atmos*., *124*, 10712–10729.

Dinku, T., Hailemariam, K., Maidment, R., and Connor, S. (2014). *Combined use of satellite estimates and rain gauge observations to generate high-quality historical rainfall time series over Ethiopia*. *Int. J. Climatol.*, *2504*(2013), 2489–2504. https://doi.org/10.1002/joc.3855

Dodd, D. E. S., and Jolliffe, I. T. (2001). Early detection of the start of the wet season in semiarid tropical climates of western Africa. *Int. J. Climatol. 21*(10), 1251–1262. https://doi.org/10.1002/joc.640

Droogers, P., and Allen, R. G. (2002). Estimating reference evapotranspiration under inaccurate data conditions. *Irrig. Drain. Syst.*, *16*, 33–45. https://doi.org/10.1023/A

Dunning, C. M., Allan, R. P., and Black, E. (2017). Identification of deficiencies in seasonal rainfall simulated by CMIP5 climate models. *Envir. Res. Lett.*, *12*(11). https://doi.org/10.1088/1748-9326/aa869e

Edoga, R. N. (2007). Determination of Length of Growing Season in Samaru Using Different Potential Evapotranspiration Models. *Au J.T.*, *11*(1), 28–35.

Egeru, A., MacOpiyo, R. L., Mburu, J., Majaliwa, M. G. J., and Aleper, D. (2014). Trend in climate variation in Karamoja Sub-region, northern eastern Uganda. *Fourth RUFORUM Bien Reg. Conf.* 449–456.

Endris, H. S., Omondi, P., Jain, S., Lennard, C., Hewitson, B., Chang’a, L., Awange, J. L. ., Dosio, A., Ketiem, P., Nikulin, G., Panitz, H. J., Büchner, M., Stordal, F., and Tazalika, L. (2013). Assessment of the performance of CORDEX regional climate models in simulating East

African rainfall. *J. Clim.*, *26*(21), 8453–8475. https://doi.org/10.1175/JCLI-D-12-00708.1

Ferijal, T., Batelaan, O., Shanafield, M., and Alfahmi, F. (2022). Determination of rainy season onset and cessation based on a flexible driest period. *Theor. Appl. Climatol.*, *148*(1–2), 91–104. https://doi.org/10.1007/s00704-021-03917-1

Gebremedhin, T., Haile, G. G., Gebremicael, T. G., Libsekal, H., and Reda, K. W. (2023). Balancing crop water requirements through supplemental irrigation under rainfed agriculture in a semi-arid environment. *Heliyon*, *9*(8), e18727. https://doi.org/10.1016/j.heliyon.2023.e18727

Gebremichael, A., Quraishi, S., and Mamo, G. (2014). Analysis of Seasonal Rainfall Variability for Agricultural Water Resource Management in Southern Region , Ethiopia. *J. Nat. Sci. Res.*, *4*(11), 56–80.

Getahun, G. W., Zewdu Eshetu, and Mekuria Argaw. (2016). Temporal and spatial variability of rainfall distribution and evapotranspiration across altitudinal gradient in the Bilate River Watershed, Southern Ethiopia. *Afr.* J. Environ. *Sci. Technol.*, *10*(6), 167–180. https://doi.org/10.5897/AJEST2015.2029

Guenang, G. M., and Mkankam Kamga, F. (2012). Onset, retreat and length of the rainy season over Cameroon. *Atmos. Sci. Lett.*, *13*(2), 120–127. https://doi.org/10.1002/asl.371

Haleakala, K., Yue, H., Alam, S., Mitra, R., and Gebremichael, A. I. B. and M. (2018). The evolving roles of intensity and wet season timing in rainfall regimes surrounding the Red Sea. *Environ. Res. Lett.*, 17 (4), 1-11, https://doi.org/DOI 10.1088/1748-9326/ac5560.

Hargreaves, G. H., and Allen, R. G. (2003). History and Evaluation of Hargreaves Evapotranspiration Equation. *J. Irrig. Drain.*, *129*(1), 53–63. https://doi.org/10.1061/(asce)0733-9437(2003)129:1(53)

Henninger, S. M. (2013). Does the global warming modify the local Rwandan climate? *Nat. Sci.*, *05*(01), 124–129. https://doi.org/10.4236/ns.2013.51A019

Ilunga, L., and Muhire, I. (2010). Comparaison des fluctuations des précipitations moyennes annuelles au Rwanda avec les épisodes EL NIÑO/LA NIÑA et les cycles des taches solaires. *Geo-Eco-Trop*, *34*(34), 75–86.

Ilunga, L., Muhire, I., and Mbaragijimana, C. (2004). Saisons pluviométriques et origine des pluies au Rwanda. *Geo-Eco-Trop*, *28*(1–2), 61–68.

Ilunga, L., Mukingambeho, D., Mugwaneza, A., and Mugiraneza, A. (2008). Probable sowing time

in Rwanda. *Geo-Eco-Tro*, 29–36.

Jena, D., Mohapatra, A. K. B., Alim, A., Pasupalak, S., and Baliarsingh, A. (2019). Assessment of onset , cessation of rain fall and length of growing period of different blocks of Dhenkanal district of Odisha for cultivation of winter pulses in rice fallow condition. *J. Pharm. Innov.*, *8*(3), 333–335.

Kalognomou, E. A., Lennard, C., Shongwe, M., Pinto, I., Favre, A., Kent, M., Hewitson, B., Dosio, A., Nikulin, G., Panitz, H. J., and Büchner, M. (2013). A diagnostic evaluation of precipitation in CORDEX models over Southern Africa. *J.Clim.*, *26*(23), 9477–9506. https://doi.org/10.1175/JCLI-D-12-00703.1

Kazora, J., Wen, W., Shahid, S., Ali, M. A., Bilal, M., Habtemicheal, B. A., Iyakaremye, V., Qiu, Z., Almazroui, M., Wang, Y., Sebaziga, J. N., and Tiwari, P. (2021). Spatiotemporal variability of rainfall trends and influencing factors in Rwanda. *J. Atmos. Sol.-Terr. Phys.*, *219*. https://doi.org/10.1016/j.jastp.2021.105631

Kijazi, A. L., and Reason, C. J. C. (2005). Relationships between intraseasonal rainfall variability of coastal Tanzania and ENSO. *Theor.Appl.Climatol.*, *82*(3–4), 153–176. https://doi.org/10.1007/s00704-005-0129-0

Kijazi, A. L., and Reason, C. J. C. (2012). Intra-seasonal variability over the northeastern highlands of Tanzania. *Int. J. Climatol.*, *32*(6), 874–887. https://doi.org/10.1002/joc.2315

Kipkorir, E. C., Raes, D., Bargerei, R. J., and Mugalavai, E. M. (2007). Evaluation of two risk assessment methods for sowing maize in Kenya. *Agric. For. Meteorol.*, *144*(3–4), 193–199. https://doi.org/10.1016/j.agrformet.2007.02.008

Kizza, M., Rodhe, A., Xu, C., Ntale, H. K., and Halldin, S. (2009). Temporal rainfall variability in the Lake Victoria Basin in East Africa during the twentieth century. *Theor. Appl. Climatol.*, *98*, 119–135. https://doi.org/10.1007/s00704-008-0093-6

Kristjanson, P., Neufeldt, H., Gassner, A., Mango, J., Kyazze, F. B., Desta, S., Sayula, G., Thiede, B., Förch, W., Thornton, P. K., and Coe, R. (2012). Are food insecure smallholder households making changes in their farming practices? Evidence from East Africa. *Food Secur.*, *4*(3), 381–397. https://doi.org/10.1007/s12571-012-0194-z

Kumi, N., Adeliyi, T. E., Asante, V. A., Abiodun, B. J., and Lamptey, B. L. (2023). Impact of rainfall onset date on crops yield in Ghana. *Front. Sustain. Food Syst.*, *7*, 1–10. https://doi.org/10.3389/fsufs.2023.1176385

Laux, P., Kunstmann, H., and Bárdossy, A. (2007). Linking the west african monsoon's onset with atmospheric circulation patterns. *IAHS-AISH Publication*, *313*, 40–50.

Laux, P., Kunstmann, H., and Bárdossy, A. (2008). Predicting the regional onset of the rainy season in West Africa. *Int. J. Climatol.*, *28*(3), 329–342. https://doi.org/10.1002/joc.1542

Linderholm, H. W. (2006). Growing season changes in the last century. *Agric. For. Meteorol.*, *137*(1–2), 1–14. https://doi.org/10.1016/j.agrformet.2006.03.006

Lipiec, J., Doussan, C., Nosalewicz, A., and Kondracka, K. (2013). Effect of drought and heat stresses on plant growth and yield: A review. *Int. Agrophysics.*, *27*(4), 463–477. https://doi.org/10.2478/intag-2013-0017

Liu, C., and Allan, R. P. (2013). Observed and simulated precipitation responses in wet and dry regions 1850-2100. *Environ. Res. Lett.*, *8*(3). https://doi.org/10.1088/1748-9326/8/3/034002

Luhunga, P., Botai, J., and Kahimba, F. (2016). Evaluation of the performance of CORDEX regional climate models in simulating present climate conditions of Tanzania Evaluation of the performance of CORDEX regional climate models in simulating present climate conditions of Tanzania. JSHESS, *66*(1), 32–54. https://doi.org/10.22499/3.6601.005

Marteau, R., Moron, V., and Philippon, N. (2009). Spatial coherence of Monsoon onset over Western and Central Sahel (1950-2000). *J. Clim.*, *22*(5), 1313–1324. https://doi.org/10.1175/2008JCLI2383.1

Mesay Abebe. (2006). The Onset , Cessation and Dry Spells of the Small Rainy Season (Belg) of Ethiopia. *Analysis*, 59067–59067.

Mikova, K. (2015). Effect of Climate Change on Crop Production in Rwanda. *Earth Sci.*, *4*(3), 120. https://doi.org/10.11648/j.earth.20150403.15

Moron, V., Robertson, A. W., and Ward, M. N. (2006). Seasonal predictability and spatial coherence of rainfall characteristics in the tropical setting of Senegal. *Mon. Weather Rev.*, *134*(11), 3248–3262. https://doi.org/10.1175/MWR3252.1

Mugalavai, E. M., Kipkorir, E. C., Raes, D., and Rao, M. S. (2008). Analysis of rainfall onset, cessation and length of growing season for western Kenya. *Agric. For. Meteorol.*, *148*(6–7), 1123–1135. https://doi.org/10.1016/j.agrformet.2008.02.013

Mugo, R. M., Ininda, J., and Okoola, R. (2016). Inter Annual Variability of Onset and Cessation of the Long Rains in Kenya. *J M R S*, *9*(12), 30–47.

https://doi.org/10.20987/jmrs.3.05.2016

Muhire, I., Ahmed, F., and Abutaleb, K. (2015). Relationships between Rwandan seasonal rainfall anomalies and ENSO events. *Theor. Appl. Climatol.*, *122*(1–2), 271–284. https://doi.org/10.1007/s00704-014-1299-4

Muhire, I., Ahmed, F., and Elbasit, M. A. M. A. (2015). Spatio-temporal variations of rainfall erosivity in Rwanda. *J. Soil Sci. Environ. 6*(4), 72–83. https://doi.org/10.5897/JSSEM14

Mupenzi, Anming, B., Lanhai, L., Ge, J., and Habiyaremye, G. (2011). Effects of climate change on Rwandan smallholder agriculture. *Afr. J. Agric. Res.*, *6*(13), 3217–3219. https://doi.org/10.5897/AJAR10.975

National institute of Statistics of Rwanda. (2023a). Gross Domestic Product – 2023 Q3. *Republic of Rwanda*.

National Institute of Statistics of Rwanda. (2023b). Main Indicators: 5th Rwandan Population and Housing Census (PHC))*; National Institute of Statistics of Rwanda: Kigali, Rwanda*.

Ndomba P. M. (2010). Development of Rainfall Curves for Crops Planting Dates: A Case Study of Pangani River Basin in Tanzania. *Nile Basin Water Sci. Eng. J.*, *3*(1), 13–27.

Ngarukiyimana, J. P., Fu, Y., Yang, Y., Ogwang, B. A., Ongoma, V., and Ntwali, D. (2017). Rwanda, East Africa. *Int. J. Climatol.*, *38*(1), 187–202. https://doi.org/10.1002/joc.5169

Ngetich, K. F., Mucheru-Muna, M., Mugwe, J. N., Shisanya, C. A., Diels, J., and Mugendi, D. N. (2014). Length of growing season, rainfall temporal distribution, onset and cessation dates in the Kenyan highlands. *Agric. For. Meteorol.*, *188*, 24–32. https://doi.org/10.1016/j.agrformet.2013.12.011

Nicholson, S. E., Some, B., and Kone, B. (2000). An analysis of recent rainfall conditions in West Africa, including the rainy seasons of the 1997 El Nino and the 1998 La Nina years. *J. Clim.*, *13*(14), 2628–2640. https://doi.org/10.1175/1520-0442(2000)013<2628:AAORRC>2.0.CO;2

Nikulin, G., Jones, C., Giorgi, F., Asrar, G., Büchner, M., Cerezo-Mota, R., Christensen, O. B., Déqué, M., Fernandez, J., Hänsler, A., van Meijgaard, E., Samuelsson, P., Sylla, M. B., and Sushama, L. (2012). Precipitation climatology in an ensemble of CORDEX-Africa regional climate simulations. *J. Clim.*, *25*(18), 6057–6078. https://doi.org/10.1175/JCLI-D-11-00375.1

Ntwali, D., Ogwang, B. A., and Ongoma, V. (2016). The Impacts of Topography on Spatial and

Temporal Rainfall Distribution over Rwanda Based on WRF Model. *ACS, 06*(02), 145–157. https://doi.org/10.4236/acs.2016.62013

Nyakaisiki, K., Mugume, I., Ngailo, T., and Nakabugo, R. (2019). The Use of Indigenous Knowledge in Predicting Changes in Seasonal Rainfall by Smallholder Farmers of Ruteete Subcounty, Kabarole District. *J. Geoscience. Environ. Prot., 07*(01), 13–22. https://doi.org/10.4236/gep.2019.71002

Nyang'au, J. O., Mohamed, J. H., Mango, N., Makate, C., and Wangeci, A. N. (2021). Smallholder farmers' perception of climate change and adoption of climate smart agriculture practices in Masaba South Sub-county, Kisii, Kenya. *Heliyon, 7*(4), e06789. https://doi.org/10.1016/j.heliyon.2021.e06789

Odekunle, T. O. (2006). Determining rainy season onset and retreat over Nigeria from precipitation amount and number of rainy days. *Theor. Appl. Climatol., 83*(1–4), 193–201. https://doi.org/10.1007/s00704-005-0166-8

Odekunle, T. O., Balogun, E. E., and Ogunkoya, O. O. (2005). On the prediction of rainfall onset and retreat dates in Nigeria. *Theor. Appl. Climatol., 81*(1–2), 101–112. https://doi.org/10.1007/s00704-004-0108-x

Odenkunle, T. O. (2004). Rainfall and the length of the growing season in Nigeria. *Int. J. Climatol., 24*(4), 467–479. https://doi.org/10.1002/joc.1012

Omay, P. O., Muthama, N. J., Oludhe, C., Kinama, J. M., Artan, G., and Atheru, Z. (2023). Changes and variability in rainfall onset , cessation , and length of rainy season in the IGAD region of Eastern Africa. *Theor. Appl. Climatol.*, 871–893. https://doi.org/10.1007/s00704-023-04433-0

Omotosho, J. B., Balogun, A. A., and Ogunjobi, K. (2000). Predicting monthly and seasonal rainfall, onset and cessation of the rainy season in West Africa using only surface data. *Theor. Appl. Climatol., 20*(8), 865–880. https://doi.org/10.1002/1097-0088(20000630)20:8<865::AID-JOC505>3.0.CO;2-R

Oyekale, A. S. (2015). Access to risk mitigating weather forecasts and changes in farming operations in east and west Africa: Evidence from a baseline survey. *Sustain. , 7*(11), 14599–14617. https://doi.org/10.3390/su71114599

Pitri, R., Soleh, A. M., and Djuraidah, A. (2018). Statistical downscaling modeling through k-means clustering. *Int. J. Sci. Res. Sci. Eng. Technol., 4*(9), 220–227.

Pope, J. O., Brown, K., Fung, F., Hanlon, H. M., Neal, R., Palin, E. J., and Reid, A. (2022). Investigation of future climate change over the British Isles using weather patterns. *Clim. Dyn.*, *58*(9–10), 2405–2419. https://doi.org/10.1007/s00382-021-06031-0

Recha, C. W., Makokha, G. L., Traore, P. S., Shisanya, C., Lodoun, T., and Sako, A. (2012). Determination of seasonal rainfall variability, onset and cessation in semi-arid Tharaka district, Kenya. *Theor. Appl. Climatol.*, *108*(3–4), 479–494. https://doi.org/10.1007/s00704-011-0544-3

Rwanyiziri, G., and Rugema, J. (2013). Climate Change Effects on Food Security in Rwanda: Case Study of Wetland Rice Production in Bugesera District. *Rwanda J.*, *1*(1), 35–51. http://www.ajol.info/index.php/rj/article/view/98944

Safari, B., Sebaziga, J. N., and Siebert, A. (2022). Evaluation of CORDEX-CORE Regional Climate Models in Simulating Rainfall Variability in Rwanda. *Int. J. Climatol., 2021*, 1–29. https://doi.org/10.1002/joc.7891

Sebaziga, J. N., Twahirwa, A., Kazora, J., Rusanganwa, F., Mbati, M. M., Higiro, S., Guhirwa, S., Nyandwi, J. C., and Niyitegeka, J. M. V. (2023). Spatial and Temporal Analysis of Rainfall Variability and Trends for Improved Climate Risk Management in Kayonza District, Eastern Rwanda. *Adv. Meteorol., 2023*, 1–17. https://doi.org/10.1155/2023/5372701

Sebaziga, N. J., Safari, B., Ngaina, N. J., Ntwali, D., Mutai, B. K., Safari, A., and Rwema, M. (2022). Rainfall variability and trends over Rwanda. *J. Clim. Chang. Sustain.*, *4*(1), 26–34. https://doi.org/10.20987/jccs.04.06.2022

Segele, Z. T., and Lamb, P. J. (2005). Characterization and variability of Kiremt rainy season over Ethiopia. *Meteorol. Atmos. Phys.*, *89*(1–4), 153–180. https://doi.org/10.1007/s00703-005 0127-x

Siebert, A., Dinku, T., Vuguziga, F., Twahirwa, A., and Kagabo, D. M. (2019). Evaluation of ENACTS-Rwanda : A new multi-decade , high- resolution rainfall and temperature data set — Climatology, *Int. J. Climatol.*, 39(6), 1–17. https://doi.org/10.1002/joc.6010

Singh, S., and Gill, N. S. (2013). *Analysis And Study Of K-Means Clustering Algorithm*. *Int. J. Eng. Res. Technol.*, *2*(7), 2546–2551.

Sivakumar, M. V. K., Das, H. P., and Brunini, O. (2005). Impacts of present and future climate variability and change on agriculture and forestry in the arid and semi-arid tropics. *Clim. Chang.*, *70*(1–2), 31–72. https://doi.org/10.1007/s10584-005-5937-9

Sobowale, A., Sajo, S. O., and Ayodele, O. E. (2016). Analysis of onset and cessation of rainfall in southwest nigeria: food security impact of of variability in the length of growing season. *Hung. Agric. Eng.*, *30*, 23–30. https://doi.org/10.17676/hae.2016.30.23

Sovacool, B. K., Griffiths, S., Kim, J., and Bazilian, M. (2021). Climate change and industrial F-gases: A critical and systematic review of developments, sociotechnical systems and policy options for reducing synthetic greenhouse gas emissions. *Renew. Sustain. Energy Rev.*, *141*(2020), 110759. https://doi.org/10.1016/j.rser.2021.110759

Sriadhi, S., Gultom, S., and Martiano, M. (2020). Accuracy of Data Cluster Accuracy of Data Cluster Using Modify K-Mean Algorithm by Local Deviation MethodS. *Int. J. Adv. Sci. Technol.*,, *29*(5), 2019–2025.

Stern, R. D., and Cooper, P. J. M. (2011). Assessing climate risk and climate change using rainfall data - A case study from Zambia. *Exp. Agric.*, *47*(2), 241–266. https://doi.org/10.1017/S0014479711000081

Sultan, B., and Janicot, S. (2003). The West African monsoon dynamics. Part II: The "preonset" and "onset" of the summer monsoon. *J. Clim.*, *16*(21), 3407–3427. https://doi.org/10.1175/1520-0442(2003)016<3407:TWAMDP>2.0.CO;2

Taye, M., Zewdu, F., and Ayalew, D. (2013). Characterizing the Climate System of Western Amhara , Ethiopia : A GIS Approach. *Am. J. Res. Commun.*, *1*(10), 319–355.

Tesfaye, K., and Walker, S. (2004). Matching of crop and environment for optimal water use: The case of Ethiopia. *Phys. Chem. Earth*, *29*(15-18 SPEC.ISS.), 1061–1067. https://doi.org/10.1016/j.pce.2004.09.024

Tubiello, F. N., Soussana, J. F., and Howden, S. M. (2007). Crop and pasture response to climate change. *PNAS USA*, *104*(50), 19686–19690. https://doi.org/10.1073/pnas.0701728104

Umuhoza, J., Chen, L., and Mumo, L. (2021). Assessing the Skills of Rossby Centre Regional Climate Model in Simulating Observed Rainfall over Rwanda. *A CS*, *11*(03), 398–418. https://doi.org/10.4236/acs.2021.113023

Umutoni, M. A., Japheth, L. P., Lipiki, E. J., Kebacho, L. L., Limbu, P. T. S., and Makula, E. K. (2021). Investigation of the 2016 March to May extreme rainfall over Rwanda. *Nat. Hazards*, *108*(1), 607–618. https://doi.org/10.1007/s11069-021-04697-7

Uwimbabazi, J., Jing, Y., Iyakaremye, V., Ullah, I., and Ayugi, B. (2022). Observed Changes in Meteorological Drought Events during 1981–2020 over Rwanda, East Africa. *Sustain.*,

14(3). https://doi.org/10.3390/su14031519

Valipour, M. (2015). Temperature analysis of reference evapotranspiration models. *Meteorol. Appl.*, *22*(3), 385–394. https://doi.org/10.1002/met.1465

Warren, F. J., Barrow, E., Schwartz, R., Andrey, J., Mills, B., and Riedel, D. (2015). Impacts et adaptation liés aux changements climatiques: *perspective canadienne*.

Wati, T., Kusumaningtyas, S. D. A., and Aldrian, E. (2019). Study of season onset based on water requirement assessment. *IOP Conf. Ser. Earth Environ. Sci.*, *299*(1). https://doi.org/10.1088/1755-1315/299/1/012042

Wickramasinghe, A., Muthukumarana, S., Loewen, D., and Schaubroeck, M. (2022). Temperature clusters in commercial buildings using k-means and time series clustering. *Energy Informatics*, *5*(1), 1–14. https://doi.org/10.1186/s42162-022-00186-8

World Meteorological Organization, W. (2012). Guide to Agricultural Meteorological Practices. In *WMO-No. 134, Geneva , Switzerland, 2010 edition* (Issue 134).

Yonah, I. B., King'uza, P. H., Chang'a, L. B., Babyegeye, M. M., Mahoo, H. F., and Kijazi, A. L. (2023). The Inter-Annual Variability of Rainfall Onset and Its Implication on Crop Planting in Selected East Africa Countries. *Am. J. Clim. Chang.*, *12*(02), 268–291. https://doi.org/10.4236/ajcc.2023.122013

Zhou, X., Chen, L., Umuhoza, J., Cheng, Y., Wang, L., and Wang, R. (2021). Intraseasonal oscillation of the rainfall variability over Rwanda and evaluation of its subseasonal forecasting skill. *A O S L*, *14*(6), 100099. https://doi.org/10.1016/j.aosl.2021.100099

Chapter 6 Observed Trends and Variability of Seasonal Extreme Rainfall Indices and Projected Changes in Rwanda

This Chapter reproduces the content of our published paper (https://doi.org/10.1007/s00704-025-05474-3).

6.1 Introduction

Globally, the frequency and intensity of climate extremes have increased, leading to disasters such as landslides, floods, and droughts that degrade the environment and potentially impact socio-economic sectors(Tank et al., 2009; Lehmann et al., 2015; Sarr et al., 2015; Attogouinon et al., 2017; Adeyeri et al., 2019). In particular, agricultural productivity is highly vulnerable to extreme precipitation variability, as the water budget during the vegetative growing season is often more affected by rainfall extremes than by total precipitation amounts (Lobell and Field, 2007; Christiansen et al., 2011; Sillmann et al., 2013). Heavy rainfall events (R20mm) cause soil erosion, root diseases, and crop failures due to excessive moisture (Posthumus et al., 2009) while prolonged dry spells, as indicated by the consecutive dry days (CDD) index, increase the risk of drought-induced crop stress (Tebaldi et al., 2006; Orlowsky and Seneviratne, 2012). These climate shocks also contribute to migration pressures, as communities affected by floods, droughts, and declining agricultural yields are forced to relocate in search of better living conditions (Nawrotzki and Bakhtsiyarava, 2017; Nawrotzki et al., 2015).

The African continent is experiencing notable shifts in extreme rainfall patterns, with declining average precipitation observed in southern and western Africa, alongside increasing dry days, daily rainfall intensity (Rx1day and Rx5day), and extreme precipitation (New et al., 2006). Positive Rx1day trends have been reported in the Sahel, Kenya, Tanzania, the Gulf of Guinea, and parts of the Middle East, whereas negative trends dominate inland West Africa, South Africa, Namibia, and central Africa from Sudan to Angola (Marra et al., 2022). Extreme precipitation shows a decreasing trend in North Africa, the Sahel, central Africa, and western South Africa, while increasing trends have been observed in West Africa, East Africa, and eastern South Africa (Habiyakare et al., 2024). Variations of these indices leads to risks on agriculture, infrastructure, and disaster management due to flooding and soil erosion. In Benin, indices such as PRCPTOT, R10mm, R20mm, Rx1day, and Rx5day show decreasing trends at most stations potentially reducing water availability for crops and increasing drought risks (Attogouinon et al., 2017), while

in the Lake Chad region, there are increasing trends in consecutive wet days (CWD) and annual total rainfall impacting water availability and heighten the risk of flooding, affecting settlements, transport networks, and food security (Adeyeri et al., 2019).

In Eastern Africa, rainfall variability presents unique challenges, especially in semi-arid and highland regions. A slight decrease in precipitation has been observed during the long rainy season, with no significant changes in annual mean daily precipitation (Ogega et al., 2020). The Arid and Semi-Arid Land (ASAL) regions have seen a decline in R10mm, R20mm, and PRCPTOT, limiting water availability for agriculture and increasing drought frequency (Ngaina and Mutai, 2013) (Ongoma et al., 2018). In Ethiopia, Kenya, and Tanzania, precipitation indices have varied without clear trends (Gebrechorkos et al., 2019). However, in semi-arid areas like Western Tigray, Ethiopia, positive trends in R10mm, R20mm, and R95pTOT suggest increasing risks of localized flooding (Berhane et al., 2020). In the equatorial and northern sub-regions, including Western Lake Victoria, Southern Sudan, and western Ethiopia, RX5day, R95pTOT, and PRCPTOT have exhibited a decreasing trend, whereas in the southern parts of the region, these indices have shown an increasing trend (Omondi et al., 2014). In Uganda, PRCPTOT has shown a rising pattern, while CDD has decreased in the Mbarara region, signalling wetter conditions (Owoyesigire et al., 2016)., whereas the eastern region has recorded declines in R10mm, R20mm, and SDII, increasing concerns about prolonged dry spells (Alex et al., 2019).

Projected changes in extreme rainfall indices suggest that future climate variability will intensify these impacts across Africa. CWD is expected to decline in the far future under SSP1-2.6, SSP2-4.5, SSP3-7.0, and SSP5-8.5 scenarios, reducing the duration of wet periods and affecting water availability (Habiyakare et al., 2024). R10mm is projected to decrease in southern Africa but increase in central, eastern, and western Africa under SSP2-4.5 and SSP5-8.5 scenarios (Bobde et al., 2024), with East Africa seeing an increase in prolonged dry spells by the late 21st century (Ayugi et al., 2021). The Lake Victoria Basin is also projected to experience longer maximum dry and wet spells, posing challenges for water resource management and ecosystem stability (Onyutha, 2020). In Rwanda, alongside neighboring regions in Uganda, Kenya, and Tanzania, rainfall extremes such as Rx5day and R95pTOT are projected to intensify under SSP4.5 and SSP8.5 scenarios for 2021-2060, increasing disaster risk (Kazora et al., 2023).

Rwanda has witnessed a rise in extreme precipitation events, consistent with trends observed across East Africa (Chang'a et al., 2020). Numerous studies in Rwanda have focused on observed

seasonal and annual rainfall variability, with a general consensus on changes in total rainfall across both timeframes (Ntwali et al., 2016; Siebert et al., 2019; Kazora et al., 2021; Umutoni et al., 2021; Umuhoza et al., 2021; Zhou et al., 2021; Safari et al., 2022; Sebaziga et al., 2022; Uwimbabazi et al., 2022; Twahirwa et al., 2023; Sebaziga et al., 2023; Sebaziga et al., 2024). Given Rwanda's complex terrain, high-resolution regional climate models are essential for capturing fine-scale precipitation patterns. Coordinated Regional Climate Downscaling Experiment-Coordinated Output for Regional Evaluations (CORDEX-CORE) regional climate models (RCMs) were evaluated in their ability to simulate the rainfall over Rwanda against the observed data (Safari et al., 2022). The study found that mean rainfall, annual cycle and their inter-annual variability were satisfactorily reproduced by all RCMs, their ensemble and multi-model ensemble means with the later outperforming individual model. Multi-model ensembles provide simulations with consistent forcing across multiple models, enabling the quantification of epistemic uncertainties and mitigating the limitations of individual models that may not fully capture the complexities of reality (Ehret et al., 2012; Adeyeri et al., 2020). Furthermore, bias correction in climate models addresses historical biases relative to observations (Adeyeri et al., 2019; Adeyeri et al., 2020; Adeyeri et al., 2023), enhancing model representation and reducing uncertainties (Adeyeri et al., 2024). This process effectively minimizes discrepancies between observed and simulated climate variables, thereby decreasing uncertainties inherent in uncorrected climate models (Adeyeri et al., 2020; Adeyeri et al., 2024). Despite evidence of changing rainfall patterns in Rwanda, no comprehensive study has assessed trends and projected changes in seasonal extreme rainfall indices. This study aims to analyse historical trends, variability, and future projected changes of extreme rainfall indices under RCP2.6 and RCP8.5 scenarios. Addressing the how extreme rainfall indices in Rwanda have evolved over time and are expected to change will offer insights to support evidence-based policymaking for climate resilience in Rwanda. In this study, the selection of extreme precipitation indices is based on their potential impacts on agriculture, water resources, and infrastructure. CWD indicates prolonged wet spells, increasing flood and landslide risks in Rwanda's mountainous regions. R10mm and R20mm capture moderate to extreme rainfall, influencing soil erosion, crop damage, and urban flooding. In the western region, where extreme rainfall is more pronounced, Rx1day assesses short-term rainfall intensity linked to flash floods and slope failures. R95pTOT highlights extreme rainfall contributions to annual totals, affecting hydrological stability, while PRCPTOT provides overall rainfall trends for long-term planning.

The selection of RCP2.6 and RCP8.5 in this study is based on the availability of CORDEX-CORE simulations for the African domain, which includes Rwanda (Safari et al., 2022). RCP2.6 represents a low-emission scenario aligned with strong mitigation efforts, while RCP8.5 reflects a high-emission, worst-case trajectory. After the introduction, the paper is structured as follows: section two offers a brief overview of the materials and methods (study area, data, and methodology). Section three presents the results, which are followed by a discussion in section four and the conclusion in section five.

6.2 Material and Methods

6.2.1 Study Area

Rwanda is situated in Eastern and Central Africa, positioned between 1°4′ and 2°51′ South latitude and 28°53′ and 30°53′ East longitude, covering a total area of 26,338 square kilometers. The agriculture sector occupies 14,020 square kilometers, which accounts for 59% of the total land area of the country (National Institute of Statistics of Rwanda, 2023). Rwanda's topography is complex, ranging from lowlands in the eastern part to highlands in the western and northern regions (Figure 6. 1). It features a mix of mountains, hills, and valleys with elevations from 900 meters to 4507 meters. The Congo Nile Trial, with elevations between 2500 and 3000 meters, dominates the western side of the country. The northern region is notable for its volcanic area, including Karisimbi, the highest peak at 4507 meters. The eastern part of the country is characterized by hills with altitudes between 1000 and 1500 meters. The central region consists of hills ranging from 1500 to 2000 meters, while the south-western lowland of Bugarama Valley sits at approximately 900 meters high (Mikova, 2015). Rwanda's rainfall climatology exhibits the typical bimodal pattern seen in East Africa. The country experiences two rainy seasons, the long rain (LR) of March-April-May and the short rain (SR) of September-October-November-December, and two dry seasons, January-February (JF) and June-July-August (JJA) (Muhire et al., 2015; Ntwali et al., 2016; Siebert et al., 2019; Kazora et al., 2021), with April and November being the two peak months for respectively, LR and SR (Ntwali et al., 2016). Rwanda's rainfall distribution is primarily influenced by its diverse topography (Ntwali et al., 2016; Ngarukiyimana et al., 2017). Rwanda presents six distinct climate zones spanning across the country (Sebaziga et al., 2024). Those are: i) the Lake Kivu zone (Zone I), located to the coast of Lake Kivu; ii) the Mountain Forest c zone (Zone II), located on the southern and south-western parts of Nyungwe

National Park; iii) the Mountain zone (Zone III), located in the area over Congo Nile Trial extended to the mountain areas of the northern volcanoes highland; iv) the Central Temperate Highlands zone of the (Zone IV) that encompasses the central mountainous part extended from the southern region to the northern region; v) the Central Plateau zone (Zone V) located between the temperate climate zone of the central highlands in the west; and vi) the Eastern Lowland zone (Zone VI) in the eastern part of the country.

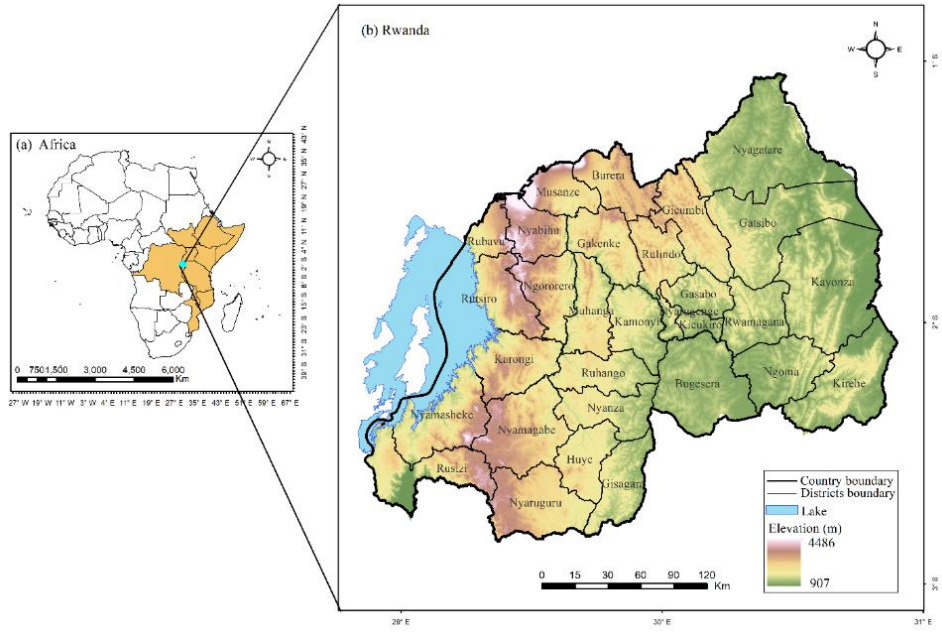

Figure 6. 1 Geographical location of Rwanda in central and eastern African, and Africa (a), Administrative and elevation map of Rwanda (b).

6.2.2 Data and methods

This study uses daily rainfall data from the Rwanda Meteorology Agency, spanning from 1983 to 2021. This dataset is represented on a grid with a spatial resolution of 4 km (0.0375°) grid. The data reconstruction adhered to the methodologies described by (Siebert et al., 2019) and (Dinku et al., 2014). Quality control measures, such checking the outliers and missing values as detailed by (Safari et al., 2022) and (Safari and Sebaziga, 2023), were applied to the observed datasets. For simulated data, we utilized CORDEX-CORE multi-model ensemble mean, generated using three Regional Climate Models (RCMs) at a spatial resolution of 25 km (0.22°). The three RCMs used were the Consortium for Small-Scale Modeling (COSMO) Climate Limited-area Modelling (CCLM5-0-15), the Regional Climatic Model Version 4.7 (RegCM4-7), and the REgional MOdel

REMO2015 (REMO2015). Each RCM was driven by three Global Climate Models (GCMs) to create the multi-model ensemble mean. The GCMs considered were the Max-Planck-Institute Earth System Model Low Resolution (MPI-ESM-LR), the Norwegian Earth System Model version 1 (NCC-NorESM1-M), and the Hadley Centre Global Environmental Model version 2 Earth System (MOHC-HadGEM2-ES). The performance of each of these models in simulating mean rainfall over Rwanda has been thoroughly documented by (Safari et al., 2022).

6.2.3 Extreme Indices

The joint World Meteorological Organization Commission on Climatology (CCl) and the Climate Variability and Prediction (CLIVAR) Expert Team on Climate Change Detection and Indices (ETCCDI) developed a core set of 27 indices (Alexander et al., 2006; Tank et al., 2009; Donat et al., 2013). In this study, six extreme rainfall indices (Table 6. 1) were computed based on the methodology provided by the Expert Team on Climate Change Detection and Indices (ETCCDI) (Tank et al., 2009; Zhang et al., 2011). The computation was carried out using RClimDex software within the R package called Climate Data Tool (CDT v8.0) (Faniriantsoa, 2017; Dinku et al., 2022). The base period from 1991-2020 was used for computing percentile-based threshold indices for each calendar day and for each grid, utilizing data for consecutive 5-day moving windows centered on that calendar day (Tank et al., 2009).

Table 6. 1 List of extreme rainfall indices used in this study.

Code	**Name**	**Definition**	**Unit**	**References**
CWD	Consecutive dry days	Maximum number of consecutive days when precipitation > 1mm	days	(Tank et al., 2009; Alexander et al., 2006; Donat et al., 2013)
R10 mm	Heavy precipitation days	Seasonal count when precipitation ≥ 10 mm	days	(Tank et al., 2009; Alexander et al., 2006; Donat et al., 2013)
R20 mm	Very heavy precipitation days	Seasonal count when	days	(Tank et al., 2009; Alexander et al., 2006; Donat et al., 2013)

		precipitation ≥ 20 mm		
Rx1day	Max 1-day precipitation amount	Seasonal maximum 1-day precipitation	mm	(Tank et al., 2009; Alexander et al., 2006; Donat et al., 2013)
R95pTOT	Precipitation due to very wet days (> 95th percentile)	Seasonal total precipitation from days with rainfall > 95th percentile	mm	(Tank et al., 2009; Alexander et al., 2006; Donat et al., 2013)
PRCPTOT	Total wet-day precipitation	Seasonal total precipitation in wet days (RR>=1mm)	mm	(Tank et al., 2009; Alexander et al., 2006; Donat et al., 2013)

6.2.4 Variability and trend detection

In this study, standard deviations were computed at each grid point for time series of extreme rainfall indices to represent their variability (Safari and Sebaziga, 2023). Trends were computed at each grid point for time series of extreme rainfall indices using the Modified Mann–Kendall test and for estimation of trend magnitude, the Theil–Sen (TS) estimator approach was used (Chechin et al., 2019) (Safari and Sebaziga, 2023). In hydrology and climate time series, the non-parametric Mann–Kendall test and the Theil–Sen slope estimator are widely used for detecting trends and estimating trend magnitudes (Safari, 2012; Tan et al., 2015). However, this method suffers from autocorrelation. Positive autocorrelation may cause the Mann–Kendall test to incorrectly identify a trend, while negative autocorrelation can lead to the opposite error (Datta and Das, 2019). To account for the effect of autocorrelation in datasets, (Ahmed et al., 2017) introduced a modified Mann-Kendall test. This method involves adjusting the variance as noted by (Hamed and Rao, 1998; Taxak et al., 2014; Mahrt, 2014; Das et al., 2022). Significant trends were considered at $\alpha = 0.05$ confidence level.

6.2.5 Errors for comparison of computed CWD, PRCPTOT, R10mm, R20mm, R95pTOT and RX1day from observation and simulated by CORDEX CORE M-M-E

Different metrics are used to compare computed CWD, PRCPTOT, R10mm, R20mm, R95pTOT and RX1day from observation and simulated by CORDEX-CORE-M-M-E. They include the Pearson correlation coefficient (r), mean bias error (MBE), root mean-square error (RMSE) and mean absolute error (MAE) for, respectively, the LR and SR. The r is a measure used to assess the linkage between observed values and the model outputs(Hargreaves & Allen, 2003; Luhunga et al., 2016). It is mathematically expressed as:

$$r = \frac{\frac{1}{n}\sum_{t=1}^{n}(R_i-R)(C_i-C)}{\sqrt{\frac{1}{n}\left[\sum_{t=1}^{n}(R_i-R)^2\right]\left[\sum_{t=1}^{n}(C_i-C)^2\right]}} \quad (1)$$

where R_i and C_i are the rainfall and rainfall characteristics, and R and C are the mean rainfall and mean rainfall characteristics, n is the total number of observations. The MBE, RMSE and MAE indicate the difference between the observation data and model outputs (Willmott & Matsuura, 2005). The positive value denote that the model overestimates the observation while a negative value denotes the underestimation of the model compared to the observation.

$$MB = \frac{1}{N}\sum_{I=1}^{N}(F_i - O_i) \quad (2)$$

$$RMSE = \sqrt{\frac{1\sum_{i=1}^{n}(F_i-O_i)^2}{N}} \quad (3)$$

$$MAE = \frac{1}{n}\left[\sum_{i=1}^{n}|F_i - O_i|\right] \quad (4)$$

where F_i is the simulated model data and O_i is the observational data.

6.2.7 Projected change

To calculate the projected changes in the extreme rainfall indices, future climate simulations were obtained for two time periods: 2026-2060 and 2066-2100, under the Representative Concentration Pathways (RCP) emission scenarios RCP 2.6 and RCP 8.5, which represent global radiative forcing levels of respectively, 2.6 W/m² and 8.5 W/m² by 2100 (IPCC, 2014; Li et al., 2016; Javaherian et al., 2021). The observed datasets are provided at a high spatial resolution of 0.0375° (~4 km), which is finer than the 0.224° (25 km) grid used by CORDEX-CORE. To enable comparison, these datasets were remapped to the CORDEX-CORE grid using bilinear

interpolation with the first-order conservative remapping method (Nikulin et al., 2012; Endris et al., 2013; Gbobaniyi et al., 2014; Safari et al., 2022). Remapping observed data to coarser grids may smooth out localized climate signals. To address scale gap effects, bias correction techniques are commonly applied to refine the model outputs. Techniques like distribution mapping and linear scaling are frequently used to adjust for biases and improve the outputs of the model (Teutschbein and Seibert, 2012). In this study, we employed the linear scaling method, which involves applying a constant correction factor calculated from the difference between observed data and the original RCM simulations for each calendar month (Teutschbein and Seibert, 2012; Crochemore et al., 2016; Luo et al., 2018; Mendez et al., 2020). For the computation of the scaling factor, we used observed and historical model data for the 1983-2005 period. This time frame was selected based on the availability of observed data that aligns with the historical model simulations. After bias correction, the mean of extreme rainfall indices for each future time period under both RCP scenarios were then computed and compared to the mean of extreme rainfall indices of the current long-term mean for the period 1986-2020. The comparison of observed extreme rainfall indices for the period 1986-2020 with projected changes for the periods 2026-2060 and 2066-2100 under RCP2.6 and RCP8.5 scenarios in different climatic zones of Rwanda was performed using student t-test (Hewer et al., 2021). The significant changes were identified at $\alpha = 0.05$.

6.3 Results

Figure 6. 2 presents the spatial distribution of long-term mean of observed seasonal extreme rainfall indices over Rwanda during LR and SR for the period of 1983-2021. CWD and R10mm exhibit high values in the southwestern and northwestern highlands during LR (15–25 days, 23–37 days) and SR (15–26 days, 26–43 days). In contrast, the central and eastern regions show lower values for LR (15–25 days, 9–23 days) and SR (4–15 days, 9–26 days). For R20mm, the southern and western parts of Nyungwe National Park, the extreme northwestern highlands, and the northwestern areas of Kigali City record high values during LR (8–13 days) and SR (8–11 days). On the other hand, the eastern region and areas bordering Lake Kivu show lower values for both LR and SR (3–8 days). RX1Day is highest in the extreme southern, central, and eastern parts of the country during both LR and SR (45–60 days), while other areas observe lower values (30–45 days). For R95pTOT and PRCPTOT, the southern, western, northern, and central regions experience significant rainfall during LR (110–170 mm, 510–790 mm) and SR (125–185 mm,

520–770 mm). In contrast, the eastern region records lower amounts for LR (50–110 mm, 230–510 mm) and SR (65–125 mm, 270–520 mm). The elevated magnitude of these extreme rainfall indices in the south-western and north-western highlands may enhance agricultural productivity due to increased water availability. However, excessive rainfall could result in soil erosion, reduced crop yields, heightened flood and landslide risks, and significant impacts on infrastructure, settlements, and human livelihoods. Meanwhile, the central and eastern regions, characterized by lower topography and relatively reduced rainfall amounts, could experience water stress, potentially affecting agriculture, livestock, and access to safe drinking water.

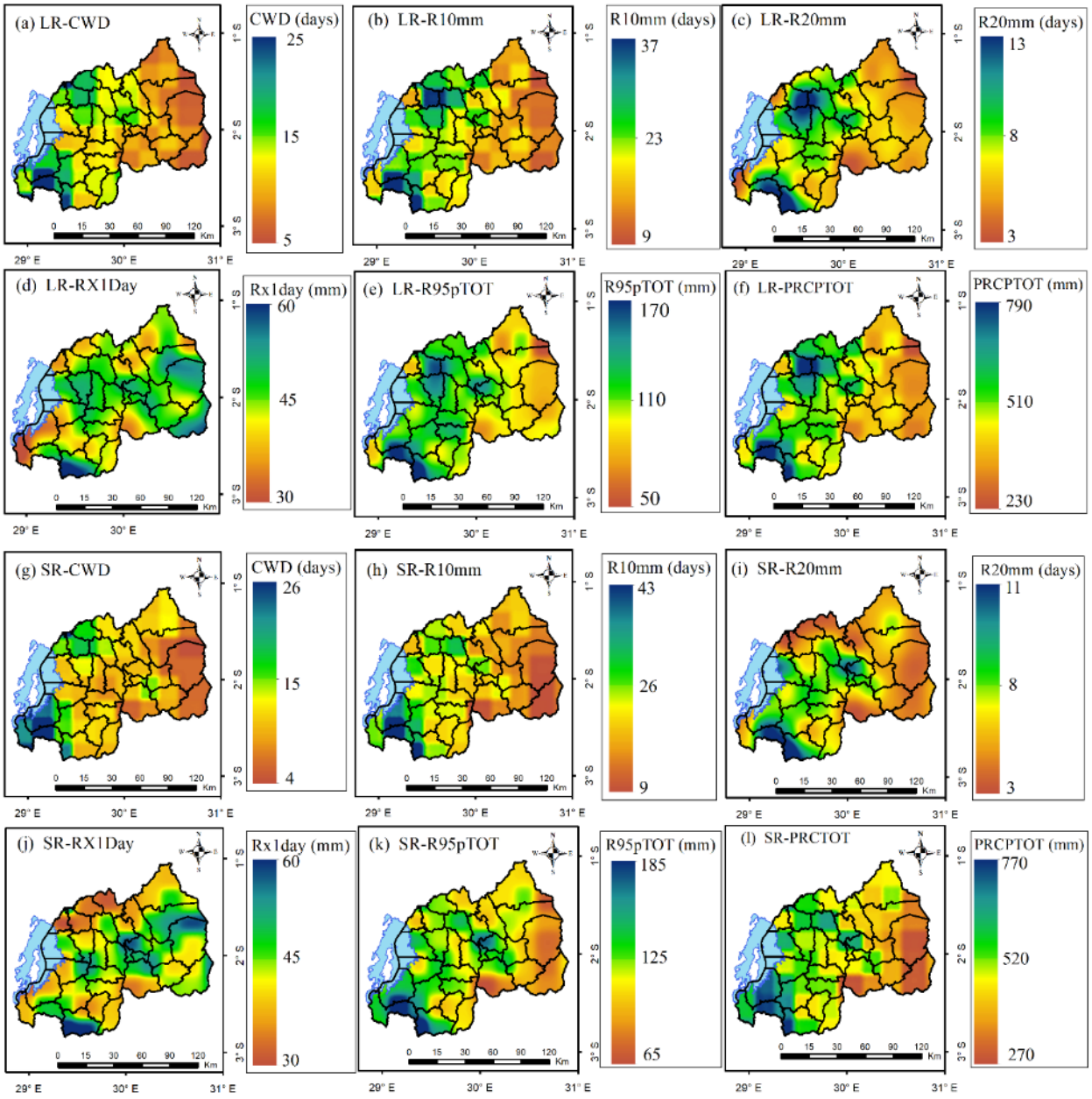

Figure 6. 2 Spatial distribution of long-term mean of observed long rain (LR) and short rain (SR) seasonal extreme rainfall indices over Rwanda during the period of 1983–2021. CWD for LR (a), R10mm for LR (b), R20mm for LR (c), RX1day for LR (d), R95pTOT for LR (f), CWD for SR (g), R10mm for LR (h), R20mm for SR (i), RX1day for SR (j), R95pTOT for SR (k), PRCPTOT for SR (l). CWD, R10mm and R20mm are expressed in days, RX1day, R95pTOT and PRCPTOT are expressed in mm.

Figure 6. 3 presents the spatial variability of the seasonal extreme rainfall indices for the LR and SR over Rwanda during the period of 1983-2021. During the LR, CWD exhibits high variability

(8-14 days) in the eastern region, while the rest of the country experiences lower variability (2-8 days). R10mm shows high variability (7-11 days) in the eastern, south-western, and north-western highlands, with lower variability (3-7 days) elsewhere. R20mm varies significantly (4-6 days) in the south-central, eastern, extreme south-western, and northern regions, while other areas observe lower variability (2-4 days). RX1Day remains relatively stable (8-21 mm) in the east but varies more widely (21-34 mm) in other regions. R95pTOT and PRCPTOT show lower variability (42-95 mm and 60-138 mm, respectively) in the southern, western, and northern regions, whereas the rest of the country experiences higher variability (95-148 mm and 138-216 mm, respectively).
During SR, CWD exhibits low variability (2-7 days) in the southwestern and northern highlands, while the rest of the country experiences higher variability (7-12 days). R10mm shows low variability (3-7 days) in the southern, central plateau, and areas around Lake Kivu, with higher variability (7-11 days) elsewhere. R20mm varies significantly (4-6 days) in the eastern and northern regions, while other areas observe lower variability (2-4 days). RX1Day remains relatively stable (8-25 mm) in the central eastern and extreme southern regions but varies more widely (25-42 mm) elsewhere. R95pTOT and PRCPTOT exhibit lower variability (47-94 mm and 73-142 mm, respectively) in the southern and central regions, whereas the eastern and northern regions experience higher variability (94-141 mm and 142-211 mm, respectively).

Higher variability in CWD can disrupt planting seasons, weaken infrastructure, and increase waterborne disease risks. Significant R10mm variability during LR may cause soil erosion, crop damage, and drainage system overload, requiring frequent maintenance. Landslides in highlands and flooding in densely populated western and northern regions pose disaster management challenges. Increased R20mm variability, particularly in south-central, eastern, and northwestern regions during LR and in eastern and northern regions during SR, threatens agriculture through crop damage, topsoil loss, and runoff-related damage to irrigation systems and roads. Flood-prone communities in western and northern highlands face heightened displacement risks, emphasizing the need for enhanced disaster preparedness. Variability in RX1Day can lead to field flooding, crop destruction, and infrastructure failure, necessitating robust designs for bridges and culverts. Greater variability in R95pTOT and PRCPTOT may disrupt water resource management, causing reservoir overflows and irrigation challenges, creating uncertainties for livelihoods reliant on

predictable rainfall. Proactive disaster strategies and infrastructure reinforcement are crucial for resilience.

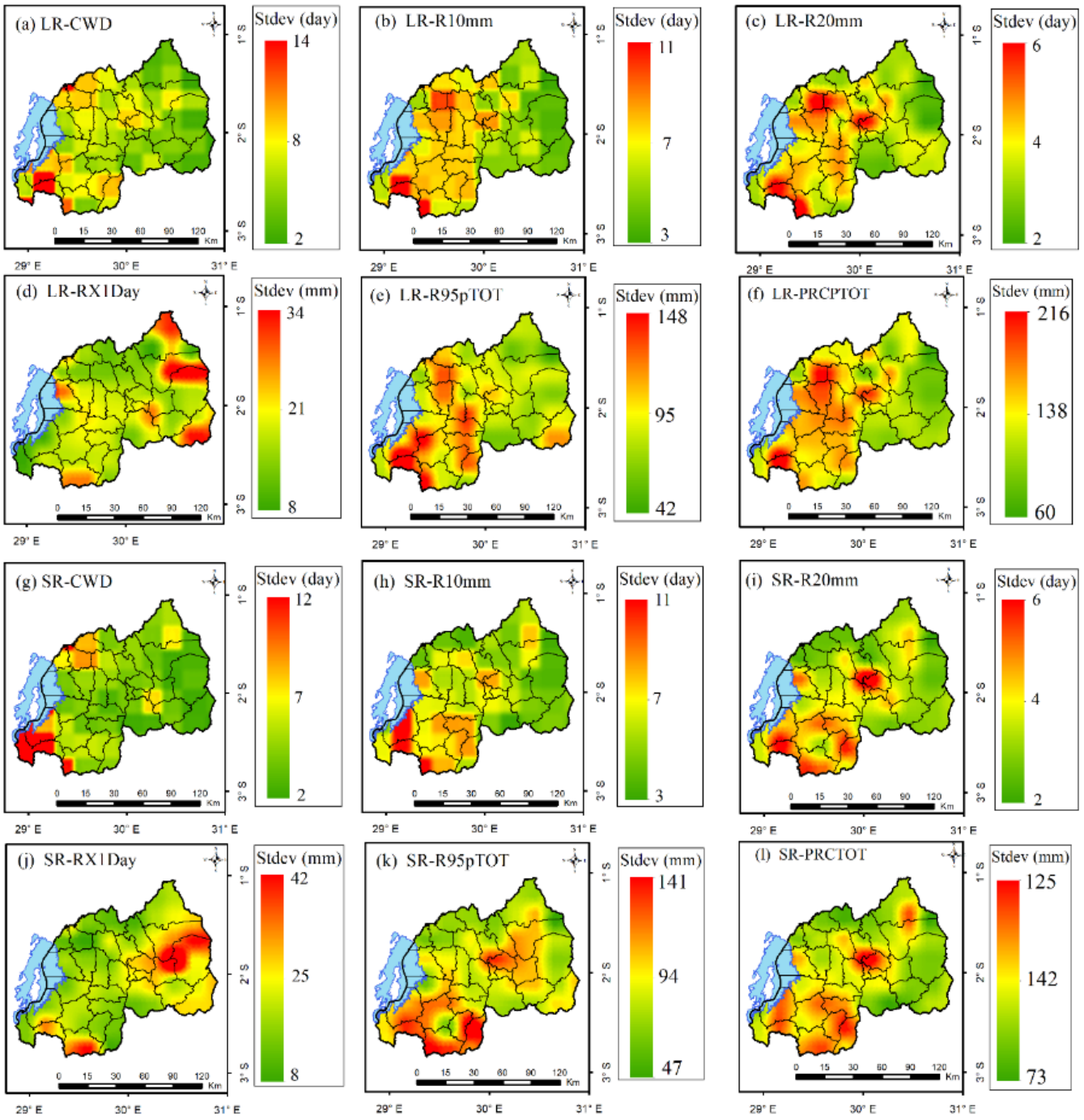

Figure 6. 3 Spatial variability of the long rain (LR) and short rain (SR) seasonal extreme rainfall indices over Rwanda during the period of 1983–2021. CWD for LR (a), R10mm for LR (b), R20mm for LR (c), RX1day for LR (d), R95pTOT for LR (e), PRCPTOT for LR (f), CWD for SR (g), R10mm for LR (h), R20mm for SR (i), RX1day for SR (j), R95pTOT for SR (k), PRCPTOT

for SR (l). CWD, R10mm and R20mm are expressed in days, RX1day, R95pTOT and PRCPTOT are expressed in mm.

Figure 6. 4 presents the spatial trends of the LR and SR seasonal extreme rainfall indices over Rwanda for the period of 1983–2021. For LR, CWD shows statistically significant increasing trends (0.3 days/year) in the south-eastern, extreme north-eastern and the western of Huye district. Statistically significant decreasing trends (-0.3 day/year) are indicated in south-western and extreme north-western of the eastern region, and the central parts of the southern region. Remaining parts of the country show no statistically significant trends. R10mm shows a statistically significant decrease (-0.33 day/year) in Kayonza District and statistically increasing trends in Ngoma and western Nyaruguru District (0.33 day/year). The remaining parts of the country show no statistically significant trends. R20mm show statistically significant decreasing trends of (-0.11day/year) in Kigali City, northern of Nyungwe National Park, Bugesera and north-eastern of Kayonza districts. The remaining parts of the country show no statistically significant trends. RX1Day show statistically significant decreasing trends (-0.8 mm/year) in southern, central plateau, eastern areas of the north region, south-eastern and north-eastern parts of the country. The rest of the country indicate no statistically significant trends. R95pTOT shows statistically significant decreasing trends (-3.3 mm/year) in southern, and eastern areas of the north region and north-eastern parts of the country. The rest of the country indicate no statistically significant trends. PRCPTOT shows statistically significant decreasing trends (-4.1 mm/year) in Kigali City, Bugesera, and the north-eastern of Kayonza district. The rest of the country indicates no statistically significant trends.

For SR, CWD shows statistically significant increasing trends (0.2 days/year) in the south-eastern. Statistically significant decreasing trends (-0.3 day/year) are indicated in south-of Kigali City, Bugesera district, and western Rwamagana and Nyagatare districts. The remaining parts of the country show no statistically significant trends. R10mm shows a statistically significant increase (0.33 day/year) in the south-eastern and north-eastern parts of the eastern region. The remaining parts of the country show no statistically significant trends. R20mm show statistically significant decreasing trends (-0.1day/year) in the north-eastern of Kayonza and the central parts of the Gatsibo districts. The remaining parts of the country show no statistically significant trends. RX1Day shows statistically significant decreasing trends (-0.6 mm/year) in north-western highlands. Statistically significant increasing trends (0.6 mm/year) in south-western, south-central,

southern Ngoma, and western Kayonza districts. The rest of the country indicates no statistically significant trends. In north-western highlands, R95pTOT shows statistically significant decreasing trends (-3.5 mm/year). Statistically significant increasing trends (3.5 mm/year) in Ngoma and western Kayonza districts. The rest of the country indicates no statistically significant trends. PRCPTOT shows statistically significant increasing trends (8.4 mm/year) in the south-eastern and extreme north-eastern Nyagatare district. The rest of the country indicates no statistically significant trends.

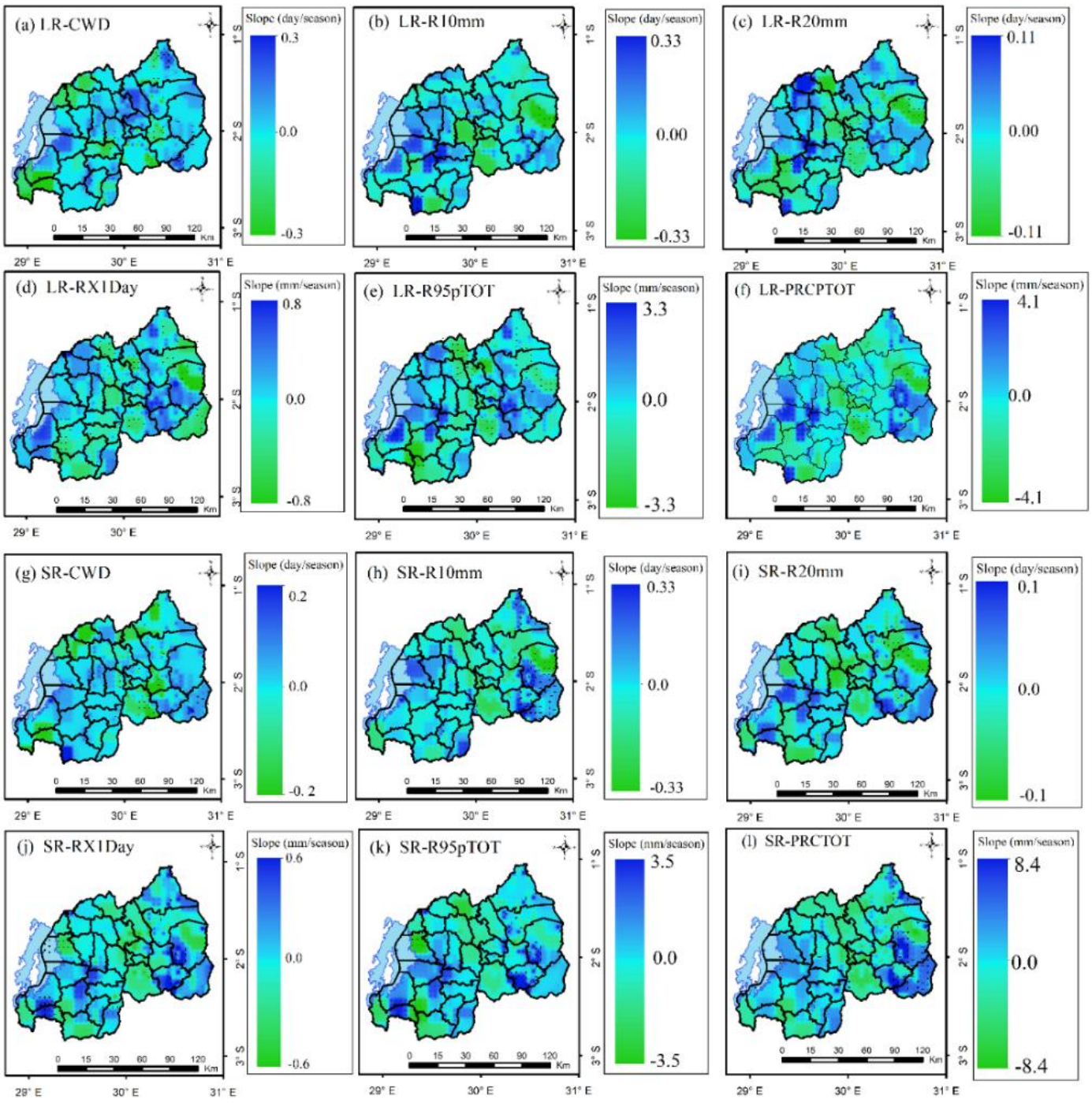

Figure 6. 4 Spatial distribution of trends of the long rain (LR) and short rain (SR) seasonal extreme rainfall indices over Rwanda during the period of 1983–2021. CWD for LR (a), R10mm for LR (b), R20mm for LR (c), RX1day for LR (d), R95pTOT for LR (e), PRCPTOT for LR (f), CWD for SR (g), R10mm for LR (h), R20mm for SR (i), RX1day for SR (j), R95pTOT for SR (k), PRCPTOT for SR (l). CWD, R10mm and R20mm are expressed in days/year, RX1day, R95pTOT and PRCPTOT are expressed in mm/year. Areas with statistically significant positive trends are

indicated with + sign, and areas with statistically significant negative trends are indicated with – sign.

Table 6. 2 show the variability and trends of country-averaged extreme precipitation indices for LR and SR. The analysis of mean values for extreme rainfall indices during the long rain season (LR) and short rain season (SR) reveals distinct patterns. For the CWD, the mean values are 10.007 days for LR and 10.082 days for SR, indicating similar wet spell durations across both seasons. The R10mm shows slightly higher mean values during SR (18.599 days) compared to LR (17.531 days), suggesting more frequent heavy rainfall events in SR. Conversely, the R20mm is slightly higher in LR (6.040 days) than in SR (5.580 days), indicating a greater occurrence of very intense rainfall in LR. The RX1Day is slightly higher in LR (42.878 mm) compared to SR (41.364 mm), reflecting more intense rainfall events in LR. For the R95pTOT, the mean value is higher in SR (109.279 mm) than in LR (95.426 mm), indicating that SR contributes more to the R95pTOT. Finally, the PRCPTOT shows higher mean values in SR (498.770 mm) compared to LR (455.675 mm), highlighting that the SR season receives more overall precipitation. These variations suggest nuanced differences in rainfall patterns between the two seasons, with SR generally exhibiting slightly more intense and frequent rainfall events. The variability for these indices demonstrates notable differences between the LR and SR seasons. For LR, CWD, R10mm, R20mm, Rx1day, R95pTOT and PRCPTOT exhibit a variability reaching 2.377 days, 3.775 days, 1.678 days, 5.772 mm, 30.876 mm and 84.363mm, respectively. For SR, these indices show a standard divarication of 2.255 days, 3.706 days, 1.486 days, 6.044 mm, 34.648 mm and 85.525 mm, respectively.

Table 6. 2 Country-averaged extreme precipitation indices for long rain (LR) and short rain (SR) seasons showing minimum values (Min), mean values, maximum values (Max), standard deviation (SD) and trend slope. Bold values indicate statistical significance at $\alpha = 0.05$. Min, Mean, Max and SD for CWD, R10mm and R20mm are expressed in days, RX1day, R95pTOT and PRCPTOT are expressed in mm. slope values are expressed in unit per year.

Extreme Rainfall indices					
INDEX	Min	Mean	Max	SD	slope
LR					
CWD	3.924	10.007	17.953	2.377	-0.003
R10mm	6.240	17.531	26.269	3.775	0.045

R20mm	1.914	6.040	9.502	1.678	-0.022
RX1Day	25.098	42.878	52.373	5.772	**-0.204**
R95pTOT	15.234	95.426	151.834	30.876	-0.900
RCPTOT	175.233	455.675	626.133	84.363	0.422
SR					
CWD	4.637	10.082	16.043	2.255	0.021
R10mm	9.938	18.599	25.446	3.706	0.045
R20mm	1.357	5.580	8.250	1.486	0.028
RX1Day	29.339	41.364	60.896	6.044	-0.002
R95pTOT	26.265	109.279	165.215	34.648	0.674
RCPTOT	274.589	498.770	662.530	85.525	1.422

Figure 6. 5 presents the country-averaged extreme rainfall indices for LR and SR. The observed trends in extreme rainfall indices are not homogeneous across the country, with significant variations between indices and seasons. Notably, RX1Day exhibits a statistically significant decrease during the LR, while other indices show no significant trends for either the LR or SR seasons. CWD and R20mm reveal contrasting trends, with both indices showing a decreasing trend (-0.003 and -0.022 days/year, respectively) during LR and an increasing trend (0.021 and 0.028 days/year) during SR. Similarly, PRCPTOT decreases during LR (-0.900 mm/year) but increases during SR (0.674 mm/year). Both R10mm and PRCPTOT exhibit positive trends in both LR and SR (0.045 days/year and 0.422 mm/year for LR; 0.045 days/year and 1.422 mm/year for SR, whereas RX1Day shows a decrease in both seasons (-0.204 and -0.002 mm/year). These results highlight the complex and regionally variable nature of extreme rainfall trends across the country.

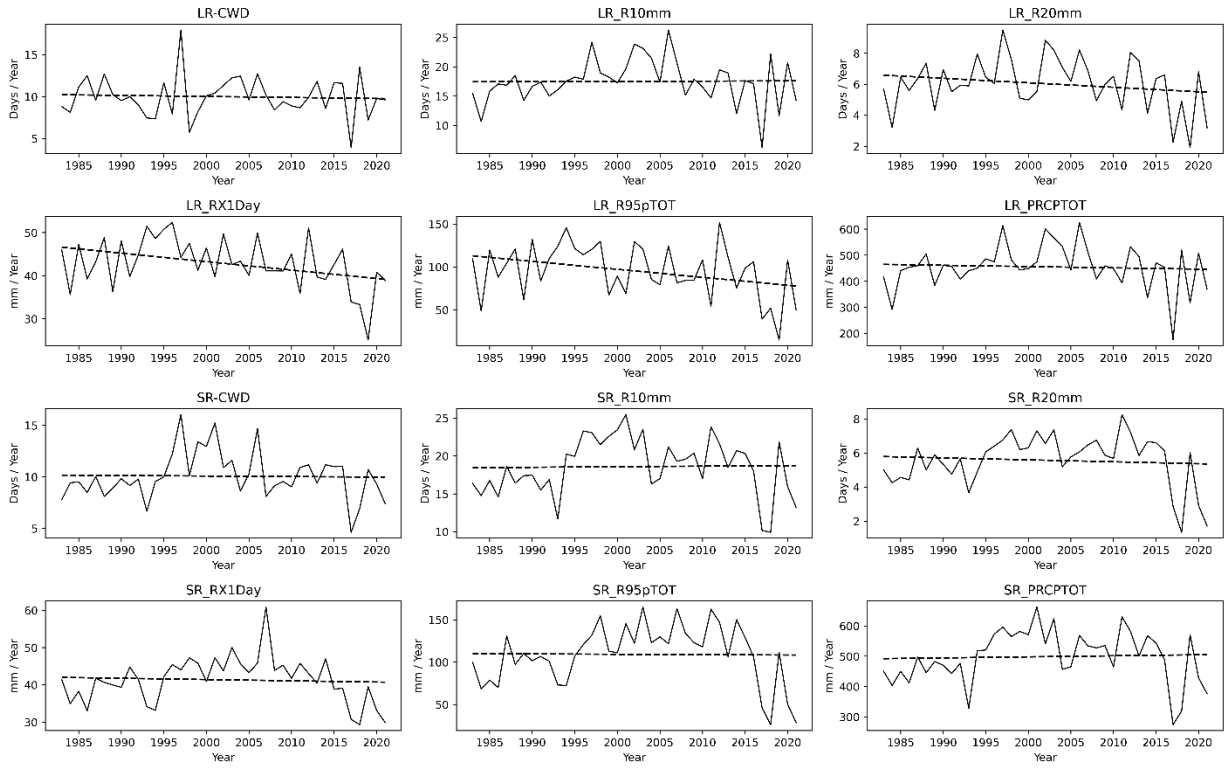

Figure 6. 5 Country-Averaged trends of the long rain (LR) and short rain (SR) seasonal extreme rainfall indices over Rwanda during the period of 1983–2021. CWD for LR (a), R10mm for LR (b), R20mm for LR (c), RX1day for LR (d), R95pTOT for LR (e), PRCPTOT for LR (f), CWD for SR (g), R10mm for LR (h), R20mm for SR (i), RX1day for SR (j), R95pTOT for SR (k), PRCPTOT for SR (l). CWD, R10mm and R20mm are expressed in days/year, RX1day, R95pTOT and PRCPTOT are expressed in mm/year.

Table 6. 3 Comparison between spatial distributions of computed CWD, PRCPTOT, R10mm, R20mm, R95pTOT and RX1day from observation and simulated by CORDEX CORE M-M-E (value in [,] is the range between minimum and maximum) for the period 1983-2005

LR				
Extreme rainfall indices LR	r (%)	MBE (mm/day)	RMSE (mm/day)	MAE (mm/day)
CWD	[20, 94]	[0, 16.01]	[0.0, 9.01]	[0.0, 22.0]
RCPTOT	[27, 90]	[-136.0, 136.0]	[0.0, 25.0]	[0.01, 37.01]
R10mm	[38, 90]	[-6.0, 6.0]	[0.0, 11.0]	[0.01, 22.01]
R20mm	[12, 99]	[-7.0, 7.0]	[0.01, 9.01]	[0.01, 9.01]
R95pTOT	[27, 92]	[-65.0, 65.0]	[0.0, 14.0]	[0.0, 17.0]

RX1Day	[3, 84]	[-18.0, 18.0]	[0.01, 21.0]	[0.02, 25.0]
SR				
Extreme rainfall indices SR	r (%)	MBE (°C)	RMSE (°C)	MAE (°C)
CWD	[21, 87]	[-7.01, 7.02]	[0.02, 6.01]	[0.01, 8.01]
RCPTOT	[3, 92]	[-100, 100]	[0.02, 38.0]	[0.02, 47.01]
R10mm	[33, 88]	[-9.01, 9.03]	[0.01, 11]	[0.03, 6.01]
R20mm	[6, 94]	[-5.03, 5.01]	[-5.5, 5.5]	[0.0, 8.01]
R95pTOT	[20, 81]	[-22.02, 22.03]	[0.0, 28.01]	[0.0, 20.01]
RX1Day	[10, 82]	[0.02, 34.01]	[0.0, 22.01]	[0.03, 16.01]

The spatial distributions of climatological mean and statistical metrics (r, MBE, RMSE, and MAE) comparing extreme rainfall indices computed from observed and CORDEX-CORE-M-M-E data during the LR in Rwanda for 1983-2005 are shown in Table 6. 3 and suppl. 6 1 (Figure 1-6). The comparisons for CWD is presented in suppl. 6 1 (Figure 1) indicates that the CORDEX-CORE-M-M-E overestimate the mean computed CWD in most parts of the country. The Pearson's correlation coefficient (r) ranges between 20% and 94%, with low values ([20, 57] %) in the north-eastern parts of the country and high values ([57, 94] %) in the other areas. MBE indicates high values ranging in the interval ([8, 16] days) in the central and extreme southern parts of the country and low values ([0, 8] days) in other regions. RMSE indicates high values ranging in the interval ([4.5, 9] days) in the extreme eastern and few areas of the south-western and low values ([0, 4.5] days) in other regions. MAE indicates high values ([11, 22] days) in the extreme south-western and low values ([0.0, 4.5] days) in other areas of the country. The comparisons for PRCPTOT presented in suppl. 6 1 (Figure 2) shows that the Pearson's correlation coefficient (r) ranges between 27% and 90%, with low values ([27, 58] %) in the south-western, southern and north-eastern parts of the country and high values ([58, 90] %) in the other areas. MBE indicates that PRCPTOT computed from CORDEX-CORE-M-M-E underestimate the PRCPTOT computed from observational data ([-136, 0] mm) in the south-western, south-eastern and northern highland and overestimate ([0, 136] mm) the observed data in other regions. RMSE indicates high values ([12.5, 25.0] mm) in southwestern and central parts of the country and low values ([0, 12.5] mm) in other regions. MAE indicates high values ([18.5, 37] mm) in the south-western, western and northern highlands and low values ([0.0, 18.5] days) in other areas of the country.

The comparisons for R10mm presented in suppl. 6 1 (Figure 3) indicates that the Pearson's correlation coefficient (r) ranges between 38% and 90%, with low values ([38, 64] %) in the western region bordering Lake Kivu, southern and extreme northern regions and high values ([64, 90] %) in the other areas. MBE indicates that R10mm computed from CORDEX-CORE-M-M-E underestimate the R10mm computed from observational data ([-6, 0] days) in the south-western, south-eastern and northern highland and overestimate ([0, 6] days) the observed data in other regions. RMSE indicates high values ([5.5, 11.0] days) in most parts of the country with few scattered areas showing low values ([0, 5.5] days) in other regions. MAE indicates high values ([11, 22] days) in the south-western and northern highlands and low values ([0.0, 11] days) in other areas of the country. The comparisons for R20mm presented in suppl. 6 1 (Figure 4) reveals that the Pearson's correlation coefficient (r) ranges between 12% and 99%, with low values ([12, 56] %) in the few areas of the western region and high values ([56, 99] %) in the other areas. MBE indicates that R20mm computed from CORDEX-CORE-M-M-E overestimate the R20mm computed from observational data ([0, 7] days) in south-western, northern highland, southeastern and extreme north-eastern and underestimate ([-7, 0] days) the observed data in other regions. RMSE indicates high values ([4.5, 9] days) in most parts of the country with few scattered areas showing low values ([0, 4.5] days) in other regions. MAE indicates high values ([4.5, 9.0] days) in the south-western and northern highlands and low values ([0.0, 4.5] days) in other areas of the country.

The comparisons for R95pTOT presented in suppl. 6 1 (Figure 5) shows that the Pearson's correlation coefficient (r) ranges between 27% and 92%, with low values ([27, 64] %) in the central western, southern and few areas of the north-eastern parts of the country and high values ([56, 99] %) in the other areas. MBE indicates that R95pTOT computed from CORDEX-CORE-M-M-E underestimate the R95pTOT computed from observational data ([-65, 0] mm) in south-eastern, central eastern and northern highland and overestimate ([0, 65] mm) the observed data in other regions. RMSE indicates low values ([0, 7] mm) in north-eastern, south-eastern, northern highland and south-western and high values ([7, 14] mm) in most parts of the country. MAE indicates low values ([0, 8.5] mm) in the central, south-eastern and northern highland and high values ([8.5, 17] mm) in other areas of the country. The comparisons for RX1day presented in suppl. 6 1 (Figure 6) indicates that the Pearson's correlation coefficient (r) ranges between 3% and 83%, with low values ([3, 43] %) in the central and southern parts of the country and high values ([43, 83] %) in

the other areas. MBE indicates that RX1day computed from CORDEX-CORE-M-M-E underestimate the RX1day computed from observational data ([-18, 0] mm) in southern, central and north-eastern regions and overestimate ([0, 18] mm) the observed data in other regions. RMSE indicates high values ([11, 21] mm) in few areas of the central, southern and northern highland and low values ([0, 11] mm) in most parts of the country. MAE indicates high values ([12.5, 25] mm) in the central western, southeastern and northeastern and low values ([0 12.5] mm) in other areas of the country.

The spatial distributions of climatological mean and statistical metrics (r, MBE, RMSE, and MAE) comparing extreme rainfall indices computed from observed and CORDEX-CORE-M-M-E data during the SR in Rwanda for 1983-2005 are shown in suppl. 6 1 (Figure 7-12). The comparisons for CWD presented in suppl. 6 1 (Figure 7) indicates that the Pearson's correlation coefficient (r) ranges between 21% and 87%, with low values (21, 54] %) observed in the central and north-eastern parts of the country and high values ([54, 87] %) in the other areas. MBE indicates that CWD computed from CORDEX-CORE-M-M-E underestimate the CWD computed from the observational data ([-7, 0] days) in the south-eastern, central, northern highlands and north-eastern parts of the country and overestimate the observation ([0, 7] days) in other regions. RMSE indicates high values ([3, 6] days) in the south-western, central and northern region and low values ([0, 3] days) in other regions. MAE indicates low values ([0, 4] days) in south-eastern and high values ([4, 8] days) in other areas of the country. The comparisons for PRCPTOT presented in suppl. 6 1 (Figure 8) indicates that the Pearson's correlation coefficient (r) ranges between 3% and 92%, with low values (3, 47] %) observed in the extreme south-western, southcentral and northern regions and high values ([47, 92] %) in the other areas. MBE shows that PRCPTOT computed from CORDEX-CORE-M-M-E overestimate the PRCPTOT computed from the observational data ([0, 100] mm) in the southern, central western and central parts of the country and underestimate the observation ([-100, 0] mm) in other regions. RMSE indicates high values ([19, 38] mm) in the south-western, northern highland and south-eastern regions and low values ([0, 3] mm) in other regions. MAE indicates low values ([0, 24] mm) in south-eastern and northern parts of the country and high values ([24, 47] mm) in other areas of the country.

The comparisons for R10mm presented in suppl. 6 1 (Figure 9) indicates that the Pearson's correlation coefficient (r) ranges between 33% and 88%, with low values (33, 61] %) observed in

the northern and southcentral parts of the country and high values ([61, 88] %) in the other areas. MBE shows that R10mm computed from CORDEX-CORE-M-M-E overestimate the R10mm computed from the observational data ([0, 9] days) in the southern and central parts of the country and underestimate the observation ([-9, 0] days) in other regions. RMSE indicates high values ([5.5, 11] days) in the south-western, northern highland and south-eastern regions and low values ([0, 5.5] days) in other regions. MAE indicates high values ([3, 6] days) in extreme southern and in northern parts of the country and low values ([0, 6] days) in other areas of the country. The comparisons for R20mm presented in suppl. 6 1 (Figure 10) indicates that the Pearson's correlation coefficient (r) ranges between 33% and 88%, with low values (33, 61] %) observed in the northern and southcentral parts of the country and high values ([61, 88] %) in the other areas. MBE shows that R20mm computed from CORDEX-CORE-M-M-E underestimate the R20mm computed from the observational data ([-5, 0] days) in the eastern, northern highland and south-western parts of the country and overestimate the observation ([0, 5] days) in other regions. RMSE indicates high values ([2.75, 5.5] days) in the south-eastern, south-western and northern highland and low values ([0, 2.75] days) in other regions. MAE indicates high values ([4, 8] days) in southcentral areas of the country and low values ([0, 4] days) in other areas of the country.

The comparisons for R95pTOT presented in suppl. 6 1 (Figure 11) indicates that the Pearson's correlation coefficient (r) ranges between 20% and 81%, with high values (51, 81] %) observed in the eastern region and low values ([20, 51] %) in the other areas. MBE shows that R95pTOT computed from CORDEX-CORE-M-M-E underestimate the R95pTOT computed from the observational data ([-22, 0] mm) in the eastern and extreme south-western parts of the country and overestimate the observation ([0, 22] mm) in other regions. RMSE indicates low values ([0, 14] mm) in the central and extreme northern parts and high values ([14, 28] mm) in other regions. MAE indicates low values ([0, 10] mm) in eastern and extreme northern parts of the country and high values ([10, 20] mm) in other areas of the country. The comparisons for RX1day presented in suppl. 6 1 (Figure 12) indicates that the Pearson's correlation coefficient (r) ranges between 10% and 82%, with low values (10, 46] %) observed in the western and northern regions and high values ([46, 82] %) in the other areas. MBE shows that RX1day computed from CORDEX-CORE-M-M-E overestimate the RX1day computed from the observational data in the whole country with high values ([17, 34] mm) in the western, southern, extreme eastern and northern regions and low values ([0, 17] mm) in other regions. RMSE indicates high values ([11, 22] mm) in few areas of

the extreme southern and north-eastern and low values ([0, 11] mm) in other regions. MAE indicates low values ([0, 8] mm) in north-eastern, central and northern regions and high values ([8, 16] mm) in other areas of the country.

Table 6. 4 Comparison between spatial distributions of computed CWD, PRCPTOT, R10mm, R20mm, R95pTOT and RX1day from observation and bias corrected simulated by CORDEX CORE M-M-E (value in [,] is the range between minimum and maximum) for the period 1983-2005

LR				
Extreme rainfall indices LR	r (%)	MBE (mm/day)	RMSE (mm/day)	MAE (mm/day)
CWD	[77, 99]	[0.0, 6.0]	[0.0, 3.001]	[0.0, 8.0]
RCPTOT	[84, 99]	[-68.0, 68.0]	[0.0, 8.8]	[0.01, 13.4]
R10mm	[95, 99]	[-2.0, 2.0]	[0.0, 4.0]	[0.0, 8.0]
R20mm	[70, 99]	[-3.0, 3.0]	[0.0, 4.02]	[0.01, 4.01]
R95pTOT	[93, 99]	[-33.0, 33.0]	[0.0, 5.0]	[0.0, 6.0]
RX1Day	[78, 99]	[-7.8, 7.8]	[0.01, 10.0]	[0.02, 8.0]
SR				
Extreme rainfall indices SR	r (%)	MBE (°C)	RMSE (°C)	MAE (°C)
CWD	[94, 99]	[-2.01, 2.02]	[0.02, 2.02]	[0.0, 1.5]
RCPTOT	[97, 99]	[-52, 0.0]	[0.02, 12.0]	[0.03, 15.01]
R10mm	[97, 99]	[-1.4, 1.403]	[0.0, 2.4]	[0.0, 1.4]
R20mm	[97, 99]	[-0.5, 0.5]	[0.0, 0.6]	[0.0, 0.8]
R95pTOT	[60, 96]	[-9.02, 9.03]	[0.0, 14.01]	[0.0, 11.02]
RX1Day	[96, 99]	[0.0, 7.01]	[0.0, 5.01]	[0.0, 4.03]

Suppl. 6 2 (Figure 1-12) and Table 6. 4 present the comparisons between spatial distributions of computed CWD, PRCPTOT, R10mm, R20mm, R95pTOT and RX1day from observation and bias corrected simulated by CORDEX CORE M-M-E for the period 1983-2005. It is clearly shown that correlations have been increased and errors have been reduced. The resulting bias corrected data were then used to analyse future projected changes in extreme rainfall indices.

Figure 6. 6 presents the projected change of the mean seasonal extreme rainfall indices for the LR over Rwanda during 2026-2060(2026-2060) and 2066-2100(2066-2100) under RCP2.6 and RCP8.5 scenarios. Future projections show a decrease in CWD for the 2026-2060 ([-8, 0] days) and for 2066-2100 ([-10, 0] days) in south-western and northern, and an increase for 2026-2060 ([0, 8] days) and for 2066-2100 ([0, 10] days) elsewhere with more decrease under RCP2.6 than RCP8.5. For R10mm and R20mm, future projection shows a decrease, respectively, ([-24, 0] days) and ([0, -14] days) for the 2026-2060 and respectively, ([-24, 0] days) and ([-13, 0 days) for 2066-2100 over the whole country with more reduction in the western and northern highland than in the central and eastern lowlands. The magnitude of change is more projected under RCP2.6 than under RCP8.5. For RX1day, future projection shows a decrease for the 2026-2060 ([-23, 0] mm) and for the 2066-2100 ([-16, 0] mm) in eastern but increase for the 2026-2060 ([0, 38] mm) and for the 2066-2100 ([0, 62] mm) elsewhere with higher magnitude of increase under RCP8.5 than RCP2.6. For R95pTOT, future projection shows for the 2026-2060, an increase ([0, 84] mm) is expected in western, southern, and northern regions with high magnitude under RCP8.5 than RCP2.6 and a decrease ([-40, 0] mm) in south-central, central and eastern regions with high magnitude under RCP2.6 than RCP8.5. For 2066-2100, an increase ([0, 380] mm) is projected in western, southern, and northern regions with high magnitude under RCP8.5 than RCP2.6 and a decrease ([-6, 0] mm) in central and southern regions. For PRCPTOT, future projection shows for the 2026-2060 a decrease ([-486, 0] mm) in southern, west and northern highlands under RCP2.6 and in the south-western and northern highland under RCP8.5. An increase ([0, 28] mm) is projected in the central and eastern under RCP2.6 and in most parts of the country under RCP8.5. For the 2066-2100, more decrease ([-380, 0] mm) is projected in the south-western, northern highland with high magnitude under RCP than under RCP8.5 and an increase ([0, 120] mm) in the eastern, central and southern region with more magnitude under RCP8.5 than RCP2.6.

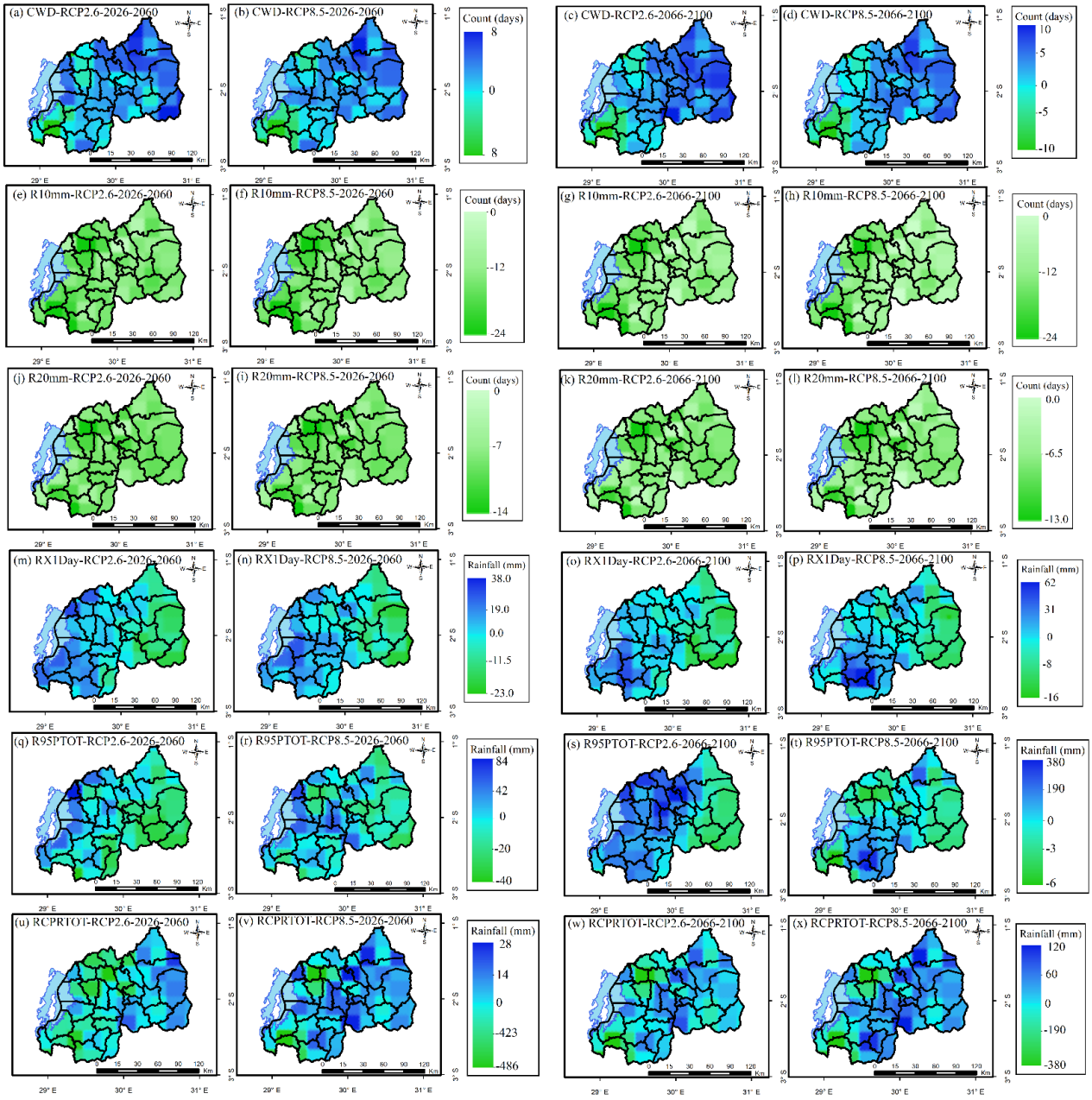

Figure 6. 6 Spatial distribution of the projected changes of mean seasonal extreme rainfall indices for long rain (LR) over Rwanda during 2026-2060 and 2066-2100 under, respectively, RCP2.6 and RCP8.5 emission scenarios relative to 1986-2020 observational period. CWD (a-d), R10mm (e-h), R20mm (j-l), RX1day (m-p), R95pTOT (q-t) and PRCPTOT (u-x). CWD, R10mm and R20mm are expressed in days, RX1day, R95pTOT and PRCPTOT are expressed in mm.

Figure 6. 7 presents the projected change of the mean seasonal extreme rainfall indices for SR over Rwanda during 2026-2060 and 2066-2100. For CWD projected increase are observed for the 2026-2060 ([2, 22] days) in most parts of the country with high magnitude under RCP2.6 than RCP8.5

and for 2066-2100 ([0, 23] days) countrywide with high magnitude in RCP8.5 than RCP2.6. For R10mm, future projection shows a decrease for the 2026-2060 (-13, 0] days) and for the 2066-2100 ([-16, 0] days) in eastern region with more reduction under RCP2.6 than RCP8.5. It is also observed an increase for the 2026-2060 ([0, 11] days) and for the 2066-2100 ([0, 16] days) in other areas with more increase expected under RCP8.5 than RCP2.6. For R20mm, future projection shows a decrease for the 2026-2060 ([-2, 0] days) and for the 2066-2100 ([-4, 0] days) in eastern region with more magnitude under RCP2.6 than RCP8.5. A projected increase is expected for the 2026-2060 ([0, 8] days) and for the 2066-2100 ([0, 10] days) in central, south, west and northern region with more increase in RCP8.5 than RCP2.6. For RX1day, a projected decrease is expected in the eastern and central regions for the 2026-2060 ([-11, 0] mm) and for the 2066-2100 ([-13, 0] mm) with more magnitude in RCP2.6 than RCP8.5. A projected increase is expected in the southern, western and northern regions for the 2026-2060 ([0, 86] mm) and for the 2066-2100 ([0, 100] mm) with more magnitude expected under RCP8.5 than RCP2.6. For R95pTOT, projected increase ([0, 313] mm) are expected for the 2026-2060 and ([0, 305] mm) for the 2066-2100 in western, southern, and northern regions with more increase under RCP8.5 than RCP2.6. A projected decrease is expected for the 2026-2060 ([-75, 0] mm) and for the 2066-2100 ([-89, 0] mm) in central and southern regions with more decrease under RCP8.5 than RCP2.6. For PRCPTOT, a projected decrease is expected for the 2026-2060 ([-38, 0] mm) and 2066-2100 ([-50, 0] mm) in the central and eastern regions with more reduction expected under RCP2.6 than RCP8.5 and increase for the 2026-2060 ([0, 582] mm) and for the 2066-2100 ([0, 765] mm) in southern, western and northern regions with more increase in RCP8.5 than in RCP2.6.

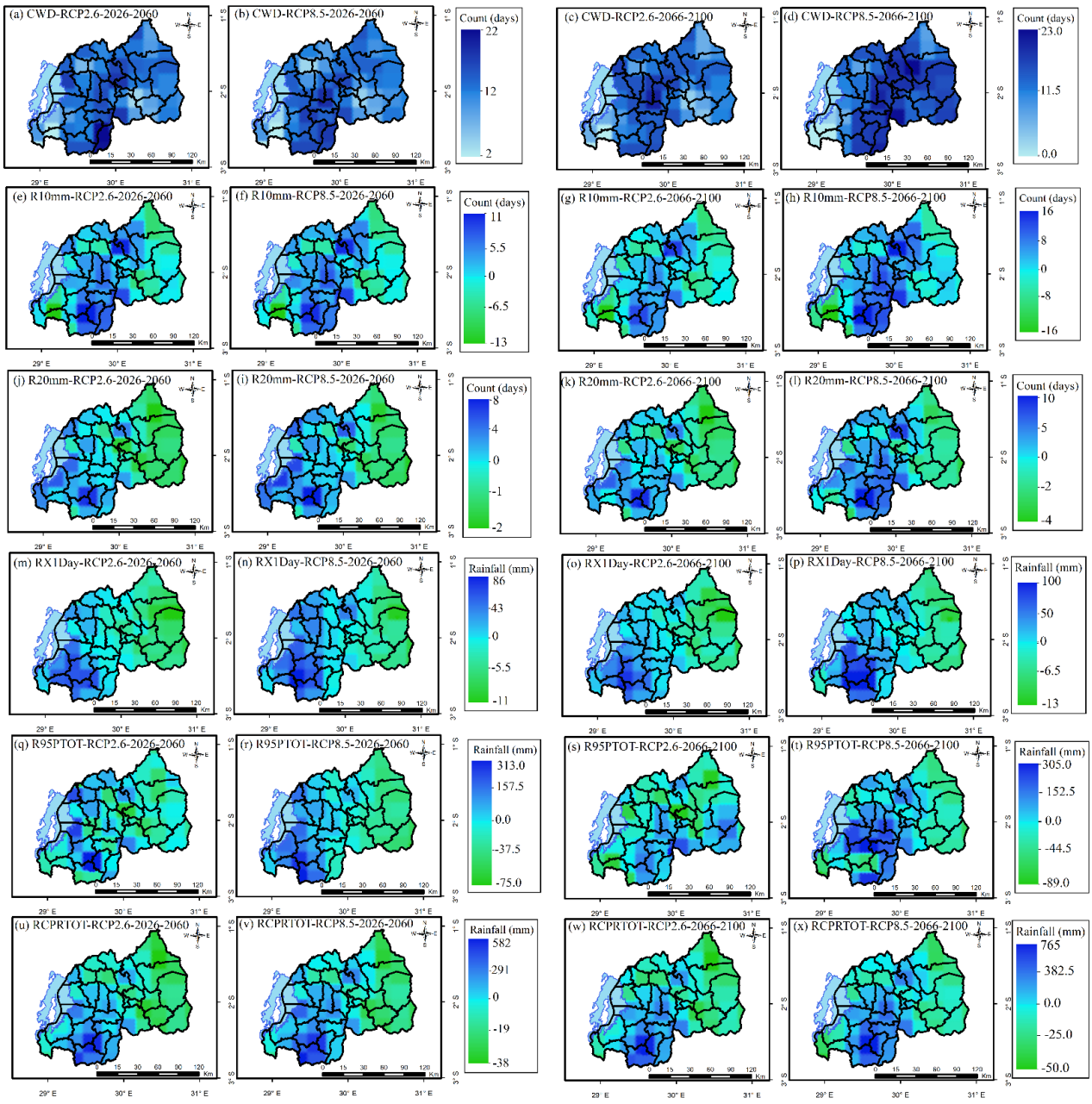

Figure 6. 7 Spatial distribution of the projected changes of mean seasonal extreme rainfall indices for short rain (SR) over Rwanda during 2026-2060 and 2066-2100 under, respectively, RCP2.6 and RCP8.5 emission scenarios relative to 1986-2020 observational period. CWD (a-d), R10mm (e-h), R20mm (j-l), RX1day (m-p), R95pTOT (q-t) and PRCPTOT (u-x). CWD, R10mm and R20mm are expressed in days, RX1day, R95pTOT and PRCPTOT are expressed in mm.

In suppl. 6 3, projected mean averaged zonal changes are presented for the periods 2026-2060 and 2066-2100 under RCP2.6 and RCP8.5 scenarios. In suppl. 6 3 (Table 1), it is observed that during

LR, in the RCP2.6 scenario, CWD shows statistically significant projected increase in Zones III, IV and VI and significant projected decrease in Zone V for 2026-2060. High values of changes corresponding to more CWDs are found in Zones III and VI. In the RCP8.5 scenario, CWD exhibits statistically significant projected increase in Zones IV and VI and decrease in Zone V with high values of changes corresponding to low CWD expected in Zone V. The same scenarios prevail for the period 2066-2100 under RCP2.6 scenario. In the RCP8.5 scenario, CWD exhibits statistically significant projected increase in Zones II, III, IV and VI and decrease in Zone V. The magnitudes of changes, when significant, are increasing following the order of zones in both RCP scenarios. During the SR, statistically significant projected increase is observed in all climatic zones for both 2026-2066 and 2066-2100 periods under both RCP2.6 and RCP8.5 scenarios. The magnitudes of changes, when significant, are increasing following the order of zones in both RCP scenarios. Overall, during the LR, patterns of changes of CWD vary from one climatic zone to another and the magnitudes of changes to more CWDs is higher in the RCP2.6 scenario than in the RCP8.5 scenario while the magnitude to low CWD is higher in RCP8.5 scenario than in the RCP2.6 scenario for both 2026-2060 and 2066-2100. For the SR, all climate zones are projected to exhibit significant changes and the magnitudes of changes to more CWDs is higher in the RCP2.6 scenario than in the RCP8.5 scenario for both 2026-2060 and 2066-2100.

In suppl. 6 3 (Table 2), it is observed during the LR, a significant changes corresponding to decrease of PRCPTOT in almost all climatic zones for 2026-2060 in both RCP2.6 and RCP8.5 scenarios.

For 2066-2100 period, significant changes corresponding to decrease are expected in Zones I, II, III, IV and VI under RCP2.6 scenario and in Zone II, III, III and IV under RCP8.5 scenario. During SR, significant projected increase in PRCPTOT is observed in all climatic zones for both 2026-2060 and 2066-2100 periods under both RCP2.6 and RCP8.5 scenarios. Overall, a projected decrease in PRCPTOT is expected during LR and increase during SR. The order of magnitudes of changes, when significant, do not follow the order of zones in both RCP scenarios.

In suppl. 6 3 (Table 3), it is found that, during LR, significant projected changes corresponding to decrease in R10mm in all zones for both 2026-2060 under both RCP2.6 and RCP8.5 scenarios. The same scenario prevails for the period 2066-2100. The order of magnitudes of changes, when significant, do not follow the order of zones in both RCP scenarios. During SR, no significant change in projected R10mm is observed in all climatic zones for both 2026-2060 under both

RCP2.6 and RCP8.5 scenarios. For the 2066-2100 period, no significant changes are observed under RCP2.6 scenario, while significant changes corresponding to decrease in R10mm are observed in Zones I and II, and increase in Zones III, IV, V and VI under RCP8.5 scenario. Overall, for LR, R10mm is projected to decrease for the two periods under both RCP scenarios while for the SR, it projected to decrease in Zones I and II and increase in Zones III, IV, V and VI under RCP8.5 scenarios for the period 2066-2100.

In suppl. 6 3 (Table 4), it is found that, during LR, significant projected changes corresponding to decrease in R20mm in all zones for both 2026-2060 under both RCP2.6 and RCP8.5 scenarios. The same scenario prevails for the period 2066-2100. The order of magnitudes of changes, when significant, follow the order of zones except for Zone IV in both RCP scenarios. During SR, significant change corresponding to increase in R20mm is observed in Zones I, II, III and IV under RCP2.6 scenario and in Zones I, II, III, IV and V under RCP8.5 scenario for the period 2026-2060. For the period 2066-2100, significant change corresponding to increase in R20mm is observed in Zones I, II, III, IV and VI under RCP2.6 scenario and in all zones under RCP8.5 scenario. The magnitudes of changes, when significant, are do not following the order of zones in both RCP scenarios. Overall, for LR, R20mm is projected to decrease for the two periods under both RCP scenarios while for the SR, it projected to increase in most zones for the two periods under both RCP scenarios.

In suppl. 6 3 (Table 5), it is found that, during LR, no significant projected changes for R95pTOT in all climate zones for 2026-2066 and 2066-2100 periods under both RCP2.6 and RCP8.5 scenarios. During SR, significant change corresponding to increase in R95pTOT is observed in all climate zones for 2026-2066 and 2066-2100 periods under both RCP2.6 and RCP8.5 scenarios. The magnitudes of changes, when significant, are do not following the order of zones in both RCP scenarios. Overall, for LR, no significant changes in R95pTOT is projected in all zones for the two periods under both RCP scenarios while for the SR, it projected to increase in all zones for the two periods under both RCP scenarios.

In suppl. 6 3 (Table 6), it is found that, during LR, no significant projected changes for RX1day in all climate zones for 2026-2066 and 2066-2100 periods under both RCP2.6 and RCP8.5 scenarios. During SR, significant change corresponding to increase in RX1day is observed in all climate zones for 2026-2066 and 2066-2100 periods under both RCP2.6 and RCP8.5 scenarios. The magnitudes of changes, when significant, are do not following the order of zones in both RCP

scenarios. Overall, for LR, no significant changes in RX1day is projected in all zones for the two periods under both RCP scenarios while for the SR, it projected to increase in all zones for the two periods under both RCP scenarios.

6.4 Country averaged projected changes of extreme rainfall indices

Figure 6 8 presents the observed and projected country averaged changes in rainfall extreme indices during LR season in Rwanda. The projections indicate a consistent decline in the number of days experiencing rainfall above 10 mm (R10mm) and 20 mm (R20mm) throughout the century. This trend reflects a decrease in the frequency of heavy and very heavy precipitation events. Conversely, indices that capture the intensity and concentration of extreme rainfall are expected to increase over time. The CWD index, which tracks the longest stretch of consecutive days with measurable rainfall, is projected to rise, suggesting longer periods of continuous wet conditions that may elevate risks of soil saturation and flooding. Additionally, the RX1Day index, measuring the highest precipitation amount recorded in a single day, is projected to increase, implying that while rainy days may become fewer, the rainfall intensity during these events could intensify. The R95pTOT, which represents the total rainfall accumulated on very wet days (those exceeding the 95^{th} percentile), is also anticipated to grow, indicating that extreme rainfall will contribute an increasing portion of total seasonal precipitation. Lastly, the total seasonal precipitation (PRCPTOT) during MAM is projected to rise despite the reduction in rainfall frequency. This suggests a shift toward heavier, more intense rainfall events contributing to overall greater precipitation amounts during the season.

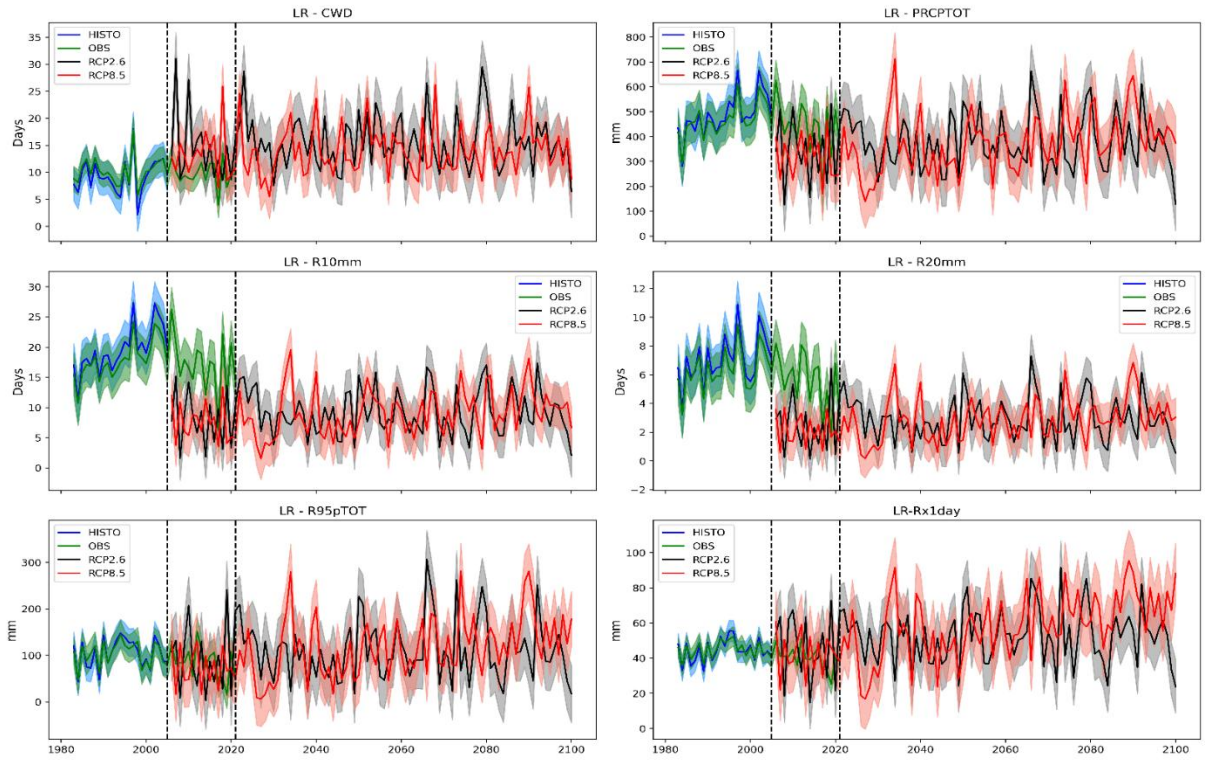

Figure 6. 8: Observations and projections of country averaged rainfall extreme indices during LRin Rwanda for observation 1983-2021 and for the future 2006-2100 under RCP2.6 and RCP8.5

Figure 6 9 presents the observed and projected country averaged changes in rainfall extreme indices during SR season in Rwanda. The projections show a steady decrease over the century in the occurrence of days with rainfall surpassing 10 mm (R10mm) and 20 mm (R20mm). This reduction implies fewer heavy to very heavy rain days. In contrast, rainfall intensity and accumulation metrics are expected to show upward trends. The CWD index, indicating the longest sequence of rainy days, is projected to increase, pointing to potentially prolonged wet periods. Similarly, the RX1Day index, reflecting the maximum single-day rainfall, is projected to rise, highlighting the possibility of more intense precipitation events, even as the frequency of rain days diminishes. The R95pTOT index, which measures total rainfall from extremely wet days (above the 95th percentile), is also expected to grow, reinforcing the likelihood that extreme rainfall will make up a larger fraction of the total precipitation in the season. Finally, total seasonal rainfall (PRCPTOT) during SOND is forecasted to increase over the century. This occurs alongside fewer

rainy days, indicating a tendency towards less frequent but heavier rainfall contributing to the overall precipitation totals.

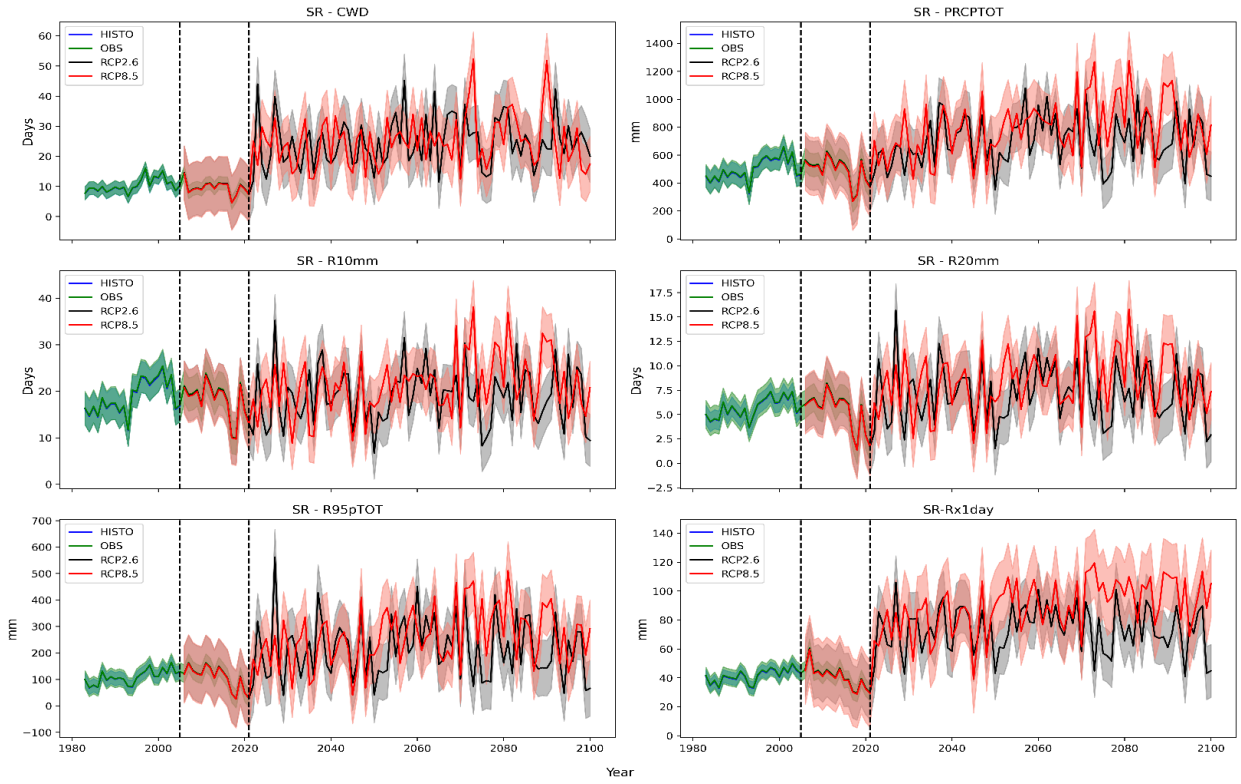

Figure 6. 9: Observations and projections of country averaged rainfall extreme indices during SR in Rwanda for observation 1983-2021 and for the future 2006-2100 under RCP2.6 and RCP8.5

6.5 Discussion

Overall, both seasons exhibit distinct patterns of spatial variability in extreme rainfall indices, with certain regions consistently showing high or low variability depending on the specific index and season. Specifically, more variabilities are observed in several parts of the country for CWD, over the western region for RX1Day, and in the eastern region for R10mm, R20mm, R95pTOT, and PRCPTOT. The spatial trends exhibit heterogeneity across the country. Among the country-averaged extremes, only RX1Day shows a statistically significant negative trend during the LR. This finding are aligned with previous findings over the southern and western Africa (New et al., 2006), while they differ from decreasing patterns observed over Benin (Attogouinon et al., 2017). Our results show non-significant changes in R10mm and R20mm which are not similar to results

obtained in the ASAL Areas of EA region (Ongoma et al., 2018), and the eastern portion of Uganda (Alex et al., 2019) and across Benin (Attogouinon et al., 2017) that indicated decreasing trends for these indices. Previous findings show a decrease trends for R95pTOT in Uganda (Alex et al., 2019) and for RCPTOT in ASAL Areas of Equatorial Eastern Africa (Ongoma et al., 2018) which are not aligned with our finding.

Projected changes in extreme rainfall indices may result in significant and multifaceted impacts on various sectors. Future projections for each climate zones for both long rain and short rain seasons show diverse projected changes with some zones indicating significant changes while other show no significant changes under different emission scenarios. Projected increases in CWD during LR in Zones III, IV, and VI, and during SR in Zones I, II, III, IV, and VI may enhance soil moisture, supporting crop growth. However, excessive wet conditions could lead to waterlogging and an increase in crop diseases, particularly in high-rainfall areas of the western and northern highlands (Zones II, III, IV). In addition, projected increase RX1day and R95pTOT during SR across all zones may intensify soil erosion, topsoil loss, and crop damage, particularly in steep agricultural regions such as Zones II and III. On the other hand, the decline in CWD in Zone V during both seasons and reductions in PRCPTOT during LR in multiple zones (I, II, III, IV, and VI under RCP2.6; II, III, and IV under RCP8.5 could lead to moisture stress, reduced crop yields, and increased reliance on irrigation, exacerbating food insecurity risks in the central plateau and eastern lowlands. Previous studies have indicated that shifts in extreme rainfall patterns may result in increased migration due to the impacts of climate-related disturbances (Nawrotzki et al., 2015; Nawrotzki & Bakhtsiyarava, 2017). Projected increase of CWD in steep mountain regions (Zones II, III, IV), increase in RX1day and R95pTOT during SR across all zones**,** R10mm during SR in several zones could increase the risks of landslides and floods that can affect infrastructure such as roads, bridges, and drainage systems leading to higher maintenance costs and disruptions to transportation networks. Landslides, especially in western and northern zones, may disrupt livelihoods and displacement of communities. Conversely, projected reductions in R10mm and R20mm during LR across all zones may decrease risks of flooding (Tubiello et al., 2007; Müller et al., 2011; Cooper et al., 2008). Heavy precipitation events can lead to flooding, which may result in root diseases, delayed planting seasons, or even crop failure due to excessive rainfall (Posthumus et al., 2009). The areas prone to landslides and floods, will likely require enhanced

measures such as development of early warning systems, evacuation plans, and resilient infrastructure (Adger et al., 2005).

Projected increases in CWD and PRCPTOT during SR could replenish reservoirs, improve groundwater recharge, and support irrigation and hydropower generation. However, excessive rainfall could increase sedimentation from heavy runoff, reducing water quality and storage capacity. On the other hand, reductions in PRCPTOT during LR across most zones may lower reservoir inflows, affecting drinking water supplies, irrigation systems, and hydropower production and negatively impacting sanitation and hygiene and the spread of waterborne diseases (Patz et al., 2005; McMichael et al., 2006). The central plateau (Zone V) and eastern lowlands (Zone VI) may be particularly vulnerable to water shortages and increased drought risks, affecting water availability for irrigation and livestock which may lead to reduced agricultural and livestock output and intensifying food insecurity (Patz et al., 2005; Tubiello et al., 2007; Funk et al., 2008; Omondi et al., 2014). In this areas, dryness conditions could adversely affect wildlife and natural reserves, reducing its attractiveness to tourists (Gössling et al., 2012). Areas prone to prolonged dryness will likely require improved water management strategies, including the construction of reservoirs, the implementation of water harvesting and recycling systems, and the adoption of drought-resistant agricultural practices (Funk et al., 2008; Adger et al., 2005). Extreme rainfall changes present challenges for Rwanda's tourism sector, particularly in highland areas reliant on eco-tourism, such as gorilla trekking in Zone III. Increased CWD and heavy rainfall during SR could result in muddy and inaccessible trails, landslides, posing safety concerns for visitors and disruptions to tourist activities. Conversely, projected reduced rainfall during LR may create opportunities for tourism growth in drier areas but could also reduce water availability for eco-tourism activities dependent on natural landscapes (Gössling et al., 2012; Ye, 2023).

These findings highlight the complex nature of rainfall patterns in Rwanda. The significant spatial differences in trends and changes of extreme rainfall indices within relatively small geographic areas underscore the importance of localized climate adaptation strategies to address the specific needs and challenges of different regions within Rwanda. For Rwanda, various climate products are available, including those provided by Meteo-Rwanda, which address diverse needs. These include daily forecasts for the general public, extreme weather warnings for disaster prevention, medium to seasonal weather forecasts, detailed information on the start and end of rainy seasons

tailored for agricultural planning, and sector-specific advisories aimed at mitigating the impacts of weather related events. However, there is a need for improvements in these services to enhance accuracy, accessibility, and responsiveness to better meet the evolving needs of all sectors.

6.6 Conclusion

This study analyses trends and variability in seasonal extreme rainfall indices over Rwanda for the period 1983-2021. The indices examined include consecutive wet days (CWD), heavy precipitation days (R10mm), very heavy precipitation days (R20mm), one-day maximum precipitation (RX1day), precipitation from very wet days (R95pTOT), and total annual precipitation (PRCPTOT). The analysis was conducted for the long rains (LR) and short rains (SR) using indices defined by the Expert Team on Climate Change Detection and Indices (ETCCDI). Trends and their magnitudes were assessed using the Modified Mann-Kendall test and Theil-Sen's slope estimator. The study also evaluates projected changes in these indices using the CORDEX-CORE multi-model ensemble under two Representative Concentration Pathways (RCP2.6 and RCP8.5). The findings reveal distinct spatial patterns of rainfall variability across Rwanda. CWD shows the most widespread variability, with RX1day being particularly variable in the western region, while R10mm, R20mm, R95pTOT, and PRCPTOT exhibit higher variability in the east. For trends, CWD generally decreases in central-eastern and western Nyagatare but increases in the southeast during both LR and SR. R10mm decreases in Kayonza for both seasons but increases in Ngoma during LR and the southeast during SR. R20mm, RX1day, R95pTOT, and PRCPTOT show decreasing trends in Kayonza, Bugesera, Kigali City, and parts of Nyungwe National Park. During LR, R95pTOT decreases in the southeast, while PRCPTOT increases during SR. The magnitude and significance of projected changes in extreme rainfall indices differ in climate zones and seasons. During LR, CWD is projected to significantly increase in Zones III, IV, and VI under RCP2.6 and in Zones IV and VI under RCP8.5 for 2026-2060. By 2066-2100, increases are expected in Zones III, IV, and VI under RCP2.6 and in Zones II, III, IV, and VI under RCP8.5, while a decline is projected in Zone V under both scenarios. R10mm and R20mm are projected to decrease in all climate zones for both scenarios during both future periods. Similarly, PRCPTOT is expected to decline in almost all climate zones during 2026-2060, and in Zones I, II, III, IV and VI under RCP2.6 and Zones II, III and IV under RCP8.5 for 2066-2100. During SR, increases in CWD, RX1day, R95pTOT, and PRCPTOT are projected across all zones under both scenarios and

time horizons. R20mm is projected to rise in Zones I–IV under RCP2.6 and Zones I-V under RCP8.5 for 2026-2060. By 2066-2100, R20mm is projected to rise in Zones I, II, III, IV, and VI under RCP2.6 and all zones under RCP8.5 by 2066-2100.

These findings underscore the complex, region-specific, and seasonally dependent nature of both historical and projected rainfall extremes in Rwanda. While increased rainfall in some regions may enhance water availability and agricultural productivity, it also poses risks such as flooding, infrastructure damage, and landslides. Conversely, reduced rainfall in other regions may threaten water security, energy generation, and agricultural outputs. Understanding these projected changes is crucial for mitigating potential socio-economic impacts. This knowledge supports informed decision-making and the development of targeted, region-specific adaptation strategies. To enhance resilience to future climate variability, it is essential to prioritize investments in climate-resilient infrastructure, improved water resource management, and strengthened early warning systems. This study utilizes the RCP2.6 and RCP8.5 emission scenarios, which are the currently available options from the CORDEX-CORE regional climate model simulations over the study area. These scenarios provide valuable insights into contrasting climate futures, representing low-emission (strong mitigation) and high-emission (business-as-usual) pathways, and thus encompass a broad range of potential climate trajectories. To enhance the comprehensiveness of future climate assessments, subsequent studies should consider incorporating intermediate scenarios such as RCP4.5 or RCP6.0, which would offer additional perspectives on potential future changes and help bridge the gap between the two extremes. Future avenues are: i) investigating regional and large-scale atmospheric systems influencing extreme rainfall indices in Rwanda to improve predictive capabilities and early warning systems; ii) assessing the socio-economic impacts associated with extreme rainfall indices on key sectors such as agriculture, infrastructure, health, biodiversity, and water resources, to support the development of targeted adaptation strategies and iii) evaluating the effectiveness of existing and proposed climate adaptation measures, identifying gaps and recommending improvements to enhance resilience against extreme rainfall events.

6.7 Reference

Adeyeri, O. E., Lawin, A. E., Laux, P., Ishola, K. A., & Ige, S. O. (2019). Analysis of climate extreme indices over the Komadugu-Yobe basin, Lake Chad region: Past and future occurrences. *Weather and Climate Extremes*, *23*(November 2018), 100194.

https://doi.org/10.1016/j.wace.2019.100194

Adeyeri, O. E., Laux, P., Lawin, A. E., & Oyekan, K. S. A. (2020). Multiple bias-correction of dynamically downscaled CMIP5 climate models temperature projection: a case study of the transboundary Komadugu-Yobe river basin, Lake Chad region, West Africa. *SN Applied Sciences*, *2*(7), 1–18. https://doi.org/10.1007/s42452-020-3009-4

Adeyeri, O. E., Zhou, W., Laux, P., Ndehedehe, C. E., Wang, X., Usman, M., & Akinsanola, A. A. (2023). Multivariate Drought Monitoring, Propagation, and Projection Using Bias-Corrected General Circulation Models. *Earth's Future*, *11*(4), 1–16. https://doi.org/10.1029/2022EF003303

Adeyeri, O. E., Zhou, W., Ndehedehe, C. E., & Wang, X. (2024). Global vegetation, moisture, thermal and climate interactions intensify compound extreme events. *Science of the Total Environment*, *912*(July 2023), 169261. https://doi.org/10.1016/j.scitotenv.2023.169261

Adeyeri, O. E., Zhou, W., Ndehedehe, C. E., Wang, X., Ishola, K. A., & Laux, P. (2024). Minimizing uncertainties in climate projections and water budget reveals the vulnerability of freshwater to climate change. *One Earth*, *7*(1), 72–87. https://doi.org/10.1016/j.oneear.2023.12.013

Adger, W. N., Hughes, T. P., Folke, C., Carpenter, S. R., & Rockström, J. (2005). Social-ecological resilience to coastal disasters. *Science*, *309*(5737), 1036–1039. https://doi.org/10.1126/science.1112122

Ahmed, K., Shahid, S., Ali, R. O., Harun, S. Bin, & Wang, X. J. (2017). Evaluation of the performance of gridded precipitation products over balochistan province, pakistan. *Desalination and Water Treatment*, *79*(January), 73–86. https://doi.org/10.5004/dwt.2017.20859

Alex, N., Jesse, K., & Neoline, N. (2019). Evaluation of Past and Future Extreme Rainfall Characteristics over Eastern Uganda. J Environ Agric Sci, 18: 38–49.

Alexander, L. V., Zhang, X., Peterson, T. C., Caesar, J., Gleason, B., Klein Tank, A. M. G., Haylock, M., Collins, D., Trewin, B., Rahimzadeh, F., Tagipour, A., Rupa Kumar, K., Revadekar, J., Griffiths, G., Vincent, L., Stephenson, D. B., Burn, J., Aguilar, E., Brunet, M., … Vazquez-Aguirre, J. L. (2006). Global observed changes in daily climate extremes of temperature and precipitation. *Journal of Geophysical Research Atmospheres*, *111*(5), 1–22. https://doi.org/10.1029/2005JD006290

Attogouinon, A., Lawin, A. E., M'Po, Y. N. T., & Houngue, R. (2017). Extreme precipitation indices trend assessment over the Upper Oueme river valley-(Benin). *Hydrology*, *4*(3), 1–24. https://doi.org/10.3390/hydrology4030036

Ayugi, B., Dike, V., Ngoma, H., Babaousmail, H., Mumo, R., & Ongoma, V. (2021). Future Changes in Precipitation Extremes over East Africa Based on CMIP6 Models. *Water*, 1–19. https://doi.org/10.1002/joc.7264

Berhane, A., Hadgu, G., Worku, W., & Abrha, B. (2020). Trends in extreme temperature and rainfall indices in the semi-arid areas of Western Tigray, Ethiopia. *Environmental Systems Research*, *9*(1). https://doi.org/10.1186/s40068-020-00165-6

Bobde, V., Akinsanola, A. A., Folorunsho, A. H., Adebiyi, A. A., & Adeyeri, O. E. (2024). Projected regional changes in mean and extreme precipitation over Africa in CMIP6 models. *Environmental Research Letters*, *19*(7). https://doi.org/10.1088/1748-9326/ad545c

Chang'a, L. B., Kijazi, A. L., Mafuru, K. B., Nying'uro, P. A., Ssemujju, M., Deus, B., Kondowe, A. L., Yonah, I. B., Ngwali, M., Kisama, S. Y., Aimable, G., Sebaziga, J. N., & Mukamana, B. (2020). Understanding the Evolution and Socio-Economic Impacts of the Extreme Rainfall Events in March-May 2017 to 2020 in East Africa. *Atmospheric and Climate Sciences*, *10*(04), 553–572. https://doi.org/10.4236/acs.2020.104029

Chechin, D. G., Makhotina, I. A., Lüpkes, C., & Makshtas, A. P. (2019). Effect of wind speed and leads on clear-sky cooling over Arctic sea ice during polar night. *Journal of the Atmospheric Sciences*, *76*(8), 2481. https://doi.org/10.1175/JAS-D-18-0277.1

Christiansen, D. E., Markstrom, S. L., & Hay, L. E. (2011). Impacts of climate change on the growing season in the United States. *Earth Interactions*, *15*(33), 1–17. https://doi.org/10.1175/2011EI376.1

Cooper, P. J. M., Dimes, J., Rao, K. P. C., Shapiro, B., Shiferaw, B., & Twomlow, S. (2008). Coping better with current climatic variability in the rain-fed farming systems of sub-Saharan Africa: An essential first step in adapting to future climate change? *Agriculture, Ecosystems and Environment*, *126*(1–2), 24–35. https://doi.org/10.1016/j.agee.2008.01.007

Crochemore, L., Ramos, M. H., & Pappenberger, F. (2016). Bias correcting precipitation forecasts to improve the skill of seasonal streamflow forecasts. *Hydrology and Earth System Sciences*, *20*(9), 3601–3618. https://doi.org/10.5194/hess-20-3601-2016

Das, S., Datta, P., Sharma, D., & Goswami, K. (2022). Trends in Temperature, Precipitation,

Potential Evapotranspiration, and Water Availability across the Teesta River Basin under 1.5 and 2◦ C Temperature Rise Scenarios of CMIP6. *Atmosphere*, *13*(6), 1–22. https://doi.org/10.3390/atmos13060941

Datta, P., & Das, S. (2019). Analysis of long-term seasonal and annual temperature trends in North Bengal, India. *Spatial Information Research*, *27*(4), 475–496. https://doi.org/10.1007/s41324-019-00250-8

Dinku, T., Faniriantsoa, R., Islam, S., Nsengiyumva, G., & Grossi, A. (2022). The Climate Data Tool: Enhancing Climate Services Across Africa. *Frontiers in Climate*, *3*, 1–16. https://doi.org/10.3389/fclim.2021.787519

Dinku, T., Hailemariam, K., Maidment, R., & Connor, S. (2014). Combined use of satellite estimates and rain gauge observations to generate high-quality historical rainfall time series over Ethiopia. *International Journal of Climate Climatology*, *2504*(November 2013), 2489–2504. https://doi.org/10.1002/joc.3855

Donat, M. G., Alexander, L. V., Yang, H., Durre, I., Vose, R., Dunn, R. J. H., Willett, K. M., Aguilar, E., Brunet, M., Caesar, J., Hewitson, B., Jack, C., Klein Tank, A. M. G., Kruger, A. C., Marengo, J., Peterson, T. C., Renom, M., Oria Rojas, C., Rusticucci, M., … Kitching, S. (2013). Updated analyses of temperature and precipitation extreme indices since the beginning of the twentieth century: The HadEX2 dataset. *Journal of Geophysical Research Atmospheres*, *118*(5), 2098–2118. https://doi.org/10.1002/jgrd.50150

Endris, H. S., Omondi, P., Jain, S., Lennard, C., Hewitson, B., Chang'a, L., Awange, J. L., Dosio, A., Ketiem, P., Nikulin, G., Panitz, H. J., Büchner, M., Stordal, F., & Tazalika, L. (2013). Assessment of the performance of CORDEX regional climate models in simulating East African rainfall. *Journal of Climate*, *26*(21), 8453–8475. https://doi.org/10.1175/JCLI-D-12-00708.1

Ehret, U., Zehe, E., Wulfmeyer, V., Warrach-Sagi, K., & Liebert, J. (2012). HESS Opinions "should we apply bias correction to global and regional climate model data?" *Hydrology and Earth System Sciences*, *16*(9), 3391–3404. https://doi.org/10.5194/hess-16-3391-2012

Faniriantsoa, R. (2017). Workshop report : Training on IRI Climate Data Tools and developing a method for integrating climate data, Kigali, Rwanda. *CGIAR Research Program on Climate Change, Agriculture and Food Security (CCAFS)*.

Funk, C., Dettinger, M. D., Michaelsen, J. C., Verdin, J. P., Brown, M. E., Barlow, M., & Hoell,

A. (2008). Warming of the Indian Ocean threatens eastern and southern African food security but could be mitigated by agricultural development. *Proceedings of the National Academy of Sciences of the United States of America*, *105*(32), 11081–11086. https://doi.org/10.1073/pnas.0708196105

Gbobaniyi, E., Sarr, A., Sylla, M. B., Diallo, I., Lennard, C., Dosio, A., Dhiédiou, A., Kamga, A., Klutse, N. A. B., Hewitson, B., Nikulin, G., & Lamptey, B. (2014). Climatology, annual cycle and interannual variability of precipitation and temperature in CORDEX simulations over West Africa. *International Journal of Climatology*, *34*(7), 2241–2257. https://doi.org/10.1002/joc.3834

Gebrechorkos, S. H., Hülsmann, S., & Bernhofer, C. (2019). Changes in temperature and precipitation extremes in Ethiopia, Kenya, and Tanzania. *International Journal of Climatology*, *39*(1), 18–30. https://doi.org/10.1002/joc.5777

Gössling, S., Peeters, P., Hall, C. M., Ceron, J. P., Dubois, G., Lehmann, L. V., & Scott, D. (2012). Tourism and water use: Supply, demand, and security. An international review. *Tourism Management*, *33*(1), 1–15. https://doi.org/10.1016/j.tourman.2011.03.015

Habiyakare, F., Jiang, T., Yahaya, I., Ndabagenga, D., Kagabo, J., & Su, B. (2024). Spatial Variation and Trend of Extreme Precipitation in Africa during 1981-2019 and Its Projected Changes at the End of 21st Century. *Journal of Geoscience and Environment Protection*, *12*(03), 192–221. https://doi.org/10.4236/gep.2024.123012

Hamed, K. H., & Rao, A. R. (1998). A modified Mann-Kendall trend test for autocorrelated data. *Journal of Hydrology*, *204*, 182–196. https://doi.org/10.1200/jco.2018.36.15_suppl. 522

Hargreaves, G. H., & Allen, R. G. (2003). History and Evaluation of Hargreaves Evapotranspiration Equation. *Journal of Irrigation and Drainage Engineering*, *129*(1), 53–63. https://doi.org/10.1061/(asce)0733-9437(2003)129:1(53)

Hewer, M. J., Beech, N., & Gough, W. A. (2021). Development and validation of the Climate Model Confidence Index (CMCI): measuring ability to reproduce historical climate conditions. *Theoretical and Applied Climatology*, *144*(3–4), 1059–1075. https://doi.org/10.1007/s00704-021-03581-5

IPCC. (2014). Climate Change 2014: Synthesis Report. Contribution of Working Groups I, II and III to the Fifth Assessment Report of the Intergovernmental Panel on Climate Change. In *(Core Writing Team, R. K. Pachauri & L. A. Meyer, eds). IPCC, Geneva, Switzerland, p. 151.*

(Vol. 541, Issue 1). https://doi.org/10.1177/0002716295541001010

Javaherian, M., Ebrahimi, H., & Aminnejad, B. (2021). Prediction of changes in climatic parameters using CanESM2 model based on Rcp scenarios (case study): Lar dam basin. *Ain Shams Engineering Journal*, *12*(1), 445–454. https://doi.org/10.1016/j.asej.2020.04.012

Kazora, J., Wen, W., Shahid, S., Ali, M. A., Bilal, M., Habtemicheal, B. A., Iyakaremye, V., Qiu, Z., Almazroui, M., Wang, Y., Joseph, S. N., & Tiwari, P. (2021). Spatiotemporal variability of rainfall trends and influencing factors in Rwanda. *Journal of Atmospheric and Solar-Terrestrial Physics*, *219*(March), 105631. https://doi.org/10.1016/j.jastp.2021.105631

Kazora, J., Zhu, W., Kyaw, T. O., & Sebaziga, J. N. (2023). Enhancement of East African Monsoon Long Rainfall (March to May) Variability from Weekly to Annual Scale by Climatic Extremes. *Atmospheric and Climate Sciences*, 491–506. https://doi.org/10.4236/acs.2023.134028

Lehmann, J., Coumou, D., & Frieler, K. (2015). Increased record-breaking precipitation events under global warming. *Climatic Change*, *132*(4), 501–515. https://doi.org/10.1007/s10584-015-1434-y

Li, K., Liao, H., Zhu, J., & Moch, J. M. (2016). Implications of RCP emissions on future PM2.5 air quality and direct radiative forcing over China. *Journal of Geophysical Research*, *121*(21), 12,985-13,008. https://doi.org/10.1002/2016JD025623

Lobell, D. B., & Field, C. B. (2007). Global scale climate-crop yield relationships and the impacts of recent warming. *Environmental Research Letters*, *2*(1). https://doi.org/10.1088/1748-9326/2/1/014002

Luhunga, P., Botai, J., & Kahimba, F. (2016). Evaluation of the performance of CORDEX regional climate models in simulating present climate conditions of Tanzania. *Journal of Southern Hemisphere Earth Systems Science*, *66*(1), 32–54. https://doi.org/10.22499/3.6601.005

Luo, M., Liu, T., Meng, F., Duan, Y., Frankl, A., Bao, A., & De Maeyer, P. (2018). Comparing bias correction methods used in downscaling precipitation and temperature from regional climate models: A case study from the Kaidu River Basin in Western China. *Water (Switzerland)*, *10*(8). https://doi.org/10.3390/w10081046

Mahrt, L. (2014). Stably stratified atmospheric boundary layers. *Annual Review of Fluid Mechanics*, *46*, 23–45. https://doi.org/10.1146/annurev-fluid-010313-141354

Marra, F., Levizzani, V., & Cattani, E. (2022). Changes in extreme daily precipitation over Africa:

Insights from a non-asymptotic statistical approach. *Journal of Hydrology X*, *16*, 100130. https://doi.org/10.1016/j.hydroa.2022.100130

McMichael, A. J., Woodruff, R. E., & Hales, S. (2006). Climate change and human health: Present and future risks. *Lancet*, *367*(9513), 859–869. https://doi.org/10.1016/S0140-6736(06)68079-3

Mendez, M., Maathuis, B., Hein-Griggs, D., & Alvarado-Gamboa, L. F. (2020). Performance evaluation of bias correction methods for climate change monthly precipitation projections over Costa Rica. *Water (Switzerland)*, *12*(2). https://doi.org/10.3390/w12020482

Mikova, K. (2015). Effect of Climate Change on Crop Production in Rwanda. *Earth Sciences*, *4*(3), 120. https://doi.org/10.11648/j.earth.20150403.15

Muhire, I., Ahmed, F., & Abutaleb, K. (2015). Relationships between Rwandan seasonal rainfall anomalies and ENSO events. *Theoretical and Applied Climatology*, *122*(1–2), 271–284. https://doi.org/10.1007/s00704-014-1299-4

Müller, C., Cramer, W., Hare, W. L., & Lotze-Campen, H. (2011). Climate change risks for African agriculture. *Proceedings of the National Academy of Sciences of the United States of America*, *108*(11), 4313–4315. https://doi.org/10.1073/pnas.1015078108

National Institute of Statistics of Rwanda. (2023). *Main Indicators: 5th Rwandan Population and Housing Census (PHC)); National Institute of Statistics of Rwanda: Kigali, Rwanda*.

Nawrotzki, R. J., & Bakhtsiyarava, M. (2017). International Climate Migration: Evidence for the Climate Inhibitor Mechanism and the Agricultural Pathway. *Population, Space and Place*, *23*(4). https://doi.org/10.1002/psp.2033

Nawrotzki, R. J., Hunter, L. M., Runfola, D. M., & Riosmena, F. (2015). Climate change as a migration driver from rural and urban Mexico. *Environmental Research Letters*, *10*(11), 114023. https://doi.org/10.1088/1748-9326/10/11/114023

New, M., Hewitson, B., Stephenson, D. B., Tsiga, A., Kruger, A., Manhique, A., Gomez, B., Coelho, C. A. S., Masisi, D. N., Kululanga, E., Mbambalala, E., Adesina, F., Saleh, H., Kanyanga, J., Adosi, J., Bulane, L., Fortunata, L., Mdoka, M. L., & Lajoie, R. (2006). Evidence of trends in daily climate extremes over southern and west Africa. *Journal of Geophysical Research Atmospheres*, *111*(14), 1–11. https://doi.org/10.1029/2005JD006289

Ngaina, J., & Mutai, B. (2013). Observational evidence of climate change on extreme events over East Africa. *Global Meteorology*, *2*(1), 2. https://doi.org/10.4081/gm.2013.e2

Ngarukiyimana, J. P., Fu, Y., Yang, Y., & Ogwang, A. (2017). *Dominant atmospheric circulation patterns associated with abnormal rainfall events over Rwanda , East Africa*. https://doi.org/10.1002/joc.5169

Nikulin, G., Jones, C., Giorgi, F., Asrar, G., Büchner, M., Cerezo-Mota, R., Christensen, O. B., Déqué, M., Fernandez, J., Hänsler, A., van Meijgaard, E., Samuelsson, P., Sylla, M. B., & Sushama, L. (2012). Precipitation climatology in an ensemble of CORDEX-Africa regional climate simulations. *Journal of Climate*, *25*(18), 6057–6078. https://doi.org/10.1175/JCLI-D-11-00375.1

Ntwali, D., Ogwang, B. A., & Ongoma, V. (2016). The Impacts of Topography on Spatial and Temporal Rainfall Distribution over Rwanda Based on WRF Model. *Atmospheric and Climate Sciences*, *06*(02), 145–157. https://doi.org/10.4236/acs.2016.62013

Ogega, O. M., Koske, J., Kung'u, J. B., Scoccimarro, E., Endris, H. S., & Mistry, M. N. (2020). Heavy precipitation events over East Africa in a changing climate: results from CORDEX RCMs. *Climate Dynamics*, *55*(3–4), 993–1009. https://doi.org/10.1007/s00382-020-05309-z

Omondi, P. A. o., Awange, J. L., Forootan, E., Ogallo, L. A., Barakiza, R., Girmaw, G. B., Fesseha, I., Kululetera, V., Kilembe, C., Mbati, M. M., Kilavi, M., King'uyu, S. M., Omeny, P. A., Njogu, A., Badr, E. M., Musa, T. A., Muchiri, P., Bamanya, D., & Komutunga, E. (2014). Changes in temperature and precipitation extremes over the Greater Horn of Africa region from 1961 to 2010. *International Journal of Climatology*, *34*(4), 1262–1277. https://doi.org/10.1002/joc.3763

Ongoma, V., Chen, H., & Omony, G. W. (2018). Variability of Extreme Weather Events over the Equatorial East Africa , a case study of Rainfall in Kenya and Uganda. *Theoretical and Applied Climatology*, *January*. https://doi.org/10.1007/s00704-016-1973-9

Onyutha, C. (2020). Analyses of rainfall extremes in East Africa based on observations from rain gauges and climate change simulations by CORDEX RCMs. *Climate Dynamics*, *54*(11–12), 4841–4864. https://doi.org/10.1007/s00382-020-05264-9

Orlowsky, B., & Seneviratne, S. I. (2012). Global changes in extreme events: Regional and seasonal dimension. *Climatic Change*, *110*(3–4), 669–696. https://doi.org/10.1007/s10584-011-0122-9

Owoyesigire, B., Mpairwe, D., Ericksen, P., & Peden, D. (2016). *Trends in variability and extremes of rainfall and temperature in the cattle corridor of Uganda*. *17*(2), 231–244.

Patz, J. A., Campbell-Lendrum, D., Holloway, T., & Foley, J. A. (2005). Impact of regional climate change on human health. *Nature*, *438*(7066), 310–317. https://doi.org/10.1038/nature04188

Posthumus, H., Morris, J., Hess, T. M., Neville, D., Phillips, E., & Baylis, A. (2009). Impacts of the summer 2007 floods on agriculture in England. *Journal of Flood Risk Management*, *2*(3), 182–189. https://doi.org/10.1111/j.1753-318X.2009.01031.x

Safari, B. (2012). Trend Analysis of the Mean Annual Temperature in Rwanda during the Last Fifty Two Years. *Journal of Environmental Protection*, *03*(06), 538–551. https://doi.org/10.4236/jep.2012.36065

Safari, B., & Sebaziga, J. N. (2023). Trends and Variability in Temperature and Related Extreme Indices in Rwanda during the Past Four Decades. *Atmosphere*, *14*(9), 1449. https://doi.org/10.3390/atmos14091449

Safari, B., Sebaziga, J. N., & Siebert, A. (2022). Evaluation of CORDEX-CORE Regional Climate Models in Simulating Rainfall Variability in Rwanda . *International Journal of Climatology*, *June 2021*, 1–29. https://doi.org/10.1002/joc.7891

Sarr, M. A., Gachon, P., Seidou, O., Bryant, C. R., Ndione, J. A., & Comby, J. (2015). Inconsistent linear trends in Senegalese rainfall indices from 1950 to 2007. *Hydrological Sciences Journal*, *60*(9), 1538–1549. https://doi.org/10.1080/02626667.2014.926364

Sebaziga, J. N., Safari, B., Ngaina, J. N., & Ntwali, D. (2024). Spatial variability of seasonal rainfall onset, cessation, length and rainy days in Rwanda. *Theoretical and Applied Climatology*. https://doi.org/10.1007/s00704-024-05086-3

Sebaziga, J. N., Twahirwa, A., Kazora, J., Rusanganwa, F., Mbati, M. M., Higiro, S., Guhirwa, S., Nyandwi, J. C., & Niyitegeka, J. M. V. (2023). Spatial and Temporal Analysis of Rainfall Variability and Trends for Improved Climate Risk Management in Kayonza District, Eastern Rwanda. *Advances in Meteorology*, *2023*, 1–17. https://doi.org/10.1155/2023/5372701

Sebaziga, N. J., Bonfils, S., Joshua, N. N., Didier, N., Bethwel, M. K., Safari, A. K., & Michel, R. (2022). Rainfall variability and trends over Rwanda. *Journal of Climate Change and Sustainability*, *4*(1), 2021–2022.

Siebert, A., Dinku, T., Vuguziga, F., Twahirwa, A., & Kagabo, D. M. (2019). Evaluation of ENACTS-Rwanda : A new multi-decade , high- resolution rainfall and temperature data set — Climatology. *International Journal of Climatology*, *January*, 1–17. https://doi.org/10.1002/joc.6010

Sillmann, J., Kharin, V. V., Zwiers, F. W., Zhang, X., & Bronaugh, D. (2013). Climate extremes indices in the CMIP5 multimodel ensemble: Part 2. Future climate projections. *Journal of Geophysical Research Atmospheres*, *118*(6), 2473–2493. https://doi.org/10.1002/jgrd.50188

Tan, C., Yang, J., & Li, M. (2015). Temporal-spatial variation of drought indicated by SPI and SPEI in Ningxia Hui Autonomous Region, China. *Atmosphere*, *6*(10), 1399–1421. https://doi.org/10.3390/atmos6101399

Tank, A. M. G. K., Zwiers, F. W., & Zhang, X. (2009). Guidelines on analysis of extremes in a changing climate in support of informed decisions for adaptation. *Climate Data and Monitoring Rep.WCDMP 72, WMO-TD 1500*, *72*, 56.

Taxak, A. K., Murumkar, A. R., & Arya, D. S. (2014). Long term spatial and temporal rainfall trends and homogeneity analysis in Wainganga basin, Central India. *Weather and Climate Extremes*, *4*, 50–61. https://doi.org/10.1016/j.wace.2014.04.005

Tebaldi, C., Hayhoe, K., Arblaster, J. M., & Meehl, G. A. (2006). Going to the extremes: An intercomparison of model-simulated historical and future changes in extreme events. *Climatic Change*, *79*(3–4), 185–211. https://doi.org/10.1007/s10584-006-9051-4

Teutschbein, C., & Seibert, J. (2012). Bias correction of regional climate model simulations for hydrological climate-change impact studies: Review and evaluation of different methods. *Journal of Hydrology*, *456–457*, 12–29. https://doi.org/10.1016/j.jhydrol.2012.05.052

Tubiello, F. N., Soussana, J. F., & Howden, S. M. (2007). Crop and pasture response to climate change. *Proceedings of the National Academy of Sciences of the United States of America*, *104*(50), 19686–19690. https://doi.org/10.1073/pnas.0701728104

Twahirwa, A., Oludhe, C., Omondi, P., Rwanyiziri, G., & Sebaziga, N. J. (2023). Assessing Variability and Trends of Rainfall and Temperature for the District of Musanze in Rwanda. *Advances in Meteorology*, *2023*. https://doi.org/https://doi.org/10.1155/2023/7177776

Umuhoza, J., Chen, L., & Mumo, L. (2021). Assessing the Skills of Rossby Centre Regional Climate Model in Simulating Observed Rainfall over Rwanda. *Atmospheric and Climate Sciences*, *11*(03), 398–418. https://doi.org/10.4236/acs.2021.113023

Umutoni, M. A., Japheth, L. P., Lipiki, E. J., Kebacho, L. L., Limbu, P. T. S., & Makula, E. K. (2021). Investigation of the 2016 March to May extreme rainfall over Rwanda. *Natural Hazards*, *108*(1), 607–618. https://doi.org/10.1007/s11069-021-04697-7

Uwimbabazi, J., Jing, Y., Iyakaremye, V., Ullah, I., & Ayugi, B. (2022). Observed Changes in

Meteorological Drought Events during 1981–2020 over Rwanda, East Africa. *Sustainability (Switzerland)*, *14*(3). https://doi.org/10.3390/su14031519

Willmott, C. J., & Matsuura, K. (2005). Advantages of the mean absolute error (MAE) over the root mean square error (RMSE) in assessing average model performance. *Climate Research*, *30*(1), 79–82. https://doi.org/10.3354/cr030079

Ye, X. (2023). Impacts of Climate Change on Tourism in Coastal Areas. *Advances in Economics, Management and Political Sciences*, *62*(1), 271–276. https://doi.org/10.54254/2754-1169/62/20231359

Zhang, X., Alexander, L., Hegerl, G. C., Jones, P., Tank, A. K., Peterson, T. C., Trewin, B., & Zwiers, F. W. (2011). Indices for monitoring changes in extremes based on daily temperature and precipitation data. *Wiley Interdisciplinary Reviews: Climate Change*, *2*(6), 851–870. https://doi.org/10.1002/wcc.147

Zhou, X., Chen, L., Umuhoza, J., Cheng, Y., Wang, L., & Wang, R. (2021). Intraseasonal oscillation of the rainfall variability over Rwanda and evaluation of its subseasonal forecasting skill. *Atmospheric and Oceanic Science Letters*, *14*(6), 100099. https://doi.org/10.1016/j.aosl.2021.100099